



**UNIVERSIDAD
DE GRANADA**

PROGRAMA DE DOCTORADO EN BIOMEDICINA (B11.56.1)

Genetic bases of endolymphatic sac hypoplasia in Meniere Disease

Base genética de la hipoplasia del saco endolinfático
en Enfermedad de Meniere

International PhD thesis

Author: Paula Robles Bolívar

Supervisors: Jose Antonio López Escámez, Álvaro Gallego Martínez

Granada, October 2023

Editor: Universidad de Granada. Tesis Doctorales
Autor: Paula Robles Bolívar
ISBN: 978-84-1195-089-3
URI: <https://hdl.handle.net/10481/85696>

El doctorando / The *doctoral candidate* **Paula Robles Bolívar**, y los directores de la tesis / and the thesis supervisor/s: **Jose Antonio López Escámez y Álvaro Gallego Martínez**:

Garantizamos, al firmar esta tesis doctoral, que el trabajo ha sido realizado por el doctorando bajo la dirección de los directores de la tesis y hasta donde nuestro conocimiento alcanza, en la realización del trabajo, se han respetado los derechos de otros autores a ser citados, cuando se han utilizado sus resultados o publicaciones.

Guarantee, by signing this doctoral thesis, that the work has been done by the doctoral candidate under the direction of the thesis supervisor/s and, as far as our knowledge reaches, in the performance of the work, the rights of other authors to be cited (when their results or publications have been used) have been respected.

Lugar y fecha / *Place and date*: **Granada, 20 de agosto de 2023**

Content

FUNDING.....	1
FIGURE INDEX.....	2
TABLE INDEX.....	7
SUPPLEMENTARY FIGURES INDEX.....	8
SUPPLEMENTARY TABLES INDEX.....	8
ABSTRACT.....	9
RESUMEN.....	11
ACRONYMS AND ABBREVIATIONS.....	13
1. - INTRODUCTION.....	2
1.1 - The inner ear.....	3
1.1.1 - The cochlea.....	3
1.1.2 - The vestibular system.....	9
1.1.3 - The regulation of endolymph and maintenance of the endocochlear potential.....	13
1.1.4 - The non-sensory organs.....	14
1.1.5 - Innervation and vascularization of the inner ear.....	21
1.2 - Meniere Disease.....	23
1.2.1 - Clinical symptoms.....	23
1.2.2 - Comorbidities.....	25
1.2.3 - Epidemiology.....	26
1.2.4 - Diagnosis and classification of MD clinical subgroups.....	27
1.2.5 - Etiology and pathophysiology of MD.....	29
1.2.6 - Endotypes of Endolymphatic Sac in MD.....	34
1.3 - The genetics of diseases.....	36
1.3.1 - NGS technologies in the discovery of genetic disease.....	36
1.3.2 - Genetic variants.....	36
1.3.3 - Variant allele frequency and phenotype effect size.....	39
2. - HYPOTHESIS AND JUSTIFICATION.....	41
3. – OBJECTIVES.....	44

4. – MATERIALS AND METHODS	46
4.1 - Materials.....	47
4.1.1 - Molecular Biology Reagents.....	47
4.1.2 - Antibodies	47
4.1.3 - IHC	48
4.1.4 - WB.....	49
4.1.5 - Equipment.....	50
4.1.6 - Informatic resources.....	50
4.2 - Methods	52
Chapter 1	52
4.2.1 – Recruitment of non-MD patient cohort.....	52
4.2.2 - ATVA radiographic marker analysis	52
4.2.3 – ATVA data analysis	54
Chapter 2	55
4.2.4 - Recruitment of hypoplastic MD patients	55
4.2.5 – Whole Exome Sequencing	56
4.2.6 - Bioinformatic analysis	57
Chapter 3	69
4.2.7 - Candidate variants validation	69
4.2.8 - Evaluation of inner ear candidate genes expression	70
4.2.9 - Evaluation of rare variants in protein structure or expression	73
4.2.10 - Functional analysis of candidate genes.....	73
5. RESULTS.....	75
5.1 - Chapter 1: study of the prevalence of ES hypoplasia in individuals without MD	76
5.1.1 - Cohort of patients without MD	78
5.1.2 - ATVA measurements	80
5.1.3 - ES hypoplasia was absent in our cohort of patients without MD.....	81
5.1.4 - Relation of ATVA with age, sex or clinical diagnosis	82
5.2 - Chapter 2: Identification of genes and variants associated with hypoplasia of ES in MD.....	84
5.2.1 - Identification of genes and variants associated with ES hypoplasia in sporadic MD patients.....	85
5.2.2 - Identification of genes and variants associated with ES hypoplasia in familiar MD patients.....	98
5.3 - Chapter 3: Validation of genes and variants associated with hypoplasia of ES in MD	108
5.3.1 - Candidate variants were validated by Sanger sequencing	109

5.3.2 - Immunohistochemical analysis revealed the expression of Adamts18 in the mice inner ear	110
5.3.3 - Western Blot assay replicated the expression of Adamts18 in the mice inner ear	115
5.3.4 - Evaluation of rare variants in protein structure or expression	117
5.3.5 - Functional analysis of GBA enriched variants genes.....	121
6. – DISCUSSION	124
6.1 - ES hypoplasia is absent in our cohort of patients without MD	126
6.2 - The characteristics of our MD and ES hypoplasia cohort are consistent with other patients with the same MD endotype	129
6.3 - The abnormal development of the temporal bone, the ES, the ED and the VA are widely related to the appearance of MD	131
6.4 - Genetic analysis of ES hypoplasia in Meniere Disease	133
6.4.1 - Candidate genes in the MD and ES hypoplastic cohort associated with audio-vestibular related function	133
6.4.2 - Candidate genes in the MD and ES hypoplastic cohort associated with bone remodeling	136
6.4.3 - Candidate genes in the MD and ES hypoplastic cohort associated with neurogenesis and neuronal circuits.....	142
6.5 - ES hypoplasia MD endophenotype is produced by alterations in the development of audio-vestibular organs, otic capsule and neural circuits inside inner ear	146
7. – CONCLUSIONS CONCLUSIONES	150
8. – LIMITATIONS AND FUTURE DIRECTIONS.....	153
9. – REFERENCES	156
10. – SUPPLEMENTARY MATERIAL	171
10.1 - Supplementary figures.....	172
10.2 - Supplementary tables	176
Original Research Articles	186



Funding

This work was supported by CECEU-PY20-00303 – EPIMEN (Papel de la regulación epigenómica en la penetrancia y expresividad en la enfermedad de Meniere); and the Schmieder-Bohrisch Foundation (Geneva, Switzerland). Paula Robles Bolívar is funded by H2020-SC1-2019-848261 – UNITI (Unification of Treatments and Interventions for Tinnitus Patients).

Figure Index

- Figure 1.1 – Schematic representation of ear anatomy. A) Differentiation of the three ear anatomical compartments: the outer (external), the middle, and the inner; B) Inner ear membranous labyrinths, and otic capsule. Created with BioRender.com..... 4
- Figure 1.2 - Anatomy of the cochlea and morphological structure of sensory cochlear epithelia. Created with BioRender.com..... 6
- Figure 1.3 - Hair bundle and sound mechanotransduction. Created with BioRender.com8
- Figure 1.4 - Morphological and simplified vestibular sensory epithelia cellular structure, including hair cells, and vestibular nerves. Created with BioRender.com..... 11
- Figure 1.5 - Schematic section of the ED and ES, showing intra (iES) and extraosseous (eES) segments. Created with BioRender.com..... 16
- Figure 1.6 - Ultrastructural details of the two types of epithelial cells in the rat ES: mitochondria-rich cells (MRC) and ribosome-rich cells (RRC) (called chief cells in rats) by transmission (A) and scanning electron microscopy (B). L: lumen; C: capillary; N: nucleus; Scale bar 1 μ m (A) and 10 μ m (B). Images from Qvortrup *et al.* (35)..... 17
- Figure 1.7 – PTA from non-affected (A) and affected (B) hearing individuals. On the X axis, the frequencies are represented in kilohertz (kHz), including low (\leq 500 kHz), medium (500 - 3000 kHz), and high (\geq 3000 kHz) tones. High frequencies are those involved in the range of speech; therefore, their alteration is the most disabling. The Y axis represents the patient's sensory thresholds in decibels (dB). Thresholds above or equal to 20 correspond to unaffected hearing. There are different levels of impairment, including mild, moderate, severe, and profound. For example, patient B has mild-to-moderate hearing impairment at low frequencies in the left ear and mild impairment in high tones in the right ear. 24
- Figure 1.8 - Timeline diagram of clinical symptoms progression in MD..... 25
- Figure 1.9 - Scheme of the different types of variants: A) SNV, B) InDels, and C) Structural variants. Created with BioRender.com..... 38

Figure 4.1 - Method to calculate ATVA marker in histological sections (A,C) and CT images (B,D). Scale bars: 1 cm. Figure adapted from Bächinger *et al.* (155). Co: cochlea IAC: internal auditory canal; LSC: lateral semicircular canal; PCF: posterior cranial fossa; pTB: petrous part of the temporal bone; VA: vestibular aqueduct; Ve: vestibule. 53

Figure 4.2 - Bioinformatics pipeline for exome data analysis in the discovery of hypoplastic cohort variants in the two types of variants i) SNV and short InDels and ii) structural variants..... 57

Figure 5.1 – Patients with overlapping MD symptoms..... 79

Figure 5.2 - A) 5 mm thickness head axial CT. B) Magnification of the TB in the area of the left ear. Co:cochlea; IAC: internal auditory canal; LSC: lateral semicircular canal; PCF: posterior cranial fossa; pTB petrous part of the TB; VA: vestibular aqueduct; Ve: vestibule..... 80

Figure 5.3 - Examples of ATVA measurements with the CoolAngle Calc software in two left ears (A and B) from two patients in our non-MD patient cohort, following the methodology previously explained in Figure 4.1. Panels A and B show sequential images of the ATVA measurement process in two ears that required one or two planes, respectively. The software provides the angle directly next to the image. In this case, ATVA angles were 95.17° in A ear, and 94.7° in B ear..... 80

Figure 5.4 - Evaluation of ATVA concordance between observers. A) Linear regression between ATVA measured by the two observers. B) Bland-Altman plot. The x-axis shows the mean ATVA between observers. The y-axis shows the difference of the ATVA values measured between observers per ear. The black line indicates the mean of the differences between observers. The dotted red lines indicate the 95% CI with respect to the mean of the ATVA differences between observers. Red points represent poor ATVA correlation between the measurements of both observers. 81

Figure 5.5 – Evaluation of ATVA association with age, sex, and patient diagnosis in the non-MD cohort. A) Linear regression of ATVA and age. The regression line (red), dispersion shading (grey) and the correlation metrics are indicated on the plot. B) and C) Box-plot of ATVA according to sex and diagnosis of the patients, respectively. * between groups indicates p value < 0.05..... 82

- Figure 5.6 - Association between SE hypoplasia and MD diagnosis according to the affected ear. 86
- Figure 5.7 – CT scan showing the left ear in a control (A) and a patient with ES hypoplasia (B). The AV exit trajectory is well visualized within the TB (orange bracket) on the control CT, finishing in the operculum (orange arrowheads). However, operculum appears abruptly in the individual with ES hypoplasia. The right panels show the corresponding ATVA measurements. 86
- Figure 5.8 – Representation of Odd ratios in the top 30 genes with an enrichment of rare variants in the highest number of MD and ES hypoplastic individuals, respecting to the reference populations nfe (left panel) and global (right panel) genomAD. Dot size indicates the number of patients with variants in that gene. Color scale refers to the total number of variants. 87
- Figure 5.9 - Clinical data, PTA and CT from both ear in the six patients (panels from A to L) with the *ADAMTS18*,g.77434661G>C variant. NA: non available. PTA: pure-tone audiometry 90
- Figure 5.10 - Clinical data, hearing thresholds (PTA) and CT scans from both ears in the five patients (panels from A to N) with the *SDK1* variants most shared between individuals. PTA: pure-tone audiometry. 93
- Figure 5.11 - Pedigrees of familiar MD patients with ES hypoplasia. Black filled symbols: MD; white filled symbols: controls for MD; strikethrough symbols: deceased individuals; oblique lined filled symbols: low-frequency SNHL; grey dotted symbols: individuals where it was not possible to collect sample or clinical information. *Hp-uni* and *Hp-bi* on the top right of the symbols indicated unilateral and bilateral ES hypoplasia, respectively; arrows point to probands; “?” inside symbols make reference to subject suspected to have course MD (in older generations) or suspected to develop MD (in younger generations). 98
- Figure 5.12 - Families where candidate variants g.77434661G>C (panel A) and g.77248008G>T (panel B) in *ADAMTS18* were found in their probands. Variants found and individuals with variants are indicated to the right of the pedigrees. Blue asterisks indicate individuals with variants. Black filled symbols: Meniere Disease; white filled symbols: controls for Meniere Disease; strikethrough symbols: deceased

individuals; oblique lined filled symbols: low-frequency SNHL; grey dotted symbols: individuals where it was not possible to collect sample or clinical information. *Hp-uni* and *Hp-bi* on the top right of the symbols indicated unilateral and bilateral ES hypoplasia, respectively; arrows point to probands; “?” inside symbols refer to subjects suspected to have developed MD (in older generations) or suspected to develop MD (in younger generations)..... 102

Figure 5.13 - PTA from individuals of family 5. Red series: left ear; blue series: right ear; dB: decibels; kHz: kilohertz..... 105

Figure 5.14 – CENPP modeled by Robetta-AB method. Shaded area includes the truncated region because of the variant, deleting from cysteine 283 onward. Amplified panels show the loss of polar interactions of glutamate 285 and alanine 284 with arginine 213 between wildtype and mutated protein..... 107

Figure 5.15 - Sanger validation of candidate variants in *ADAMTS18* (panel A); *SDK1* (panel B) and *CENPP* (panel C). The different variants are indicated with arrows of different colors, whose correspondence is indicated in the legend..... 109

Figure 5.16 – General view of mouse TB in the axial plane (A, B), with magnification of Organ of Corti (C,D) and *stria vascularis* (E-H) areas. Specific staining for *Adamts18* label as a brown precipitate. B, D, G and H are negative technical controls. BM: basilar membrane; bLab: boundaries of membranous/osseous labyrinth in the cochlear duct; bSGN: bodies of spiral ganglion neurons; IHC: inner hair cells; OC: Organ of Corti; OHC: outer hair cells; RM: Reissner membrane; SL: spiral ligament; SMe: scala media; STi: scala timpani; SV: stria vascularis; SVe: scala vestibuli; TB: temporal bone; TM: tectorial membrane. Scale bar: 100µM (A, B), 50µM (C-H). 111

Figure 5.17 – Axial section in the mouse vestibular organs area. General view (A, B) and magnification of SSC crista ampullaris (C, D) and utricular maculae (E, F). B, D, and F show negative technical controls. bLab: boundaries of Labyrinths (membranous and osseous) in the vestibular organs. Co: cochlea; Cu: cupula; ISC: inferior semicircular canal; SSC-A: ampulla of superior semicircular canal; SSC-Ca: *crista ampullaris* of superior semicircular canal; TB: temporal bone; U:utricle; U-Ma: utricular maculae. Scale bar: 100µM (A,B), 50µM (C-F). 112

Figure 5.18 – General view of the mouse TB. The PCF and SS area (A, C) and magnification (B, D). Specific staining for Adamts18 label as a brown precipitate. B and D show negative technical controls. eES: extraosseous PCF; LSC: lateral semicircular canal; PCF: posterior cranial fossa; TB: temporal bone; SS: sigmoid sinus SSC: superior semicircular canal. Scale bar: 100µM (A,B), 50µM (C-F)... 113

Figure 5.19 – Mouse axial section in the otic capsule surrounding cochlear and vestibular organs. General view (A, B) and magnifications (F, E) in several areas of bone remodeling. Lower panels C, D, G and H are negative technical controls. I: schematic figure of bone maturation by endochondral ossification, modified from (197). bLab: boundaries of labyrinths (membranous and osseous); HC: hypertrophic chondrocytes; PC: proliferative chondrocytes; preHP: pre-hypertrophic chondrocytes; RC: resting/germinal chondrocytes; SMe: scala media; SL: spiral ligament; SV: stria vascularis; PCF: posterior cranial fossa; SSC: superior semicircular canal; OC: ossified chondrocytes; U: utricle. Scale bar: 100µM (A-D), 50µM (E-J)..... 114

Figure 5.20 – Western Blot expression assays identifying Adamts18 expression in the inner ear organs. A) Membrane revealed in four different biological replicates (R1-R4). B) Signal quantification. Ce: cerebellum; Co: cochlea; V.O.: vestibular organs; TB: temporal bone; Sp: spleen. Error bars: SEM; Significant differences (p value < 0.05) are indicated with *. 116

Figure 5.21 - Structural information of ADAMTS18 and location of the rare variants found in the hypoplastic cohort. A) Scheme of the structure of ADAMTS18 in terms of the domains that compose it, the cellular compartmentalization of each segment and the post-transcriptional modifications to which it is subjected. B) Variants in ADAMTS18 found in the hypoplastic cohort. The legend for variants indicates the number of patients in which each variant is found depending on color..... 117

Figure 5.22 - Structural information of SDK1 and location of the rare variants found in the hypoplastic cohort. A) Scheme of the structure of SDK1 in terms of the domains that compose it, the cellular compartmentalization of each segment and the post-transcriptional modifications to which it is subjected. B) Variants in SDK1 found in the MD and ES hypoplastic cohort. The legend for variants indicates the number of patients in which each variant is found depending on color. 119



Figure 5.23 - Significantly enriched cellular compartments, pathways and diseases with our 94 GBA rare variants enriched genes 122

Table Index

Table 1.1 - Chemical composition of endolymph in the inner ear (Adapted from Kim et al. (25))..... 13

Table 1.2 - Molecules related to ion transport, transporters, and exchangers in the ES epithelium. Adapted and updated from Mori et al., 2017 and Kim et al., 2019 (39,40). 19

Table 1.3 - Diagnostic criteria for definite and probable MD (108) 28

Table 1.4- Clinical subgroups and prevalence per group in MD according to Frejo et al., (86,101). 29

Table 4.1 - List of antibodies used in the IHC and WB assays..... 48

Table 4.2 – Consequences of variants according to VEP IMPACT categories 60

Table 5.1 – Cohort of non-MD patients. Continuous variables are described as the mean \pm standard deviation. Discrete variables are indicated as the number of individuals per category and the percentage represented. 78

Table 5.2 - Distribution of clinical variables in the MD hypoplastic cohort. Continuous variables are described as the mean \pm standard deviation. Discrete variables are indicated as the number of individuals per category and the percentage represented. * per each population..... 85

Table 5.3 - List of *ADAMTS18* variants in the ES hypoplastic cohort 89

Table 5.4 - List of *SDK1* variants in the ES hypoplastic cohort..... 92

Table 5.5 - List of candidate LSV in the ES hypoplastic cohort 96

Table 5.6 - List of candidate CNV in the ES hypoplastic cohort 97



Table 5.7 - Clinical evaluation of familiar MD patients and affected relatives or controls.	99
Table 5.8 - List of candidate rare variants in the family 5	106
Table 5.9 - Functional analysis enriched pathways using input genes from our GBA analysis.	123

Supplementary Figures Index

Supplementary Figure 1 – Top 20 of the most enriched routes and pathways (although not significantly enriched) in the rest of databases contrasted in the functional analysis. A) GO including go_bp: biological processes; go_cc: cellular compartment; and go_mf: molecular function; B) KEGG; C) Reactome; D) Panther; E) Phenotype databases including MGI and HPO.....	173
---	-----

Supplementary Tables Index

Supplementary Table 1 – List of primers used to validate candidate variants in <i>ADAMTS18</i> , <i>SDK1</i> and <i>CENPP</i> genes.....	177
Supplementary Table 2 – Complete list of the 94 genes enriched in rare variants as a result of GBA analysis.	178
Supplementary Table 3 – Complete list of LSV	181
Supplementary Table 4 – Complete list of CNV	183
Supplementary Table 5 – Predicted structural models evaluation of <i>CENPP</i>	185



Abstract

Introduction - Meniere disease (MD) is a complex disease of the inner ear, characterized by wide symptomatological heterogeneity that includes sensorineural hearing loss, episodic vertigo and tinnitus, which can overlap with various comorbidities and appears as partial clinical pictures. It has a multifactorial etiology that includes an immune component, a genetic origin, and disorders related to endolymph flow. In fact, the most consistent findings in the temporal bones of patients with MD have been: i) the presence of endolymphatic hydrops, which consists of endolymph accumulation in the sensory audiovestibular organs; ii) abnormalities in the endolymphatic sac (ES) and the endolymphatic duct, being the two non-sensory organs of the inner ear that are responsible for regulating the endolymph composition and drainage, including the narrowing and collapse of their lumens and fibrosis in their epithelia, and iii) malformations of the temporal bone such as shortening and compression of the vestibular aqueduct.

Hypothesis and Objectives - Recently, two endotypes of MD have been described based on the histopathological malformation of the ES. Specifically, in the hypoplastic endotype, the ES abruptly disappears at the level of the operculum, with a total absence of the extraosseous region. These patients had a family history of sensorineural hearing loss, vertigo, or MD, a tendency to present early onset, temporal bone abnormalities, a male predominance, and a higher bilateral prevalence than other MD patients. Based on these findings, the authors suggest that ES hypoplasia originates during development and may have a genetic origin. Thus, the objective of this work is to decipher the genetic basis of ES hypoplasia in patients with MD.

Material and methods - A cohort of 42 patients with MD and ES hypoplasia was recruited, and exome sequencing was performed. The endotype was identified by calculating the angular trajectory of the vestibular aqueduct (ATVA) on computed tomography (CT) and magnetic resonance (MRI) images. The approach for the genetic study incorporated gene burden analysis of SNVs and InDels variants and structural variants discovery, pointing out candidate genes with higher variant enrichment in our cohort compared to the reference populations. The functional analysis highlighted the possible pathways and biological processes affected. Candidate genes were validated by



immunohistochemical assays on tissue sections and western blot in the mouse inner ear. The absence of the hypoplastic endotype in the general population was addressed by ATVA analysis in a complementary study on 332 ears of otologic patients without MD.

Results - Gene burden analysis pointed to 94 genes with enrichment for rare variants. Among them, the best candidates were *ADAMTS18* and *SDK1*, whose variants were present in a large number of individuals in the cohort (35.7% and 33.3%, respectively), and showed a high number of variants (15 and 14, respectively), some of which were shared by a large number of individuals. The expression of *Adamts18* has been verified in mice in the first postnatal stage, both in the sensory epithelia and the otic capsule. The functional analysis taking into account the results of the genes enriched in variants, and the genes with more represented structural variants, has highlighted certain pathways and biological processes, indicating a possible alteration in the development and function of the sensory epithelia of the inner ear, the transmission of information to higher information centers, and the generation of abnormalities in the bone matrix of the otic capsule.

Conclusions - In this doctoral dissertation, the possible candidate genes and biological pathways for the development of ES hypoplasia in MD patients have been defined. The genetic and molecular characterization of this endophenotype could help to stratify different types of patients within MD, a complex and diverse pathology, improving diagnosis, prediction of evolution, and clinical decision-making.



Resumen

Introducción - La enfermedad de Meniere (EM) es una enfermedad compleja del oído interno, con gran heterogeneidad sintomatológica que incluye hipoacusia neurosensorial, vértigo episódico y tinnitus, que puede solapar con diversas comorbilidades y que se manifiesta con cuadros clínicos parciales. Tiene una etiología multifactorial que incluye un componente inmune, un origen genético y desórdenes relacionados con el flujo de endolinfa. De hecho, los hallazgos más consistentemente encontrados en huesos temporales de pacientes con EM han sido: i) la presencia de *hydrops* endolinfáticos, que consiste en la acumulación de endolinfa en los órganos audiovestibulares sensoriales; ii) anomalías en el saco endolinfático (SE) y el conducto endolinfático, siendo estos los dos órganos no sensoriales del oído interno que se encargan de la regulación de la composición de la endolinfa y su drenaje, incluyendo el estrechamiento y colapso de sus lúmenes y la fibrosis en sus epitelios, y iii) malformaciones del hueso temporal como el acortamiento y compresión del acueducto vestibular.

Hipótesis y Objetivos - Recientemente, se han descrito dos endotipos de EM basados en la malformación histopatológica del SE. Concretamente, en el endotipo hipoplásico, el SE desaparece bruscamente a nivel del opérculo, con ausencia total de la región extraósea. Estos pacientes tenían antecedentes familiares de hipoacusia neurosensorial, vértigo o EM, una tendencia a presentar inicio temprano, alteraciones de hueso temporal, predominio masculino y mayor prevalencia bilateral que el resto de pacientes con EM. De acuerdo con estos descubrimientos, los autores sugieren que la hipoplasia de SE se origina durante el desarrollo y tendría un origen genético. Así, el objetivo de este trabajo es descifrar la base genética de la hipoplasia de SE en pacientes con EM.

Material y métodos - Se reclutó una cohorte de 42 pacientes con EM e hipoplasia del SE, sobre los que se realizó secuenciación de exoma. El endotipo fue identificado mediante el cálculo de la trayectoria angular del acueducto vestibular sobre imágenes de tomografía axial computerizada y resonancia magnética. La aproximación para el estudio genético se ha basado en el análisis de agregación de variantes SNVs e InDels raras y descubrimiento de variantes estructurales, señalando genes candidatos con mayor enriquecimiento de variantes en nuestra cohorte frente a las poblaciones de referencia.



El análisis funcional destacó las posibles rutas y procesos biológicos afectados. Los genes candidatos fueron validados mediante ensayos de inmunohistoquímica sobre secciones de tejido y electrotransferencia-immunoblot en oído interno de ratón. La ausencia del endotipo hipoplásico en la población general fue abordada mediante el análisis de ATVA en un estudio complementario sobre 332 oídos de pacientes otológicos sin EM.

Resultados - El análisis de agregación señaló 94 genes con enriquecimiento de variantes raras. Entre ellos, los mejores candidatos fueron *ADAMTS18* y *SDK1*, cuyas variantes estaban presentes en gran cantidad de individuos de la cohorte (un 35,7% y 33,3%, respectivamente) y mostraron un alto número de variantes (15 y 14, respectivamente), estando algunas de estas compartidas en gran cantidad de individuos. La expresión de *Adamts18* ha sido comprobada en ratón en la primera etapa postnatal, tanto en los epitelios sensoriales como en la cápsula ótica. El análisis funcional teniendo en cuenta los resultados de los genes enriquecidos en variantes, y los genes con variantes estructurales más representadas, han apuntado ciertas rutas y procesos biológicos señalando una posible alteración en el desarrollo y función de los epitelios sensoriales del oído interno, la transmisión de la información a centros superiores de información, y la generación de anomalías en la matriz ósea de la cápsula ótica.

Conclusiones - En esta disertación doctoral se han definido los posibles genes y rutas biológicas candidatas para el desarrollo de la hipoplasia del SE en pacientes de EM. La caracterización genética y molecular de este endofenotipo podría ayudar a estratificar distintos tipos de pacientes dentro de EM, una patología compleja y diversa, mejorando el diagnóstico, la predicción de la evolución, y la toma de decisiones clínicas.



Acronyms and abbreviations

ACMG: American College of Medical Genetics and Genomics guidelines	LSC: lateral semicircular canal
AIED autoimmune inner ear disease	LSV: large structural variants
ATVA: angular trajectory of the vestibular aqueduct	MD: Meniere Disease
BAM: Binary Alignment Map	MET: mechanotransduction channels
CADD: Combined Annotation Dependent Depletion	MGI: Mouse Genome Informatics
CI: confidence interval	MMP: matrix metalloproteases
CNV: copy number variants	MRC: mitochondria rich cells
CT: computed tomography	MRI: magnetic resonance imaging
ECM: extracellular matrix	NFE: Non-Finish European
ED: endolymphatic duct	OMIM: Online Catalog of Human Genes and Genetic Disorders
EDTA: Ethylenediaminetetraacetic acid	OR: Odd ratio
eES: extraosseous part of ES	PBS: Phosphate Buffered Saline
EH: endolymphatic hydrops	PCF: posterior cranial fossa
ENT: Ear, Nose, Throat (~ Otorhinolatingology)	pLi: probability of being Loss of function Intolerant
ES: endolymphatic sac	PSC: posterior semicircular canal
FLAGS: FrequentLy mutAted GeneS	PTA: pure-tone audiometry
FMD: familiar Meniere Disease	RNA-seq: RNA sequencing
gnomAD: Genome Aggregation Database	RRC: ribosome rich cells
GO: gene ontology	RT-PCR: real time PCR
HC: hair cells	SC: supporting cells
HPO: Human Phenotype Ontology	SCC: semicircular canals
iES: intraosseous part of ES	SGN: spiral ganglion neurons
IGV: Integrative Genome Viewer	SMD: sporadic Meniere Disease
IHC: immunohistochemistry	SNHL: sensorineural hearing loss
InDels: Insertions and Deletions	SNV: single nucleotide variants
LOEUF: loss-of-function observed/expected upper bound fraction	SS: sigmoid sinus
LoF: loss of function	SSC: superior semicircular canal
	SV: structural variants
	TB: temporal bone
	TM: tectorial membrane



VA: vestibular aqueduct

VCF: Variant Call Format

VEP: Variant Ensembl Predictor

VGN: vestibular ganglion neurons

VM: vestibular migraine

WES: whole exome sequencing

WGS: whole genome sequencing



1. - Introduction

1.1 - The inner ear

The ear can be divided into three anatomical compartments: the outer, the middle, and the inner ear (Figure 1.1, A). In the outer ear, the auricle captures sound waves propagating through the external auditory canal to reach the eardrum or tympanic membrane. In the middle ear, three small, coupled bones, the ossicles (the malleus, the incus, and the stapes), transmit the vibration that eardrum receives to the oval membrane, where the inner ear begins (1).

The inner ear is a remarkable structure composed of a complex network of interconnected membranous tubes called the membranous labyrinth, which is housed inside a bony cover designated as the osseous labyrinth or otic capsule (Figure 1.1, B) (2). Differing from the aerial outer and middle ear, the inner ear labyrinths are filled with two types of fluids with distinct compositions: endolymph inside the membranous labyrinth; and perilymph between the membranous labyrinth and the otic capsule. These fluids move in response to various stimuli, which are detected by two sensory systems: the organ of Corti in the cochlea, which is sensitive to auditory input, and the vestibular system, which can detect linear and angular accelerations (1).

In addition to sensory organs, the membranous labyrinth extends out of bone cover, giving rise to two non-sensory organs: the endolymphatic duct (ED) and the endolymphatic sac (ES). The inner ear complex is housed within the petrous part of the temporal bone (TB) in the posterior cranial fossa (PCF) (3,4).

1.1.1 - The cochlea

The cochlea is responsible for the sense of hearing, managing the translation of sound vibrations into nerve impulses (5).

The bony and membranous labyrinths of the cochlea are arranged in a spiral shape with three turns, apical, medial, and basal turns (Figure 1.2, A) (6). Along its length, different auditory frequencies gradually stimulate distinct areas of the cochlea. The part closer to the base is more sensitive to high frequencies, and the nearer to the apex responds better to low tones. This spatial-frequency capacity is designated as tonotopy and depends on the basilar membrane's width, thickness, and stiffness, which produces variations in the distance over which waves of different frequencies can propagate (5,7). The basilar membrane supports the organ of Corti, which contains the sensory epithelium (Figure 1.2, A).

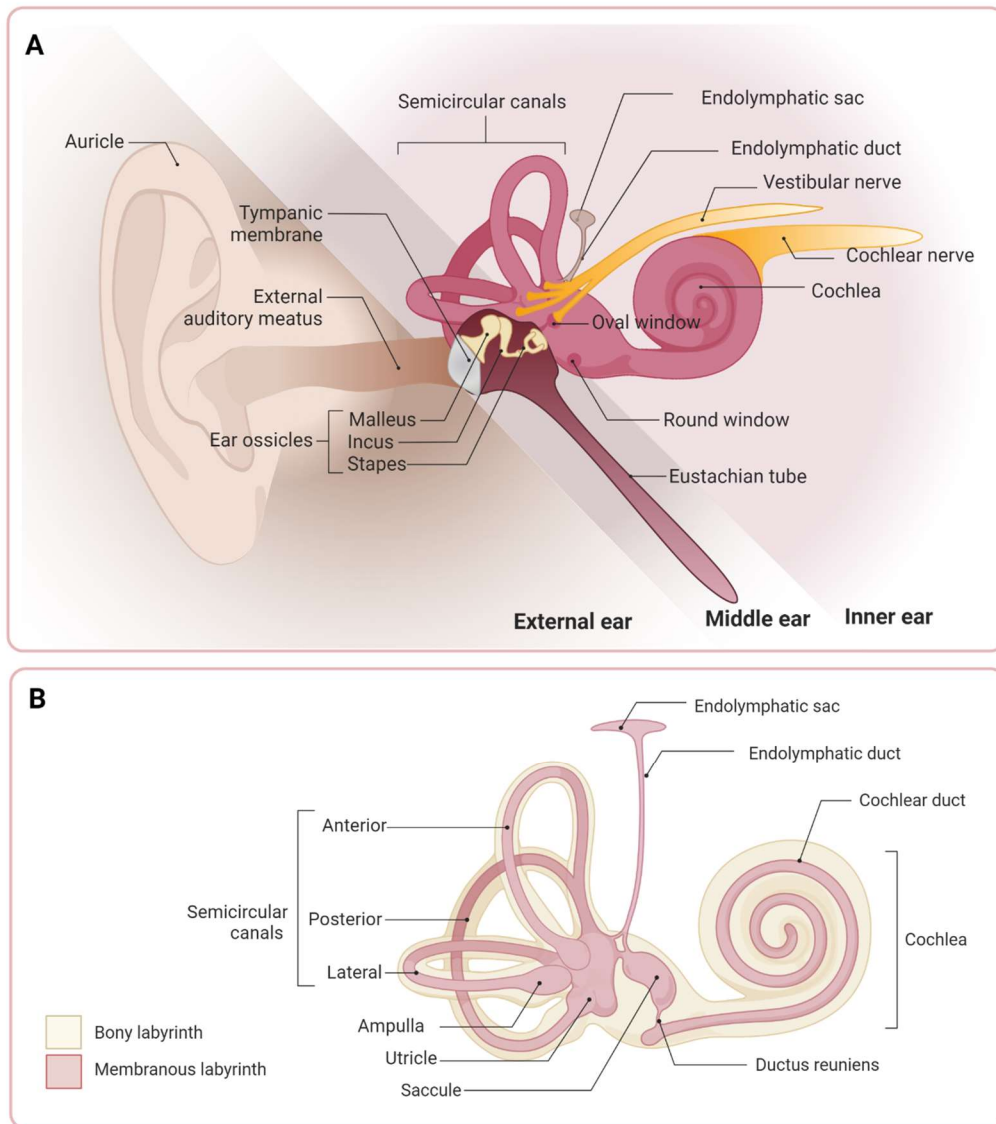


Figure 1.1 – Schematic representation of ear anatomy. A) Differentiation of the three ear anatomical compartments: the outer (external), the middle, and the inner; B) Inner ear membranous labyrinths, and otic capsule. Created with BioRender.com

The cochlear membranous labyrinth is divided into three cavities: the scala vestibuli, the scala media, and the scala tympani (Figure 1.2, A). The scala vestibuli and the scala tympani contain perilymph and communicate at the helicotrema level in the cochlea's apex. The scala media is bathed by endolymph and sealed without communication with other compartments. The correct separation of the scales is necessary to preserve the different compositions of the two fluids, which is essential for the proper functioning of the cochlea. Thus, Reissner's membrane separates the scala tympani and the scala media, and the basilar membrane separates the scala media from the scala vestibuli (5).

Therefore, the scala media appears as a triangular chamber with three walls in a cross-section of the membranous labyrinth. The upper wall would be the Reissner's membrane, the lateral wall would include the *stria vascularis* and the spiral ligament, and the lower wall would be the basilar membrane, on which rests the Organ of Corti (5) (Figure 1.2, A).

1.1.1.1 - Morphological and molecular structure of the Organ of Corti

The Organ of Corti comprises several types of cells and structures with specialized functions: hair cells (HC), supporting cells (SC), and tectorial membrane (TM) (5) (Figure 1.2, B).

Hair cells

Two types of cochlear HC can be distinguished: inner HC, disposed in one row and responsible for converting mechanical stimuli into electrochemical signals, and three rows of outer HC, that amplify signals and connect to efferent neurons. The hair bundle is situated on the apical surface of HC, each containing around 50-200 microvilli-like projections called stereocilia. These are arranged in a V-like shape with a staircase pattern, where stereocilia increase in height ordered up to the tallest (Figure 1.2, B) (6,7).

Internally, stereocilia exhibit a skeleton of actin chains arranged in parallel and crosslinked by several proteins. The intersection pattern frequency is higher in the middle part, more rigid and stable (8). In the flexible base, on the contrary, the number of crosslinked unions is lower, which allows stereocilia to pivot towards the neighbor stereocilia. The tips of stereocilia house the MET complex, the functional mechanosensitive transduction channels responsible for HC depolarization in response to sound (5,8).

Each stereocilium is attached to the stereocilia immediately anterior and posterior in height by different junctions: tip link at the surface; and top connectors, shaft connectors, and ankle links at different heights on the lateral side. While shaft connectors and ankle links stabilize the stereocilia during its development, only tip links and top connectors remain once it matures (9). Among them, we can highlight the function and structure of the tip links (Figure 1.3, A).

Tip links are comprised of dimers of the proteins protocadherin-15 (*PCDH15*) and cadherin-23 (*CDH23*). Protocadherin-15 interacts with the MET complex in the anterior stereocilia and the cytoplasmic part of cadherin-23 is anchored to the actin backbone in

the posterior stereocilia. This union creates a force of tension between the stereocilia that intervenes in the deflection of the hair bundle (7,8).

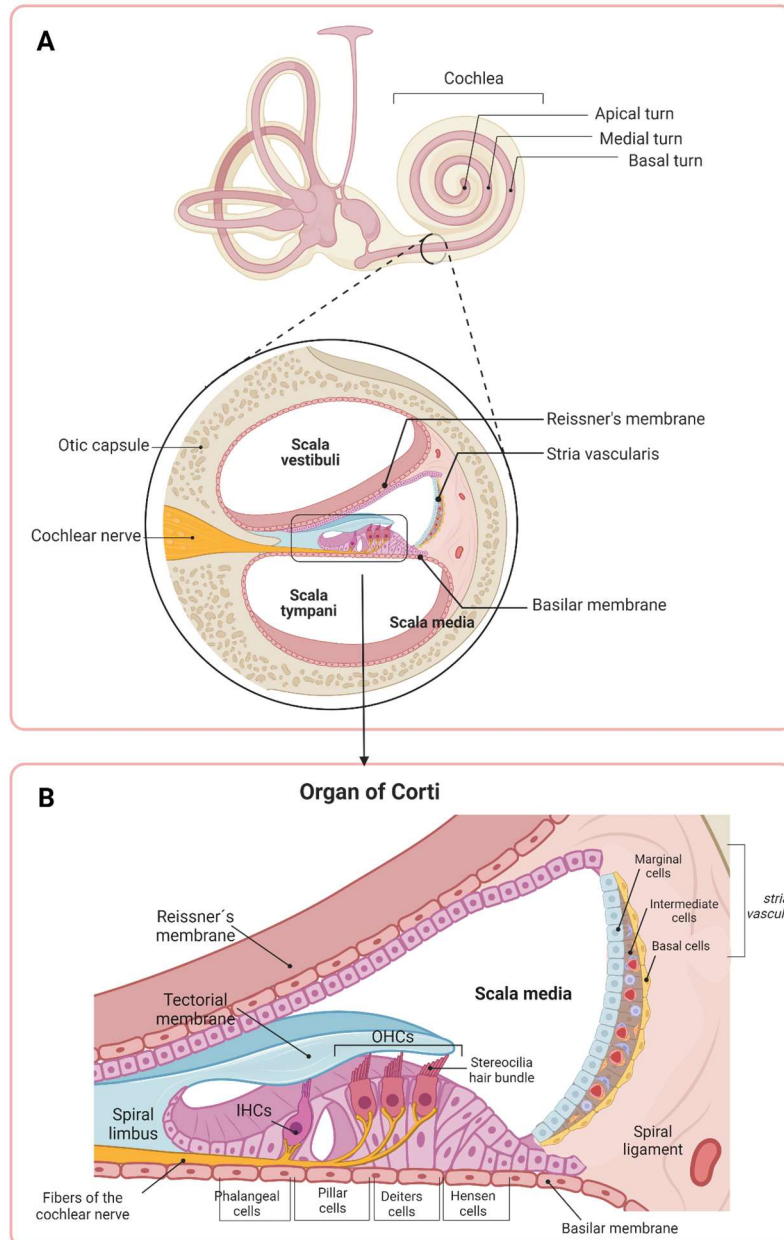


Figure 1.2 - Anatomy of the cochlea and morphological structure of sensory cochlear epithelia. Created with BioRender.com

Supporting cells

Accompanying HC, several types of non-sensory SC form a base on which the HC are anchored. Although they are not directly involved in the mechanotransduction process, their functions are essential for hearing (5,10) (Figure 1.2, B).

On the one hand, they form a rigid structural base that is simultaneously vibratile, which transmits movement from the basilar membrane. They contribute to the maintenance of endocochlear potential, thanks to the tight junctions with the HC in their luminal domain. Meanwhile, on their basolateral side, they mediate phagocytosis, debris removal, and recycling of neurotransmitters and ions. In addition, they participate in the maintenance of the TM, synthesizing and secreting proteins that constitute it. During development, they are involved in cell patterning, polarity, and synaptogenesis of the sensory epithelium (10,11)

There are several types of SC, from the spiral limbus to the spiral ligament disposed of as follows: Hensen's cells, Deiters' cells (outer phalangeal cells), pillar cells, and inner phalangeal cells (Figure 1.2, B) (5,10,11).

Tectorial membrane

Above HC resides the TM, an extracellular protein matrix that extends from the spiral limbus above the sensory epithelium, submerging the stereocilia hair bundle (Figure 1.2, B). Its composition is predominantly water (95%), glycosaminoglycans, several types of collagens (II, V, IX, and XI), and seven non-collagenous glycoproteins (tectorins, CEACAM16, otogelin, otogelin-like, otoancorin, and otolin) (12). The matrix is built as a network of collagen II fibers arranged in parallel, interconnected by the rest of the proteins that give consistency to the framework. In addition, some of these proteins interact in the anchor with the stereocilia in their upper part (12–14).

The function of the TM is still being elucidated (12). Several studies suggest that TM experiences movement due to sound stimulation and the basilar membrane's movement. In this way, it creates a plate that slides over the surface of the Organ of Corti, subjected to compression and expansion in the radial plane (15). Due to its union with the hair bundle, the TM amplifies the input signal received by HC (16). In addition, the TM regulates the concentration of Ca^{2+} ions near the stereocilia, thus regulating the responsiveness of the MET channels (17,18).

1.1.1.2 - Mechanotransduction of sound

Sound perception is based on HC ability to convert mechanical stimuli into electrochemical signals, thanks to the MET complex located on the stereocilia surface (Figure 1.3, B). These complexes are formed by dimers of non-selective cation channels

TMC1/2, with high Ca^{2+} permeability and TMIE proteins. TMC1/2 and TMIE are attached to the CDH23 N-terminus of the tip links (7).

As previously explained, the vibrations received in the oval membrane move fluids inside the inner ear labyrinths. These currents generate deflection of the hair bundle: each stereocilium flexes toward its nearest tallest stereocilia due to the tension created by tip links. This stiffness triggers the opening of the MET complex, leading to the entrance of K^+ , which depolarizes the HC. Subsequently, an increase in Ca^{2+} concentration provokes the release of neurotransmitters in the HC basolateral side to the synaptic space, exciting afferent endings which will take the information to the central (7) (Figure 1.3, B).

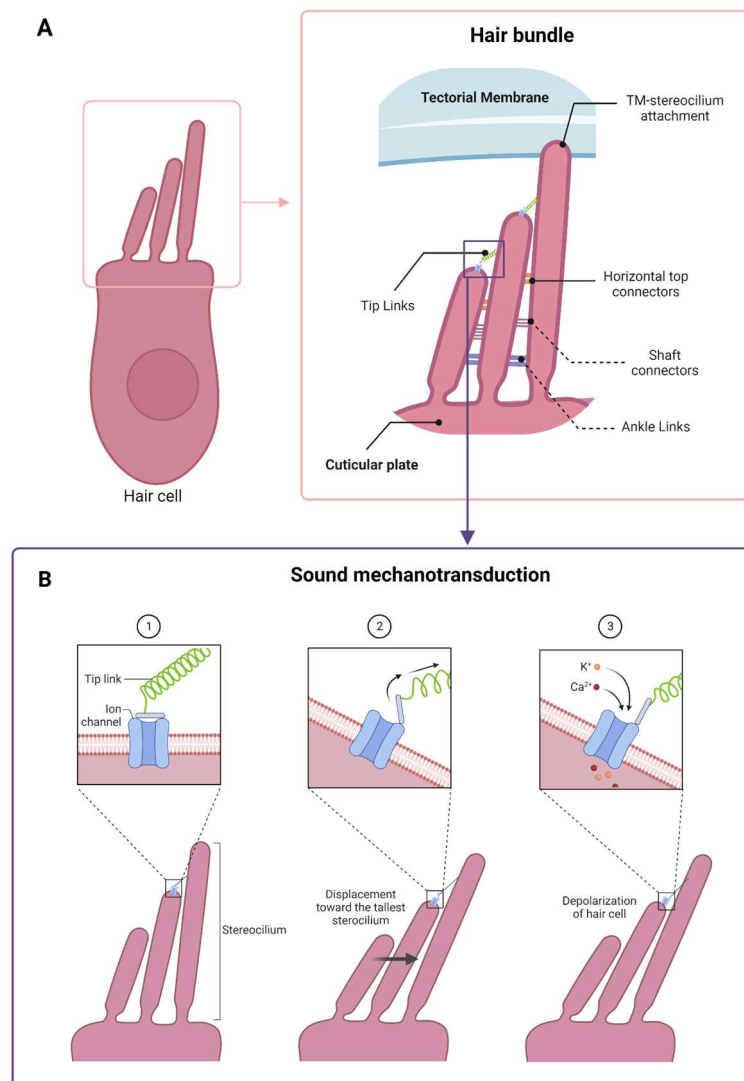


Figure 1.3 - Hair bundle and sound mechanotransduction. Created with BioRender.com

Most spiral ganglion fibers that project to the brain come from INNER HC since they are the actual sensory receptors. However, nerve endings contacting with outer HC come from efferent fibers of intermediate centers as pons (1).

1.1.1.3 - The stria vascularis

The third wall of the scala media is formed by the *stria vascularis*, a highly vascularized structure that performs several essential functions (19,20) (Figure 1.2, B). It comprises three cell layers arranged from the scala media to the spiral ligament: marginal, intermediate, and basal. The primary function of those cell layers is to generate the endocochlear potential through recycling ions, especially K^+ , involved in the depolarization of HC, to maintain the electrochemical gradient inside the scala media within acceptable mean ranges for cochlear function. Therefore, it has been shown that they express numerous ionic channels, transporters, and gap-junctions. Moreover, the intermediate cell layer constitutes the blood-labyrinth barrier, composed of pericytes, which are involved in angiogenesis and maintenance of vascular integrity; and macrophage-like-melanocytes that communicate with tight junctions, controlling the entrance of molecules from the blood, in addition, to prevent pathogen infiltration. The basal cell layer is in contact with the spiral ligament fibrocytes (19–21).

1.1.2 - The vestibular system

The vestibular system is responsible for collects information about balance, including angular rotation and linear acceleration. It comprises the vestibule and the semicircular canals (SCC) (2) (Figure 1.4).

1.1.2.1 - The semicircular canals

The three SCC are sensitive to angular rotations. They are arranged in the three axes of space: two vertically, superior (SSC) (or anterior) and posterior (PSC), and one horizontally, called lateral (LSC) (Figure 1.4). SSC and PSC converge in part of their lengths in the structure known as common crus. In this way, they notice any type of head rotation (22).

In the area of termination of each SCC near the utricle, there is a sac-shape widening called ampulla (ampullae in plural), where the sensitive epithelium or *crista ampullaris* is located (Figure 1.4). This structure contains different and specialized cell types and structures: vestibular HC, vestibular SC, the cupula, connective tissue, and a

network of vascular and nerve fibers (22). Most of these structures have a morphology and functioning mechanism very similar to those described for the sensory epithelium of the cochlea. However, there are some notable differences to be highlighted.

The vestibular HC display about 70-100 stereocilia of different heights placed on their apical surface, arranged in increasing order, forming a ladder. The tallest stereocilium, also known as kinocilium, is located eccentrically at the edge of the surface, and all of them point in the same direction (22,23).

Instead of the TM, over the sensory epithelium lies the cupula, a gelatinous complex cover of mucopolysaccharides and keratin. This matrix extends from the *crista ampullaris* through the entire membranous labyrinth along SCC, immersed in endolymph (22) (Figure 1.4).

The SC in the vestibular system are less heterogeneous than in the sensory epithelium of the cochlea, and only two types of cells have been described. Vestibular dark cells are the most studied, constituting the structural base in which HC scaffold. They participate in the same functions as the *stria vascularis* in the cochlear duct, intervening in regulating endolymph composition by regulating the flux of ions and small molecules and in producing proteins. They exhibit several signs of secretory activity in their cytoplasm and basolateral side, including a well-established Golgi, mitochondria, lipid droplets, and secretory granules. Moreover, they are involved in cell patterning, polarity, and synaptogenesis of the sensory epithelium during development. Along with dark cells, a distinct subtype of vestibular SC that is still relatively unknown appears to have regenerative abilities and contribute to replacing damaged vestibular HC (10,21,22).

HC and SC are joined together with tight junctions and desmosomes, which ensure the seal between the apical zone bathed by endolymph and the zone below the basement membrane filled with perilymph (22).

1.1.2.2 - The vestibule

The vestibule is sensitive to kinetic linear accelerations or decelerations but is also responsible for localizing the static position of the head in space. It consists of two otolith organs: the utricle, arranged in the horizontal plane, and the saccule in the vertical (22,23) (Figure 1.4). The saccule connects with the membranous labyrinth of the cochlear duct through the *ductus reuniens* canal.

The sensory epithelium of both otoliths is called macula (maculae in plural) (Figure 1.4). The morphology and disposition of cells and structures in the utricular and saccular maculae are similar to the *crista ampullaris*, with some variations (22).

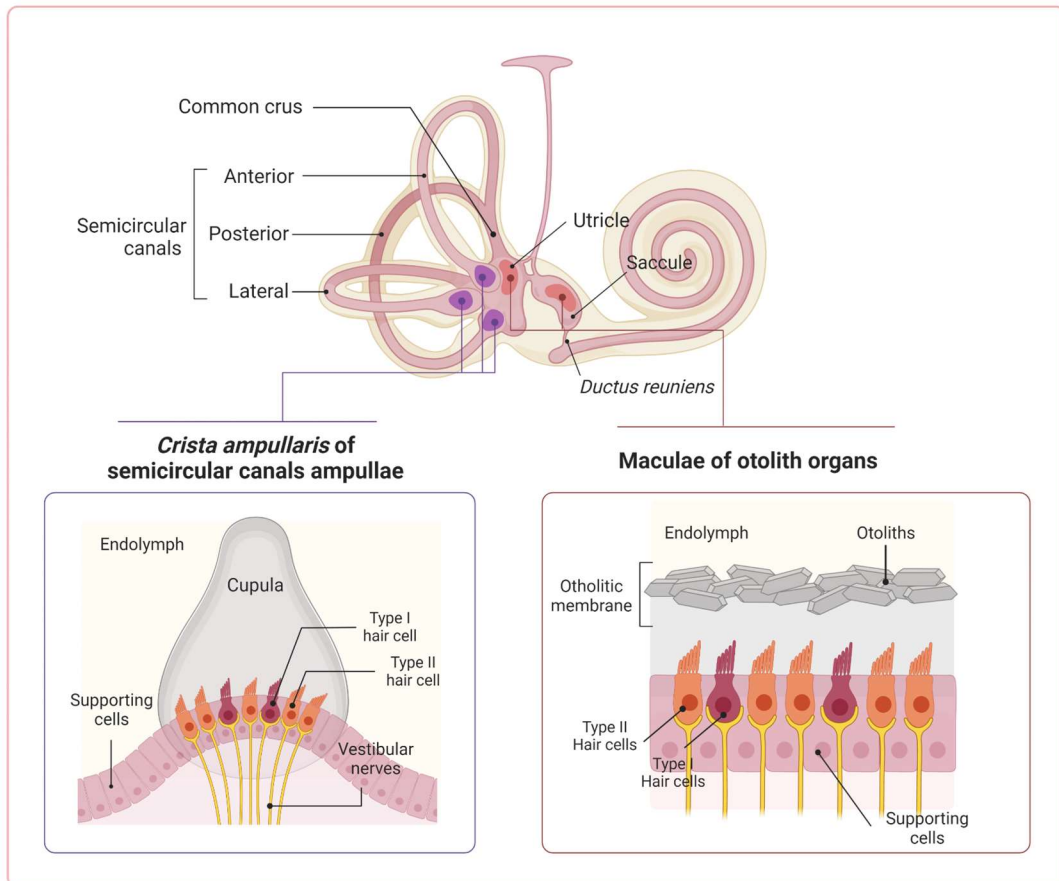


Figure 1.4 - Morphological and simplified vestibular sensory epithelia cellular structure, including hair cells, and vestibular nerves. Created with BioRender.com

As a notable difference, the gelatinous covering that extends over the sensory epithelia is designated as an otolithic membrane and contains minuscule crystals called otoconia, formed by inorganic particles of calcium carbonate (Figure 1.4) (22,23). There is only one type of SC, which carry out the same functions described in the ampulla of the SCC. SC are responsible for the synthesis and maintenance of the otolithic membrane. The expression of the otopetrin protein, which is involved in anchoring otoconia to the gelatinous membrane, is predominantly expressed in the apical microvilli of SC (10).

Towards the central area of the maculae, there is a distinctive-looking area called striola, which divides HC zones with stereocilia showing opposite morphological



polarizations. Thus, a stimulus that excites the HC on one of these zones would inhibit those on the other. The difference in striola appearance is given by the orientation of HC kinocilia, the thickness of the otolithic membrane, and the change in the size of the otoconia. In the saccular striola, the otolithic membrane thickness increases, and HC kinocilia point away from the striola. On the contrary, in the utricular striola, the otolithic membrane thickness is reduced, and HC kinocilia point toward the striola. In addition, in both striolae, the otoconia size is reduced from 5-7um to 1um (22).

1.1.2.3 - Mechanotransduction of angular rotation and linear acceleration

Just like in the cochlear HC, vestibular HC can depolarize in the presence of a stimulus. In this case, the head's angular rotations and linear accelerations/decelerations move the endolymph, displacing the cupula and otolithic membranes in the crista ampullaris and maculae, respectively. This causes deflection of stereocilia toward the kinocilium, tension transmitted by tip links which ultimately trigger the opening of the MET channels. The entry of K^+ depolarizes the cell, and subsequent Ca^{2+} entry triggers the formation of the synaptic vesicles, their fusion with the plasma membrane in the basal surface of HC, and the release of neurotransmitters to afferents (22,23).

Three types of afferents that innervate vestibular HC can be distinguished: calyx afferents, bouton afferents, and dimorphic afferents. Calyx afferents are so named because they surround the HC except for the apical part. They are usually located in the striolar region. The HC that synapse with these afferents are vessel-shaped and are called type I. In bouton afferents, mainly found in the extrastriolar region, the synapse occurs only in the basal zone of HC. These afferents contact vestibular HC type II, with a typical cylindrical configuration. In addition to afferents, type II cells are also innervated by efferent fibers. For its part, dimorphic afferents interact with type I and type II HC, spanning across the entire sensory epithelia. Afferent buttons transmit the impulses to the vestibular nuclei. Efferent contact afferents and type II HC, and transmit the impulses to the brainstem (22,23).

1.1.3 - The regulation of endolymph and maintenance of the endocochlear potential

The lumen of the membranous labyrinth is filled with endolymph, the fluid that bathes the sensory epithelia of the cochlea and vestibular organs. Another fluid, the perilymph, is located between the membranous labyrinth and the otic capsule. Both have a different chemical composition at basal states, showing the endolymph high concentration in K^+ and low in Na^+ , unlike the perilymph, with low levels of K^+ and high levels of Na^+ . This difference generates an ionic force called endocochlear potential, whose maintenance is necessary for a correct response to auditory and balance stimuli (24).

Endolymph composition varies throughout the membranous labyrinth, giving rise to a different resting potential between the different structures, summarized in Table 1.1 (24,25).

Table 1.1 - Chemical composition of endolymph in the inner ear (Adapted from Kim et al. (25)).

Structure	Vestibule	Cochlea	ES
Na⁺	9mM	1.3mM	129mM
K⁺	149mM	157mM	8-13mM
Cl⁻	nd	132mM	124mM
Protein	nd	38mg/dl	1600mg/dl
Resting potential	-2mV	+80mV	+15mV

ES: endolymphatic sac; nd: not described

Inside the inner ear, endolymph experiences two types of flows: i) a slow longitudinal flow from where it is produced to where it is reabsorbed, and ii) a rapid radial flow responsible for ions recycling after HC depolarization (26).

The slow course was defined as the theory of longitudinal endolymphatic flow, postulated by Guild et al. in 1927 (27). Endolymph is produced mainly in the cochlear duct, thanks to ion transport from the stria vascularis and the perilymphatic space through Reissner's membrane. Numerous ion channels, enzymes, and selective transporters are involved in this process. A small proportion of endolymph is also produced in the vestibular dark cells. Later, endolymph reaches the saccule through the *ductus reuniens*, navigates across the ED, and finally arrives at the lumen of the ES, where it is eventually reabsorbed



into the vascular system through the sigmoid sinus (SS) (24,26,27). Some authors tested the slow course of endolymph with experiments in which different traceable molecules were introduced into the cochlear duct, and its route was followed through the various structures over time (3,27).

The quick course involves several regulatory mechanisms that return endolymph and HC cytoplasm to basal ion levels after depolarization, restoring the endocochlear potential and making the system sensitive again to new stimuli. In the cochlear duct, K^+ from the HC basolateral side travels across SC and fibrocytes in the spiral ligament thanks to the gap-junction proteins. Once in the stria vascularis, K^+ is transported across marginals, basal and intermediate cells and released to the scala media (20,21). In the vestibule, after the stimulus, the K^+ of the HC is captured by the dark cells. These cells form a single monolayer that separates perilymph from endolymph. Thanks to tight junctions, K^+ ions navigate across this epithelium and are finally secreted to endolymph through ion carrier transporters (21).

1.1.4 - The non-sensory organs

The ED and ES are the non-sensory organs of the membranous labyrinth, and, in contrast to the cochlear and vestibular systems, they have been less studied, and their exact labors are still being delineated (4).

The membranous labyrinth in the cochlear duct and vestibular organs are cloistered within the otic capsule. However, the ED and the ES cross this bony covering through the vestibular aqueduct (VA). This bony canal runs parallel to the common crus, the part in which SSC and PSC converge. VA gradually widens until its exit from the TB through an opening called operculum, emerging into the epidural space in the PCF (Figure 1.5) (4,28).

The anatomical and morphological structure in the ED and ES does not differ a lot between mammals such as rats, guinea pigs, rabbits, mice, and humans, taking into account the morphology and ultrastructure of its different cell types, the composition of its lumen fluid, or the vasculature and innervation of the tissue that surrounds it (2).

1.1.4.1 - The endolymphatic duct

The ED emerges from the vestibule, where the saccule and utricle meet. It is a simple tubular structure with a cuboidal epithelium surrounding an interior lumen. Two

parts can be differentiated in the ED: the sinus constituted as a fusiform bag from the fusion of the utricular and saccular ducts and the isthmus, the narrow intraosseous part that enters the VA (Figure 1.5) (3,4,29).

1.1.4.2 - The endolymphatic sac

The ES begins after the distal area of the isthmus. In contrast to the ED, the ES varies greatly in dimensions throughout its length and shows a gradual widening in width but not in thickness, giving it a sail-like appearance (30,31).

The ES can be divided into different parts depending on the criteria used: macrostructural/anatomical or morphological/structural (Figure 1.5). According to anatomical standards, we can differentiate the intraosseous ES (iES), which runs from the internal opening to the external exit of the VA and the extraosseous ES (eES), which originates from the operculum, rests on the dura and is exposed to the subarachnoid space in the posterior fossa (32). Concerning morphology and ultrastructure, three segments can be distinguished: proximal, intermediate, and distal ES (Nordstrom 2020 thesis). The first studies on the morphology and ultrastructure of the ES epithelium cells were carried out on guinea pigs (3,27,29), and later, on mice (33), rats (34,35), rabbits and humans (36–38). Although different nomenclatures have been designated for the different parts and cells in the different models, the similarity of the structures suggests that there are not many differences between vertebrates.

The proximal part begins after the distal area of the isthmus at the beginning of the VA, and the otic capsule surrounds it. The epithelium is formed by thin squamous cells showing well-developed basolateral processes. The intermediate section runs inside the VA, continues to the operculum's external opening, and adheres shortly to the dura mater in the PCF. The epithelium is mostly cuboidal, except for the part immediately behind the VA exit, which briefly becomes columnar. The walls of this portion form an intricate network of epithelial folds that give rise to tubules and cisterns, the reason why it is also called *pars rugosa* or *pars canalicularis*. These tubules protrude into the lumen and can fuse, resulting in ES compartmentalization. This network significantly increases the epithelial surface in this segment. The distal part, which lies entirely in the dura crossing in front of the SS, is called *pars intraduralis*. This structure is simpler than the intermediate zone and consists of a simple lumen surrounded by an epithelium of cuboidal or squamous cells (Figure 1.5) (29,30,33,36).

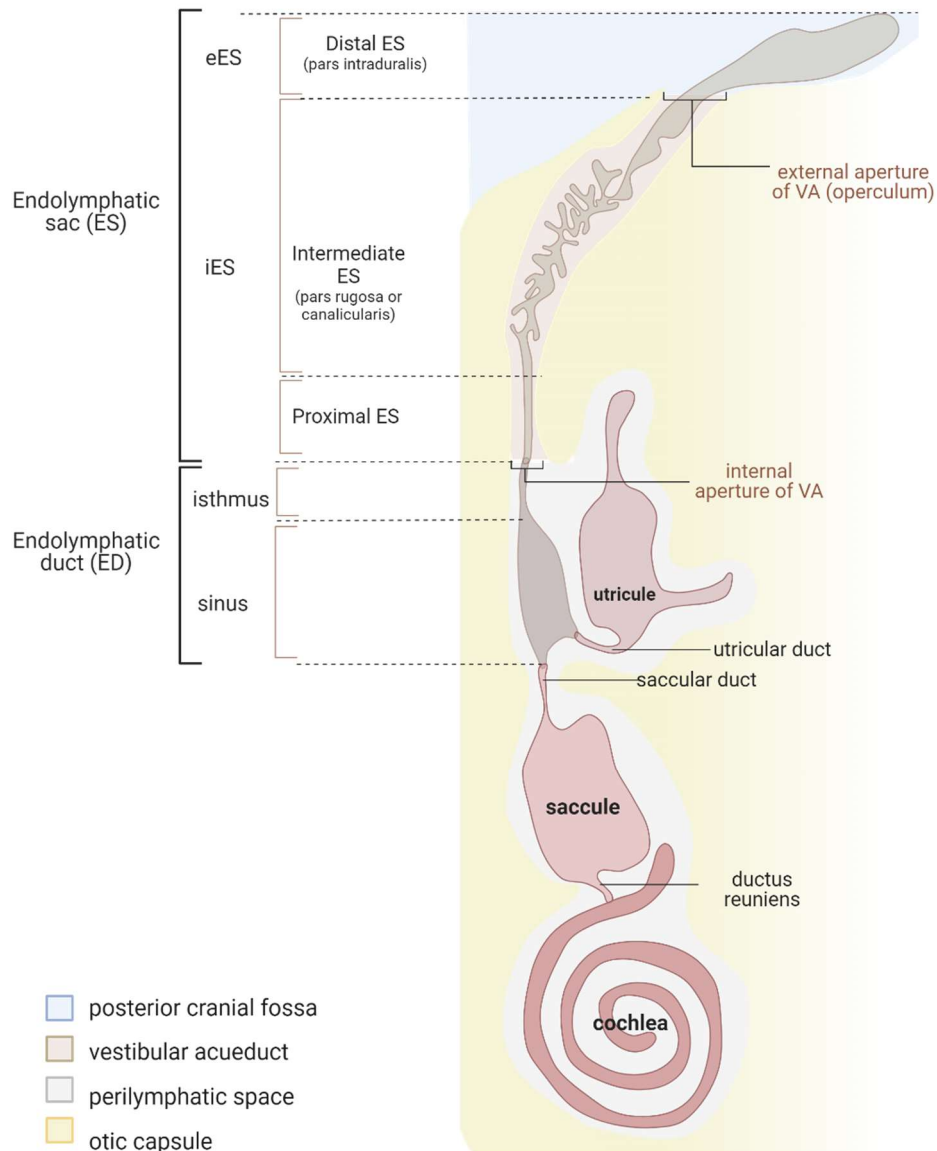


Figure 1.5 - Schematic section of the ED and ES, showing intra (iES) and extraosseous (eES) segments. Created with BioRender.com

The pars *canalicularis* has been described as the most active. Ultrastructural studies in human and animal models distinguished two similar cell types in this ES section: mitochondria-rich cells (MRC) and ribosome-rich cells (RRC) (Figure 1.6). The RRCs are the most abundant (~70%) and were characterized by cytoplasm full of ribosomes, cytoskeletal components, Golgi complexes, and well-developed rough endoplasmic reticulum. Multiple organelles such as pinocytotic vesicles, vacuoles, multivesicular bodies, and lysosomes can be differentiated. On the other hand, MRCs occupy around ~20-25% of the total ES epithelium. As its name suggests, it exhibits a cytoplasm with a

high number of mitochondria, a low amount of organelles, and numerous microvilli in their apical side (29,33–35,38).

These findings suggest different functions for the two cell types (28,33,34,38). Thus, the MRCs would maintain the endolymph ionic composition thanks to many ion channels, transporters, and exchangers arranged in the microvilli of its apical part. The numerous characteristic mitochondria would provide the necessary energy to co-transport ions and molecules (39,40). For their part, the RRCs would be specialized in protein synthesis and secretion into the ES lumen, given the well-developed protein synthesis machinery that can be observed in the cytoplasm of these cells (35). Honda *et al.*, differentiated in 2017 both profiles using single-cell RNA-seq, where RRCs displayed a transcriptomic profile of protein synthesis and secretion, and immunity-related, while MRCs indicated ionic transport processes (41).

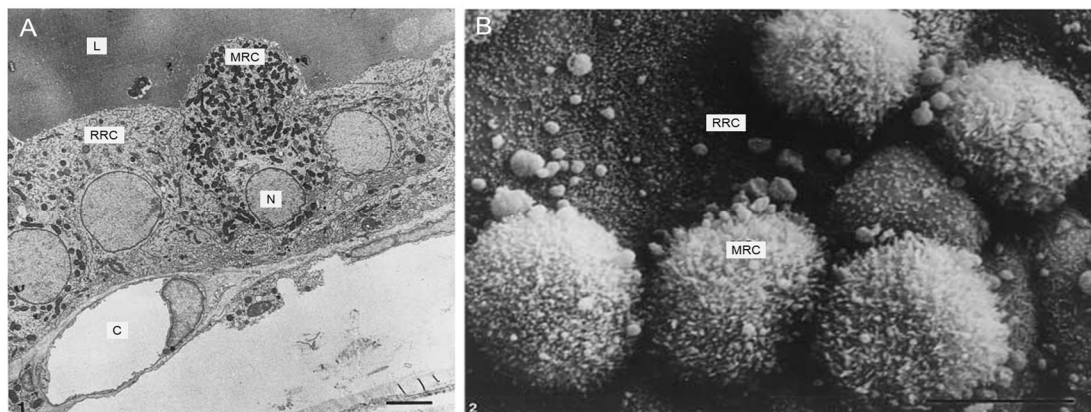


Figure 1.6 - Ultrastructural details of the two types of epithelial cells in the rat ES: mitochondria-rich cells (MRC) and ribosome-rich cells (RRC) (called chief cells in rats) by transmission (A) and scanning electron microscopy (B). L: lumen; C: capillary; N: nucleus; Scale bar 1 μ m (A) and 10 μ m (B). Images from Qvortrup *et al.* (35).

1.1.4.3 - Functions of the endolymphatic sac

Diverse functions have been attributed to the ED and ES, among which are the regulation of the ionic composition, the pH, the volume, and the pressure of the endolymph in the complete membranous labyrinth, but also the elimination of waste products, and the immune response in the inner ear (4).

1.1.4.3.1 - Regulation of the ionic homeostasis of endolymph

As previously explained, the endolymph is subjected to a slow or longitudinal flow throughout the entire membranous labyrinth. This pathway extends from the production

areas (*stria vascularis* and Reissner's membrane in the cochlea, and vestibular dark cells in the vestibular organs) to the ES, where it is finally reabsorbed (26). This process is carried out by a broad battery of ion channels, transporters, and exchangers expressed in ES epithelial cells. Numerous studies have investigated these molecules in animal models and human ES tissue. In some of them, it was possible to identify that they are mainly expressed in the abovementioned MRCs.

Table 1.2 summarizes these molecules, considering the animal or human model used in the study, the technique used for its detection, and the localization of the molecule in the epithelial ES membrane. Among them, it can be highlighted: i) molecules related to water reabsorption, such as aquaporins AQP1–4, 6–9; ii) Na^+ channels, such as non-selective ion channels (amiloride-sensitive Na^+ channel and epithelial Na^+ channel (ENaC)) and co-transporters bumetanide-sensitive $\text{Na}^+ - \text{K}^+ - 2\text{Cl}^-$ cotransporter (NKCC2, NKCC1), thiazide-sensitive $\text{Na}^+ - \text{Cl}^-$ cotransporter (NCC, SLC12A3) and Na^+ -phosphate cotransporter (SLC34A2); iii) pH regulators such as ATPases ($\text{Na}^+ - \text{K}^+ - \text{ATPase}$ and $\text{H}^+ - \text{ATPase}$), carbonic anhydrase (CA), and ion exchangers, both cationic ($\text{Na}^+ - \text{H}^+$ exchanger (NHE)) or anionic ($\text{Cl}^- - \text{HCO}_3^-$ exchanger (SLC4A2) or Pendrin ($\text{Cl}^- - \text{HCO}_3^-$) exchanger SLC26A4); and v) Cl^- transporters, such as cystic fibrosis transmembrane conductance regulator ion channel (CFTR) (39,40).

1.1.4.3.2 - Regulation of pressure as an endocrine organ

The extraosseous distal part of the ES rests on the SS and jugular bulb, which gives it a privileged position to monitor and regulate the pressure not only of the endolymph in the inner ear but also intracranial or in the systemic venous blood (4,35).

Moller *et al.* described the expression of natriuretic peptides and regulators of vascular tone in the human ES epithelium (42). Thus, ES may be an endocrine/paracrine organ, influencing the hypothalamic-pituitary-adrenal axis and vasopressin-aquaporin-2 pathway. Several analogies have been observed with the vasopressin system in the ES, similar to the regulation of systemic blood pressure in the kidney. The vasopressin receptor (V2R) is expressed in the ES epithelium, and the binding of its ligand increases the expression of aquaporin-2 (AQP2) and its translocation to the basolateral side of the ES epithelium for subsequent water transport. Plenty of studies have shown the expression of both AQP2 and V2-R in the PCF in several organism, such as human, rat and mouse (Table 1.2) (43–48), and endolymphatic volume increases are observed in animals following the administration of vasopressin (49,50). In addition, Eckhard *et al.*,

demonstrated that the epithelium of the eES is sensitive to salt intake and that the regulation of Na⁺ through the aldosterone - mineralocorticoid receptor – epithelial sodium channel (ALDO-MR-EnaC) pathway occurs in the same way as in the kidney (32).

Table 1.2 - Molecules related to ion transport, transporters, and exchangers in the ES epithelium. Adapted and updated from Mori et al., 2017 and Kim et al., 2019 (39,40).

Molecule	Methods and techniques	ES epithelial localization	Organism	Study
ION CHANNELS				
Na ⁺ channel (amiloride-sensitive)	Electrophysiology	apical membrane	guinea pigs	(51)
Epithelial sodium channel (ENaC)	RT-PCR, IHC	more likely on the apical side	human, rat	(52,53)
K ⁺ channel (outward delayed rectifier)	Electrophysiology	basolateral membrane	guinea pigs	(54)
Non-selective cation channel (ATP-activated)	Electrophysiology	apical membrane	guinea pigs	(55,56)
Cystic fibrosis transmembrane conductance regulator (CFTR)	RT-PCR, IHC	apical membrane	rat, human	(53)
Transient receptor potential vanilloid: TRPV4, TRPV2, TRPV1	IHC	apical membrane	rat, mouse, human	(45,57,58)
K ⁺ channels KCNN2, KCNK2, KCNK6, KCNJ14	Electrophysiology / pharmacology, LC-MS/MS, RT-PCR, IHC	MRC, apical membrane	human	(25)
ATPase				
Na ⁺ -K ⁺ -ATPase	IHC, ME, LC-MS/MS	more likely on the apical side	guinea pigs, human	(25,59,60)
H ⁺ -ATPase	IF, IHC	apical membrane	guinea pigs, mouse	(61,62)
Carbonic anhydrase membrane (CA)	IHC, ME	cytoplasm, vacuoles	guinea pigs, mouse, chinchilla	(63–65)
ION EXCHANGERS				
Cation exchanger Na ⁺ -H ⁺ exchanger (NHE)	RT-PCR, Electrophysiology, Fluorimetry	more likely on the apical side for NHE2 and NHE3; and basolateral for NHE1	guinea pigs, human	(66,67)
Anion exchangers Cl ⁻ -HCO ₃ ⁻ - exchanger (SLC4A2)	IF	basolateral membrane	guinea pigs	(61)
Pendrin (HCO ₃ ⁻ /Cl ⁻ exchanger; SLC26A4)	Electrophysiology, IHC, TEM, RT-PCR	MRC, apical membrane	mouse, human	(25,62,68–70)

Molecule	Methods and techniques	ES epithelial localization	Organism	Study
CO-TRANSPORTERS				
Bumetanide-sensitive Na ⁺ -K ⁺ -2Cl ⁻ cotransporter (NKCC2, NKCC1)	RT-PCR, ISH, IHC, IF, cDNA microarray	apical membrane	rat, human	(46,70-72)
Thiazide-sensitive Na ⁺ -Cl ⁻ cotransporter (NCC, SLC12A3)	RT-PCR, ISH, IHC, IF, cDNA microarray	apical membrane	rat, human	(70,73)
Na ⁺ -phosphate cotransporter (SLC34A2)		apical membrane	human	(70)
AQUAPORINS (AQPS)				
AQPs 1-4, 6-9	RT-PCR, IF	Basolateral: AQP3,4; apical: AQP2; both AQP1.	rat	(43,46)
AQPs 1-3	IF	AQP1 and AQP3 (slight) basolateral; AQP2 apical;	mouse	(48)
AQPs 1-4	IHC, ISH	Basolateral: AQP3,4; apical: AQP2; both AQP1.	human	(44,45,48)

ES epithelial localization refers to the type of cells: mitochondria-rich cells (MRC) or ribosome-rich-cells (RRC), and the side in which the signal was observed (apical or basolateral side). RT-PCR: reverse transcription polymerase chain reaction; IHC: Immunohistochemistry; IF: immunofluorescence; LC-MS/MS: liquid chromatography tandem mass spectrometry; EM: electron microscopy; ISH: in situ hybridization.

1.1.4.3.3 – Immune response in the inner ear

The membranous labyrinth was initially thought to be immunologically inactive and, as the brain, isolated from the bloodstream in a way similar to the blood-brain barrier. However, early evidence of immune cells was found in the membranous labyrinth, mainly in the ED and ES (74).

Macrophages and lymphocytes have been found to interact in the epithelium and perisaccular tissue of the ED and ES, just in the way they usually are seen in lymphoid tissues during antigen presentation. These findings have been discovered in human tissue and animal models, such as mice or guinea pigs (33,38,74,75). In addition to macrophages and lymphocytes, plasma cells, monocytes, or mast cells have also been seen in the perisaccular tissue. In general, these cells expressed surface markers, molecules for extravasation and migration, or immunoglobulins IgG and IgM, suggesting an active role in inner ear defense (74-76). In fact, Moller *et al* analyzed gene expression from human ES tissue, obtaining many expressed genes related to the innate humoral



and cellular immune response, including Toll-like receptors 4 and 7, β -defensin, and lactoferrin (77).

Besides, it seems that the inner ear carried out an active immune activity. On the one hand, pathogens or antigens in the inner or middle ear would be intercepted by macrophages and transported to the distal part of the ED lumen. There, they would be phagocytosed by macrophages and present their antigens to lymphocytes, triggering innate and adaptive responses. But increases of Na^+ in ES or stria vascularis could also activate inflammasome, promoting macrophage activation, and generating an inflammatory response. Debris of phagocytic processes is observed in the lumen of the distal part of the ES (75,76).

In addition to ES and ED, macrophages also reside in the stria vascularis and spiral ligament, where they control tight junction permeability and phagocytose cellular debris (78); but also in the synapses of SC and HC with SGN, implicated in immunomodulatory and nerve regeneration functions (79,80).

1.1.5 - Innervation and vascularization of the inner ear

1.1.5.1 - Innervation of the inner ear

The inner ear is innervated by the vestibulocochlear nerve or cranial nerve VIII, which emerges from the brainstem and splits into a vestibular and a cochlear division. The vestibular division turns posteriorly to form the vestibular ganglion and supply the vestibular system. The cochlear division turns anteriorly to form the spiral ganglion and innervates the cochlea (22,23).

Neurons from the cochlear and vestibular divisions, called spiral and vestibular ganglion neurons (SGN and VGN), respectively, are bipolar, hosting their cell bodies in the spiral and vestibular ganglions, respectively, while their dendrites terminate ultimately in synaptic boutons making contact with HC of the sensory epithelia (22).

1.1.5.2 - Vascularization of the inner ear

The labyrinthine artery provides the main blood supply to the inner ear, dividing into two branches: the anterior vestibular artery and the common cochlear artery. The anterior vestibular artery supplies the utricle, ampullae of SSC and LSC, and a small fraction of the



sacculae. The common cochlear artery supplies the cochlea, the PSC ampulla, and most of the saccule (81).

On the other hand, venous blood is drained by vestibular veins from the vestibular system and spiral modiolar veins from the cochlea. Both branches merge to form the labyrinthine vein, which crosses the VA and bails into the SS, on which the ES rests (81).



1.2 - Meniere Disease

Meniere Disease (MD, OMIM 156000) is a disorder of the inner ear characterized by recurrent episodes of spontaneous vertigo and ipsilateral cochlear symptoms, such as fluctuating episodes of sensorineural hearing loss (SNHL), tinnitus, and aural pressure (82). In addition, manifestations may not be limited to the inner ear and may be accompanied by other comorbidities such as migraine, allergic processes, and several autoimmune or autoinflammatory disorders (26,82).

The disease does not manifest in the onset with the complete clinical picture: vertigo, SNHL, and tinnitus. Most commonly, it appears as a partial syndrome with vertigo attacks but without hearing symptoms, although some patients also initiate with intermittent SNHL with or without tinnitus.

1.2.1 - Clinical symptoms

1.2.1.1 - Vertigo

Vertigo is the most disabling symptom at the beginning of the disease, appearing in around 90% of patients. It consists of the perception of rotation in the individual's environment without real movement, producing an imbalance sensation that implicates the risk of falling. It occurs as a consequence of vestibular dysfunction, probably due to changes in endolymph pressure or composition that cause abnormal excitation of the utricle, saccule, or SCC (83). Vertigo attacks appear spontaneously at the onset, lasting from minutes to hours. Episodes accumulate in periods of several weeks, where at least one day separates each attack from the next, followed by remission intervals. These vestibular events may be preceded by tinnitus, decreasing hearing, and aural fullness in the affected ear and can be accompanied by nausea and vomiting. In the first 10 years of the disease, the frequency of vertigo decreases significantly, the following 10 years stabilizes, and then gradually disappears (84,85).

1.2.1.2 - Sensorineural hearing loss

SNHL is a fluctuating symptom at the onset of MD but is more stable over time than vertigo. Initially, SNHL appears acutely in the affected ear/ears as a prequel to vertigo attacks and disappears after the crisis. As the disease progresses, the SNHL worsens with each event, becoming permanent and reaching moderate to severe levels. The presentation of SNHL can be unilateral or bilateral if it affects one ear or both, respectively.

When SNHL appears bilaterally at the onset, it is described as synchronic SNHL, while if it started unilaterally and affected the contralateral ear over the years, it is termed metachronic SNHL (85,86). In unilateral patients, SNHL typically affects low and middle tones and usually aggravates during the first 5-15 years to stabilize later. In contrast, bilateral cases finally influence all frequencies to produce a flat audiogram. The severity of SNHL is usually greater in bilateral cases (87). SNHL monitoring is performed by pure-tone audiometry (PTA) (Figure 1.7), considering impaired frequencies those with thresholds lower than 20dB.

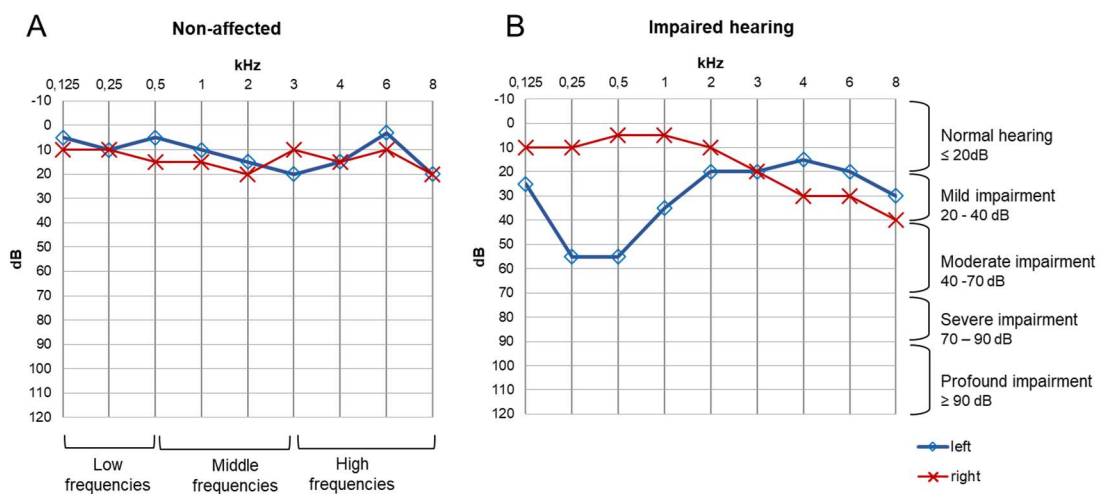


Figure 1.7 – PTA from non-affected (A) and affected (B) hearing individuals. On the X axis, the frequencies are represented in kilohertz (kHz), including low (≤ 500 kHz), medium (500 - 3000 kHz), and high (≥ 3000 kHz) tones. High frequencies are those involved in the range of speech; therefore, their alteration is the most disabling. The Y axis represents the patient’s sensory thresholds in decibels (dB). Thresholds above or equal to 20 correspond to unaffected hearing. There are different levels of impairment, including mild, moderate, severe, and profound. For example, patient B has mild-to-moderate hearing impairment at low frequencies in the left ear and mild impairment in high tones in the right ear.

1.2.1.3 - Tinnitus

Tinnitus is defined as the perception of sound inside the ear in the absence of real sound. Some patients describe it as a low-tone noise, like a seashell or smooth engine, while it is perceived whistle to others. The prevalence of tinnitus in patients with MD is more frequent than in other etiologies. Initially, it is intermittent and appears as a prequel to vertigo attacks. As the disease progresses, matching with the improvement of vertigo, the tinnitus disappears in 80% of patients but can also become persistent and louder (83,85). Furthermore, as the SNHL worsens over time, the patient becomes more isolated,

and tinnitus becomes more evident (83,88). Tinnitus can become the most disabling symptom of MD in advanced stages and has been widely associated with anxiety and (89).

1.2.1.4 - Aural fullness

As tinnitus, aural fullness usually appears acutely preceding the vertigo attacks in the early stages of MD. However, constant manifestations have also been described. It arises as a feeling of pressure and blockage inside the ear. Around 20% of patients do not experience this symptom (85).

As a summary of this section, Figure 1.8 outlines a timeline of the onset and progression of symptoms.

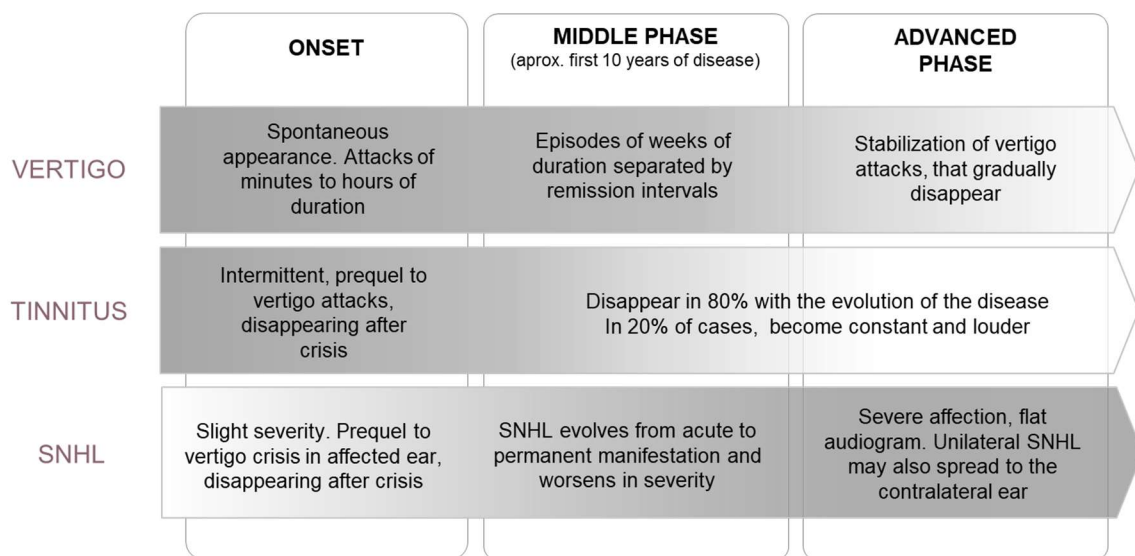


Figure 1.8 - Timeline diagram of clinical symptoms progression in MD.

1.2.2 - Comorbidities

MD shows overlapping symptoms with other pathologies, such as vestibular migraine or migraine. Vestibular migraine is defined by past or ongoing history of migraineous events accompanied by vertigo in at least 50% of the episodes. It is essential to consider the accompanying symptoms to discard an incorrect diagnosis of MD and VM. In VM, vestibular attacks coincide with migraine-type headache, visual aura, or photo/phonophobia, meanwhile, MD vestibular episodes coexist with tinnitus, aural fullness, and SNHL (90). However, hearing loss may also occur in VM, usually showing

bilateral affection from the onset that does not progress to severe levels over time. On the contrary, SNHL in MD often starts as unilateral, worsening with disease development (91). In 2019, Flook et al., initiated research on the molecular differentiation of MD and MV, identifying two profiles of proinflammatory cytokines between both groups (92). On the other hand, migraine without vestibular symptoms can also mislead between MD and VM since migraine occurrence is more frequent in MD patients than in the general population (86,93).

Immune-related comorbidities have been described in MD patients, suggesting that the immune system plays a role in the etiology or progression of the disease (94,95). Some systemic autoimmune diseases have been described as more frequent in MD patients than in the general population, like rheumatoid arthritis, asthma, chronic fatigue syndrome, irritable bowel syndrome, gastro-esophageal reflux disease, psoriasis, systemic lupus erythematosus, and ankylosing spondylitis (94,96,97). Allergic processes are also present in more than 50% of MD patients, of which 44% usually have high IgE levels in their blood. It has been observed that allergen exposure can trigger the symptoms of MD (98,99).

Another disease that can also be confused with MD during diagnosis is autoimmune inner ear disease (AIED). During its development, the inner ear itself is the target of the autoimmune reaction. This condition is characterized by recurrent bilateral SNHL episodes spanning several weeks to months. It can start as unilateral but usually spreads rapidly to the contralateral ear. Vestibular involvement can also appear in 50% of patients. AIED is considered primary when the ear is the only organ affected or secondary when it coexists with other systemic autoimmune diseases, which occurs in 30% of patients. People with AIED often have elevated levels of proinflammatory cytokines such as IL-1 β and TNF- α (100).

1.2.3 - Epidemiology

The prevalence of MD varies according to ethnic background and world region, ranging from 3-500 out of 100.000 individuals. European descending populations expose the most significant disease rates, being the highest at 513 per 100.000 in Finland. Asian or Native American regions exhibit the lowest abundance, with 3.5 per 100.000 in Japan (83,85).

MD can be classified as familial (FMD) or sporadic (SMD). Most described cases are sporadic (86,101), being familiar aggregation described in 5-20% of patients in European descendants (102,103). FMD is considered when at least one relative in the first or second degree satisfies probable or definitive MD criteria. In a scenario where the proband has several family members with a history of migraine, vertigo, or SNHL, relatives' medical history must be deeply investigated to confirm or discard MD incomplete phenotypes (104,105).

The distribution by sex depends on the population studied, but it generally displays female dominance (82,83). Referring to onset, patients exhibit wide variations concerning the age of onset, but the first symptoms begin in the fourth or fifth decade of life. About 10% of patients debut with 65 years or more. Pediatric MD is rare, described in 0.5-7% (83,85). In the onset, it usually starts as a partial syndrome, being 5-10 years between the first symptoms and the complete clinical picture (83,106) (Figure 1.8).

Focusing on SNHL, the proportion of unilateral and bilateral changes dramatically depends on the stage of the disease in the patients studied. Typically, bilaterals account for about 25% of patients, of which about 10% started as synchronous SNHL and 15% evolved from unilateral to bilateral (metachronic SNHL). This means up to half of the unilateral patients have the contralateral ear affected over time, in a range of 10-20 years (83,85,107).

1.2.4 - Diagnosis and classification of MD clinical subgroups

The clinical heterogeneity of MD makes its diagnosis difficult. For this reason, during the last decade, several clinical consortiums have proposed unifying the diagnostic standards guidelines. In 2015, the Classification Committee for Vestibular Disorders of the Bárány Society, The Japan Society for Equilibrium Research, the European Academy of Otolaryngology and Neurotology (EAONO), the Equilibrium Committee of the American Academy of Otolaryngology-Head and Neck Surgery (AAO-HNS) and the Korean Balance Society redefined an updated the diagnosis criteria (108). Thereby, i) definite Meniere and ii) probable Meniere can be distinguished (Table 1.3). These criteria are essentially symptomatologic since no radiological or biological markers are normalized for diagnosing the disease (108).

Table 1.3 - Diagnostic criteria for definite and probable MD (108)

Definite MD
A. Two or more spontaneous episodes of vertigo, each lasting 20 minutes to 12 hours.
B. Audiometrically documented low- to medium-frequency sensorineural hearing loss in one ear, defining the affected ear on at least one occasion before, during, or after one of the episodes of vertigo.
C. Fluctuating aural symptoms (hearing, tinnitus, or fullness) in the affected ear.
D. Not better accounted for by another vestibular diagnosis

Probable MD
A. Two or more episodes of vertigo or dizziness, each lasting 20 minutes to 24 hours.
B. Fluctuating aural symptoms (hearing, tinnitus, or fullness) in the affected ear.
C. Not better accounted for by another vestibular diagnosis

These efforts to standardize MD seek to improve accuracy in diagnosis, avoiding the overdiagnosis in patients with overlapping audiovestibular symptoms, mainly vestibular migraine or hearing loss, but also the other MD comorbidities such as migraine, allergies, or autoimmune diseases (108). With this purpose, several clinical predictors have been utilized to define clinical subgroups within MD, differentiating unilateral or bilateral, including history of autoimmunity, history of migraine, presence, or absence of affected relatives, and SNHL onset. The clustering of MD patients based on these predictors has allowed the definition of five subgroups (Table 1.4). Types 3, 4, and 5 are the same for unilateral and bilateral MD types: Type 3 includes patients with FMD without migraine; Type 4 contains SMD patients with migraine; and Type 5 are those with autoimmune diseases. In bilateral MD: Type 1 comprises patients with metachronic hearing loss, without migraine and autoimmune diseases, and Type 2 consists of patients with synchronic hearing loss, without migraine and autoimmune history. In unilateral MD, Type 1 includes SMD without migraine and autoimmune diseases; Type 2 contains those with hearing loss that preceded the vertigo events by months or years (delayed), without migraine and autoimmune diseases. In both classifications, sporadic cases were the most abundant (86,101).

Table 1.4- Clinical subgroups and prevalence per group in MD according to Frejo et al., (86,101).

Subgroup	Patients (%)	Definition
BILATERAL MD		
Type 1	46	SMD, with metachronic SNHL
Type 2	17	SMD, with synchronic SNHL
Type 3	13	FMD
Type 4	12	SMD accompanied by migraine
Type 5	11	SMD accompanied by autoimmune disease
UNILATERAL MD		
Type 1	53	SMD
Type 2	8	Delayed MD
Type 3	13	FMD
Type 4	15	SMD accompanied by migraine
Type 5	11	SMD accompanied by autoimmune disease

1.2.5 - Etiology and pathophysiology of MD

MD is a multifactorial disorder with disparate symptoms and comorbidities. Therefore, its pathophysiology must be approached by different etiologies: i) immune-related etiology, ii) alterations in the endolymphatic flow, and iii) genetic background. The different factors may be more or less relevant in each MD group.

1.2.5.1 - Impaired endolymphatic flow

Endolymphatic hydrops

One of MD most characteristic histopathological findings was the presence of endolymphatic hydrops (EH), which refers to the distention or swelling in the membranous labyrinth by increment in the endolymph volume. It occurs mainly in the inferior end organs: the cochlear duct and the saccule. EH rarely appear in the vestibular organs but can be observed confined to the cochlear duct (26).

EH were primarily noticed in extensive post-mortem studies of TB from MD patients. In the tissues of patients in the early stages, EH began in the saccule and the cochlear



duct as a slight expansion of the scala media. Reissner's membrane displaces when the disease advances and the scala media enlarges to almost or entirely occupy the scala vestibuli. In the saccule, the walls expand until they meet the stapes and can even displace the utricle. As the most drastic consequence, the membranous labyrinth breaks, rupturing more frequently in Reissner's than in vestibular membranes (109,110). Rupture of the membranous labyrinth was more common in MD patients than in individuals only with EH (110). In general, EH were found in all ears affected by MD, but not all ears with EH had developed symptoms of MD (111,112).

In addition to EH, TB from MD individuals had poor pneumatization (113,114) and displaced lateral sinus (115). Affections of the SGN have also been described, both loss of neurons and decreased synapses with HC (116–118).

Abnormalities of the ED and ES

In addition to EH, other macrostructural features were evident between the TB of MD patients and controls. VA appeared shortened, hypoplastic, or with a narrower cranial fossa opening (113,114). The ED and ES were also affected, with a smaller ED isthmus and partial or complete reduction of the ES lumen volume (119,120). At the microstructural level, loss of integrity by fibrotic processes in the epithelium of the ES and saccule was described, which were either fibrotic or absent (32,119,120). Therefore, the presence of EH was linked to other abnormalities in the ED and ES.

Numerous studies have proposed endolymph malabsorption in the ED and ES as the basis for explaining the etiology of MD. In this hypothesis, abnormal function/structure/anatomy of the VA, ED, and ES will create a deficit of endolymph absorption that would start to accumulate (117). These alterations could develop EH slowly and silently in the patient, increasing in severity with the progression of the disease. The onset of symptoms could coincide with advanced EH, in which extreme events like membranous labyrinth ruptures would produce a mixture of perilymph and endolymph. Loss of the endocochlear potentials would result in depolarization/hyperpolarization of the sensory epithelia, causing acute vestibular or auditory symptoms (117). These theories have been supported by animal studies in which part of the ED or ES were obstructed or dissected led to the production of EH in the cochlear duct, although vestibular findings or symptoms were never observed (109,121)

1.2.5.2 - Autoimmunity, autoinflammation, and allergy

Since various studies have indicated that some autoimmune disorders are more prevalent among MD patients than in the general population, autoimmunity has been suggested as another potential triggering factor in MD (94,96). Some of these include rheumatoid arthritis, psoriasis, systemic lupus erythematosus, atopic dermatitis, non-allergic asthma, and thyroid diseases (94,96,97,122,123). Supporting this hypothesis, circulating immune complexes in blood of MD patients were increased in 7% of patients during the inter-crisis period (124), and autoantibodies and antigens, including interferon regulatory factor 7 and various immunoglobulins have been found elevated in the inner ear fluid from MD patients compared to healthy individuals (125). In patients with AIED, high levels of proinflammatory cytokines, including IL-1 β and TNF- α , have been described. Interestingly, some of the AIED patients resistant to corticosteroids improved their auditory response and decreased IL-1 β levels after treatment with IL-1 receptor antagonists (126,127). Moreover, immune-related genes (*MICA*, *TLR10*, *NFKB1*, *PTPN12*, *HCFC1*) carrying genetic variants have been described in MD patients and associated with the development of the disease (128). One of the variants in *NFKB* was present in 18% of patients with MD and a comorbid autoimmune disease (129).

On the other hand, an autoinflammatory etiology has been proposed based on consistently detecting elevated proinflammatory molecule levels in patients with MD. Several cytokines, including CCL18, CCL22, and CCL4, significantly differed in cultured PBMC from MD, migraine patients, and healthy individuals (130). TNF- α , IL-6, and INF- γ were upregulated in the luminal fluid of the ES in affected unilateral MD patients compared with the contralateral control ear (131). Some autoinflammatory diseases that course with SNHL seem to have a similar pathogenesis mechanism, in which an abnormal activation of the NLRP3 inflammasome is observed in the resident macrophages within the mouse cochlea, producing a release of IL-1 β that would mediate local inflammation and trigger the associated symptoms (132).

Allergic processes are also more frequent in MD patients, both to inhaled and ingested allergens. Available antihistamine treatments and allergy-causing foods removal from the diet improve audiovestibular symptoms in some MD patients (133,134). According to this premise, several investigations have shown that MD patients show higher serological levels of IgE and proinflammatory cytokines such as IL-4, IL-5, IL-10, IL-13, IL-6, IL-1 β , IL-1RA, and TNF- α (99,135–138). IgE and histamine receptors have



been found in the inner ear of human and animal models, such as mice and rabbits (139–142). Frejo *et al.*, described that stimulation of PBMC with *Aspergillus* and *Penicillium* in patients with MD and elevated basal cytokines triggered an exacerbated inflammatory response with the release of TNF- α (99).

1.2.5.3 - Genetics

Numerous pieces of evidence suggest a genetic contribution in MD, according to the ethnic prevalence and the familial aggregation described for the European and Asian populations. In the last 10 years, several advances have been made in understanding the genetic basis of MD, both sporadic and familial, but the underlying mechanisms are still not fully understood (103,128). Candidate genes have different functions, from structural proteins in the hair bundle to oxidative stress or axonal guidance proteins (103,143).

FMD has been found in 5-20% of cases in European descendants, with a predominantly autosomal dominant inheritance pattern with incomplete penetrance and anticipation (102–104). However, families with autosomal recessive, digenic, and multiallelic inheritance have also been described (Roman-Naranjo 2020; Gallego-Martinez 2020).

According to the autosomal dominant inheritance pattern, 9 genes are involved in FMD, including *FAM136A*, *DTNA*, *PRKCB*, *COCH*, *DPT*, *SEMA3D*, *TECTA*, *GUSB*, and *SLC6A7* (143,144). Most variants in these genes have not been replicated in other families, which suggests they could be private causal variants in specific families. However, Roman-Naranjo *et al.*, reported variants in the *TECTA* gene shared between 2 unrelated Spanish families with MD (144).

In autosomal recessive inheritance, 4 genes have been identified, including *HMX2*, *LSAMP*, *OTOG*, and *STRC* (145–148). *OTOG* seems crucial in recessive MD Spanish cohorts since 16% of MD families showed segregation of variants in this gene, and several unrelated families shared the same rare variants (148).

Another possible genetic model considers digenic inheritance. This hypothesis has been extrapolated from some families where co-segregation of variants in at least two genes previously related to different types of SNHL has been found. In these MD families, rare and novel variants in *MYO7A* segregate in some relatives with other variants in *CDH23*, *PCDH15*, and *ADGRV1* (149).

Many of the previously highlighted genes have an essential structural function being part of the junctions between stereocilia, as fundamental components of the TM and otolithic membranes, or binding the stereocilia to these gelatinous matrices. These findings support a structural cause in FMD. First, α -tectorin and otogelin (codified by *TECTA* and *OTOG*, respectively) are fundamental components of the tectorial and otolithic membranes (150,151). Tectorin interconnects the collagen fibers and anchors the TM to the surface of the stereocilia. Abnormal collagen assembling and glycoprotein diffusion have been observed when the anchoring C-terminal extreme of α -tectorin is impaired, as occurs in the shared variants discovered by Roman-Naranjo *et al.*, (144,151). Second, *MYO7A*, *CDH23*, *PCDH15*, *ADGRV1*, *STR*, and *OTOG* (encoding for myosin VIIa, cadherin-23, protocadherin-15, adhesion G-protein coupled receptor V1, stereocilin and otogelin, respectively), play a role in the junctions between stereocilia (8,14,152,152). Myosin VIIa intervenes in the organization of the actin cytoskeleton in the stereocilia backbone but also connects actin to tip links (formed by cadherin-23 and protocadherin-15) on the surface of the stereocilia and to ankle links (constructed by adhesion G-protein coupled receptor V1 units) in the anchorage of stereocilia to the cuticular plate (8,152). Furthermore, the transmembrane zone of protocadherin-15 interacts with MET channels in the anterior stereocilia, and the accumulation of variants in these genes could impair the interaction and opening of the MET channels during sound mechanotransduction (8,103). Stereocilin and otogelin play a joint role since stereocilin anchors top horizontal connectors, formed by otogelin and otogelin-like dimers, between stereocilia membranes (14). Third and last, stereocilin on the surface of the stereocilia interacts with tectorins to anchor the membrane to the hair bundle (14). A correct anchorage between the stereocilia and the otolithic and TM is essential to ensure the ionic microenvironment in the hair bundle, ensuring the responsiveness of MET channels. *Tecta*^{-/-} knockout mice, characterized by decreased hearing sensitivity, showed deficient TM anchoring and abnormal Ca²⁺ ion composition near the hair bundle environment (17,18).

The analysis of sporadic cases has been approached through genetic studies of large cohorts. In these investigations, the accumulation of rare variants in the cases is compared with control databases for that specific population (128). Gallego *et al.* described a burden of rare variants in genes previously associated with SNHL in a Spanish cohort of 890 patients. Among these, some have been previously related to autosomal dominant or recessive SNHL, such as *GJB2* and *ESRRB*, respectively; genes involved in the ionic regulation of endolymph, such as *SLC26A4* and *CLDN14*; and genes

related to syndromic vestibular hypofunction in Usher syndrome such as *USH1G* (153). In addition, genes involved in axonal guidance pathways, such as *NTN4* or *NOX3*, have also revealed a load of variants in MD patients (154). Although these studies have shed light on the genetic basis of MD in sporadic individuals, replication of the genes found in other cohorts is required to give weight to the causality of these genes.

The variability in the function of the genes pointed out in these studies would explain the phenotypic heterogeneity of MD among patients.

1.2.6 - Endotypes of Endolymphatic Sac in MD

In 2019, Eckhard *et al.* described two histopathological subtypes of ES, designated as i) hypoplastic and ii) degenerative. The findings were found in a postmortem study of the TB of 24 patients with idiopathic MD and EH. Evaluation of the epithelium described that the eES in the degenerative endotype contained mainly shrunken or extruded epithelial cells, pyknotic nuclei, and fibrosis in areas of complete epithelial loss. In contrast, in the hypoplastic subtype, the ES ended abruptly in the operculum, with the eES completely absent. The iES was intact in both cases (32). Both alterations would result in the alteration of the epithelium and its functions in regulating the composition of the endolymph, the pressure within the membranous labyrinth, and immunological or secretory roles. Inspection of the medical records of the patients whose TB had been examined indicated a clinical-histopathological correlation. Specifically, the hypoplastic group showed a family history of MD, early onset, bilateral involvement, and greater severity of EH, while the degenerative group showed late onset and unilateral MD affection. The finding of ES hypoplasia, both bilateral and unilateral, was correlated with a diagnosis of MD in the affected ear or ears (32).

Subsequently, the method for distinguishing the two subtypes was adapted for examination in computed tomography (CT) images by calculating the Angular Trajectory of the Vestibular Aqueduct (ATVA) marker. This approximation calculates the angle formed by the entrance trajectory of the VA into the TB from the vestibule and the exit trajectory of the VA from the TB towards the PCF at the level of the operculum. Therefore, hypoplastic cases were those with an $ATVA > 140^\circ$ and degenerative cases with an $ATVA < 120^\circ$. In the TB for which histological sections and CT scans were available, ATVA measurements were replicated with low variability (maximum 10° difference) between the two techniques for both controls and MD cases. The development of this method

facilitated the screening of these endotypes in the population, as a CT scan is a simple and routine test used in otolaryngology medical units (155).

Bachinguer *et al.* thus sought to confirm the clinical-histopathological correlation between the two subtypes proposed by Eckhard *et al.* This retrospective study was based on a larger cohort of 92 MD individuals who underwent high-resolution computed tomography (CT) or gadolinium-based magnetic resonance imaging. The results refined the clinical differences that distinguish the two groups. The degenerative patients revealed a higher frequency of vertigo attacks and severely reduced vestibular function, and their condition was almost exclusively unilateral. The hypoplastic subtype showed male preponderance, higher frequency of bilateral involvement, findings of TB abnormalities such as dehiscence of the semicircular canal, and a positive family history of hearing loss, vertigo, and MD. These results validated that these subtypes can be considered different disease endotypes (156).

As in the study of Eckhard *et al.*, (2019), unilateral and bilateral ES hypoplasia displayed in the same ear or ears affected by MD (32). Furthermore, it is suggested that there is a high risk that patients with bilateral ES hypoplasia, but unilateral MD will eventually develop bilateral MD. This hypothesis was verified in posterior studies, where 69% of patients with bilateral ES hypoplasia and unilateral MD developed symptoms in the contralateral ear in an average of 12 years. On the contrary, patients with unilateral ES hypoplasia and unilateral MD remained only affected in one ear (157).

Identifying different endotypes within a disease can help to establish the diagnosis, improve clinical decision-making, and predict the evolution and prognosis of the disease. Therefore, the main objective of this project is to describe the association between the phenotypic variability observed in individuals with ES hypoplasia and the possible genetic variants that may be involved in its pathogenesis. The results will improve the genetic and molecular characterization of these endotypes in MD.

1.3 - The genetics of diseases

1.3.1 - NGS technologies in the discovery of genetic disease

In recent decades, the technology for sequencing genetic material has evolved significantly, from Sanger sequencing to next-generation sequencing. In this process, we have progressed from sequencing small fragments of DNA, with expensive cost and time-consuming procedures, to being able to sequence large-scale projects where the entire genome and exome of thousands of individuals can be addressed in a considered time and at a lower cost (158,159).

Massively parallel DNA-sequencing or Next Generation Sequencing (NGS) methodology has revolutionized our approach to medical genetics, becoming an indispensable tool for identifying genetic variants associated with diseases. The most used procedures are genetic panels, whole exome sequencing (WES), and whole genome sequencing (WGS), ordered in increasing cost, difficulty in analysis, and scope. Genetic panels are fast and cheap, with low production of artifacts and low complexity in the analysis. However, it is a targeted methodology that does not reveal new disease-causal genes. WES has dominated rare disease research in recent years. In this procedure, only the exomes are sequenced, that is, the coding parts of genes that will be translated into proteins. These regions represent only 1-2% of the total genome, which makes WES a more profitable method in terms of cost, time, and complexity of analysis than WGS. Furthermore, over 85% of the variants associated with disease pathogenesis have been found in exonic regions. Therefore, WES can potentially discover the genetic causes of a rare disease, mainly in monogenic disorders, but also in complex or common pathologies (158,159). However, we must remember that with WES, we are losing those variants found in non-coding regions, mainly regulatory regions that affect gene expression and epigenetic modifications (160).

It is expected that this technology will continue to advance and, in a few years, will allow a personalized study of the genetics of diseases.

1.3.2 - Genetic variants

Sequencing technologies allow us to identify the genetic variants of an individual or cohort with a particular pathology. In this way, we can obtain information about the genetic

basis of the disease and the biological pathways affected and thus develop specific treatments.

Genetic variants are alterations in the DNA sequence that contribute to the diversity observed among individuals. These variations can be inherited or arise spontaneously, and they play a crucial role in determining our unique traits and susceptibility to certain diseases.

There are several types of genetic variants, including single nucleotide variants (SNV), short Insertions and Deletions (InDels), copy number variants (CNV), and large structural variants (LSV).

1.3.2.1 - Single Nucleotide Variant

SNV are the most common type of genetic variation. They involve a change in a single nucleotide base pair in the DNA sequence.

SNV are referred to as coding or non-coding if they affect the coding-protein regions or not, respectively. Coding SNV may be non-synonymous if they produce an amino acid change or synonymous if there is a nucleotide modification but no amino acid change due to the degeneracy of the genetic code. Non-synonymous SNV can be non-sense, also called loss-of-function variants (LoF), if the amino acid change results in the appearance or disappearance of a stop/start codon; or missense if the change produces an amino acid replacement (Figure 1.9, A).

Non-coding SNV are found in areas of the genome whose functional significance is still being elucidated, such as untranslated regions, non-coding RNA, or alternative splicing sites. These areas are thought to have regulatory effects on the coding regions.

1.3.2.2 - Short Insertions and Deletions

InDels are genetic variants that involve inserting or deleting nucleotides in the DNA sequence. These variants can range in size from a single base pair to larger sections of DNA (2-10.000bp). Indels are classified as frameshift or non-frameshift, depending on if they alter the reading frame of a gene. Frameshift or non-frameshift InDels are also classified as LoF variants, potentially pathogenic in the protein production or function (Figure 1.9, B).

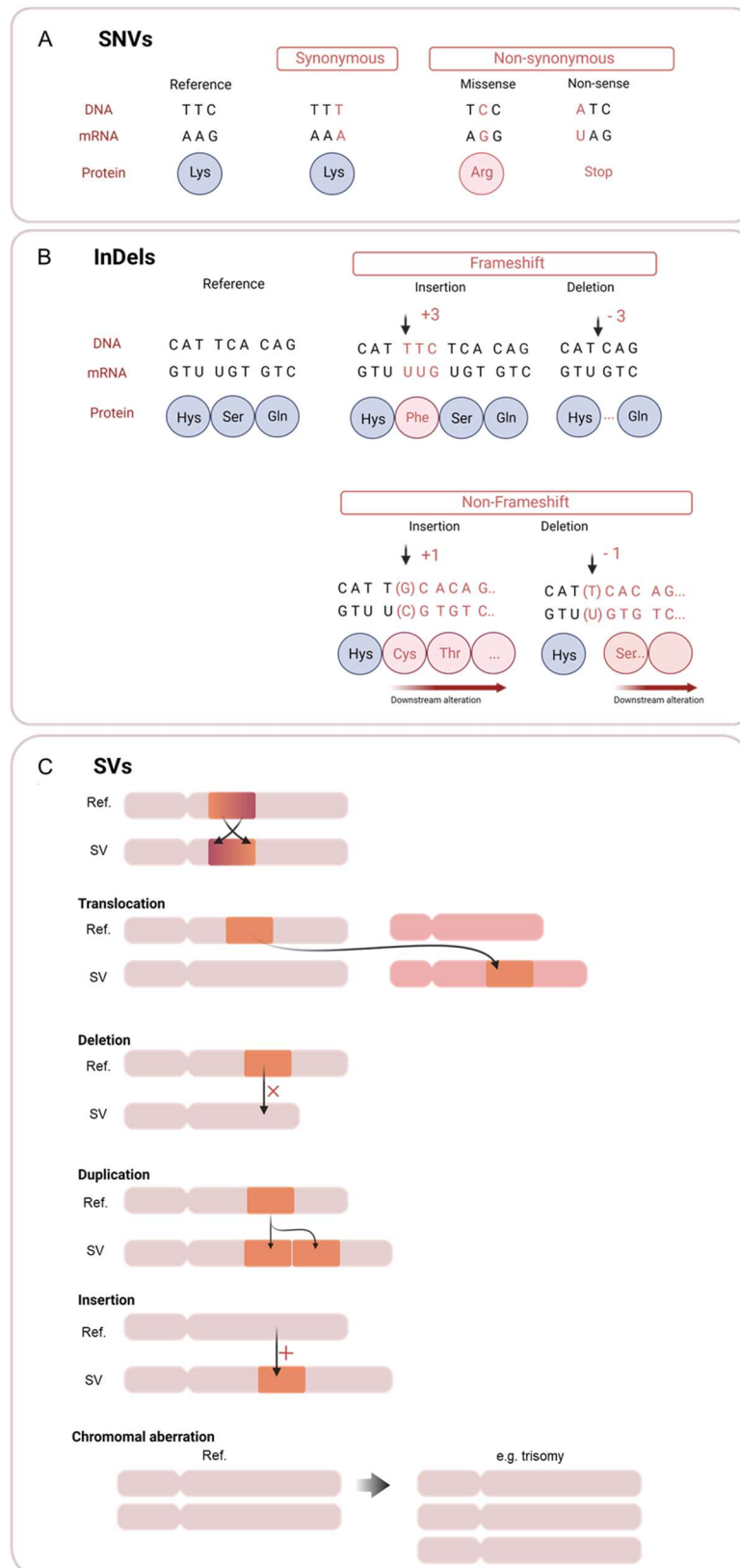


Figure 1.9 - Scheme of the different types of variants: A) SNV, B) InDels, and C) Structural variants. Created with BioRender.com



1.3.2.3 - Structural variants

SVs include events where a DNA region shows changes in the number of copies, orientation, or location (161) (Figure 1.9, C).

Copy Number Variations

CNV are structural changes in the DNA that involve the variable repetition of a segment of DNA compared with the reference genome. These variants can range in size from kilobases to megabases and can encompass multiple genes. CNV can significantly impact gene dosage, disrupting normal gene function (161).

CNV are classified as deletions or duplications. Deletions can be heterozygous deletions (remove one copy), resulting in a reduction of half the amount of the protein(s) involved, or homozygous deletions (affecting two copies) with the complete absence of the protein(s). Duplications are detected by the presence of 3 or more copies (up to hundreds of copies) of the altered region.

Large Structural Variants

LSV are genomic alterations implying more than 10.000bp. Several types of LSV can be differentiated, such as translocations, consisting of DNA segment transferences between different genomic zones; inversions, appearing as reversed sequence fragments; or large-scale deletions, duplications, or insertions.

Chromosomal Aberrations

Chromosomal aberrations are large-scale alterations that involve changes in the structure or number of chromosomes, such as trisomy 21 in Down syndrome.

1.3.3 - Variant allele frequency and phenotype effect size

The allele frequency of disease-causing variants is closely related to the nature and prevalence of the disease and the effects of these variants on the phenotype. In common diseases, the causative variants usually have relatively high allele frequency in the general population, their impact on the phenotype is small, and they may also interact with environmental factors that may increase/decrease the risk of disease development. In contrast, Mendelian diseases are due to rare mutations in a single gene that usually have low allele frequency in the general population. These mutations have a dominant or recessive effect on the phenotype and usually manifest markedly and early in the affected



individual's life. Complex diseases have a multifactorial genetic basis resulting from causal variants and environmental factors. These variants typically have low/medium allele frequency in the general population, and their effects on phenotype can be challenging to discern (162,163).

As previously exposed, MD is a complex, multifactorial disorder with a prevalence of approximately 1 in every 2000 individuals in the European population and shown heritability of around 20%, with autosomal dominant or recessive inheritance patterns and incomplete penetrance. Therefore, the approach would focus on multiple genes or causative variants with moderate and additive effects on phenotype and rare allele frequency in the general population.



2. - Hypothesis and justification



Since the opening of the study of this complex disease, the most relevant histopathological discovery has been EH, hence it is clear that it should play an important role in MD. And it makes sense that the accumulation of endolymph within the membranous labyrinth leads to an increase in pressure, which would produce abnormal excitation of the sensory epithelia, resulting in the associated symptoms.

Therefore, EH seem to be more the consequence of the inadequate drainage of the endolymph in the ED and ES, discarding their origin directly in the organs where they appear: the cochlea and the saccule. This hypothesis is based on several considerations. First, the theory of longitudinal endolymph flow, according to which endolymph originates in the cochlear duct and vestibule, travels through the ED, and finally reaches the ES, where it is reabsorbed into the systemic circulation through the SS. Second, animal models for EH have been developed by ES ablation or blockade. Third, the presence of abnormalities in the VA, ED, and ES in patients with MD associated with EH, such as shortened VA, narrowed VA openings to the subarachnoid space, smaller ED isthmus, or ES with collapsed lumen or even absent. Ultrastructural changes also included fibrosis of the ES epithelium, with the consequent alteration of its functionality.

Studies conducted by the researchers Andreas Eckhard and David Bächinger, briefly explained in the section *Endotypes of Endolymphatic Sac in MD* (in the introductory chapter of this thesis), also contributed to consolidate these ideas, describing the two ES histopathological subtypes. However, these investigations provide the innovative definition of endotypes inside MD: hypoplastic and degenerative, integrating histopathology and clinical profile.

Based on the variables associated with the degenerative endotype: late onset, vertigo crisis and reduced vestibular function, it has been suggested that there may be a disruptive vestibular etiology in adult life. The adult ear has a reduced ability to compensate for homeostatic imbalances. Thus, loss of epithelium in the adult eES would lead to changes in the composition of the endolymph, whose lowest potential difference and therefore the most vulnerable is found in the vestibular organs. As a consequence of the regulatory failure, it would produce the associated phenotype.

In contrast, the phenotype associated with the hypoplastic endotype supports the hypothesis of a genetic cause, especially because these patients have a family history of SNHL, vertigo or MD and a tendency to present early onset. Therefore, the collapse in the formation of the extraosseous part of the ES could occur at early developmental stages



and would affect both ears, as we observed in the higher bilateral prevalence. Genetic segregation would lead to ES hypoplasia between members of the same family, causing complete or partial clinical pictures as described. Anomalies in the TB have also been associated, which support that abrupt ES termination in the operculum could be caused not only by malformations in the membranous labyrinth itself, but also in osseous, as VA alterations previously reported in MD studies.

In this thesis, our interest focuses on the hypoplastic endotype. Our working hypothesis is that there is a genetic component that may describe the hypoplastic endotype of the ES in MD patients. In this scenario, it is possible that the accumulation of rare variants in different genes with a large influence on the phenotype would determine the occurrence of the clinical picture.

The identification of molecular and genetic markers associated with MD endotypes may be promising to define personalized subgroups with regards to improve the diagnosis, the clinical decision-making, and predict patient evolution and prognosis.



3. – Objectives



Main goal

The main objective of this project is to decipher the genetic background of the ES hypoplasia in MD.

Secondary goals

For this purpose, three chapters within this manuscript are differentiated, where it is expected to achieve the following secondary objectives:

Chapter 1 - Analysis of the prevalence of ES hypoplasia in patients without MD

- To identify the prevalence of ES hypoplasia in patients without MD
- To evaluate the replicability of the ATVA measurement method
- To determine if ATVA is associated with others ontological features in the patients without MD

Chapter 2 - Identification of genes and variants associated with ES hypoplasia in MD

- To identify genes and variants associated with ES hypoplasia in sporadic MD patients.
- To identify genes and variants associated with ES hypoplasia in familial MD patients.

Chapter 3 - Validation of genes and variants associated with with ES hypoplasia in MD

- To evaluate the effect of rare variants on protein structure or expression in genes associated with sac hypoplasia.
- To define the biochemical pathways and biological processes involved in the development of the PCF.



4. – Materials and Methods



4.1 - Materials

4.1.1 - Molecular Biology Reagents

Molecular Biology reagents include those used for sample preservation, DNA extraction, preparation of WES libraries, preparation of amplicons for Sanger sequencing, and quality control (electrophoresis and concentration measurements).

- Oragene®DNA (#OG-510, Genotek, Ottawa, Canada)
- prepIT L2P (#PT-2LP, Genotek, Ottawa, Canada)
- Direct Load 1 Kb DNA ladder (#D3937, Sigma-Aldrich)
- 100bp DNA ladder (#15628019, Invitrogen)
- Water molecular biology reagent (#7732-18-5, Sigma-Aldrich)
- Qubit dsDNA BR Assay Kit (#Q32850, Invitrogen)
- Loading buffer (#10816015, Invitrogen, Thermo Fisher)
- Agarose routine grade (#MB14403, NZYtech)
- Tris-acetate-EDTA buffer (TAE) (#B49, ThermoFisher Scientific)
- SureSelectXT Human All Exon V6 (Agilent Technologies, Santa Clara, CA, USA)
- TapeStation DNA screenTape D1000 (Agilent Technologies, Santa Clara, CA, USA)
- NovaSeq 6000 platform (Illumina, San Diego, CA)
- Gelred Nucleic Acid Gel Stain 10.000x in water 1*0.5 ml (Biotium, #41003)
- MicroElute® Cycle Pure Kit (#D6293-01, Omega, BioTek)
- AmpliTaq 360 DNA polymerase (#4398886, ThermoFisher Scientific)

4.1.2 - Antibodies

Table 4.1 summarizes the antibodies or reagents including antibodies used for immunohistochemistry (IHC) and western blot (WB) assays.

Table 4.1 - List of antibodies used in the IHC and WB assays.

	Host, reactivity, target	Provider	Catalogue reference	Working Dilution
IHC				
1° AB	Rabbit anti mouse Adamts18	Origene	TA321964	1:100
2° AB	Ready-to-use Horse Anti-Rabbit Antibody labelled with Peroxidase	Vector	MP-7401	ready to use
WB				
1° AB	Adamts18 rabbit anti mouse	Aviva System Biology	ARP53478_P0 50-FITC	1:1000
	Anti-β-Actin monoclonal antibody, Clone AC-15	Sigma-Aldrich	A1978	1:10000
2° AB	Goat anti-Rabbit IgG (H+L) HRP Conj.	Promega	W4011	1:5000
	Goat anti-Mouse IgG (H+L) HRP Conj.	Promega	W4021	1:5000

4.1.3 - IHC

Paraffin sections preparation

- Formaldehyde solution 4% (#FN-1020-4-1, SAV LP GmbH)
- Soft Decalcification EDTA-25% EDTA solution pH 7.4 (#6484.2, Carl Roth GmbH Co. KG, Germany)
- PBS Tablets (#18912-014, Life Technologies Limited, UK)
- Ethanol absolute (# UN1170, VWR Chemicals, Belgium)
- Paraffin (#39502004, McCormick, Canada)
- Glass slides (# J1800AMNZ, Thermo Scientific, USA)
- Cover glasses 24x50 mm (#7695030, Th. Geyer GmbH & Co. KG, Germany)

Immunolabelling

- Normal Horse Serum 2,5% (#30022, Vector Laboratories, Burlingame, CA)
- 10x Casein Solution SP (#5020, Vector Laboratories, Burlingame, CA)



- Xilol substitute (#10524305, ThermoFisher Scientific)
- Ethanol (#20821.310, VWR Chemicals, Belgium)
- Citrate Buffer, pH 6.0, 10×, Antigen Retriever (#C999-100ML, SigmaAldrich)
- Methanol (#107018, Merk)
- Hydrogen peroxide solution (#H1009, SigmaAldrich)
- Ready-to-use Horse Anti-Rabbit Antibody labelled with Peroxidase (#MP-7401, Vector, Burlingame, CA)
- Papanicolaou Harris hematoxylin (#05-12011E, Bio-optica)
- Diaminobenzidine (DAB) Substrate Kit (#SK-4100, Vector Laboratories, Burlingame, CA)
- DPX Mountant for histology (#44581, SigmaAldrich)

4.1.4 - WB

- Non-Fat Dry Milk (#B501-0500, Rockland)
- PBS-TWEEN Tablets (#524653-1EA, Calbiochem)
- SuperSignal West Femto Maximum Sensitivity Substrate (#34095, ThermoScientific)
- 10x Tris/Glycine Blotting Buffer (#161-0771, Bio-Rad)
- Ethanol absolute, denatured (#K928.4, ROTH)
- Chromatography Paper 17 CHR (#3017915, Whatman)
- Roti-Load sample loading solution (#K929.1, Carl Roth GmbH, Karlsruhe, Germany)
- Novex 4-20% Tris-Glycine Gel, 12 well (#XP04202BOX, Invitrogen, Thermo Fisher)
- Page Ruler Plus Prestained Protein Ladder (#26619, Thermo Scientific)
- Immobilon-P Transfer Membrane, PVDF, 0.45µm pore size (#IPFL00010, Millipore, Thermo Fisher Scientific)
- SuperSignal West Femto Maximum Sensitivity Substrate (#34095, Thermo Fisher Scientific)



4.1.5 - Equipment

- Savant DNA120 SpeedVac Concentrator (ThermoFisher Scientific)
- PowerPac™ Basic Power Supply (Bio-Rad)
- ImageQuant™ LAS 4000 (GE Healthcare Life Sciences).
- Nanodrop 2000C Spectrophotometer (ThermoFisher Scientific)
- XCell SureLock® Mini-Cell gel electrophoresis system (#EI0001, Thermo Fisher Scientific)
- XCell II Blot Module (#EI9051, Invitrogen)
- LI-COR C-Digit Blotscanner (LI-COR Biotechnology-GmbH, Bad Homburg vor der Höhe, Germany).
- Power supply device Biometra (Biometra GmbH, Göttingen, Germany)
- MicroStart 17R microcentrifuge (VWR)
- 5804 R Centrifuge (Eppendorf)
- Dry Bath/Block (#88870001, ThermoFisher Scientific)
- SureCycler 8800 (Agilent Technologies)
- EpreDia™ Lab Vision™ PT Module (#A80400012, Fisher Scientific)
- RM2125 RTS Microtome (Leica)
- Tecan Infinite M200 PRO microplate reader (Tecan, Männedorf, Switzerland).
- Olympus BX43 Microscope (Olympus, Shinjuku, Tokio, Japan)
- Olympus DP22-SAL camera
- Chromas v2.6.6 (Technelysium Pty. Ltd. Australia)
- Nanodrop2000 v1.4.1 (ThermoFisher Scientific)

4.1.6 - Informatic resources

Online tools

- ClinVar - <https://www.clinicalgenome.org/>
- Cool Angle Calc - <https://danielzuerrer.github.io/CoolAngleCalcJS/>
- DisGeNet - <https://www.disgenet.org/>



- gEAR portal - <https://umgear.org/>
- Gene Burden Tool Kit - https://github.com/AlbaEB/gene_burden_toolkit
- Gene Ontology (GO) - <http://geneontology.org/>
- GeneCodis - <https://genecodis.genyo.es/>
- Hereditary Hearing Loss Homepage - <https://hereditaryhearingloss.org/>
- HPO - <https://hpo.jax.org/app/>
- KEGG - <https://www.genome.jp/kegg/>
- MANTA - <https://github.com/Illumina/manta>
- MGI - <https://www.informatics.jax.org/>
- OligoAnalyzer™ Tool - <https://eu.idtdna.com/calc/analyzer>
- OMIM - <https://www.omim.org/>
- Panther - <https://www.pantherdb.org/pathway/>
- Primer3web - <https://primer3.ut.ee/>
- PrimerBlast - <https://www.ncbi.nlm.nih.gov/tools/primer-blast/>
- Reactome - <https://reactome.org/>
- SAMTOOLS - <https://samtools.github.io>
- SVDB - (<https://github.com/J35P312/SVDB>,
- TIDDIT - <https://github.com/SciLifeLab/TIDDIT>
- Uniprot - <https://www.uniprot.org/>
- BioGPS - <http://biogps.org/#goto=welcome>
- GTEX - <https://www.gtexportal.org/>

Equipment

- Workstation: AMD Threadripper RX with 32 cores and 128 GB RAM.
- Server: NAS Synology Rack (3 U) RS3617xs with 100TB of storage.



4.2 - Methods

The methods section is also separated according to the three chapters indicated in the objectives.

Chapter 1

Analysis of the prevalence of ES hypoplasia in patients without MD

4.2.1 – Recruitment of non-MD patient cohort

A retrospective analysis of five millimeters thick ear CTs, in the axial plane, and without intravenous contrast were performed in the Radiodiagnostic Department of Hospital San Cecilio Granada (Spain), and Hospital Reina Sofía in Córdoba (Spain). The corresponding patients were evaluated to eliminate patients with MD or suspected MD from the study. Exclusion criteria were: i) Definitive diagnosis of MD, according to the diagnostic criteria described by the International Classification Committee for Vestibular Disorders of the Barany Society (108); and ii) young patients (<40 years old, and CT performed with <40 years old) with a clinical history of low-frequency SNHL, recurrent vertigo and tinnitus. The set of patients finally included will be referred as "non-MD cohort".

Patients were anonymized by clinical specialty students in the Radiodiagnostic Departments of both hospitals. Age, sex, and clinical diagnosis were collected in the study database.

Axial CT planes were obtained for both ears of each control. As many CT images axial planes were collected per ear as necessary to visualize correctly i) the vestibule and the horizontal semicircular canal, and ii) the exit of the VA from the TB (operculum).

4.2.2 - ATVA radiographic marker analysis

ES endotype classification was carried out analyzing ATVA marker on CT images. In MD cases, ES hypoplasia is defined when ATVA $>140^\circ$ and ii) ES degeneration when ATVA $<120^\circ$ (155). In the case of controls, our reference ATVA values were defined in a cohort of 62 control adults with an ATVA of 102.3 ± 9.8 degrees, with maximum value of 76.8° and minimum of 119.1° (155) ATVA was calculated with the Cool Angle Calc online tool (<https://danielzuerrer.github.io/CoolAngleCalcJS/>). Two double-blind measurements were performed for each image by two independent researchers.

As indicated in the section *Endotypes of Endolymphatic Sac in MD* (in the introductory chapter of this thesis), the ATVA marker was defined in histological sections, and later adapted to use it in CT and MRI imaging (Figure 4.1) (155). In histological sections, ATVA marker refers to the angle formed between: i) the entrance trajectory of the VA from the vestibule into the TB (red line I₁), situated most parallel as possible to the walls of the VA and perpendicular to the internal aperture of VA; and ii) the exit trajectory of the VA in the PCF (green line I₂), drawn most parallel as possible to the walls of the VA and perpendicular to the operculum aperture (Figure 4-1, A and C).

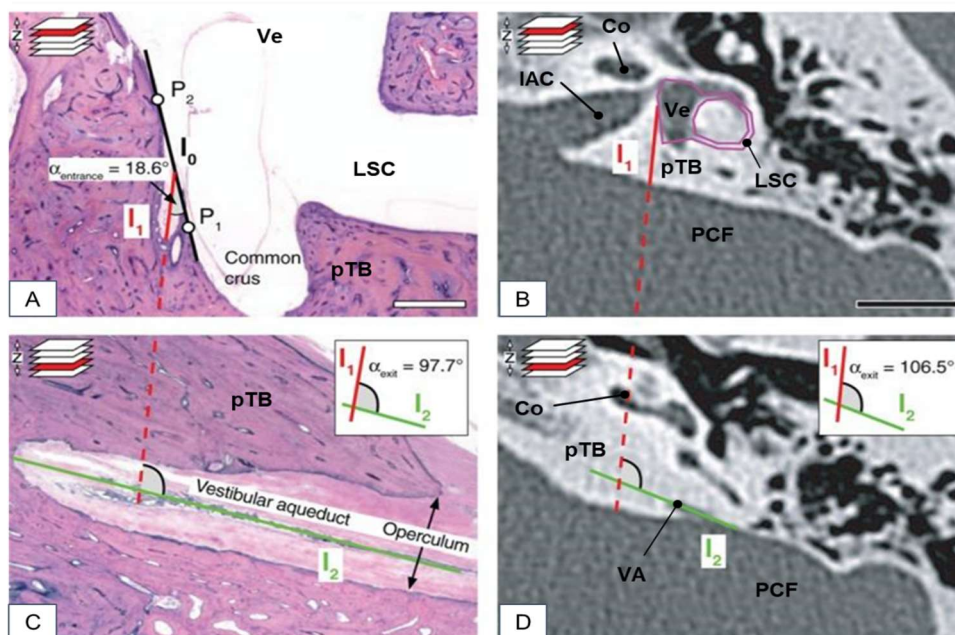


Figure 4.1 - Method to calculate ATVA marker in histological sections (A,C) and CT images (B,D). Scale bars: 1 cm. Figure adapted from Bächinger *et al.* (155). Co: cochlea IAC: internal auditory canal; LSC: lateral semicircular canal; PCF: posterior cranial fossa; pTB: petrous part of the temporal bone; VA: vestibular aqueduct; Ve: vestibule.

In CT sections, a correct visualization of the VA trajectory in its origin from the vestibule is not possible due to the resolution of this type of image. Therefore, the entrance trajectory is predefined as a 14° angle, that is directly placed using the purple shape attached to red line I₁ (Figure 4-1 B). This fixed angle was calculated as the average of multiple entrance trajectories (I₁) from TB of adults control (155). The purple shape must be fitted to the bony limits of the vestibule and the LSC, in the axial plane in which both structures are visualized. The exit trajectory (green line I₂) is correctly visualized and positioned in a similar way as in histological sections (Figure 4-1, B and D).



4.2.3 – ATVA data analysis

The prevalence of the hypoplastic endotype in patients without MD was calculated. Reproducibility between ATVA measurements between the two observers was analyzed by linear regression and visualized with the Bland-Altman method. Normality of the ATVA values was contrasted with the Shapiro-Wilk test, and the relationship of ATVA with the clinical variables (sex, age, and clinical diagnosis) was contrasted with two-tailed T-test. Patients with ATVA between 120-140° were further evaluated to rule out possible hidden MD with less pronounced ES hypoplasias.

Chapter 2

Identification of genes and/or variants associated with hypoplasia of ES in MD

4.2.4 - Recruitment of hypoplastic MD patients

Retrospective analysis of ear CT and MRI images were performed in the ENT (Ear, Nose, Throat – Otorhinolatingology) department of the University Hospital of Zurich. CT and MRI images of patients with a definitive diagnosis of MD, according to the diagnostic criteria described by the International Classification Committee for Vestibular Disorders of the Barany Society (108) were collected. MD patients were excluded; i) if they showed secondary otological pathologies (such as otosclerosis, vestibular schwannoma, history of TB fracture or Cogan syndrome); ii) if they have been diagnostic by probable MD; and iii) if they were affected by comorbidities with MD such as vestibular migraine or AIED. The clinico-radiological study was approved by the local ethics committee (application ZHNr. 2016-01619, Kantonale Ethikkommission, Zurich, Switzerland) in accordance with the Declarations of Helsinki.

As in *Chapter 1*, ATVA marker was measured with the online Cool Angle Calc software. ES endotype classification was carried out on CT images, defining i) hypoplasia when ATVA marker $>140^\circ$, and ii) degeneration when ATVA marker $<120^\circ$, according to Bächinger *et al.* (155) (Figure - 4.1). Two double-blind measurements were performed for each image by two independent researchers.

After the radiodiagnostic ATVA marker analysis, MD patients with ES hypoplastic endotype were included in a clinical database, distinguishing familial or sporadic cases. They were subjected to audio-vestibular evaluation, including PTA.

Individuals were considered as familiar when at least one relative in first or second degree satisfies the criteria for probable or definitive MD. During the meticulous study of familial cases, audio-vestibular assessment and CT/MRI was performed to confirm the presence/absence of hypoplastic endotype in: i) relatives with definitive diagnosis of MD; ii) relatives with overlapping MD audio-vestibular symptoms, and iii) familial controls.



4.2.5 – Whole Exome Sequencing

In the genetic analysis of hypoplastic MD patients classified as sporadic, individuals with disease onset older than 65 years were excluded from WES, trying not to include patients whose ES alterations could be caused by age. In those defined as familiar cases, the relatives that could be useful to discern the segregation of variants in the phenotype in each family, such as individuals showing symptoms overlapping with the disease and/or controls were also sequenced in addition to the proband.

4.2.2.1 - Sample collection, DNA extraction and quality controls

Saliva samples were obtained from patients using the Oragene®DNA kit (Oragene). DNA extraction was performed preiT®.L2P kit (DNA Genotek) following the manufacturer's instructions. To ensure the quality of the genomic DNA, we conducted concentration and quality controls using Nanodrop 2000C (ThermoFisher Scientific) and Qubit (dsDNA BR Assay, ThermoFisher Scientific), respectively. Additionally, to assess the integrity of the gDNA, samples and loading buffer were prepared in (1:4 volume) and loaded in 1.2% agarose gel in 1X TAE buffer marked with GelRed as staining agent and using Direct Load 1kb DNA as molecular weight marker. Electrophoresis was run at 90V and 400mA using PowerPac supply for 1 hour and revealed in ImageQuant LAS 4000.

4.2.2.2 - WES libraries preparation and sequencing

In the preparation of libraries targeting coding regions, SureSelectXT Human All Exon V6 (Agilent Technologies, Santa Clara, CA, USA) (Agilent Technologies, Santa Clara, CA, USA) was conducted following manufacturer instructions (Chen 2015). First, gDNA is fragmented, denatured and hybridized with biotin conjugated oligos targeting coding regions. Streptavidin-paramagnetic beads are used to purify biotin captured fragments that are subsequently amplified and indexed by PCR. This procedure targets around 50Mb of human exonic regions. The quality of the libraries was confirmed using the TapeStation DNA screenTape D1000 (Agilent Technologies, Santa Clara, CA, USA). Sequencing was performed on NovaSeq 6000 platform (Illumina, San Diego, CA) and generated pair-end reads, ensuring a minimum coverage of 100X on average (Macrogen, South Korea)

4.2.6 - Bioinformatic analysis

Several steps can be distinguished in bioinformatics processing of WES data: i) preprocessing, including alignment of reads with reference genome and filtering of low-quality mapped reads; ii) variant calling, identifying changes differing between samples and reference genome; iii) annotation, retrieving information of variant in public databases; and iv) data analysis, to finally discover candidate genes and variants (Figure 4.2). Except for the first step, the approaches for analyzing SNV and short indels on the one hand and structural variants on the other hand were slightly different, so distinct sections for each of these types of variants are distinguished.

Nf-core/sarek nextflow pipeline v2.6.1 was followed as a workflow for the alignment and variant calling for SNV, shorts Indels and SV (164).

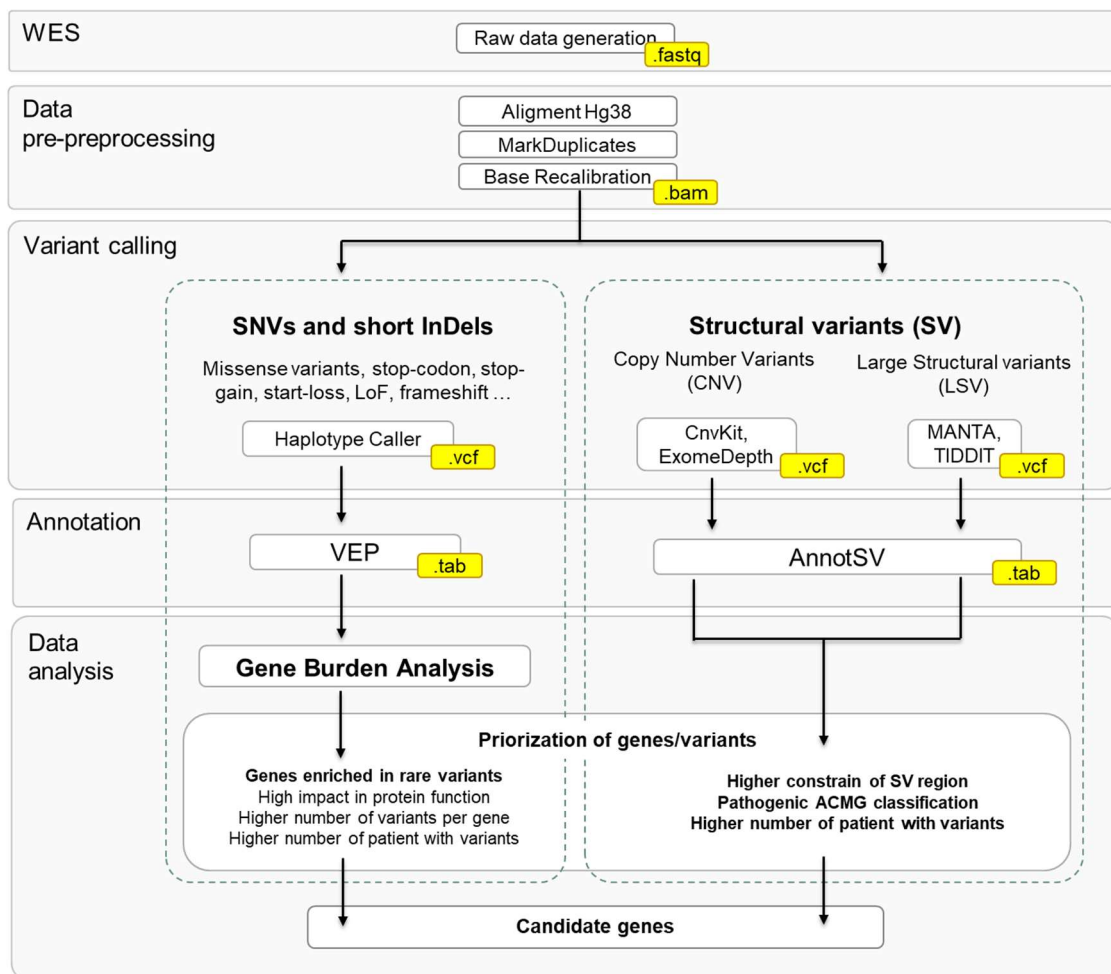


Figure 4.2 - Bioinformatics pipeline for exome data analysis in the discovery of hypoplastic cohort variants in the two types of variants i) SNV and short InDels and ii) structural variants.

4.2.6.1 - Data pre-processing

Paired-end FASTQ files were generated per sample after the sequencing. FASTQ sequences were aligned to the GRCh38/Hg38 reference genome using the Burrows-Wheeler Aligner's Maximal Exact Matches algorithm (BWA-MEM), producing a sorted and indexed SAM (Sequence Alignment Map) file (164). This output is transformed using SAMtools into BAM (Binary Alignment Map) files, the compressed binary version of a SAM file. Smaller BAM files management is more efficient in terms of computation and storage.

Post-alignment processing includes several steps of quality filtering of the BAM files. GATK MarkDuplicates is used for identifying and removing duplicated reads that are likely to have originated from duplicates of the same original DNA fragments, mitigating potential biases from PCR and library preparation. GATK BaseRecalibrator and GATK ApplyBQSR tools apply machine learning to model the accuracy of each base call according to the site where it was aligned, detecting systematic errors made by the sequencing machine (165,166)

Once the recalibrated BAM files are available, they will be used as input for variant calling. Two different protocols are distinguished in the following steps, depending on the type of variant called i) short indels and SNV; and ii) Structural variants.

4.2.6.2 - SNV and short InDels

4.2.6.2.1 - Variant calling

After applying clean-up operations, GATK HaplotypeCaller (164) function was employed to determine genetic germline variants. The resulting VCF (Variant Call Format) files captured SNV and short InDels (< 50bp) from each individual.

To ensure variant quality assessment, hard filtering following by the Variant Quality Score Recalibration (VQSR) was utilized. VCFs from each patient were filtered by the same parameters as gnomAD database: Allele balance (AB) ≥ 0.2 and $AB \leq 0.8$ (for heterozygous genotypes only), genotype quality (GQ) ≥ 20 , and depth (DP) ≥ 10 (5 for haploid genotypes on sex chromosomes) (165,166). After that, filtered VCFs from each patient were combined into a single file using BCFtools from SAMTOOLS (<https://samtools.github.io>), resulting in a VCF dataset containing all variants in our ES hypoplastic cohort (167).

Apart from hard filtering, VQSR was applied to the merged dataset. This tool trains a machine learning model that learns from our dataset and gives us a well-calibrated score (VQSLOD) for the probability of each variant being true or false positive. Subsequently, variants VQSLOD > 10 are excluded (168). This method for quality filtering is more sensitive, flexible, and adapted to our samples than hard filtering, and the scoring results are better the higher the number of samples the model is trained on.

4.2.6.2.2 - Variant annotation

To annotate our hypoplastic VCF dataset file, we utilized the Variant Ensembl Variant Predictor v104 (VEP) platform from Ensembl (169). VEP is a powerful bioinformatics tool designed to recruit information among a vast collection of public databases, providing information about:

- *Consequences of variants*, according to VEP classification as HIGH, MODERATE, MODIFIER and LOW impact, summarized in Table 4.2.
- *Variants frequency on different populations*, incorporating information from gnomAD v3.1 (Genome Aggregation Database) (170).
- *Pathogenicity of variants*, and predictions of deleteriousness, highlighting scores as CADD and ACMG classification.
 - CADD v1.6 (Combined Annotation Dependent Depletion) score integrates annotation based on allelic diversity, conservation, protein functionality and regulatory effects (experimentally tested), pathogenicity and severity of associated traits or diseases. The resulting C score is used to prioritize potentially pathogenic diseases when CADD score is ≥ 20 (171).
 - ACMG consists of a standard guide for variant interpretation updated by the American College of Medical Genetics and Genomics (ACMG), the Association for Molecular Pathology (AMP) and the College of American Pathologists (CAP) in 2015 (172). It classified variants in five categories: 'pathogenic', 'likely pathogenic', 'uncertain significance', 'likely benign' and 'benign', taking into account criteria such as the frequency of the variant in the population and cohort, segregation data, functional data or computer predictive models, among others.

- *Gene conservation and constraint*, with scores as pLi (probability of being Loss of function Intolerant). This metric indicates the probability that a LoF variant in one allele causes an haploinsufficient phenotype, identifying intolerant ($pLi \geq 0.9$) or tolerant ($pLi \leq 0.1$) to LoF variation (173).

Table 4.2 – Consequences of variants according to VEP IMPACT categories

VEP IMPACT categories	Variant consequences	
HIGH	<ul style="list-style-type: none"> • Transcript ablation • Splice acceptor variant • Splice donor variant • Stop gained 	<ul style="list-style-type: none"> • Frameshift variant • Stop lost • Start lost • Transcript amplification
MODERATE	<ul style="list-style-type: none"> • Inframe insertion • Inframe deletion 	<ul style="list-style-type: none"> • Missense variant • Protein altering variant
MODIFIER	<ul style="list-style-type: none"> • Coding sequence variant • Mature miRNA variant • 5 prime UTR variant • 3 prime UTR variant • Non coding transcript exon variant • Intron variant • NMD transcript variant • Non coding transcript variant • Upstream gene variant 	<ul style="list-style-type: none"> • Downstream gene variant • TFBS ablation • TFBS amplification • TF binding site variant • Regulatory region ablation • Regulatory region amplification • Feature elongation • Regulatory region variant • Feature truncation • Intergenic variant
LOW	<ul style="list-style-type: none"> • Splice region variant • Splice donor 5th base variant • Splice donor region variant • Splice polypyrimidine tract variant 	<ul style="list-style-type: none"> • Incomplete terminal codon variant • Start retained variant • Stop retained variant • Synonymous variant

4.2.6.2.3 - Data analysis: Gene Burden Analysis

To find causative genes for SE hypoplasia in MD, Gene Burden Analysis (GBA) approach of SNV and InDels was performed. This method determines whether there is a greater accumulation or “burden” of potentially causative genetic variants in one or more genes in individuals affected by the disease, compared to healthy individuals. With this purpose, several steps can be distinguished: the filtering of potentially causative variants, the calculation of Odd Ratios, and the statistical validation of variants enriched genes. The GBA was carried out with the Gene Burden Tool Kit developed by Alba Escalera-Balsera (https://github.com/AlbaEB/gene_burden_toolkit).



Filtering of potentially causal variants

First, we performed a filtering of the potentially causal variants. Hypoplastic cohort variant dataset will be filtered based on the predicted impact of the variant on protein function, allele frequency and type of variant. We selected:

- Those with rare allele frequency ($MAF < 0.05$) in the general population, following the genetic strategy that multiple genes or causative variants with moderate and additive effects cause the phenotype.
- Those with a great impact on phenotype, which contain HIGH and MODERATE variants described by VEP calculated consequences. HIGH variants comprise InDels, being more deleterious those that involve a change in the reading frame, or punctual LoF variants that can cause the disappearance or appearance of start or stop codons, resulting in total loss of expression, abrupt truncations, or abnormally long non-functional proteins. MODERATE variants include non-synonymous missense variants in which there is an amino acid change as a result of the point base change. These punctual changes may involve crucial amino acids, such as charged amino acids that maintain the structure of the protein through interactions with other residues, amino acids involved in anchorage between subunits or scaffolding with structures, or active site residues in the case of enzymes (169).

Calculation of Odd Ratios

Next, for the filtered dataset of variants, it was examined whether there was a significant accumulation of variants in specific genes in the hypoplastic cohort compared to healthy individuals. In this case, global population and Non-Finish European (NFE) from gnomAD v3.1 (including 76156 genomes) were utilized as control reference population.

For each gene, the number of alleles (AC) with variants for that gene were summarized, where A and C were the allele count in the hypoplastic cohort with and without variants in the X gene, respectively; and B and D the allele count in the control population with and without variants in the X gene, respectively.

Next, Odds Ratio (OR) was calculated by gene. OR is a “measure of association” that compares the probabilities that one event occurs (in this case, the accumulation of variants in a gene of interest) and the risk that the consequence appears (in this case, ES hypoplasia in MD). Thus, the 2x2 contingency table would be as shown:

	Hypoplastic cohort	Control population
AC with variant in gene X	A	B
AC without variant in gene X	C	D

And the OR is then calculated as follow:

$$\text{OR (gene X)} = \frac{\text{AC ratio with/without variants in hypoplastic cohort}}{\text{AC ratio with/without variants in control population}} = \frac{A / C}{B / D}$$

OR significantly greater than 1 indicates that accumulation of rare variants in that gene increases the risk of developing the phenotype. OR significantly lower than 1 denotes a protective relationship, so the absence of variants in that gene minimizes the risk of developing the pathology. OR equal to 1 shows there is no association with this gene.

The magnitude of the association is greater the further OR is from 1. For example, for predisposing factors, the risk of finding ES hypoplasia due to variant accumulation in gene X, with an OR of 10 is much greater than if the variants are present in gene Y, with an OR of 1.2, being both OR relative to the same control population.

Statistical significance of variants enriched genes

To assess the significance of the OR, p value and 95% confidence interval (CI) were calculated. The p value indicates the probability of obtaining the estimated OR if null hypothesis of no association were true. So, real association was considered statistically significant with typical p value < 0.05. To reduce the number of these false positives due to multiple testing, the p-value was corrected for multiple comparisons by the number of genes tested for each data set, following Bonferroni correction. On the other hand, CI provided a range of values around estimated OR in which real OR is with 95% of certainty.

In summary, p value indicates the statistical significance of the association between the enrichment of variants in that gene and the phenotype, and 95% CI provides a measure of the precision of this estimated OR. Genes significantly enriched in accumulation of variants in our cohort versus population databases were taken into account for the prioritization of candidate genes and variants.

4.2.6.2.4 - Prioritization of candidate genes and variants

In the gene prioritization process, the following was taken into account: i) the significance of variants enrichment genes; ii) the presence of FLAG genes; iii) the allele frequency per gene in the ES hypoplastic cohort, and lastly iv) the information available in different databases about gene expression (systemically and in the inner ear), or previous association with specific phenotypes, especially audio-vestibular ones. In the variant prioritization, it was considered: i) the number of variants per gene and the segregation of these variants among affected individuals; ii) the consequence of the variant, the allelic frequency and the prediction of pathogenicity. A list of candidate genes was generated once the prioritization process was completed.

Enriched variants genes vs control population

Genes that showed significant variants enrichment, p-value corrected < 0.05 , with respect to the two reference populations: gnomAD global and gnomAD nfe were considered.

FLAGS genes

FLAGS genes (from FrequentLy mutAted GeneS) were excluded. These genes have been observed to accumulate rare variants in healthy individuals due to their larger length, or high mutation rate due to genomic instability or DNA repair deficiencies (174).

Allele frequency per gene in the ES hypoplastic cohort

An additional filter was made to retain only those genes whose variants were present in 5% or more of our hypoplastic cohort. This 5% threshold was the same as that used in the variant filtration process prior to the GBA.

Expression data and associated phenotypes

Functional annotations available in public databases were consulted, such as:

- ***Expression data.*** We focused on expression data from gEAR portal (<https://umgear.org/>). gEAR is a web platform that provides access to gene expression profile of inner ear and related organs (cochlea, vestibule, PCF, spiral ganglia, etc) from numerous studies, including RNA-seq, single cell RNA-seq, microarray-based gene expression data, and in situ hybridization (ISH) analysis. In addition, expression data is available from a wide range of model organisms and during different stages of development.



- *Previous association with specific phenotypes.* Phenotypic HPO or MGI terms previously related to our genes were consulted. Human Phenotype Ontology (HPO) (<https://hpo.jax.org/app/>) terms have been described from associations of patient clinical data and phenotypes with genes or genotypes in numerous diseases, disorders and syndromes in humans. On the other hand, Mouse Genome Informatics (MGI) (<https://www.informatics.jax.org/>) gives access to phenotypes described in mice mutant strains altered in specific genes (<https://www.informatics.jax.org/>). Terms can be filtered to obtain those of interest, for example, with an audiovestibular phenotype.
- *Previous association with audiovestibular diseases, SNHL, sporadic or familial Meniere's disease.* With special consideration to genes previously associated with SNHL retrieved from the Hereditary Hearing Loss Homepage (<https://hereditaryhearingloss.org/>) (175).

Number of variants and segregation between individuals

The most important aspect was the number of variants per gene and if they are shared between affected individuals. Variants with higher number of variants and those shared between higher number of individuals were prioritized.

Within these genes, it was observed if variants were close in their chromosomal coordinates, which could suggest that modifications in these specific protein domains could be related to function impairment and risk of developing the phenotype.

Variant consequence, allele frequency, and prediction of pathogenicity

Discovered variants were annotated using VEP, adding information about impact/consequence of variant in the protein, allele frequencies from gnomAD (v3.1), and pathogenicity prediction from CADD. Variants with lower MAF, higher variant consequence according to VEP, and more pathogenic scores (CADD \geq 20 and to “pathogenic” or “likely pathogenic” ACMG classifications) were prioritized.

4.2.6.3 - Structural variants

4.2.6.3.1 - Variant calling

Each type of SV, LSV and CNV, were called by two different tools using BAM files as inputs. In this way we will be able to compare the reproducibility that exists for SV calling in exome data. LSV were called by the tools MANTA v2.6.0 (Illumina, <https://github.com/Illumina/manta>) (176) and TIDDIT v3.5.2 (SciLife, <https://github.com/SciLifeLab/TIDDIT>) (177), within the Nf-core/sarek nextflow pipeline. Meanwhile, CNV were called by CnvKit v0.9.10 (<https://github.com/etal/cnvkit>) (178).

MANTA, TIDDIT and CnvKit generated a VCF with SV calls for each individual, including large insertions, deletions, duplications and transversion in the case of LSV, and duplication and deletion for CNV.

4.2.6.3.2 - Filtering of false positive SV

These tools carry out several filtering steps to detect artifacts caused by contamination and sequencing errors, misalignments of repetitive regions with the reference genome, and inconsistencies with the ploidy of the studied species. High quality variants are labeled as PASS in the FILTER column. Quality filtering steps were performed in each VCF separately, removing i) low-quality variants not marked as PASS and ii) variants with length outside the range of 100,000bp. Variants longer than 100,000bp are usual artifacts generated by the tool.

4.2.6.3.3 - Overlapping of SV

Subsequently, filtered variants of each individual were merged using the SVDB merge toolkit v2.8.1 (<https://github.com/J35P312/SVDB>), specifying to join those variants whose starting point were not far than 10,000bp and overlapped in length by at least 60%. Two datasets of overlapped LSV, from TIDDIT and MANTA, and one dataset of overlapped CNV from CnvKit were generated. LSV replication between TIDDIT and MANTA was compared by contrasting both sets of calls obtained at this level.

4.2.6.3.4 - SV annotation

The overlapped SV datasets were then annotated with AnnotSV v3.3.6 (179). AnnotSV collects available information on public databases about structural variants in the same way as VEP for SNV and short InDels, with some additional information specific to SV.



- SV frequency, from databases such as DGV, 1000G, or gnomAD.
- Mutation tolerance and constraint data, including pLi (180) from gnomAD and ExaC, and LOEUF bin (181). LOEUF, the loss-of-function observed/expected upper bound fraction" (LOEUF), represents a conservative estimation of the ratio of observed to expected LoF variants. LOEUF is binned into deciles ranging from 0 (most depleted/evolutionarily constrained) to 9 (not depleted/constrained). A LOEUF bin value ≤ 2 was subsequently considered constrained to prioritize SV.
- Pathogenicity of genes or genomic regions and predictions of deleteriousness with scores such as the ACMG classification for SV.
- Phenotypes associations from databases such as Exomiser and HPO.
- Disease associations from databases such as ClinVar (<https://www.clinicalgenome.org/>) or the Online Catalog of Human Genes and Genetic Disorders (OMIM - <https://www.omim.org/>)

4.2.6.3.5 - SV Data analysis and prioritization of candidate variants

After filtering, overlapping, and annotation, SV in non-coding regions were removed, since exome capture does not include these regions and coverage is not sufficient for variants discovery. SVs were then prioritized based on conservation and pathogenicity scores. Candidate variants were those shared by more individuals, localized in regions with higher constraint ($pLi \geq 0.9$) and classified as "pathogenic" or "likely pathogenic" by ACMG. Variants in FLAGs genes were also discarded.

4.2.6.4 - Candidate variants in hypoplastic MD families

Due to the low number of samples per family, it was not possible to perform segregation analysis itself. For this reason, the study of families was limited to detecting whether the candidate variants in the MD and ES hypoplasia cohort study were present in the probands and available relatives, and if so, whether they segregated with the phenotype.

4.2.6.5 - Candidate variants for low-frequency SNHL in family 5

In family 5, in addition to the presence of hypoplasia and MD disease in some of their relatives, low-frequency SNHL segregated in five individuals across three generations with a clear pattern of autosomal dominant inheritance.

Since SNHL is a pathology associated with genetic causes in its different types: syndromic or non-syndromic, described in various inheritance patterns (autosomal dominant or recessive, sex-linked and mitochondrial), and knowing that SNHL affecting low frequencies have been associated with early stages of MD, this phenotype within this family was studied to find candidate variants that could explain SNHL.

4.2.6.5.1 – Data pre-processing

Exome data pre-processing steps were carried out with the rest of the hypoplastic cohort, including alignment of reads with GRCh38/Hg38 reference genome, generation of BAMs files, filtering of low-quality mapped reads, variant calling of SNV and InDels, VQSR quality assessment and annotation, as described in chapter 4.2.6.1 and 4.2.6.2.

Following this, variants from family 5 including low-frequency SNHL affected individuals and one control for the phenotype were separated in a database for subsequent analysis.

4.2.6.5.2 – Filtering and prioritization of candidate variants

Familiar database was filtered including those variants shared between the five relatives segregating low frequency SNHL (I-4, II-4, II-5, III-1, and III-2), but absent in II-3. A Single Variant Analysis (SVA) strategy was followed, where it is expected that one single variant with great effect in the phenotype will be the cause of the phenotype.

Therefore, selected variants were those classified as “HIGH” or “MODERATE”, according to VEP protein consequences. Taking into account that the prevalence of SNHL at low frequencies is a very rare condition, which has been estimated at 18 out of 100,000 individuals, a MAF ≤ 0.001 in the non-Finnish European population (gnomADv3.1) has been used to filter variants. In addition, a pathogenic CADD score ≥ 20 thresholds were used as threshold. Variants found in FLAGS genes were discarded.

Finally, of the filtered variants, those with higher impact on protein consequence, a “pathogenic” or “probably pathogenic” classification according to the ACMG, and higher



CADD were prioritized. It was also taken into account that the gene had expression data in the inner ear (gEAR portal).

4.2.6.5.3 – Computational modelling

The human CENPP amino acid sequence was retrieved from Uniprot (Q6IPU0). To find a suitable template for CENPP (greater than 40% identity between aligned primary amino acid) a protein BLAST was performed. No structures were found that could be used for template-based modelling.

Besides, structural model template-free (fold-recognition and de novo or ab initio methods) prediction employing Robetta-AB (182), C-QUARK (183) and C-I-TASSER (184) servers. These model structures were also compared with the model generated by AlphaFold (185). The quality and reliability between modelled and predicted models were assayed by calculation of Molprobity Score, Verify3D, ERRAT, ProSA-web and QMEANDisCo metrics.

Subsequently, the mutated version of CENPP protein (C283*) was generated by comparative homology modelling using Modeller 10.1 (186). The wild type CENPP protein model previously obtained as a template. Stability prediction of mutated CENPP was assessed by SCOOP (187).

Chapter 3

Validation of genes and variants associated with hypoplasia of of ES in MD

4.2.7 - Candidate variants validation

The final list of candidate variants (SNV, InDels and SV) were inspected in the Integrative Genome Viewer (IGV, v2.16.0) (188). Variants suspected to be false positives or variants with lower coverage were validated by capillary Sanger sequencing.

Primers were designed flanking the variant regions using Primer3web v4.1.0 (189) (Kõressaar 2018) (<https://primer3.ut.ee/>). The specificity for amplification of the region of interest in human and the absence of heterodimer formation between forward and reverse primers were verified in PrimerBlast (<https://www.ncbi.nlm.nih.gov/tools/primer-blast/>) (190) and OligoAnalyzer™ Tool (<https://eu.idtdna.com/calc/analyzer>), respectively. The sequence of the primers are indicated in Supplementary Table 1.

The specific region was amplified by PCR following 15 times of major cycle (95°C for 15s, 61°C for 15s, and 72°C for 30s), 10 times of medium cycle (95°C for 15s, 60°C for 15s, and 72°C for 30s) and 10 times of end cycle (95°C for 15s, 59°C for 15s, and 72°C for 30s) in a SureCycler 8800 thermocycler (Agilent). The reaction volume was 20ul including the sample, isovolumetric mixture of forward and reverse primers, Master Mix and molecular biology grade water in 1:2:7:10 proportions. To verify amplification to the expected size, PCR products were diluted 1:5 with loading buffer and loaded in 2% agarose gel in 1X TAE buffer marked with GelRed as staining agent and using 100bp DNA Ladder as molecular weight marker. Electrophoresis was run at 90V and 400mA using PowerPac supply for 1 hour and revealed in ImageQuant LAS 4000. PCR fragments were then purified with MicroElute® Cycle Pure Kit and sequenced by using Sanger technology in an ABI 3730XL sequencer (STAB-VIDA. Caparica, Portugal). Chromatograms were inspected for variant validation using Chromas v2.6.6 (Technelysium Pty. Ltd. Australia).



4.2.8 - Evaluation of inner ear candidate genes expression

4.2.8.1 - Animals

57BL/6 mice of both sexes and aged 3 to 5 days were acquired from the Charité-Universitätsmedizin Berlin animal facility. The study was conducted in accordance with the recommendations of the EU Directive 2010/63/EU on the protection of animals used for scientific purposes. The experimental protocol was approved by the Government Ethics Commission for Animal Welfare.

4.2.8.2 - IHC

Preparation of mouse head paraffin section

Mice were sacrificed by decapitation. The top of the skull was cut off to expose the inner ear tissues for fixation. Unnecessary tissues such as the ears, mouth and most of the skin were trimmed as much as possible to facilitate the fixative entry.

The materials were immediately placed in 10 ml 4% formaldehyde fixative solution for 3 hours while shaking at room temperature. Excess of fixative was removed by three baths in 1X PBS of 15 minutes each. Subsequently, pieces were placed in EDTA decalcification solution overnight. On the second day, dehydration begins by placing the tissues in 50% ethanol for 30 minutes and later in 70% ethanol overnight at 4°C. On the third day, dehydration was continued as follows: 80% ethanol, 90% ethanol, 95% ethanol, 2x 100% ethanol, each for one hour. All the indicated steps of fixation, decalcification and dehydration were carried out at room temperature with shaking (100 rpm), except for the incubation with 70% ethanol, which was performed at 4°C to avoid evaporation overnight. The amount of the different reagents was sufficient to generously cover the tissue.

Afterwards, the tissues were transferred to paraffin block cassettes and embedded in 70°C pre-warmed paraffin for 1 hour inside the oven. Later, the cassettes were immersed in new, fresh paraffin overnight.

On the last day, the pieces were placed in the metal molds that will form the blocks for subsequent cutting. The heads were positioned to obtain axial cuts sections. After covering the tissue with hot paraffin, new cassettes were put on top forming a solid block with the paraffin, and were left to solidify at 4°C.

Once hardened, the cassette was separated from the metal block and cut. Axial sections of the mouse head were made on an RM2125 RTS microtome (Leica) with a



thickness of 5 micrometers. They were allowed to dry on the slides in an oven at 37°C for at least 16 hours.

Immunolabelling

The sections were deparaffinized by 2 xylene baths of 10 minutes each. Dehydration was then initiated with 5-minute baths in descending concentration of ethanol until distilled water. Next, antigenic retrieval was performed in an EpreDia™ Lab Vision PT Module (Fisher Scientific) for 20 minutes at 95°C in citrate buffer. The tissues were then tempered in distilled water.

The sections were incubated with 3% H₂O₂ in methanol to block endogenous tissue peroxidase. This was followed by 3X 5-minute washes in 1X PBS. Specific antigenic sites were then blocked by incubating with normal horse serum for 30 minutes and 1x Casein Solution for 30 minutes. Once the last blockade has been removed, the necessary volume of diluted primary Ab is added to cover the tissue (approximately 50-70 ul) and incubated at 4° C overnight. The appropriate primary Ab dilutions were previously optimized (Figure 4.1). The technical controls were incubated with 1X casein solution only.

The next day, the tissues were bathed 3X in 1x PBS, 5 minutes each, and then a few drops of 2nd Ab are added, and incubated for 1 hour at RT. This 2nd Ab is conjugated with the enzyme horseradish peroxidase. Three 5-minute baths with 1X PBS are performed to remove excess of 2° Ab. After the last bath, revealing is carried out by adding peroxidase Diaminobenzidine substrate solution, being observed under the microscope. The target-protein tissues were observed first and allowed to react until a specific signal was seen but no general background was yet apparent (45 seconds for Adamts18). Negative controls for both proteins were each incubated for the same time respectively.

Finally, counterstaining and mounting is performed. Sections were stained with haematoxylin for 30 seconds and then dehydrated by rapid washing in increasing ethanol solutions until xylene. Finally, DPX mounting fluid was added, covered with a coverslip and dried for 24 hours. All 1X PBS washes in this protocol are performed with shaking.

The sections were observed in a light microscope Olympus BX43 (Olympus, Shinjuku, Tokio, Japan), and the images captured with an Olympus DP22-SAL camera at different magnifications.



4.2.8.3 - WB

Protein extraction and quantification

Mice were sacrificed by decapitation and target tissues were dissected including the cochlea, vestibular organs, otic capsule and control tissues. Positive cerebellum and negative spleen control tissues were chosen according to the expression data in both mouse and human systemic expression databases BioGPS (<http://biogps.org/#goto=welcome>) and GTEX (<https://www.gtexportal.org/>). Pieces were immediately placed in 1X RIPA buffer at 4°C and homogenized mechanically using a pestle. Proportions tissue/RIPA buffer were: 6 cochlear ducts from both ears of 3 animals in 100ul RIPA, 1 complete vestibular system (part of vestibule and 3 SCC) from one ear in 100ul RIPA, and 5mg of tissue from cerebellum, spleen and otic capsule in 300ul RIPA. Extracts were then incubated at 4°C for 10 minutes with regular vortexing. Not disaggregated tissue residues were precipitated by centrifugation at 14,000 rpm for 10 minutes, and the supernatant was stored in a new tube.

The Micro BCA™ Protein-Assay-Kit (Thermo Scientific) was used to quantify protein concentration according to the manufacturer's instructions. In brief, 1:20 dilutions of the samples were prepared in 0.9% NaCl. For both samples and standards, 150 µm of the dilutions were added to a plate along with 150 µm of the reaction mixture (isovolumetric mixture of reagents A, B, and C from the kit). The mixture was incubated at 37° for 2 hours and revealed by measuring absorbance at 595 nm in the Tecan Infinite M200 PRO microplate reader (Tecan, Männedorf, Switzerland). Proteins are stored at -80° until use.

SDS-page and immunoblot

For each extract, mixtures containing 30 ug protein were prepared with Roti-Load loading buffer and heated at 90°C for 5 min to denature the proteins. Samples were then loaded onto a 4-20% Tris-Glycine Mini Gel. Electrophoresis was performed in an XCell SureLock® Mini-Cell tank at 180 V for 1 hour. Page Ruler Plus Prestained (Thermo Fischer Scientific) was used as a molecular weight marker.

For membrane transfer, the PVDF membrane was previously activated in absolute ethanol for 30 seconds and equilibrated in transfer buffer (distilled water:Tris-Glycin Blotting buffer:ethanol absolute 8:1:1) for 5 minutes. The transference sandwich was prepared in the XCell II Blot module including sponges, gel, and activated PVDF membrane. The transference took 44 minutes at 300 mA generated by the Biometra Power supply device. Later, the membranes were incubated in blocking solution (5%

skimmed milk powder in 0.1% Tween20 in PBS 1X) for 1 hour. After blocking, the membrane is incubated with primary antibody at a dilution of 1:1000 in blocking buffer overnight at 4°C in orbital shaking. Next day, the membrane was washed three times for 10 minutes in 0.1% Tween20 in 1X PBS and incubated for 1 hour at room temperature with the secondary antibody at a dilution of 1:5000 in blocking solution. Excess of secondary antibody was removed from the membrane by washing three times for 10 minutes. Chemiluminescent signal was revealed by incubation with SuperSignal West Femto Maximum Sensitivity Substrate (Thermo Fisher Scientific) according to the manufacturer's instructions and visualized using the LI-COR C-Digit scanner.

Membrane quantification was measured using ImageJ (v1.53). Intensity signals per organ were normalized against the constitutive β -catenin gene. The means of expression between organs were compared with T-test, considering significant differences with p value < 0.05.

4.2.9 - Evaluation of rare variants in protein structure or expression

Information on the different proteins, including their domains and their subcellular compartmentalization, the presence of post-translational modifications (glycosylation, disulfide bonds ...) and their isoforms was obtained from UniProt (<https://www.uniprot.org/>). The candidate variants identified as a result of GBA in our cohort of patients with ES hypoplasia and MD was evaluated in the protein motifs. The modification of the residues was evaluated in terms of hydrophobicity and charge.

4.2.10 - Functional analysis of candidate genes

Genomic studies give us a large number of altered genes for our hypothesis. Instead of addressing each entity (gene) separately, an enrichment analysis or functional analysis will allow us to manage the entire results. In this way, the number of genes in the input dataset belonging to a specific is counted and compared with the total number of genes of that reference pathway. Therefore, it is calculated if there is a significant enrichment of entities in my dataset for that pathway, estimating a p-value that represents the significance of this association (181).

To perform the functional analysis, we used the GeneCodis (191) to explore the gene dataset that we obtain from our GBA of patients with MD and ES hypoplasia. The



idea is to elucidate the biological pathways that could be involved in our phenotype. In our study, we explore the pathways databases Gene Ontology (GO - <http://geneontology.org/>) including molecular functions (GO-mf), biological pathways (GO-bp) and cellular compartments (GO-cc), Panther (<https://www.pantherdb.org/pathway/>), Reactome (<https://reactome.org/>) and KEGG (<https://www.genome.jp/kegg/>); but also phenotypes databases, such as MGI and HPO; and diseases databases OMIM and DisGeNET (<https://www.disgenet.org/>).

Since diseases databases usually associated one single gene with a pathology, obtaining high amount of enriched diseases, co-annotation analysis will be perform with OMIM and DisGeNET, where we will obtain only the entities that replicate between both databases for the same genes, specifying a minimum number of 3 genes.



5. Results



5.1 - Chapter 1: study of the prevalence of ES hypoplasia in individuals without MD



Brief justification of Chapter 1

The main hypothesis of this thesis is that there is a genetic contribution explaining ES hypoplasia in patients with MD. For this purpose, in Chapter 2 we have performed a rare variant analysis ($MAF \leq 0.05$) by gene burden tests to target candidate gene for ES hypoplasia.

According to the studies carried out by Andreas Eckhard and David Bachinger (32,155), ES hypoplasia has been found in approximately 1 of 4 MD patients. Taking into account that the prevalence of MD in the European population is 1-2 per 2000 individuals (0.0005), the inferred prevalence of ES hypoplasia in the general population would be 1/4 of 0.0005, that is, 0.000125 (1-2 each 10.000), or practically nonexistent. However, in these studies, less than 100 CT and their respective TB were available from control individuals. This number of controls is not enough to confirm that ES hypoplasia is absent in the general population.

Therefore, the Chapter 1 of this thesis was proposed to confirm that ES hypoplasia does not exist among the general population, and if it exists, to estimate its real prevalence.

Since we cannot obtain CT images from the general population, we design a cross-sectional study to estimate the prevalence of ES hypoplasia by selecting CT images that have been requested in the ENT Department for different pathologies. We selected 5 mm thick CT scans focused in the ear planes, which have sufficient resolution to visualize the vestibule, the SSC and AV. These specific CT scans are performed on patients who had attended the ENT service, and therefore, patients suspected of suffering from some audio-vestibular or TB pathology. So, we finally got a "non-MD patient" cohort, rather than a "control" cohort.

Patients with a diagnosis of MD, indications that they may develop, or patients younger than 40 years and who had two or three overlapping symptoms, including vertigo, tinnitus, or SNHL were excluded.

5.1.1 - Cohort of patients without MD

Bearing in mind that 1-2 hypoplastic ES can be found every 10,000 individuals, our control cohort without MD should at least have such a number of individuals. However, given the magnitude of these amounts, the real target was established to get 500 individuals (1000 ear CT). Since this is a longitudinal study that has not yet been completed, data from 175 patients processed so far are shown in this chapter as our non-MD patients. Finally, 332 CTs were evaluated, after removing 25 ears in which it was not possible to measure ATVA due to image quality. The distribution of age, sex, country of origin, enrolled hospital and patient diagnosis is described in table 5.1.

Table 5.1 – Cohort of non-MD patients. Continuous variables are described as the mean \pm standard deviation. Discrete variables are indicated as the number of individuals per category and the percentage represented.

Variable		Variable	
Age	59.3 \pm 11.9	Diagnosis	
Sex		Chronic otitis media	60 (38.2%)
Female	84 (52.90%)	Conductive hearing loss	29 (18.50%)
Male	74 (47.10%)	No specific diagnostic	17 (10.8%)
Hospital		External ear pathology	13 (8.3%)
Cordoba	68 (42.70%)	Acute otitis media	12 (7,60%)
Granada	89 (56.70%)	Sensorineuronal hearing loss	10 (6,4%)
Country		Vertigo	5 (3.2%)
Spain	154 (98.01%)	Serous otitis media	4 (2,5%)
Germany	1 (0,6%)	Tinnitus	3 (1.9%)
UK	1 (0,6%)	Facial paralysis	2 (1.3%)
Morocco	1 (0,6%)	Mixed hearing loss	2 (1.3%)

The categories for which patients underwent CT were classified into 11 diagnostic categories including: vertigo, tinnitus, sensorineural hearing loss, conductive hearing loss, mixed hearing loss, serous otitis media, acute otitis media, chronic otitis media, external ear pathology and facial paralysis. External ear pathology included tympanic perforation, granuloma, polyp, external otitis, osteoma, exostosis and stenosis. Patients who did not fit into the previous categories were included in the category of "without specific diagnosis"

including tympanoplasty, otorrhea, bone labyrinth alteration, ear cyst, otalgia, occupation, unspecified ear pain or discomfort, mastoid pain, trauma/contusion, headache, cancer or eardrum collapse.

Patients presenting any of the symptoms of MD or vertigo were carefully examined (Figure 5.1), finding 41 (83.7%), 5 (10.2%), and 3 (6.1%) individuals with hearing loss, vertigo, and tinnitus, respectively. Of the 5 patients with vertigo and 3 with tinnitus, only one woman with tinnitus over 40 years of age was also affected with hearing loss in the right ear, but it had a conductive origin. In the patients with hearing loss, the 70.7% had conductive hearing loss, discarding the neurosensorial basis of the hearing loss in most of these individuals, and therefore MD. None of the 10 (24.4%) patients with SNHL and 2 (4.9%) patients with mixed hearing loss had also experienced vertigo or tinnitus.

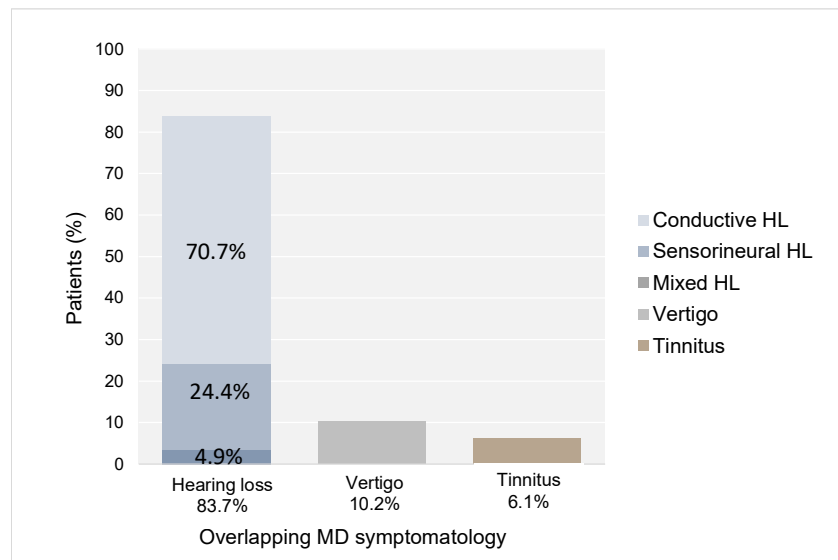


Figure 5.1 – Patients with overlapping MD symptoms.

5.1.2 - ATVA measurements

ATVA measurements were performed on magnifications of axial planes in the petrous part of the TB, in the area corresponding to the ear (Figure 5.2).

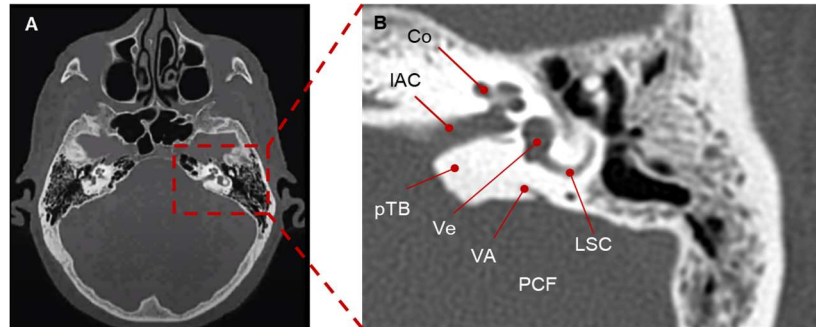


Figure 5.2 - A) 5 mm thickness head axial CT. B) Magnification of the TB in the area of the left ear. Co: cochlea; IAC: internal auditory canal; LSC: lateral semicircular canal; PCF: posterior cranial fossa; pTB: petrous part of the TB; VA: vestibular aqueduct; Ve: vestibule.

In most ears, two CT planes for each ear were needed, one to visualize the vestibule and LSC and a second one where the AV exit to the PCF could be differentiated (Figure 5.3, A). Only in some patients the complete measurement could be performed on the same image (Figure 5.3, B).

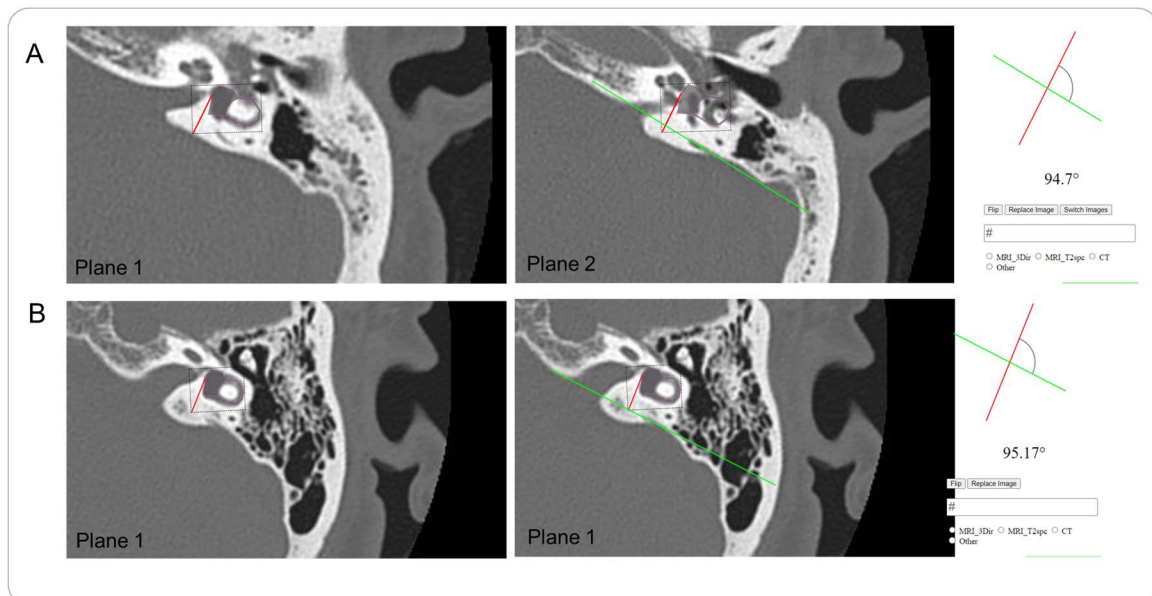


Figure 5.3 - Examples of ATVA measurements with the CoolAngle Calc software in two left ears (A and B) from two patients in our non-MD patient cohort, following the methodology previously explained in Figure 4.1. Panels A and B show sequential images of the ATVA measurement process in two ears that required one or two planes, respectively. The software provides the angle directly next to the image. In this case, ATVA angles were 95.17° in A ear, and 94.7° in B ear.

The agreement between the ATVA measurements between both observers was evaluated with a linear regression and the Bland-Altman plot. The regression indicates that there is a positive linear correlation between the measurements of the two observers, with a correlation coefficient of 0.7, showing some dispersion (Figure 5.4, A). The Bland-Altman plot shows bad inter-observers ATVA concordance in only 15 ears of 332 (4.5%) (Figure 5.1, B).

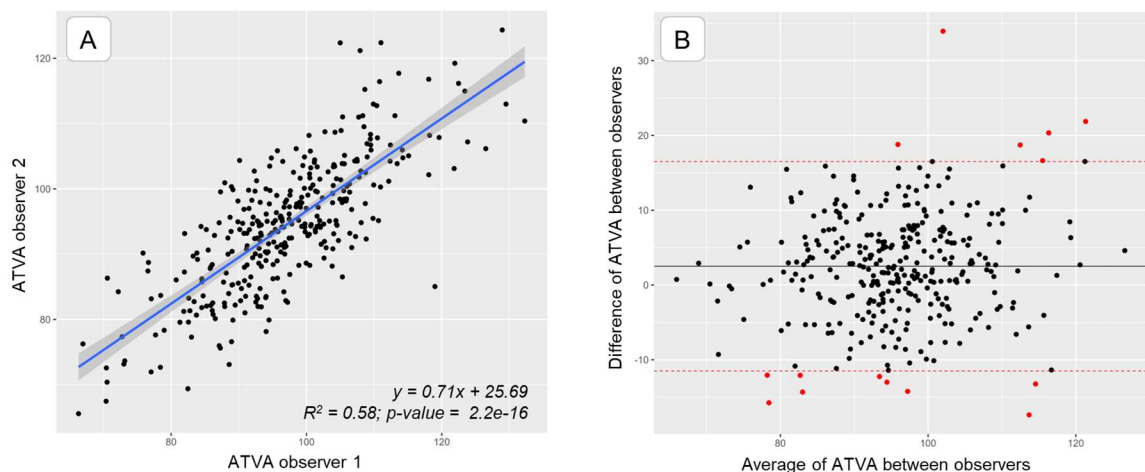


Figure 5.4 - Evaluation of ATVA concordance between observers. A) Linear regression between ATVA measured by the two observers. B) Bland-Altman plot. The x-axis shows the mean ATVA between observers. The y-axis shows the difference of the ATVA values measured between observers per ear. The black line indicates the mean of the differences between observers. The dotted red lines indicate the 95% CI with respect to the mean of the ATVA differences between observers. Red points represent poor ATVA correlation between the measurements of both observers.

5.1.3 - ES hypoplasia was absent in our cohort of patients without MD

Henceforward, and if not otherwise specified, ATVA marker values would refer to the average of ATVA values measured by two observers.

ATVA markers greater than or equal to 140° were not found in the ears CT analyzed from the cohort of individuals without MD. This means that ES hypoplasia is absent in our non-MD patient cohort, or if this exists, it would occur in less than 1/175 (0.0057, 0.57%) if the calculation refers to the number of patients; or 1/332 (0.003, 0.3%) considering the number of ears. These thresholds may be lowered further with the analysis of our 1000 CT images database. Average ATVA was $95.6 \pm 9.8^\circ$, with a maximum value of 126.63° and minimum of 65.95° .

5.1.4 - Relation of ATVA with age, sex or clinical diagnosis

No associations were found between ATVA and age or sex ($p= 0.11$). Significant differences were observed between ATVA with mixed hearing loss and tinnitus (Figure 5.5)

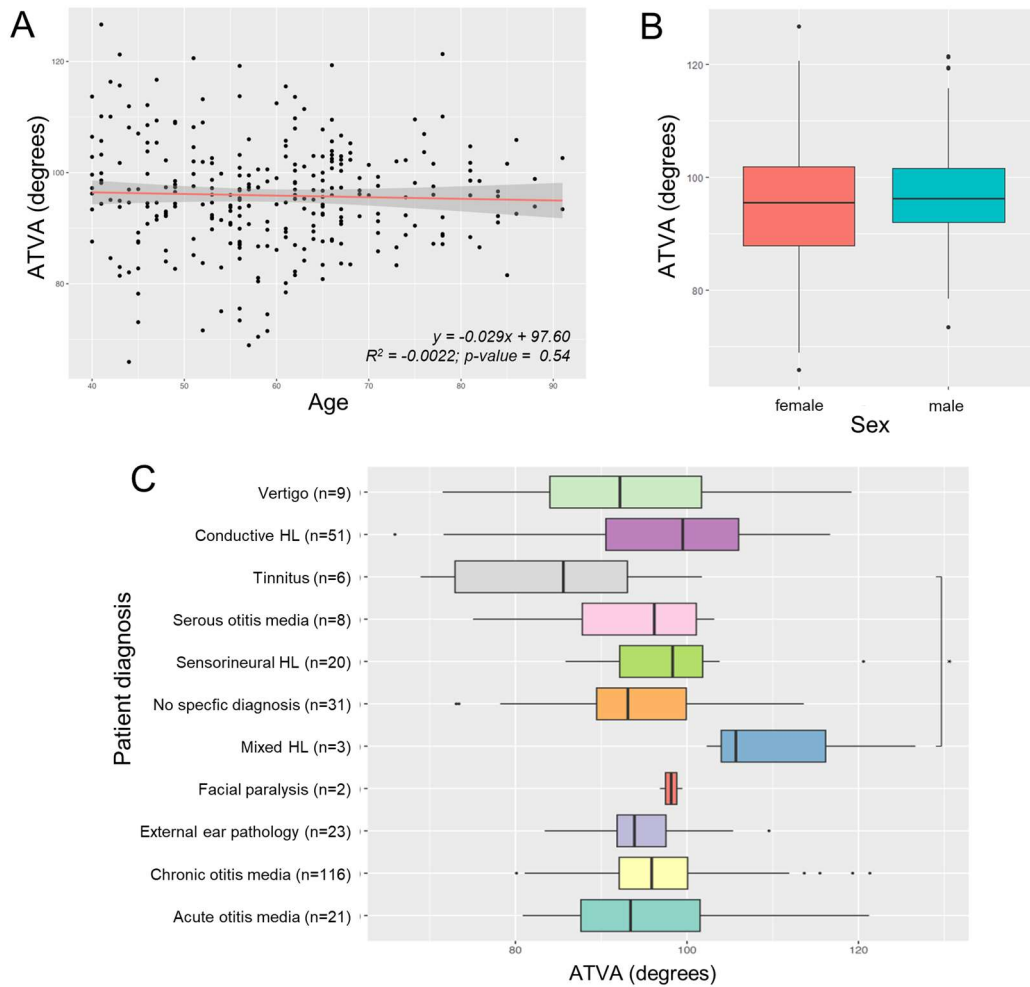


Figure 5.5 – Evaluation of ATVA association with age, sex, and patient diagnosis in the non-MD cohort. A) Linear regression of ATVA and age. The regression line (red), dispersion shading (grey) and the correlation metrics are indicated on the plot. B) and C) Box-plot of ATVA according to sex and diagnosis of the patients, respectively. * between groups indicates p value < 0.05 .



5.1.5 - ATVA values close to the finding of ES hypoplasia

Since the ATVA angle moves on a continuous scale from normal ($<120^\circ$ with a mean of $95.6^\circ \pm 9.8^\circ$) to the hypoplastic phenotype ($>140^\circ$), patients with ATVA in the $120 - 140^\circ$ interval were examined exhaustively. Four patients displayed ATVAs in this range, but none of them showed symptoms that could suggest a non-diagnosed MD. Two of them presented middle ear pathology: first with left ATVA of 121.3° had a contralateral cholesteatoma, and second with right ATVA of 115.7° an ipsilateral middle ear otitis. The third patient was a 41 years old woman with an ATVA of 126.6° in the right ear, but had undergone the CT scan to assess mixed hearing loss in the left ear. The fourth patient, a woman of 51 years old with an ATVA of 120.6° , attended the CT for evaluation of cochlear implant, showing a severe-profound bilateral SNHL. But since the ATVA was quite close to the normal limit and the other ear gave a normal ATVA of 105.7 , it is ruled out that it could be a possible MD. None of these patients also had vertigo or tinnitus.



5.2 - Chapter 2: Identification of genes and variants associated with hypoplasia of ES in MD

5.2.1 - Identification of genes and variants associated with ES hypoplasia in sporadic MD patients

5.2.1.1 - Sporadic MD hypoplastic cohort

After the identification of the endotype in the patients with MD and the exclusion of those with an onset greater than 65 years, a total of 42 individuals formed the final sporadic MD hypoplastic cohort. Table 5.2 shows the distribution of the patients according to sex, age, age of onset and years of evolution of MD, laterality of the MD and ES hypoplasia (endotype), family history, and evaluation of some comorbidities such as migraine or vestibular migraine.

Table 5.2 - Distribution of clinical variables in the MD hypoplastic cohort. Continuous variables are described as the mean \pm standard deviation. Discrete variables are indicated as the number of individuals per category and the percentage represented. * per each population.

Variable	mean (years) \pm sd	Variable	Individuals (%)
Age	51 \pm 11	Family history	
Onset MD	37 \pm 11	Familiar/sporadic	6 (14%) / 36 (86%)
Years of evolution	14 \pm 12		
		Comorbidities	
Variable	Individuals (%)	migraine (yes/no)	2(5%) / 40 (95%)
Sex		VM (yes/no)	3 (7%) / 39 (93%)
Female/male	8 (19%) / 34 (81%)		
		Country	
MD laterality		CH/DE	27 (64%)
Bilateral/unilateral	18 (43%) / 24 (57%)	Portugal/ Turkey	3 (7%)*
Unilateral right/left	13 (31%) / 11 (26%)	Spain	2 (5%)
		Croatia, India, Italy, Kosovo, Pakistan, Serbia/Montenegro, UK	1 (2%)*
Hypoplasia laterality			
Bilateral/unilateral	28 (67%) / 14 (34%)		
Unilateral right/left	4 (10%) / 10 (24%)		

Among the 42 individuals of MD hypoplastic cohort, 6 (14%) had relatives with MD or symptoms overlapping with the disease. An in-depth analysis of these individuals and their families is made in section 5.2.2.

In our cohort, bilaterality was fully associated between the diagnosis of MD and the findings of ES hypoplasia, since bilateral ES hypoplasia was found in all the 18 patients (43% of the cohort) with bilateral MD. The remaining patients (24 individuals, 57.1% of the

cohort) had a diagnosis of unilateral MD, where 41.7% (10 individuals) exhibit hypoplasia bilaterally, and 58.3% (14 individuals) unilaterally (p value < 0.01, $X^2 = 13.23$). In the patients with unilateral MD and unilateral ES hypoplasia, the hypoplasia was always in the ipsilateral ear with MD (p value < 0.01).

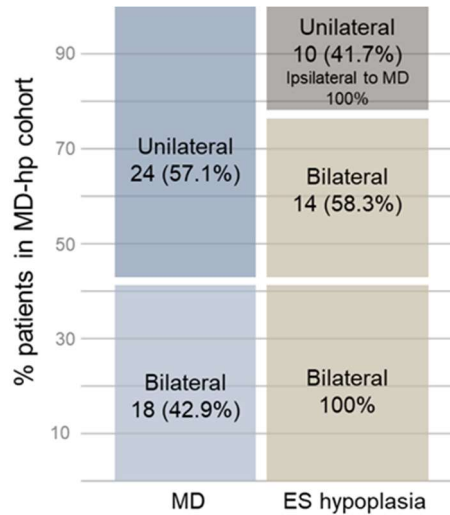


Figure 5.6 - Association between SE hypoplasia and MD diagnosis according to the affected ear.

Finally, to illustrate ES hypoplasia finding, representative CT scans from control and ES hypoplastic patients are shown in Figure 5.7.

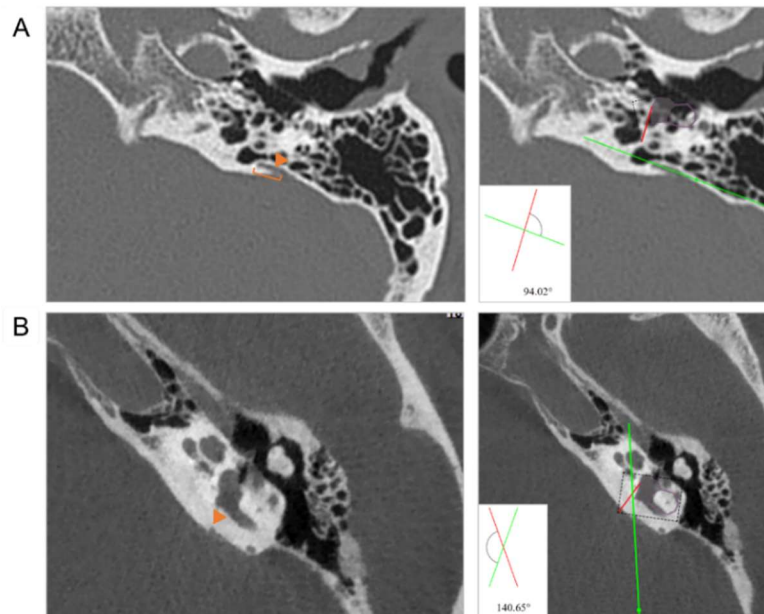


Figure 5.7 – CT scan showing the left ear in a control (A) and a patient with ES hypoplasia (B). The AV exit trajectory is well visualized within the TB (orange bracket) on the control CT, finishing in the operculum (orange arrowheads). However, operculum appears abruptly in the individual with ES hypoplasia. The right panels show the corresponding ATVA measurements.

5.2.1.2 - Enrichment of SNV and short indels in the sporadic MD hypoplastic cohort

5.2.1.2.1 - Enrichment of SNV in the sporadic cohort: candidate genes

A database of SNV and Indels was created for the ES hypoplastic cohort with 134.692 variants. After the annotation step, potential 20.780 causal variants with $MAF \leq 0.05$ and HIGH or MODERATE impact were retained and used as input for GBA.

Significant enrichment of rare variants was found in 1150 genes *versus* both gnomADg global and gnomADg nfe reference populations, reduced to 1132 genes after removal of FLAGS genes. Final list included 94 genes, whose summarized variants had an allele frequency greater than or equal to 5% in our ES hypoplastic. Figure 5.8 shows the top 30 genes with the largest number of individuals. The complete list and their metrics are in Supplementary Table 2.

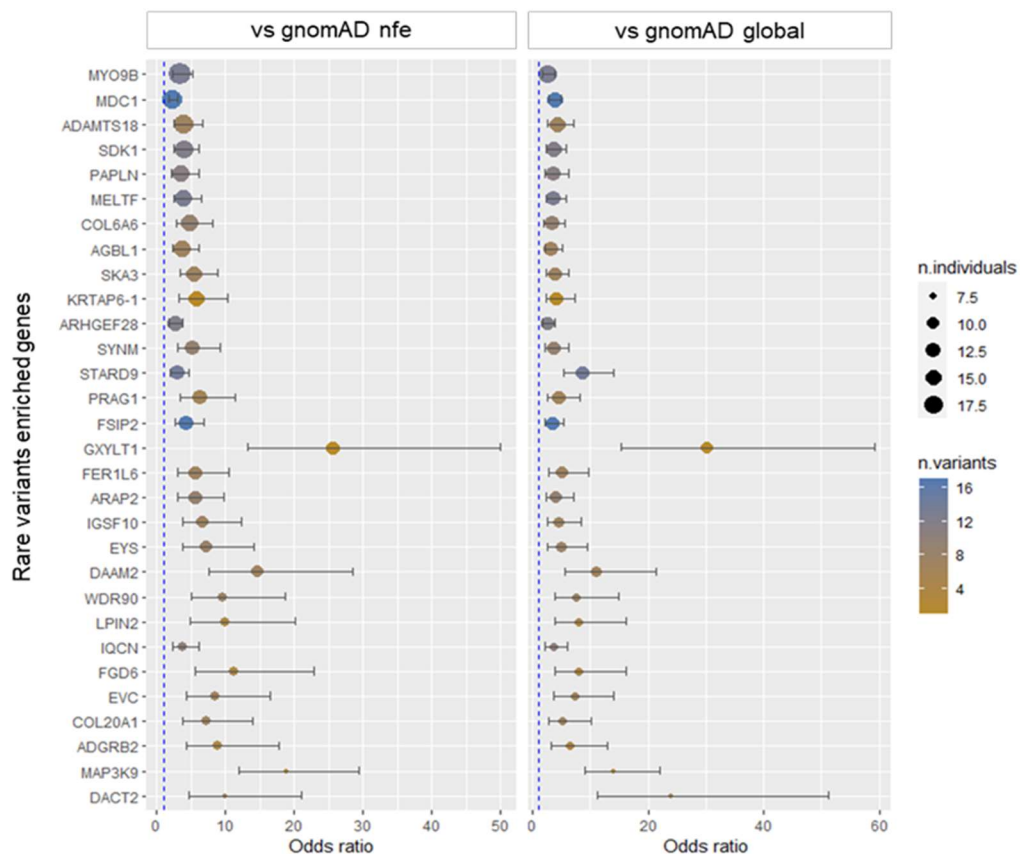


Figure 5.8 – Representation of Odds ratios in the top 30 genes with an enrichment of rare variants in the highest number of MD and ES hypoplastic individuals, respecting to the reference populations nfe (left panel) and global (right panel) gnomAD. Dot size indicates the number of patients with variants in that gene. Color scale refers to the total number of variants.

These genes were prioritized and ranked according to: i) the number of rare variants; ii) the number of individuals segregating the variants; and iii) the gene expression levels in the inner ear databases. Finally, 2 genes were selected as candidate genes for ES hypoplasia: *ADAMTS18* and *SDK1*.

5.2.1.2.2 - ES hypoplastic phenotype and MD clinical picture in patients with candidates ADAMTS18 variants

The *ADAMTS18* gene showed 7 missense variants in 15 different individuals (37,5% of MD-ES hypoplastic cohort), all in heterozygous (Table 5.3). The g.77434661G>C variant was shared in 6 individuals, g.77248008C>T in 4, and g.77367582G>A in 2. The remaining 4 variants were only found in 1 individual. In addition, one of the individuals had 2 variants: g.77326001G>A and g.77248008C>T. No InDels were significantly enriched and prioritized on this gene. Some of the *ADAMTS18* variants selected were validated by Sanger sequencing (section 5.3.1).

The clinical picture of the patients with the shared variants of *ADAMTS18* was examined to assess the segregation of the phenotype. In the six patients with the g.77434661G>C variant of *ADAMTS18* in the cohort, four had a diagnosis of bilateral MD, and finding of bilateral ES hypoplastic endotype (Figure 5.9, B, C, F and L). Three of them show asymmetric audiometry, where one of the two ears is more affected than the other (Figure 5.9, B, C and L), and one patient has a symmetric condition (Figure 5.9, F). Of the 2 unilateral MD patients, one of them had ES hypoplasia in the right ear, ipsilateral to the MD diagnosis (Figure 5.9, A), but SNHL was detected as fluctuating in the affected ear. The other patient with right unilateral MD has clearly affected hearing in his right ear, but has a finding of ES hypoplasia in both ears (Figure 5.9, D). As a summary, the auditory phenotype does not appear to follow a similar audiometric profile among these patients, neither according to the laterality of the disease nor the presence of ES hypoplasia. The letter that designates the patients in Figure 5.9 agrees with that given in Table 5.3 for each individual with a variant in *ADAMTS18*.

		A	B	C	D	F	L
General	Procedence	CH/De	Serbia/Montenegro	CH/DE	CH/DE	CH/DE	CH/DE
	Age	44	52	55	59	66	45
	Sex	female	male	male	male	male	male
Meniere disease	MD onset	20	28	28	50	49	25
	Years of evolution	24	24	27	9	17	20
	MD laterality	unilateral right	bilateral	bilateral	unilateral right	bilateral	bilateral
ES endotype	Hypoplasia laterality	unilateral right	bilateral	bilateral	bilateral	bilateral	bilateral
PTA							
CT	Left CT		NA			NA	NA
	Right CT		NA			NA	NA
Variants	g.77434661G>C	●	●	●	●	●	●

Figure 5.9 - Clinical data, PTA and CT from both ear in the six patients (panels from A to L) with the ADAMTS18,g.77434661G>C variant. NA: non available. PTA: pure-tone audiometry

5.2.1.2.2 - ES hypoplastic phenotype and MD clinical picture in patients with candidates SDK1 variants

The SDK1 gene had 12 missense variants in 14 different individuals with the ES hypoplasia (33,3% of MD-ES hypoplastic cohort), all heterozygous (Table 5.4). The g.3951870G>T variant was shared by 4 individuals, g.3951025C>T by 3, meanwhile g.3974407C>T and g.3951861C>T were in 2 different individuals, each of them. The remaining 8 variants were only found in 1 individual. Moreover, the 3 patients with the g.3951025C>T variant had also g.3951870G>T, thus sharing 2 variants in the 3 same individuals. One of these three individuals is also the carrier of one of the variants in a single individual g.4221325A>C, having 3 rare variants in this gene. No InDels were enriched and prioritized on this gene. The SDK1 variants selected were validated by Sanger sequencing (section 5.3.1).

The clinical information of patients with shared variants in SDK1 was examined to verify the segregation of the phenotype (Figure 5.10). Three individuals shared the same two variants, g.3951025C>T,A317V and g.3951870C>T,P367L (A,K,L). Two of them (K, L) had bilateral MD involvement and ES hypoplasia, and their audiograms showed a descending symmetric profile with moderate-severe impairment (L left ear not available in the figure). The third (A) had MD and ES hypoplasia unilaterally in the left ear, although SNHL fluctuated. A fourth patient (N) shared the variant g.3951870C>T,P367L with the previous three, and also had another variant g.3951861C>T,A364V shared with another individual (patient I, not shown in the figure). This case showed bilateral MD and hypoplasia, with a symmetrical descending audiogram with moderate-profound impairment. The clinical characteristics of patients with the same variants in SDK1 do not seem to segregate the audiometric profile and show different laterality of MD and ES hypoplasia.

		A	I	K	L	N
General	Procedence	CH/De	CH/DE	Pakistan	Portugese	CH/DE
	Age	44	48	47	52	65
	Sex	f	m	f	m	m
Meniere disease	MD onset	20	46	44	18	44
	Years of evolution	24	2	3	34	21
	MD laterality	unilateral right	unilateral left	bilateral	bilateral	bilateral
ES endotype	Hypoplasia laterality	unilateral right	bilateral	bilateral	bilateral	bilateral
PTA						
CT	Left CT					
	Right CT					
Variants	7:3951025C>T,A317V	●		●	●	
	7:3951870C>T,P367L	●		●	●	●
	7:3951861C>T,A364V		●			●

Figure 5.10 - Clinical data, hearing thresholds (PTA) and CT scans from both ears in the five patients (panels from A to N) with the *SDK1* variants most shared between individuals. PTA: pure-tone audiometry.

5.2.1.3 - Analysis of structural variants in the sporadic MD hypoplastic cohort

5.2.1.3.1 - Large structural variants

The SVDB overlapping LSV dataset from TIDDIT resulted in a total of 44 LSV. After removing 1 LSV located in a FLAG gene and those mapped in non-coding regions, 21 LSV were retained (Supplementary Table 3). Of these 21 LSV, only 2 variants present in more than one individual were prioritized (Table 5.5, bold and gray background). The first of these is a tandem duplication in the TBC1 Domain Family Member 16 (*TBC1D16*) gene, present in 3 individuals. Its conservation metrics are not very high, and its pathogenicity prediction uncertain. The other one is an 6590bp inversion in Long Intergenic Non-Protein Coding RNA 917 (*LINC00917*) gene, present in 4 individuals, one homozygous and 3 heterozygous.

On the other hand, MANTA identified 13 LSV after SVDB overlap and FLAGs removal (Supplementary Table 3). Five variants in *CASP8*, *CHROMRM-PRKPA* and *SKA3* were found in more than 1 individual and prioritized (Table 5.5, bold and gray background). Variants in one individual but overlapping in prioritized genes were also shown. The deletion in the caspase 8 (*CASP8*) gene was found in the largest number of individuals. Six patients had this tandem duplication of around 3000bp, classified as “uncertain significance”. This gene did not show very high constraints. In addition, five deletions of different lengths were found along the Spindle And Kinetochores Associated Complex Subunit 3 gene (*SKA3*), present in the same five individuals. These span from position 21155811 to 21167989 on chromosome 13, over more than 12,000 bp. The third most frequent LSV was in the Protein Activator Of Interferon Induced Protein Kinase EIF2AK2 (*PRKRA*) gene, another deletion of around 3000bp occurred in 3 individuals. Its constraint score was not high, but it was classified as “Likely pathogenic” by ACMG guidelines. Interestingly, this variant separates around 3000bp from another 5290bp deletion that also involves the *PRKRA* gene and upstream Cholesterol Induced Regulator Of Metabolism RNA (*CHROMR*) gene. This second variant in *PRKRA* is heterozygous in a single individual and cataloged as “benign”. The rest of the LSV found by MANTA were only found in 1 patient.

Only 1 SV in the *WWP2* gene was replicated between both tools, but it was in only 1 individual (Supplementary Table 3).

5.2.1.3.2 – Copy number variants

The SVDB overlapping variant dataset from CnvKit resulted in a total of 852 CNV. After removing those mapped in non-coding regions and FLAG genes, and selecting those located in regions with high constraint ($pLi > 0.9$ in gnomAD or ExAC) and “pathogenic” or “likely pathogenic” ACMG classified, 21 CNV were selected (Supplementary Table 4). CNV present in more than 1 individual are showed in Table 5.6, and those in the largest number of individuals were prioritized (bold and gray background).

The most represented CNV were presented in four individuals. The first are duplications involving the Transforming Growth Factor Beta 2 (TGFB2) and MicroRNA 548f-3 (MIR548F3) genes in heterozygosity, where there are 176, 256, 189 and 57 more expected copies in each patient, respectively. The second was a deletion in homozygosity, affecting the Glucose-Fructose Oxidoreductase Domain Containing 2 (GFOD2) and RAN Binding Protein 10 (RANBP10) genes. Interestingly, two different CNV were called in the same Ring Finger Protein 43 (RNF43) and Heat Shock Transcription Factor 5 (HSF5) genes, starting at the same position but differing by almost 70,000bp at their end. The longer variant also comprises the downstream Myotubularin Related Protein 4 (MTMR4) gene. The 3 and 2 affected individuals in homozygosity in both variants are different, which makes a total of 5 affected individuals in these two genes.

5.2.1.3.3 – Replication of genes enriched in SNV-Indels and SV

The *SKA3* gene showed LSV overlapping an enrichment of rare SNV/InDels. In addition to the 5 LSV deletions, 7 SNV/InDels were found in 12 individuals as a result of the GBA (Supplementary Table 2, line 10). These variants span across chromosome 13 from positions 21155150 to 21172498 and include 2 missense variants, 2 frameshift insertions, and 2 splice site acceptor variants. Four of the 5 individuals with the LSV also have at least 1 SNV or InDels in *SKA3*. However, the quality of those variants is not very good and it would be necessary to validate them.

In no other gene were replicated the enrichment of SNV or Indels and presence of SV.

Table 5.5 - List of candidate LSV in the ES hypoplastic cohort

Tool	Gene/s	Chr	Start	End	Length	Type	AF cohort	N ind (hom/het)	GnomAD pLI	ExAC pLI	ACMG
TIDDIT	<i>LINC00917</i>	16	86345402	86352129	6596	INV	0.060	4 (1/3)	ND	ND	ND
	<i>TBC1D16</i>	17	80021923	80025068	3146	TDUP	0.071	3 (3/0)	0	0.01	US
MANTA	<i>CASP8</i>	2	201281925	201284727	-2792	DEL	0.119	6 (4/2)	0	0	US
	<i>CHROMR; PRKRA</i>	2	178436319	178441609	-5290	DEL	0.012	1 (0/1)	0.42	0.15	B
		2	178444501	178447508	-3007	DEL	0.036	3 (0/3)	0.42	0.15	LP
	<i>SKA3</i>	13	21155811	21157923	-2110	DEL	0.012	1 (0/1)	0	0	B
		13	21158122	21159902	-1776	DEL	0.060	5 (0/5)	0	0	B
		13	21158126	21161789	-3663	DEL	0.012	1 (0/1)	0	0	B
		13	21159987	21161790	-1802	DEL	0.060	5 (0/5)	0	0	B
	13	21161875	21167989	-6112	DEL	0.060	5 (0/5)	0	0	B	

Gene/s: LSV mapped gene or genes; Chr: chromosome; Start and End: SV starting and ending position in GRCh38/Hg38; Length: size of SV in base pairs; Type of SV including DEL (deletion), DUP (duplication); INV (inversion); N ind (hom/het): number of individuals with the SV, specifying in brackets how many present SV in homozygosity and heterozygosity; pLI: probability of being Loss of Function variant intolerant gene in GnomAD and Exac databases. pLi >= 0.9 regions are considered as high-constrained. ACMG: American College of Medical Genetics guideline classification. LB: likely-benign; US: uncertain significance; LP: likely-pathogenic. ND: non-describe

Table 5.6 - List of candidate CNV in the ES hypoplastic cohort

Gene/s	Chr	Start	End	Length	Type	AF cohort	N ind (hom/het)	GnomAD pLi	ExAC pLi	ACMG	CN
<i>MIR548F3; TGFB2</i>	1	218346476	218441728	95252	DUP	0.048	4 (0/4)	1.00	0.99	P	+176, +256, +189, +57
<i>MYT1L</i>	2	1789112	1887121	-98009	DEL	0.071	3 (3/0)	1.00	1.00	LP	-2
<i>TSC1</i>	9	132895943	132928955	33012	DUP	0.024	2 (0/2)	1.00	1.00	P	+9, +10
<i>CPSF7; CYB561A3; TKFC; TMEM138; TMEM216</i>	11	61346832	61404704	-57872	DEL	0.048	2 (2/0)	1.00	0.99	P	-2
<i>GFOD2; RANBP10</i>	16	67677765	67726021	-48256	DEL	0.095	4 (4/0)	0.97	0.95	P	-2
<i>ANKRD11; ZNF778</i>	16	89228836	89268146	-39310	DEL	0.048	2 (2/0)	1.00	1.00	P	-2
<i>CHD3; CYB5D1; NAA38</i>	17	7859908	7887081	-27173	DEL	0.071	3 (3/0)	1.00	1.00	LP	-2
<i>HSF5; RNF43</i>	17	58402639	58421864	-19225	DEL	0.071	3 (3/0)	0.98	0.74	LP	-2
<i>HSF5; RNF43 MTMR4;</i>	17	58402639	58491583	-88944	DEL	0.048	2 (2/0)	1.00	1.00	LP	-2
<i>METTL2A; TLK2</i>	17	62449643	62508553	-58910	DEL	0.071	3 (3/0)	1.00	1.00	P	-2
<i>CERS1; GDF1; UPF1</i>	19	18866520	18878756	-12236	DEL	0.071	3 (3/0)	1.00	1.00	P	-2

Gene/s: LSV mapped gene or genes; Chr: chromosome; Start and End: SV starting and ending position in GRCh38/Hg38; Length: size of SV in base pairs; Type of SV including DEL (decreases in the number of copies) or DUP (increases in the number of copies); n ind: number of individuals with SV in homozygosity (n hom) and heterozygosity (n het); pLi: probability of being Loss of Function variant intolerant gene in GnomAD and Exac databases. pLi \geq 0.9 regions are considered as high-constrained. ACMG: American College of Medical Genetics guideline classification. LP: likely-pathogenic; P: pathogenic. ND: non-described; CN: number of copies in the CNV. In duplications, the incremented number of copies are specified per individual. In deletions are indicated as -2 (homozygous deletion) or -1 (heterozygous deletion)

5.2.2 - Identification of genes and variants associated with ES hypoplasia in familial MD patients

5.2.2.1 - Familial patients in the MD hypoplastic cohort

In the 42 individuals of the MD and ES hypoplastic cohort, 6 (14%) had relatives with MD or symptoms overlapping with the disease. These probands were classified as familial MD patients and their families cataloged as families 1 to 6. Pedigrees and detailed clinical evaluation of probands and relatives, both affected and controls, is found in Figure 5.11 and Table 5.7, respectively.

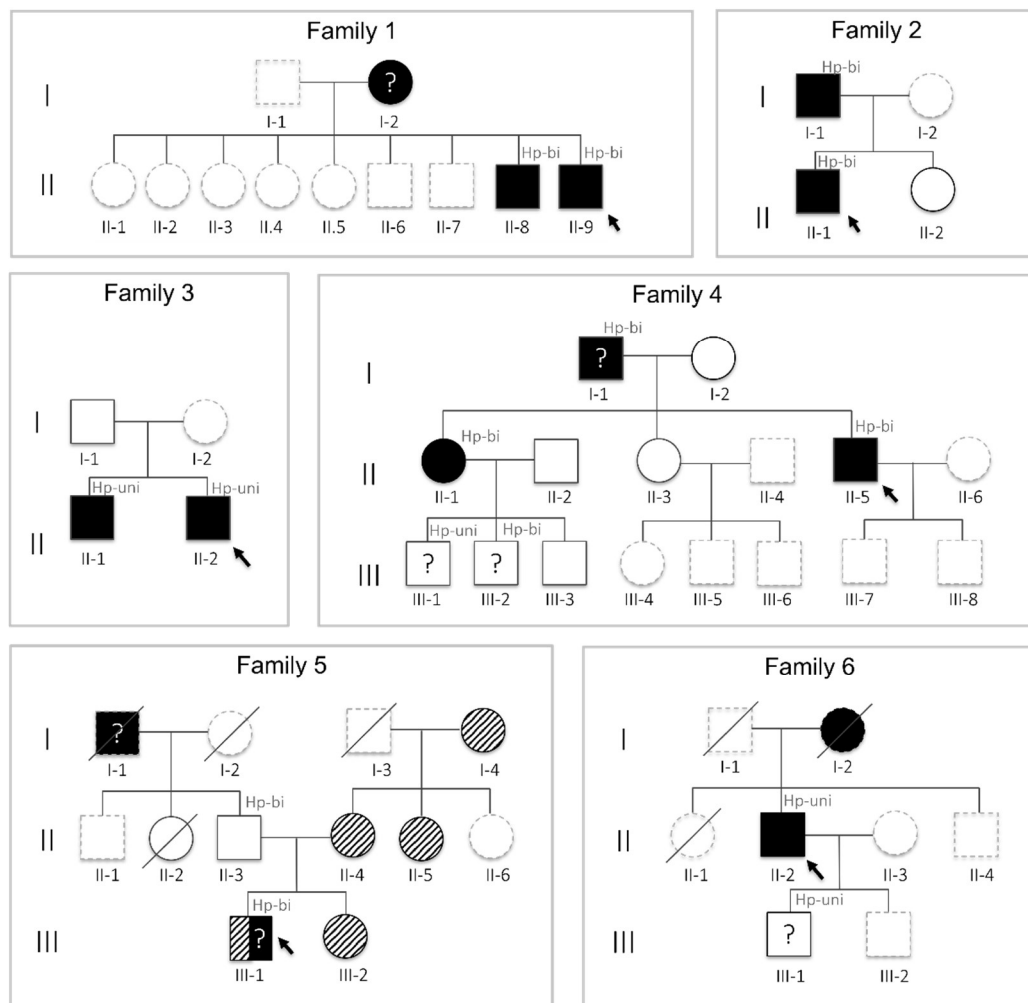


Figure 5.11 - Pedigrees of familial MD patients with ES hypoplasia. Black filled symbols: MD; white filled symbols: controls for MD; strikethrough symbols: deceased individuals; oblique lined filled symbols: low-frequency SNHL; grey dotted symbols: individuals where it was not possible to collect sample or clinical information. *Hp-uni* and *Hp-bi* on the top right of the symbols indicated unilateral and bilateral ES hypoplasia, respectively; arrows point to probands; “?” inside symbols make reference to subject suspected to have course MD (in older generations) or suspected to develop MD (in younger generations).

Table 5.7 - Clinical evaluation of familiar MD patients and affected relatives or controls.

PC	Status	General			Meniere disease				ES endotype		Symptoms / Comorbidities			Comments
		Proc.	Age	Sex	Diag.	Onset	YOE	Lat.	ES-hp	Hp-Lat.	SNHL	M	VM	
Family 1														
I-2	suspected	SM	na	f	susp	na	na	na	-	na	na	na	na	not-available
II-8	affected	SM	53	m	def	38	15	bilat.	hp	bilat.	nd	nd	nd	
II-9	proband	SM	52	m	def	28	24	bilat.	hp	bilat.	nd	nd	nd	
Family 2														
I-1	affected	CH/DE	78	m	def	30	48	bilat.	hp	bilat.	nd	yes	nd	
II-1	proband	CH/DE	55	m	def	28	27	bilat.	hp	bilat.	nd	nd	nd	
I-2	control	CH/DE	52	f	no	-	-	-	normal	-	nd	nd	nd	
Family 3														
II-1	affected	CH/DE	59	m	def	51	8	left	hp	left	nd	nd	nd	
II-2	proband	CH/DE	60	m	def	30	30	left	hp	left	nd	nd	nd	
Family 4														
I-1	suspected	CH/DE	83	m	susp	45	38	bilat.	hp	bilat.	nd	nd	nd	suspected to have coursed MD
I-2	control	CH/DE	81	f	no	-	-	-	-	-	nd	nd	nd	
II-1	affected	CH/DE	51	f	def	46	5	left	hp	bilat.	nd	nd	yes	
II-2	control	CH/DE	52	m	no	-	-	-	-	-	nd	nd	nd	
II-3	control	CH/DE	57	f	no	-	-	-	-	-	nd	nd	nd	
II-5	proband	CH/DE	59	m	def	30	29	bilat.	hp	bilat.	nd	nd	nd	
III-1	suspected	CH/DE	29	m	susp	-	-	-	hp	left	nd	nd	nd	suspected to develop MD
III-2	suspected	CH/DE	27	m	susp	-	-	-	hp	bilat.	nd	nd	nd	suspected to develop MD
III-3	control	CH/DE	26	m	no	-	-	-	no	-	nd	nd	nd	



PC	Status	General			Meniere disease				ES endotype		Symptoms / Comorbidities			Comments
		Proc.	Age	Sex	Diag.	Onset	YOE	Lat.	ES-hp	Hp-Lat.	SNHL	M	VM	
Family 5														
I-1	suspected	CH/DE	deceased	m	susp	nd	nd	nd	hp	bilat.	nd	nd	nd	suspected to have coursed MD
I-4	control	CH/DE	89	f	no	-	-	-	-	-	low-freq	nd	nd	
II-3	control	CH/DE	62	m	no	-	-	-	hp	bilat.	high-freq	nd	nd	epilepsy, disabled suspected to develop bilateral affection. EHs in left ear.
II-4	control	CH/DE	62	f	no	-	-	-	-	-	low-freq	nd	nd	
II-5	control	CH/DE	53	f	no	-	-	-	-	-	flat audiogram	nd	nd	
II-6	nd	CH/DE	nd	f	nd	nd	nd	nd	nd	nd	nd	nd	nd	
III-1	proband	CH/DE	23	m	def	17	6	left	hp	bilat.	low-freq	nd	nd	epilepsy, disabled suspected to develop bilateral affection. EHs in left ear.
III-2	control	CH/DE	26	f	no	-	-	-	-	-	low-freq	nd	nd	
Family 6														
I-2	suspected	Turkey	deceased	f	susp	nd	nd	nd	nd	nd	nd	nd	nd	suspected to have coursed MD
II-2	proband	Turkey	57	m	def	33	24	left	hp	left	nd	nd	nd	
II-4	nd	Turkey	nd	f	no	-	nd	-	-	-	-	-	-	waiting for evaluation suspected to develop MD
III-1	suspected	Turkey	23	m	susp	-	-	-	hp	left	nd	nd	nd	
III-2	nd	Turkey	nd	m	no	-	nd	-	-	-	-	-	-	waiting for evaluation
Family 7														
II-1	control	Kosovo	24	f	no	-	-	-	normal	-	nd	nd	nd	
I-2	proband	Kosovo	50	f	def	40	10	right	hp	right	nd	yes	nd	

Information of table 5.7 include: pedigree familiar code (PC); Status of individuals referring to MD: MD affected, suspected to have coursed or to develop MD, differentiating the proband, and control; General column include procedence (Proc.), Age in years and Sex (f-female or m-male); MD column include: diagnosis of MD (Diag.) - definitive (def), suspected (susp) or no MD; Years old in the onset of MD; years of evolution (YOE) and MD laterality (Lat.); ES endotype column include: ES-hp being "hp" or "normal" when ES hypoplasia or normal ES is found, respectively, and "-" when ES have not been evaluated, and hp-Lat. indicating laterality of ES hypoplasia; Symptoms/Comorbidities column display some information about presence of migraine (M); vestibular migraine (VM) and sensorineural hearing loss (SNHL). na: not available. SM: Serbia/Montenegro; CH/DE: Swiss/Deutschland.

5.2.2.2 - Candidate variants in familial MD patients

Four candidate variants from the GBA performed in the MD and ES hypoplastic sporadic cohort were present in 4 familial probands, all in *ADAMTS18*. Specifically, the *ADAMTS18* variant g.77434661G>C shared by 6 individuals was found in the probands of family 1 (II-9) and family 2 (II-1) (Figure 5.12, A). On the other hand, the *ADAMTS18* variant g.77248008C>T was discovered in the probands of family 4 (II-5) and family 5 (III-1) (Figure 5.12, B). Sanger validation for some of these variants displays in Section 5.3.1. Any of the candidate variants in *SDK1* was found in a familial patient.

In the family 1, g.77434661G>C was heterozygous in proband II-9 and his brother II.8. Both show bilateral MD and bilateral ES hypoplasia. Unfortunately, we do not have more samples of this family. The mother does not have a definitive diagnosis of MD but she appears to have experienced vestibular and auditory symptoms throughout her life. Samples and CT from the mother as affected individual, and from controls (including father and some sisters/brothers) would be necessary to confirm segregation of the variant with the phenotype and ES hypoplasia in this family. In family 2, the g.77434661G>C variant was also described in the proband II-1. Both he and his father (I-1) have the heterozygous variant and a diagnosis of bilateral MD and bilateral ES. The sister (II-2) has shown no vestibular or auditory symptoms at age 52, and her CT confirms that she does not show ES hypoplasia. However, the variant g.77434661G> C was also present in this woman. Lastly, it is noteworthy that these four familial patients with this g.77434661G>C variant, II-8 and II-9 in family 1, and I-1 and II-1 in family 2, had bilateral affection of both de MD diagnosis and the ES hypoplasia laterality.

In family 4, the variant g.77248008C>T was found in proband II.5. Her sister (II-1) has left MD and bilateral ES hypoplasia. Her father (I-1), now 83, never had a definitive MD diagnosis, but he suffered from vestibular and auditory symptoms. A CT performed at a younger age revealed the presence of bilateral ES hypoplasia, so it is suspected that this individual could have developed MD. Two sons of his affected sister, nephew III-1 and III-2, exhibit unilateral and bilateral ES hypoplasia, respectively, both still without audiovestibular symptoms. The third brother, III-3, displays a normal ES endotype in his CT, and no symptoms. Evaluated familiar controls (I-2, II-2, II-3, III-1 and III-3) did not display MD compatible symptoms. When the segregation of the variant g.77248008C>T was sought in the members of this family, the affected II-1 and the suspected of have been affected I-1 also displayed the variant. However, it was also found in the unexpected control sister II-3. None of the nephews with ES hypoplasia III-1 and III-2 had it.

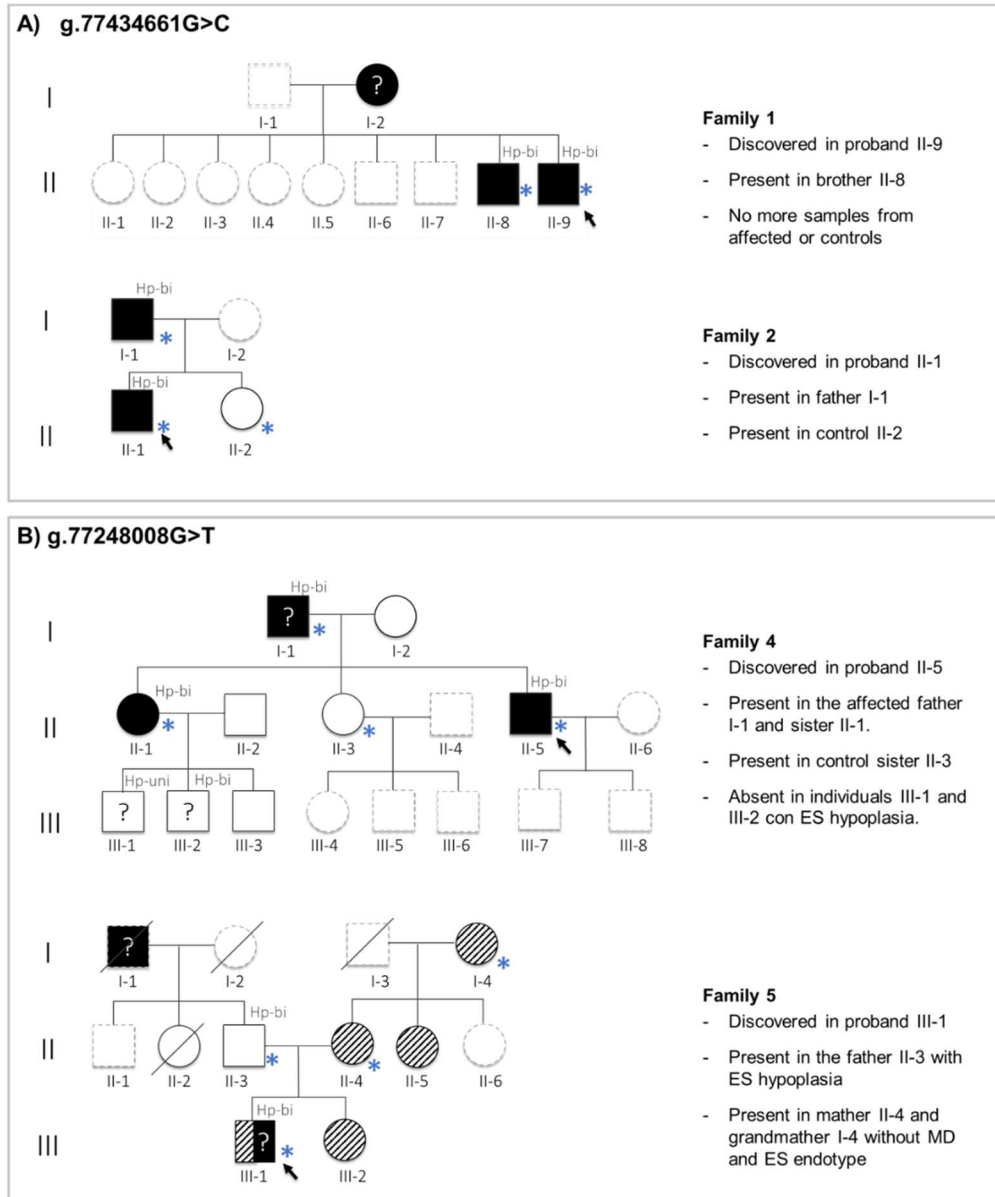


Figure 5.12 - Families where candidate variants g.77434661G>C (panel A) and g.77248008G>T (panel B) in *ADAMTS18* were found in their probands. Variants found and individuals with variants are indicated to the right of the pedigrees. Blue asterisks indicate individuals with variants. Black filled symbols: Meniere Disease; white filled symbols: controls for Meniere Disease; strikethrough symbols: deceased individuals; oblique lined filled symbols: low-frequency SNHL; grey dotted symbols: individuals where it was not possible to collect sample or clinical information. *Hp-uni* and *Hp-bi* on the top right of the symbols indicated unilateral and bilateral ES hypoplasia, respectively; arrows point to probands; “?” inside symbols refer to subjects suspected to have developed MD (in older generations) or suspected to develop MD (in younger generations).

The variant g.77248008C>T was found in proband III-1 in family 5. This individual was diagnosed with MD when he was only 17 years old and currently has 6 years of evolution. His symptomatology is unilateral to the left and he has ES hypoplasia bilaterally. His father (II-3) has ES bilateral hypoplasia, but at his current 62 years he has not manifest



vestibular symptoms or tinnitus, although he exhibits a moderate drop in hearing at high frequencies, typically related to age. His paternal grandfather (I-1), now deceased, suffered from auditory and vestibular symptoms that suggest MD, although he was never diagnosed. The maternal part of his family does not show MD, but is characterized by a rare audiometric profile with low-frequency hearing loss that segregates in three generations in 5 individuals, including II-1. The study of this phenotype is addressed below, in section 5.2.2.3. The g.77248008C> T variant was present also in his father II-3, in his mother II-4 and in his grandmother I-4, in all cases in heterozygosity.

5.2.2.3 - Low-frequency SNHL in family 5

In family 5, in addition to hypoplasia and MD disease, low-frequency SNHL segregated in five individuals across three generations with a clear pattern of autosomal dominant inheritance. This phenotype was studied to find a candidate variant that could explain the phenotype.

5.2.2.3.1 - Audiovestibular evaluation

In family five, subject III-1 was diagnosed with unilateral right MD at age 17, accompanied by episodes of rotational vertigo lasting several hours, aural pressure, and moderate SNHL in the ipsilateral ear. EHs were also found in the affected ear. All three, III-1, his father II-3 and his grandfather I-1 showed bilateral ES hypoplasia. II-3 had no symptoms of MD and was considered as control for the disease, since it is not expected to develop the pathology by the age of 62. I-1 was suspected of having MD, since he suffered from symptoms overlapping with the disease during his life, but he did not receive a definitive diagnosis. In addition, retrospective analysis of his CT images described bilateral ES hypoplasia (Figure 5.11, panel for family 5).

Apart from MD and ES hypoplasia, low-frequency SNHL segregated in five individuals in this family (I-4, II-4, II-5, III-1, and III-2) across three consecutive generations, suggesting an SNHL autosomal dominant inheritance pattern (Figure 5.12). PTA described bilateral and symmetrical audiograms, excepting III-1 with unilateral left affection (Figure 5.13). SNHL showed anticipation, beginning in the 50s, 30s and 20s years old in the first, second and third generation, respectively. Taking into account the profile of each generation, evolution over time can be delineated. In this way, mild hearing loss would start early (about the 2nd-3rd decade of life) affecting frequencies below 500 Hz (20–40 dB), as in the case of III-2. After 10-20 years, moderate thresholds (30-50 dB) would be reached at low-tones, and middle-high frequencies impairment would start, typical of hearing loss related to mature age (as in II-4). In the older generation, low-tone hearing loss stabilizes but rest of frequencies deteriorate, resulting in the usual flat audiogram in the elderly. II-3 displayed a symmetric and decreasing audiogram profile with different configuration, affected at high frequencies (> 3000 Hz) in mild to severe levels (from 30 to 70 dB), usually of age-related SNHL. Therefore, this individual can also be considered as a control for low-frequency SNHL exhibited by their offspring and his wife's family.

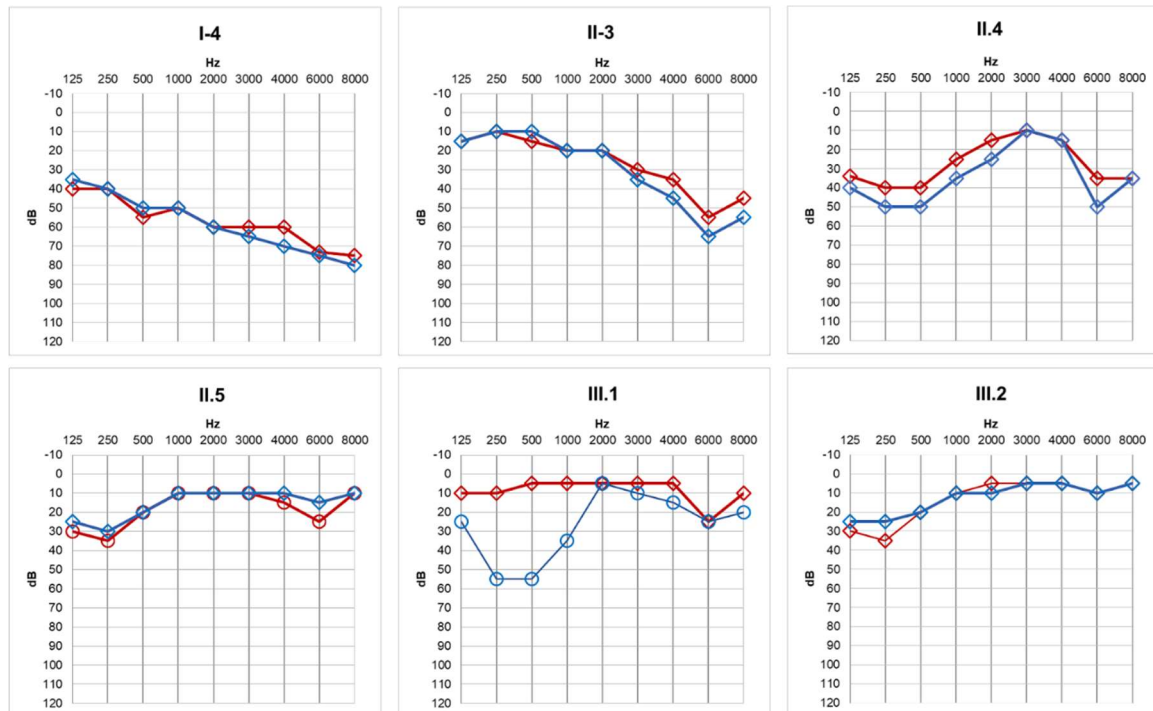


Figure 5.13 - PTA from individuals of family 5. Red series: left ear; blue series: right ear; dB: decibels; kHz: kilohertz.

5.2.2.3.2 - Prioritization of candidate variants

Family variants dataset contained 51,423 SNVs and short InDels. After retaining those shared among the individuals with low-frequency hearing loss (I-4, II-4, II-5, III-1 and III-2), but absent in control (II-3), there remained 2654 variants. Of these, 626 were identified as having a HIGH or MODERATE impact according to VEP. Among them, 10 variants had been described in gnomAD with a MAF less than or equal to 0.001 and 5 with a CADD score ≥ 20 . These 5 final candidates consist of 1 stop gain variant and 4 missense variants, summarized in Table 5-8.

5.2.2.3.3 – The candidate *CENPP* gene and variant

The novel variant in the *CENPP* gene g.92613131T>A,C283* was top-ranked due to the HIGH impact of the LoF variants, their more elevated CADD and their classification as “pathogenic” by the ACMG. This variant affects the canonical transcript in exon 8 producing an early stop codon from cystein 283 and onwards, truncating the protein at the amino-terminal end. Chromatograms of Sanger sequencing validation of the variant in patients I-4, II-4, II-5 and III-2 is shown in section 5.3.1.

Table 5.8 - List of candidate rare variants in the family 5

Gene	Chrom	Position	ID	Ref	Alt	Consequence	Impact	gnomAD AF nfe	gnomAD AF global	CADD	ACMG
<i>CENPP</i>	chr9	92613131	.	T	A	Nonsense	High	ND	ND	32	P
<i>NEIL3</i>	chr4	177322544	rs1338708417	A	G	Missense	Moderate	4.60E-05	2.10E-05	29.4	US/LP
<i>PPP1R1A</i>	chr12	54582069	rs202211027	C	T	Missense	Moderate	0.0011	0.000572	24.9	US
<i>FRMPD3</i>	chrX	107602107	rs183198624	C	G	Missense	Moderate	0.0005	0.000387	22.9	LB/US
<i>PIPOX</i>	chr17	29043230	rs747657795	C	T	Missense	Moderate	1.50E-05	1.40E-05	22.4	US

ND: non-described. Chrom: chromosome; Pos: position; Ref: allele in reference genome; Alt: alternative variant allele; Consequence: variant consequence according to Variant Effector Predictor tool (Ensembl); gnomAD AF global/nfe: variant allele frequency worldwide/in non-Finnish European population; CADD: Combined Annotation Dependent Depletion pathogenic score; ACMG: American College of Medical Genetics guidelines classification: likely benign (LB), uncertain significance (US), likely pathogenic (LP), pathogenic (P).

CENPP expression in the inner ear was contrasted in the gEAR portal in mice. RNA-seq assays have shown that, both in vestibular organs and cochlea, the highest expression is registered during the embryonic stage (E16), decreasing to minimum levels at birth (P0). It increases again postnatally, although not to levels as high as during embryonic development (192,193). Comparing between structures in stage P0, the expression is higher in the vestibular sensory epithelium than in the cochlear, and in both structures the HC show lower levels compared to SC (193–195).

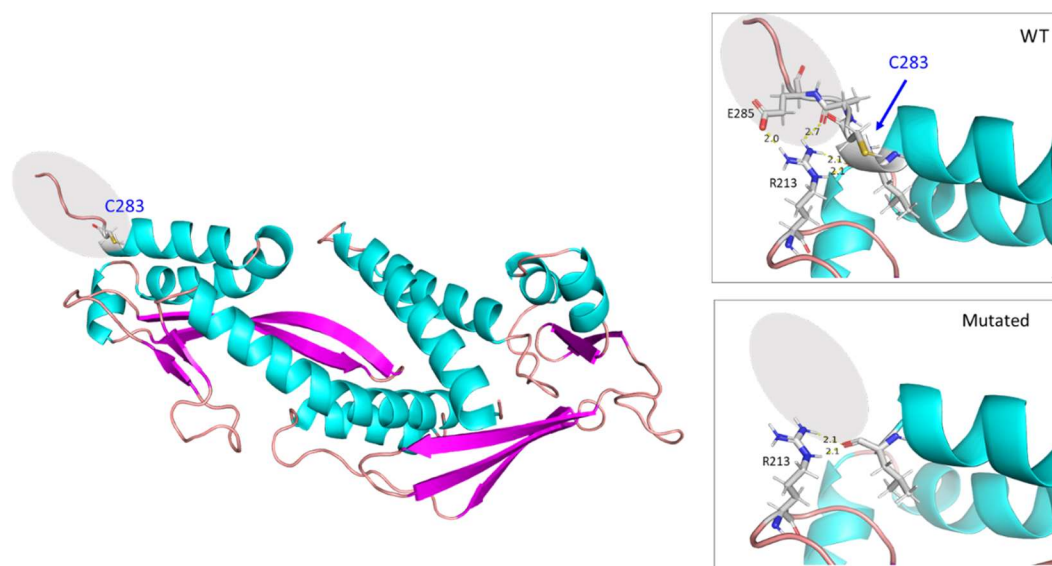


Figure 5.14 – CENPP modeled by Robetta-AB method. Shaded area includes the truncated region because of the variant, deleting from cysteine 283 onward. Amplified panels show the loss of polar interactions of glutamate 285 and alanine 284 with arginine 213 between wildtype and mutated protein.

Best validations were obtained with Robetta-ab models (Supplementary Table 5). Protein modeling using the Robetta-ab method is comparable to models created by experimental techniques (196). The trimming of the final five amino acids produces a slight reduction in stability ($\text{SCOOP}:\Delta\Delta G = 0.4 \text{ kcal/mol}$), and leads to the loss of the polar interaction between glutamate 285 and alanine 238 with arginine 213 (Figure 5.14, amplified region).



5.3 - Chapter 3: Validation of genes and variants associated with hypoplasia of ES in MD

5.3.1 - Candidate variants were validated by Sanger sequencing

Candidate variants of patients with MD and ES hypoplasia in the sporadic and familial cases with lower coverage or quality were validated by Sanger sequencing to confirm their presence (Figure 5.15). The patients nomenclature and the color of the variants are the same as those used in figures 5.9 and 5.10 in sporadic patients, or pedigree codes in familial cases.

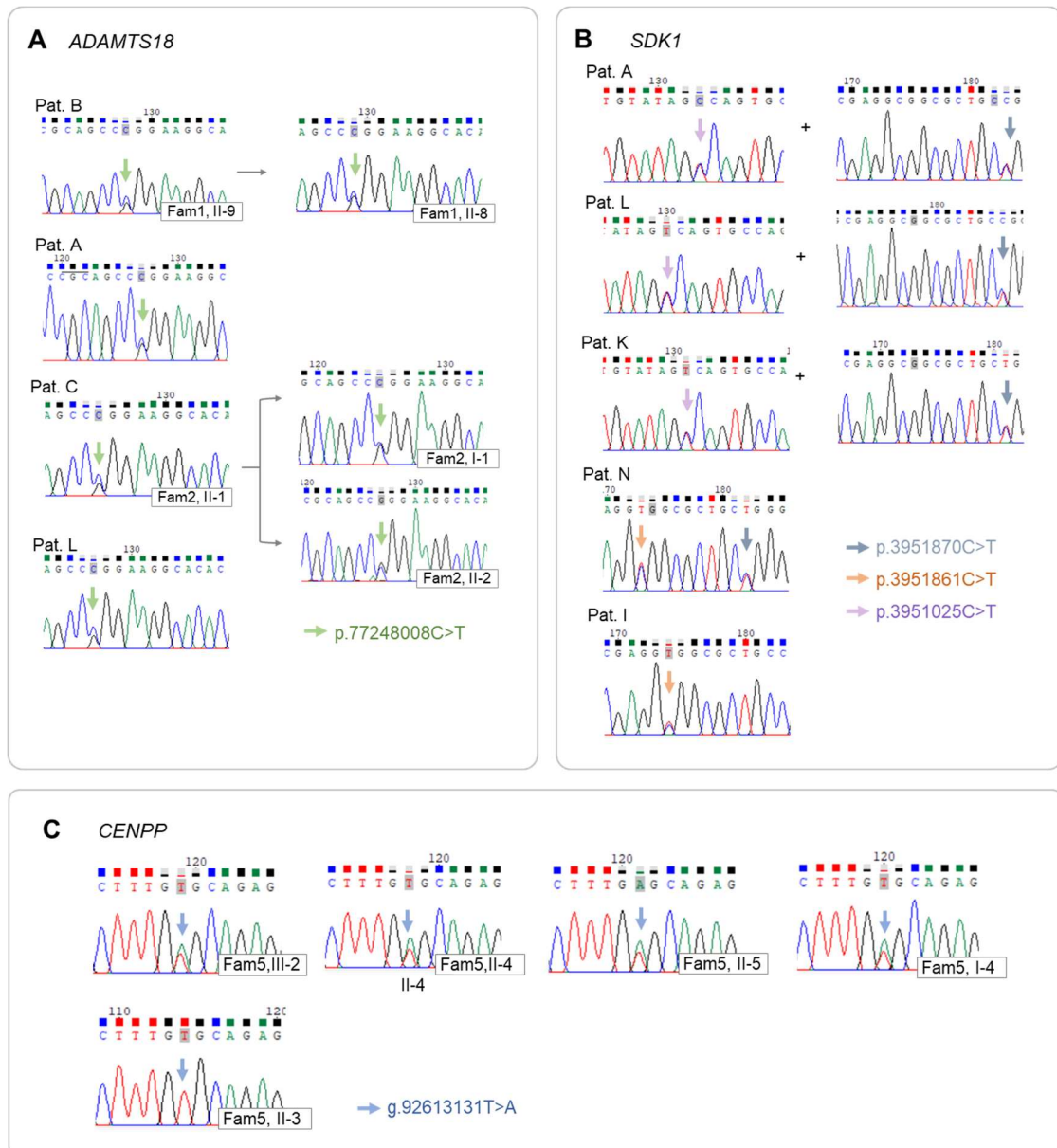


Figure 5.15 - Sanger validation of candidate variants in *ADAMTS18* (panel A); *SDK1* (panel B) and *CENPP* (panel C). The different variants are indicated with arrows of different colors, whose correspondence is indicated in the legend.

5.3.2 - Immunohistochemical analysis revealed the expression of Adamts18 in the mice inner ear

Hereunder, the results of the IHC on the axial sections in the mouse head are exposed, separating the cochlear duct, the vestibular organs, the SE region and the remodeling bone surrounding cochlea and vestibular organs (Figure 5.16, Figure 5.17, Figure 5.18 and Figure 5.19), respectively.

In the general view of the cochlea (Figure 5.16, A), clear specific signal for Adamts18 is observed in the organ of Corti, the *stria vascularis* and the bodies of the SGN. This staining can be observed with more precision on the magnification (Figure 5.16, C), where it is possible to distinguish the different cells that constitute the organ of Corti. Labeling can be differentiated on both sides of the tunnel of Corti, the inner HC and outer HC. Panels E and F focus on the *stria vascularis*, where obvious signaling can be differentiated along its entire length. Remarkably, a slight signal is observed at the edge of the membranous and osseous labyrinths, in the border between both types of tissues, specifically between the fibrocytes of the spiral ganglion and the remodeling bone (label as “bLab” in the figure). No signal was observed in the negative controls (figure 5.16, B, D, G and H).

The vestibular organs and SCC were also investigated. Due to the three-dimensional complexity of the vestibular system, only the utricle and SSC are visualized in these sections (Figure 5.17). In the magnifications, staining is unequivocally distinguished in the utricular maculae and crista *vascularis* of the SSC, (Figure 5.17, C and E, respectively). Surprisingly, the similar signal observed at the membranous and osseous labyrinths borders (bLab) in the cochlear duct is again revealed in vestibular organs. No signal was observed in the negative controls (figure 517, B, D, F).

The course of the ES is observed emerging from the inner surface of the otic capsule in the PCF, running along the SS (Figure 5.18). The narrower and more tubular proximal part of the sac (*pars canalicularis*) is not yet completely surrounded by bone at this 3-day postnatal stage. In the extraosseous zone (eES), the ES reaches its greatest volume, resting on the SS. The bone canal that forms the AV, which starts from the vestibule and reaches the PCF through the otic capsule, is not observed in these sections. In the ES and surrounding structures, no specific signal was observed, nor in the lumen or the ES epithelial cells (Figure 5.18, A, B).

The Adams18 signal was observed, as indicated, in the limits of the membranous and osseous labyrinths around the cochlear duct and vestibular organs (bLab) (Figure 5.16 and Figure 5.17). Therefore, more distal areas of the otic capsule were also investigated (Figure 5.19). Interestingly, Adams signal is observed in chondrocytes in an intermediate stage between hypertrophy and ossification (Figure 5.19, A, B, F, E) during the endochondral ossification process, schematized in Figure 5.19, I. In this step the heterogeneous cartilage matrix is digested by osteoclasts and calcified by osteoblasts to produce mature bone. Cells in this stage are characterized by loss of cells tabication, collapse of cytoplasm, and caking of nuclei.

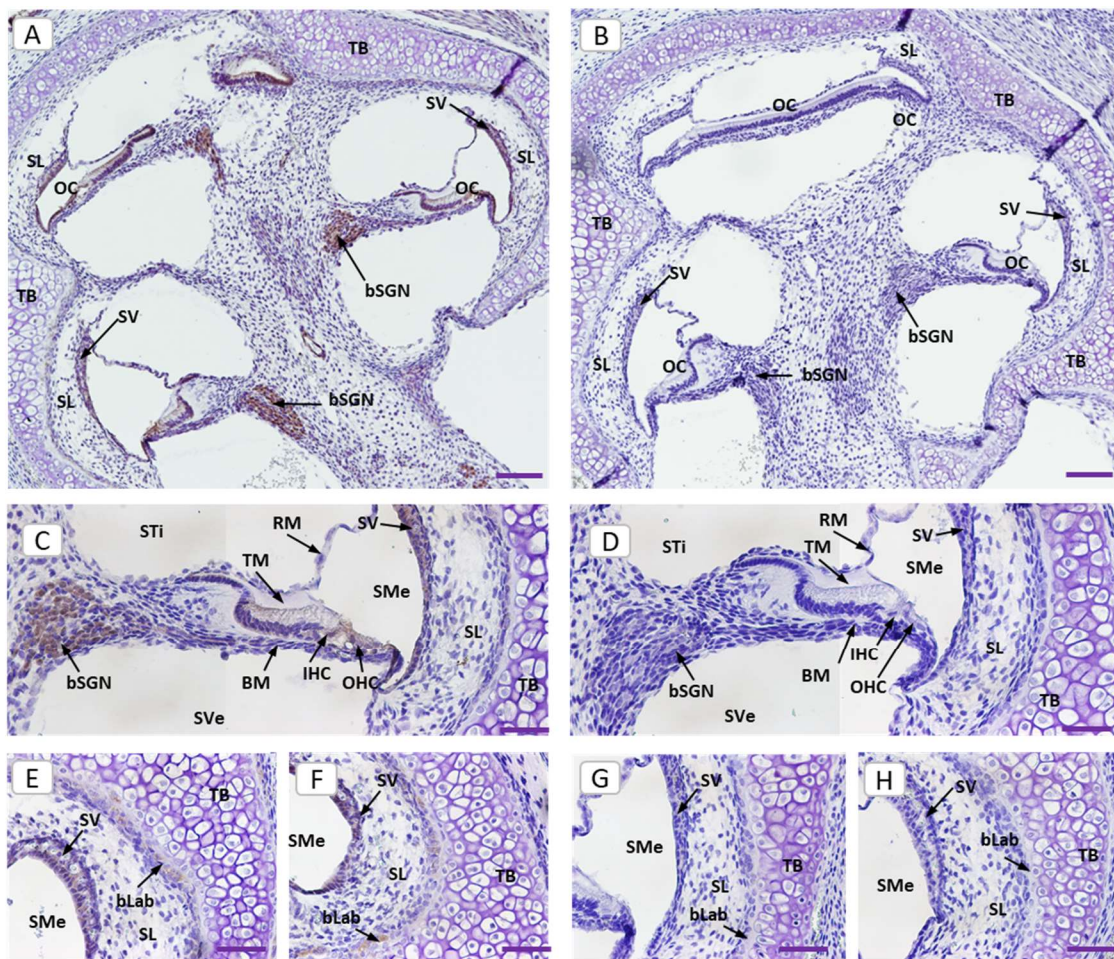


Figure 5.16 – General view of mouse TB in the axial plane (A, B), with magnification of Organ of Corti (C,D) and *stria vascularis* (E-H) areas. Specific staining for Adams18 label as a brown precipitate. B, D, G and H are negative technical controls. BM: basilar membrane; bLab: boundaries of membranous/osseous labyrinth in the cochlear duct; bSGN: bodies of spiral ganglion neurons; IHC: inner hair cells; OC: Organ of Corti; OHC: outer hair cells; RM: Reissner membrane; SL: spiral ligament; SMe: scala media; STi: scala timpani; SV: stria vascularis; SVe: scala vestibuli; TB: temporal bone; TM: tectorial membrane. Scale bar: 100µM (A, B), 50µM (C-H).

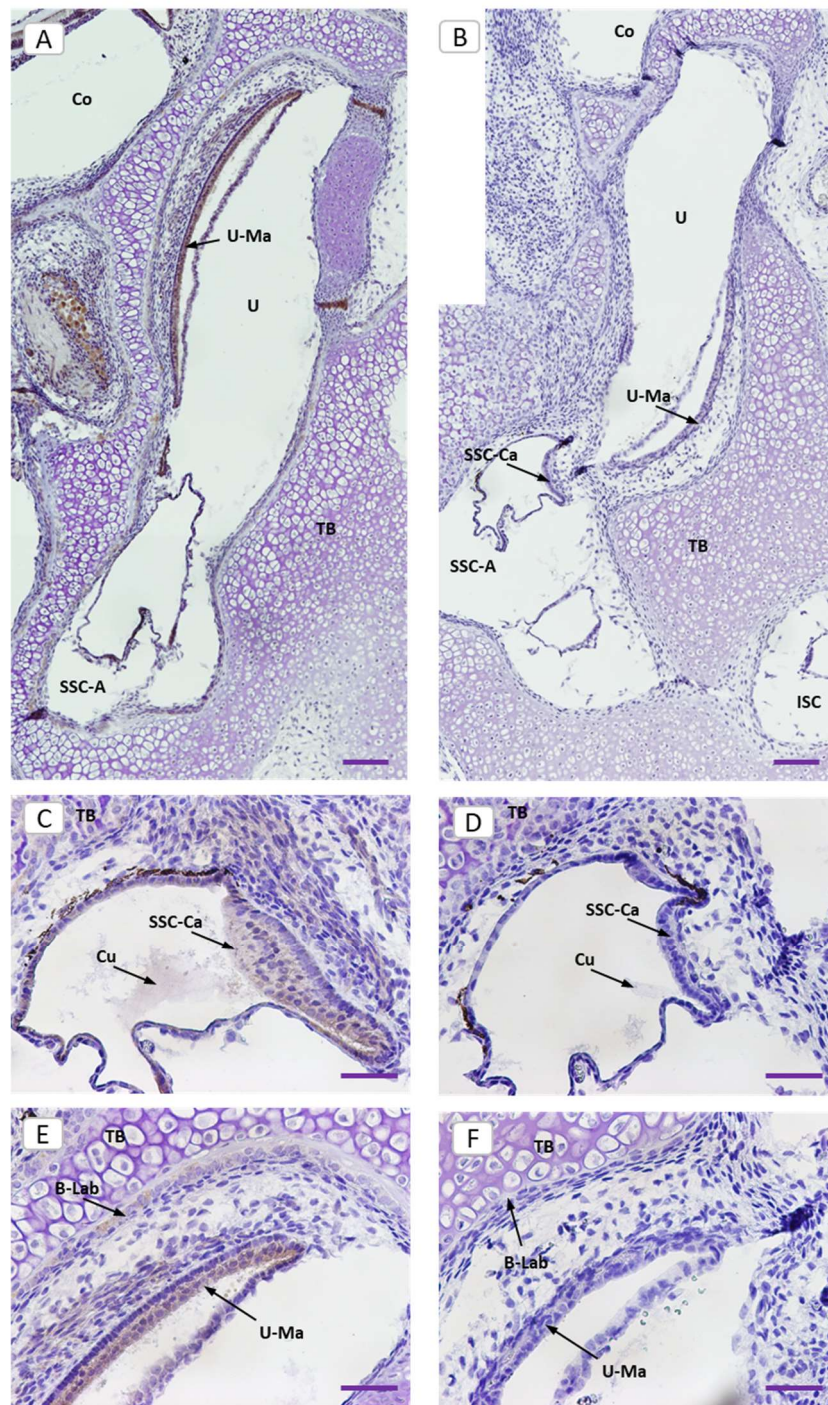


Figure 5.17 – Axial section in the mouse vestibular organs area. General view (A, B) and magnification of SSC crista ampullaris (C, D) and utricular maculae (E, F). B, D, and F show negative technical controls. bLab: boundaries of Labyrinths (membranous and osseous) in the vestibular organs. Co: cochlea; Cu: cupula; ISC: inferior semicircular canal; SSC-A: ampulla of superior semicircular canal; SSC-Ca: *crista ampullaris* of superior semicircular canal; TB: temporal bone; U:utricle; U-Ma: utricular maculae. Scale bar: 100µM (A,B), 50µM (C-F).

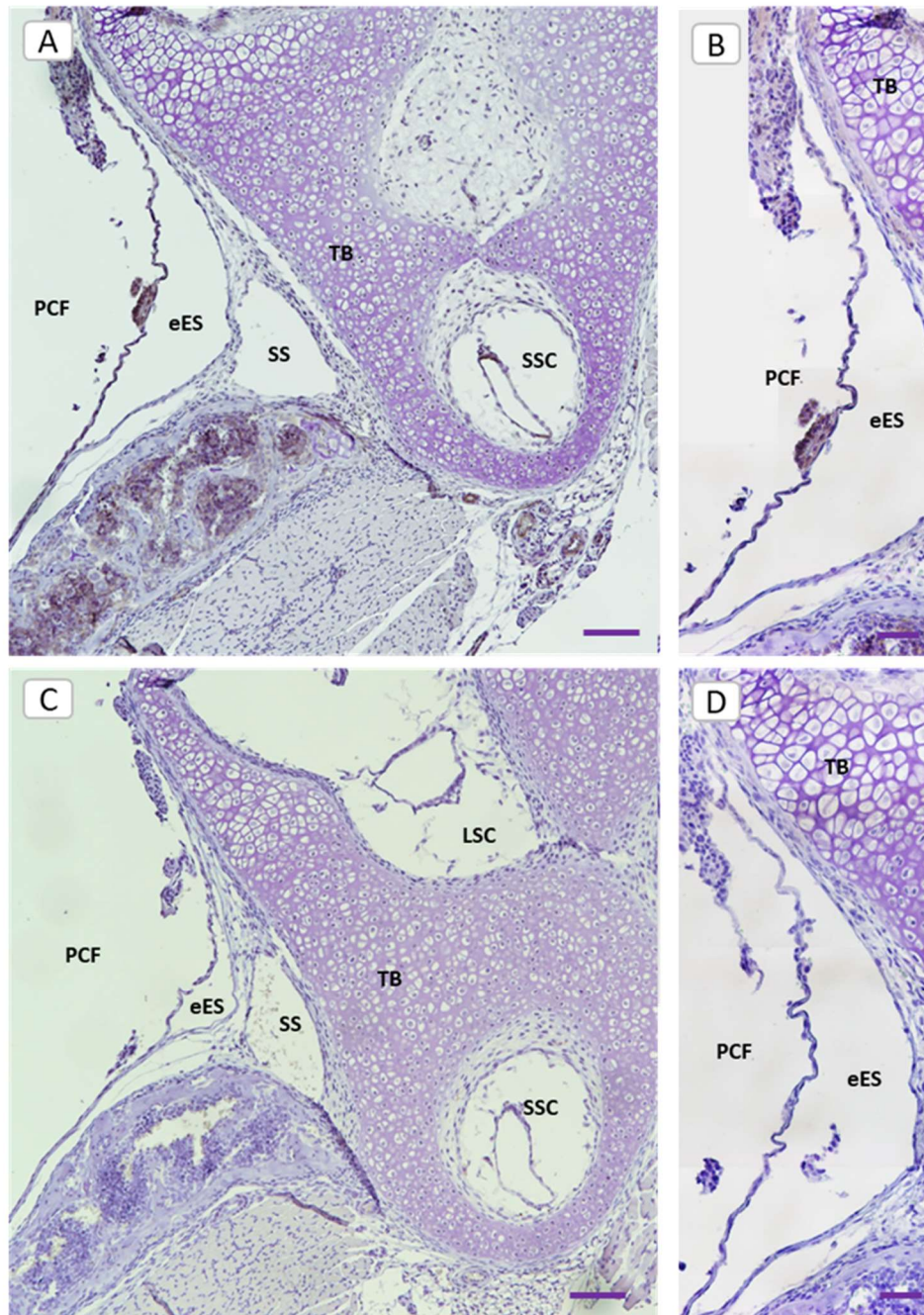


Figure 5.18 – General view of the mouse TB. The PCF and SS area (A, C) and magnification (B, D). Specific staining for Adamts18 label as a brown precipitate. B and D show negative technical controls. eES: extraosseous PCF; LSC: lateral semicircular canal; PCF: posterior cranial fossa; TB: temporal bone; SS: sigmoid sinus SSC: superior semicircular canal. Scale bar: 100µM (A,B), 50µM (C-F).

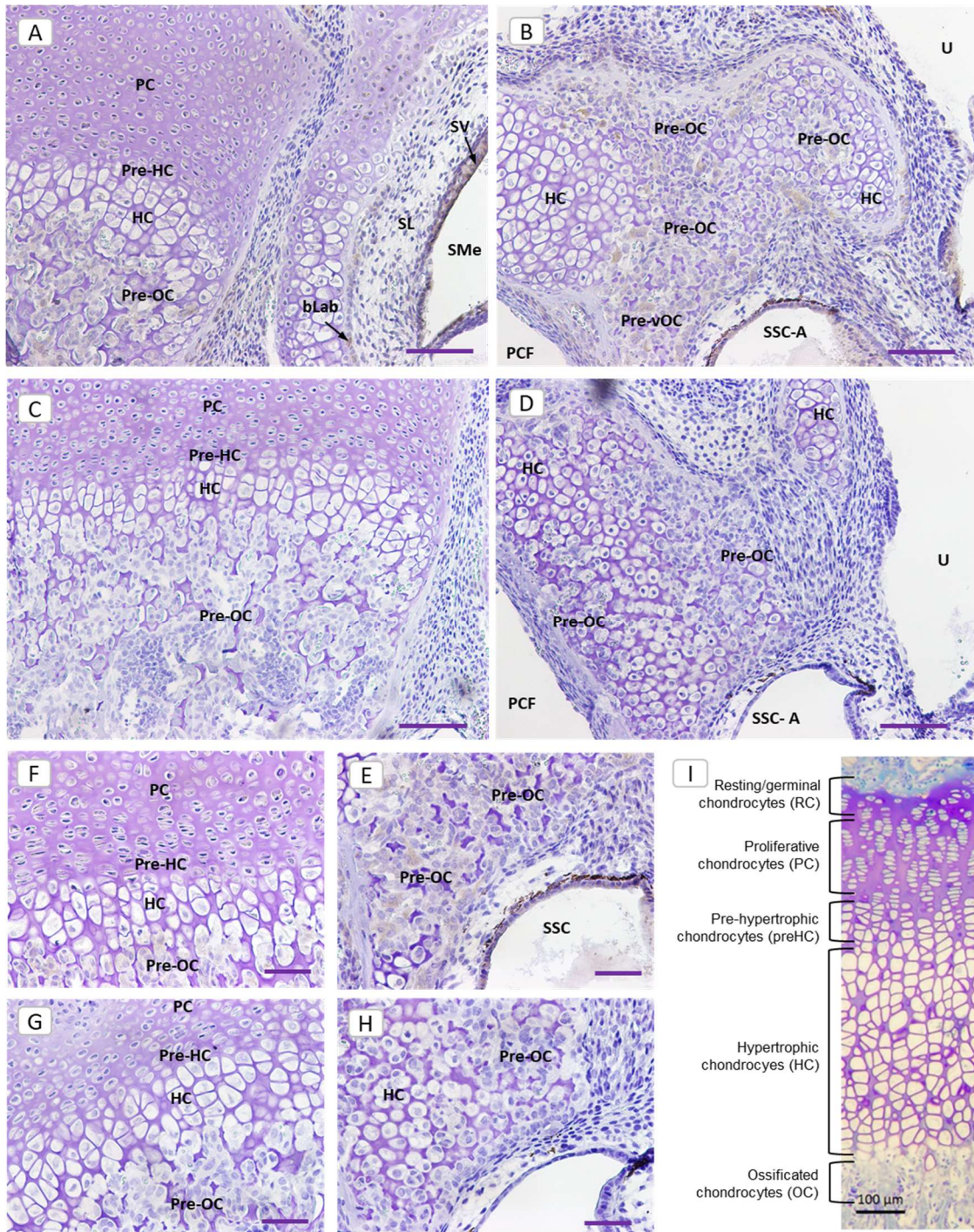


Figure 5.19 – Mouse axial section in the otic capsule surrounding cochlear and vestibular organs. General view (A, B) and magnifications (F, E) in several areas of bone remodeling. Lower panels C, D, G and H are negative technical controls. I: schematic figure of bone maturation by endochondral ossification, modified from (197). bLab: boundaries of labyrinths (membranous and osseous); HC: hypertrophic chondrocytes; PC: proliferative chondrocytes; preHP: pre-hypertrophic chondrocytes; RC: resting/germinal chondrocytes; SMe: scala media; SL: spiral ligament; SV: stria vascularis; PCF: posterior cranial fossa; SSC: superior semicircular canal; OC: ossified chondrocytes; U: utricle. Scale bar: 100µm (A-D), 50µm (E-J).

5.3.3 - Western Blot assay replicated the expression of Adamts18 in the mice inner ear

Western blot assays replicated Adamts18 expression in the inner ear organs observed in the IHC. The cerebellum was chosen as a positive control, and the spleen as a negative control, according to the expression data in both mouse and human consulted in BioGPS and GTEX systemic databases.

The figure 5.20 shows 4 revealed membranes including organs of 4 different biological replicates (R1-R4), except in cochlea, where at least 6 ears from 3 different animals were used per line. It is necessary to specify that the line "Co" includes the sensory epithelium of the cochlea without bone, "V.O." carries part of the vestibule and the SCs plus the surrounding bone, and "O.C." include only bone, specifically the otic capsule that surrounds the sensory epithelium of the cochlea. Replica 1 did not include the line with only the otic capsule. The ES was not included due to the difficulty in dissecting this structure at the P3 stage in mice.

The expression of both controls was found as expected, giving signal in the cerebellum and being absent in the spleen. In the target organs, the cochlea showed the highest expression, even more than the positive control. The expression in vestibular organs plus otic capsule was lower than in cochlea, although it was also evident. Expression in the otic capsule surrounding the sensory epithelium of the cochlea was less appreciable. Significant differences were found in the expression levels between cerebellum and cochlea versus negative control.

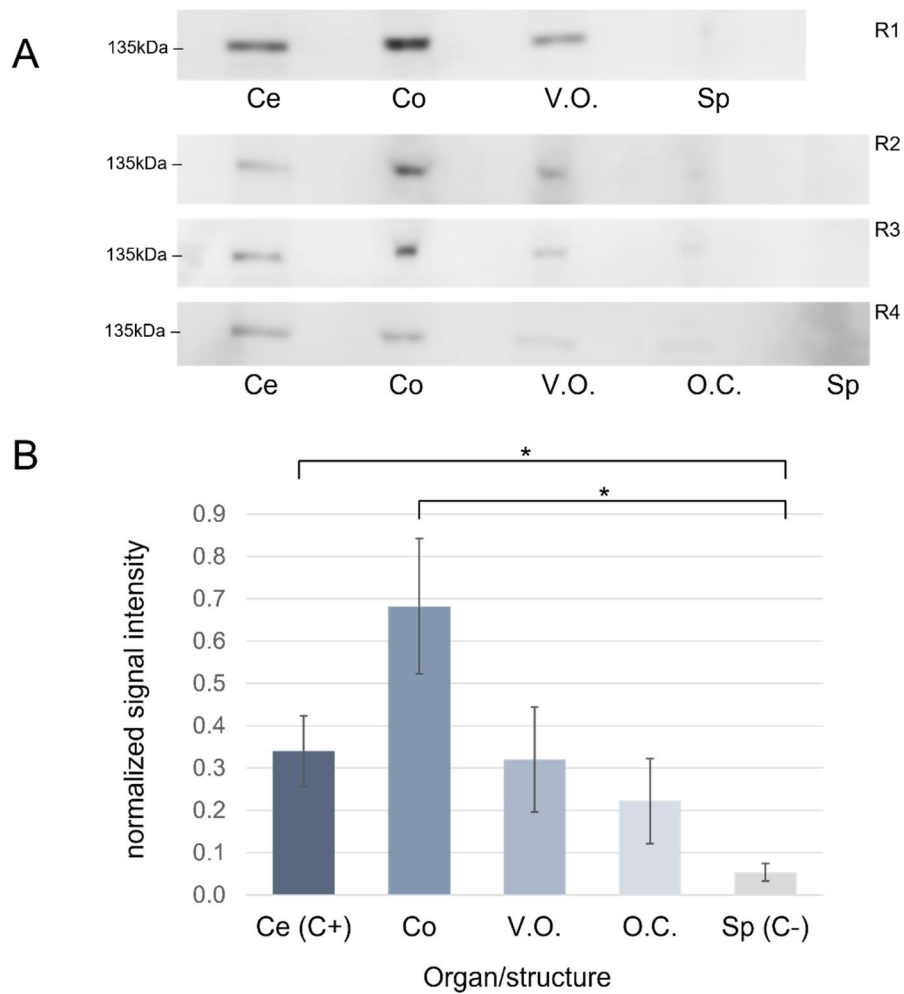


Figure 5.20 – Western Blot expression assays identifying Adamts18 expression in the inner ear organs. A) Membrane revealed in four different biological replicates (R1-R4). B) Signal quantification. Ce: cerebellum; Co: cochlea; V.O.: vestibular organs; TB: temporal bone; Sp: spleen. Error bars: SEM; Significant differences (p value < 0.05) are indicated with *.

5.3.4 - Evaluation of rare variants in protein structure or expression

5.3.4.1 - *ADAMTS18* variants

To understand the effects of the uncommon variations in the *ADAMTS18* protein, we analyze the location of these variants across the secondary structure of the protein. This includes examining the specific areas (or domains) within the protein where they occur, how each segment of the protein is organized, and the changes that happen to the protein after its initial creation (post-translational modifications) (Figure 5.21).

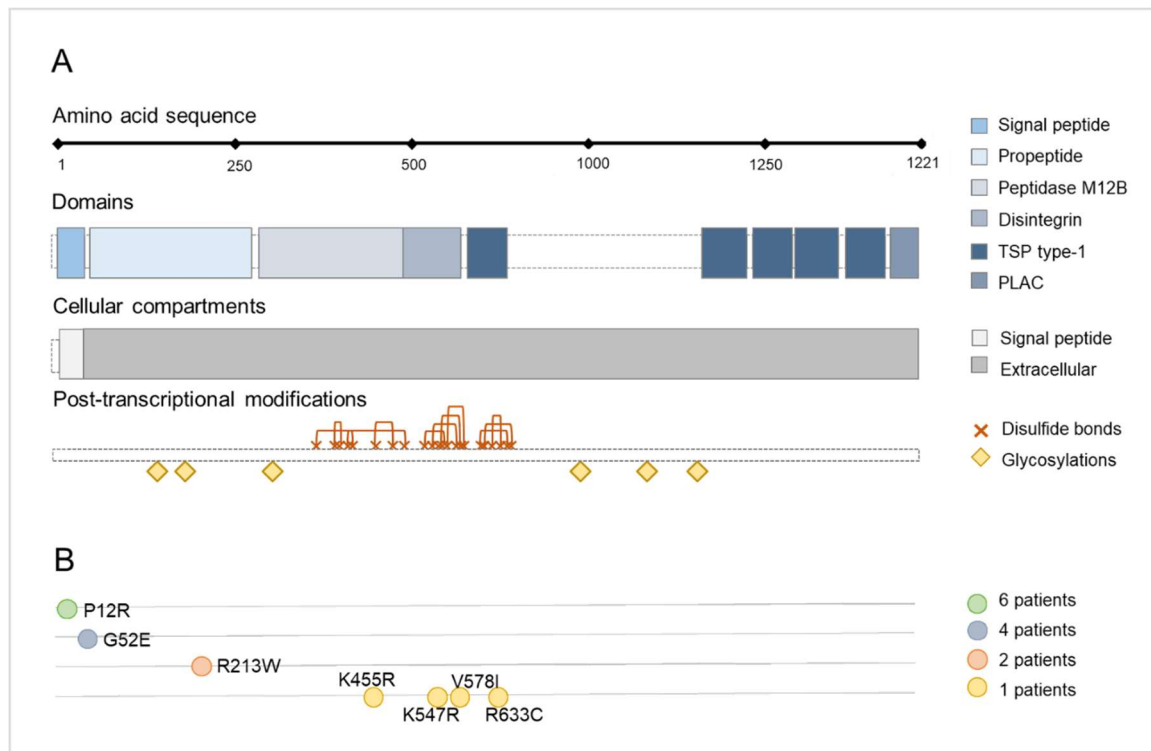


Figure 5.21 - Structural information of *ADAMTS18* and location of the rare variants found in the hypoplastic cohort. A) Scheme of the structure of *ADAMTS18* in terms of the domains that compose it, the cellular compartmentalization of each segment and the post-transcriptional modifications to which it is subjected. B) Variants in *ADAMTS18* found in the hypoplastic cohort. The legend for variants indicates the number of patients in which each variant is found depending on color.

Human *ADAMTS18* (Uniprot Accession Number Q8T660) has 1221 aminoacids and a molecular mass of 135,167 kDa. *ADAMTS18* is a member of metallopeptidases family with enzymatic activity. In their structure, *ADAMTS* enzymes include from amino to carboxi-terminal extremes: a signal peptide, a pro-peptide region, and the mature chain composed of a catalytic domain with a reprotolysin-type zinc-binding motif, a disintegrin-like



region, a central thrombospondin type-1 (TSP) motif, a cystein-rich region, a spacer region, five additional C-terminal TSP repeats and a protease and lacunin motif (PLAC). Carboxi-terminal regions from the first TSP motif to PLAC determine substrate specificity. In fact, the different types of forms in ADAMTS family differ in the number of these TSP domains. The pro-peptide of about 280 amino acids is cleaved to generate the mature protein. The cysteine switch motif including residues 252-259 housed the active site with the catalytic conserved cysteine. Its binding and dissociation to ion Zn^{2+} produces inhibition and activation of the enzyme, respectively.

ADAMTS18 is a secreted protein, found mainly in the extracellular space. The protein is subject to various glycosylations that mediate for proper secretion. This enzyme has been associated with biological processes including ion binding, metalloendopeptidase activity, and organization of the extracellular matrix.

In this work we have found an enrichment of 7 missense variants in 15 individuals in *ADAMTS18*. The g.77434661G>C,P12R variant shared in 6 individuals involves a change from proline to arginine at amino acid 12, in the signal peptide from a polar uncharged amino acid proline to a positively charged arginine. The second most represented variants, 16:77248008C>T,G52E and 16:77367582G>A,R213W in 4 and 2 individuals, respectively, are found in the propeptide. The rest of the variants in 1 individual are distributed in the peptidase, disintegrin and TSP-type-1 domain. The variants g.77341774T>A,H547L and g.77335883C>T,V578I are located one residue close to an amino acid that forms disulfide bonds. The amino acid changes produced, from histidine to lysine (both positively charged) and from valine to isoleucine (both hydrophobic) should not sterically alter the formation of the bond and the three-dimensional protein structure. None affect a glycosylation residue or active site.

5.3.4.2 - *SDK1* variants

In order to assess the consequences of our rare variants, the location of the variants is studied in relation to the domains of *SDK1* protein, the cellular compartmentalization of each motif, and the post-transcriptional changes to which it is subjected (Figure 5.22).



Figure 5.22 - Structural information of *SDK1* and location of the rare variants found in the hypoplastic cohort. A) Scheme of the structure of *SDK1* in terms of the domains that compose it, the cellular compartmentalization of each segment and the post-transcriptional modifications to which it is subjected. B) Variants in *SDK1* found in the MD and ES hypoplastic cohort. The legend for variants indicates the number of patients in which each variant is found depending on color.

Sidekick molecule 1 (*Sdk1*) is a transmembrane member of *Sdk* proteins, included in the immunoglobulin superfamily. *Sdk* proteins have an important role as adhesion molecules promoting the synaptic connections in the membrane of interneurons.

Human *SDK1* (Uniprot Accession Number Q7Z5N4) has 2213 aminoacids and a molecular mass of 242,112 kDa. In its structure, from the amino to the carboxy terminus, several domains are arranged as follows: the signal peptide and propeptide composed by one ectodomain with 6 Ig-like motifs and 13 fibronectin-type III (FNIII) motifs, and a short cytoplasmic domain with a PDZ motif. Ig-like domains intervene in protein dimerization and cell-cell adhesion, PDZ interact with cytoplasmic molecules and define the synaptic localization, and FNIII is thought to be involved in adhesion to the neighboring cell membrane (Yamagata 2020).



In this work we have found an enrichment of 12 missense variants in 14 individuals in *SDK1*. Those shared between higher individuals are found in the Ig-like domains in the protein. The g.3951870C>T,P367L variant in Ig-like 3 present in 4 individuals produce a change from a proline to a lysine, changing a bulky and hydrophobic amino acid to a positively charged polar one. Also g.3951025C>T,A317V, and g.3951861C>T,A364V, found in 3 and 2 individuals respectively, are located in the Ig-like 3 domain. Both generate a change of alanine for valine, two very similar hydrophobic amino acids, which only differ in one more carbon in the valine side chain. The other variant determined in 2 individuals (g.3974407C>T,S619L) is found in the Ig-like 6 domain, changing a non-charged polar serine to a positively charged lysine.

The rest of the variants are only found in 1 individual. Of note, the variant g.4220247A>G,N1893S in the FNIII 3 motif makes disappear an asparagine that undergoes glycosylation, modifying to a serine, also an uncharged polar amino acid but with a shorter side chain. The two variants g.4149315C>T,R1493C and g.4149316G>A,R1493H affect the same residue 1493 of the FNIII 9 domain. The change from arginine to histidine maintains a charged residue, while the change to serine adds an SH group. The rest of the variants are found in Ig-like 1 (g.3619104C>T,T108M), Ig-like 4 (g.3962743G>A,G441R), FNIII 1 (g.3987268C>T,P693S) and FNIII 4 (g.4077067C>T,T1027M) domains, and do not affect any amino acid that forms disulfide bridges or undergoes glycosylation.

5.3.5 - Functional analysis of GBA enriched variants genes

Among the eight databases contrasted in the functional analysis and using as input the 94 enriched genes resulting from the SNV/InDels GBA, only those appearing in Figure 5.23 were significantly enriched. Detailed information from these pathways is shown in Table 5.9.

GO according to “cellular compartments” (cc) and Reactome revealed similar pathways referring to the formation and maintenance of the ECM, including “collagen-containing extracellular matrix”, “extracellular matrix” and “extracellular matrix organization”. The encoded proteins in these pathways included ECM constituents (COL6A6 and COL20A1, MTN4, TECTA), interactors between ECM and cells (NID1, ITGA1), enzymes or enzymes regulators (ADAMTS18, PAPLN, ITH4), and transcription factors ligands (LTBP2, LTBP3).

According to disease annotation databases, OMIM and DisGeNET co-annotation revealed the relationship with non syndromic hearing loss of *WHRN*, *MYO7A* and *TECTA*, widely associated with the organization of stereocilia HC and constituent of TM in the inner ear sensory epithelia.

The top 20 of the most enriched routes and pathways (although not significantly) contrasted in the rest of the databases are shown in the Supplementary Figure 1.

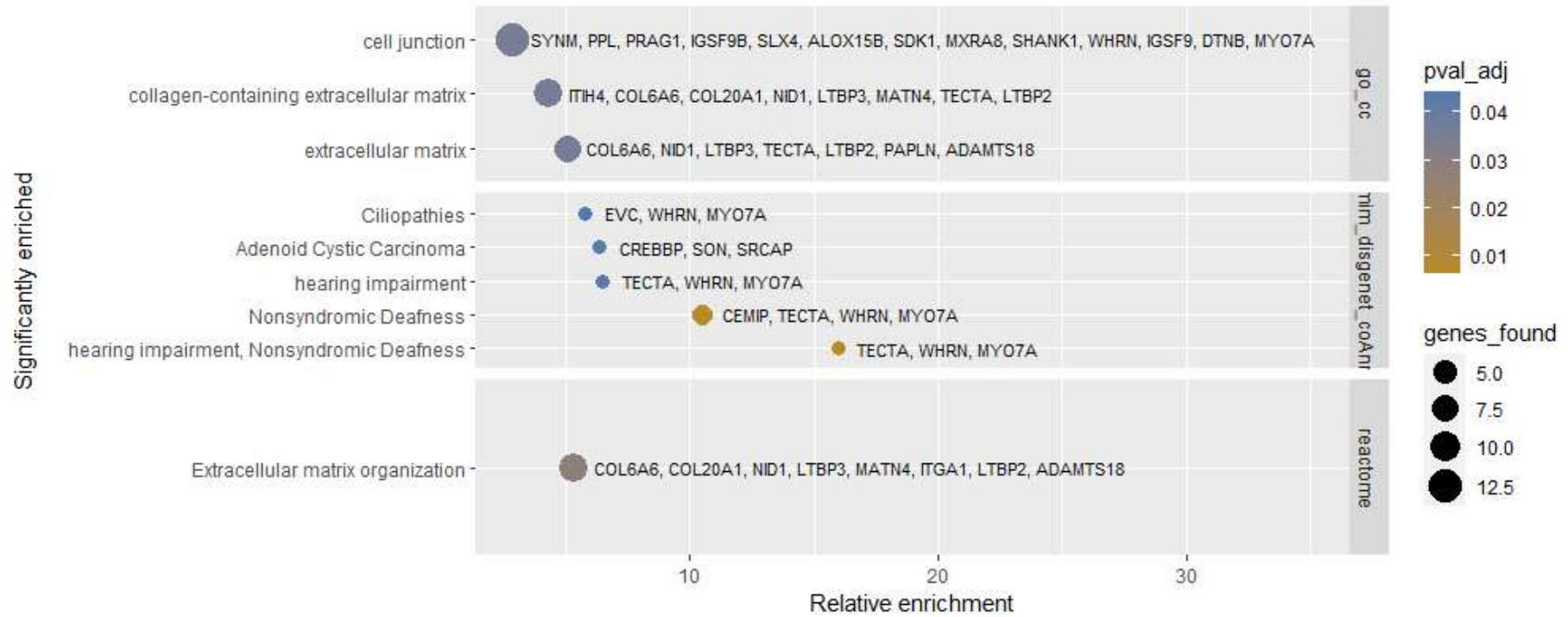


Figure 5.23 - Significantly enriched cellular compartments, pathways and diseases with our 94 GBA rare variants enriched genes.

Table 5.9 - Functional analysis enriched pathways using input genes from our GBA analysis.

Database: entity ID	Description	Genes found	Input size	Total genes	p value adj	Relative enrichment	Genes
GO (cc): GO:0030054	cell junction	13	92	938	3.6E-02	2.84	<i>SYNM, PPL, PRAG1, IGSF9B, SLX4, ALOX15B, SDK1, MXRA8, SHANK1, WHRN, IGSF9, DTNB, MYO7A</i>
GO (cc): GO:0031012	extracellular matrix	7	92	284	3.6E-02	5.06	<i>COL6A6, NID1, LTBP3, TECTA, LTBP2, PAPLN, ADAMTS18</i>
GO (cc): GO:0062023	collagen-containing extracellular matrix	8	92	379	3.6E-02	4.33	<i>ITIH4, COL6A6, COL20A1, NID1, LTBP3, MATN4, TECTA, LTBP2</i>
Reactome: R-HSA-1474244	Extracellular matrix organization	8	52	301	2.9E-02	5.36	<i>COL6A6, COL20A1, NID1, LTBP3, MATN4, ITGA1, LTBP2, ADAMTS18</i>
OMIM-Disgenet co-annotation: C3711374	Nonsyndromic Deafness	4	46	81	6.4E-03	10.51	<i>CEMIP, TECTA, WHRN, MYO7A</i>
OMIM-Disgenet co-annotation: C1384666; C3711374	hearing impairment, Nonsyndromic Deafness	3	46	40	6.4E-03	15.96	<i>TECTA, WHRN, MYO7A</i>
OMIM-Disgenet co-annotation: C0010606	Adenoid Cystic Carcinoma	3	46	100	4.3E-02	6.38	<i>CREBBP, SON, SRCAP</i>
OMIM-Disgenet co-annotation: C1384666	hearing impairment	3	46	98	4.3E-02	6.52	<i>TECTA, WHRN, MYO7A</i>
OMIM-Disgenet co-annotation: C4277690	Ciliopathies	3	46	110	4.4E-02	5.80	<i>EVC, WHRN, MYO7A</i>

Columns (left to right) indicate: Database and standardized code for that term in each database; description of term; genes found: entities (genes) found in our input list in that particular reference pathway; input size: number of genes in our input list annotated in each reference database. Total genes: number of total genes in that particular reference pathways; p value adj: Benjamini/Hochberg FDR corrected p value; Relative enrichment: proportion between i) the ratio of input genes found in the pathway respecting to the input genes found in the database, and ii) the ratio of total genes in the pathway referring to the total genes in the database; and the name of genes. (Additional information in <https://genecodis.genyo.es/>).



6. – Discussion



Our work goal was to characterize the molecular genetics of ES hypoplasia and to confirm that this histopathological condition defines an endophenotype in MD.

The studies carried out by Andreas Eckhard and David Bächinger defined the foundations in the definition of both histopathological findings, hypoplasia and degeneration of the ES in MD patients. The significant differences existing in the clinical picture and pathological findings in the TB may define two distinct endophenotypes within the disease. Intriguingly, the presence of a family history of MD, SNHL, or vertigo, TB abnormalities, primarily bilateral involvement, and a propensity for early onset were associated with the ES hypoplastic phenotype (32,156).

In patients with ES hypoplasia, the diagnosis of MD, unilateral or bilateral, is associated always with the same ear, or ears in which the ES finding was found (32,156). In a posterior investigation, Bächinger described that in the case of bilateral ES hypoplasia but a diagnosis of unilateral MD, 69% developed symptoms in the contralateral ear in a mean of 12 years (157). All together suggests that the presence of hypoplasia is clearly related to the development of MD, and it supports the hypothesis of a genetic cause during the formation of the ES. In this way, the abnormalities found in the TB during development would lead to the abrupt termination of the ES at the exit of the AV in the operculum, producing an alteration in the endolymph drainage and increasing the pressure inside the inner ear, thus producing the clinical picture of symptoms associated with MD, including the presence of EH.

Therefore, the main objective of this Thesis is to identify the genes associated with the hypoplastic endotype of the ES in MD patients.

MD is considered a complex disease with great heterogeneity, including variable symptoms at its onset, which can manifest with different severity, presence of comorbidities and with a multifactorial etiology, comprising an immune-related facet, alterations in the endolymphatic flow, and the genetic background. Over 20% of patients have a family history, where autosomal dominant or recessive inheritance patterns, sometimes with incomplete penetrance, and partial clinical pictures (85). Therefore, the genetic approach will be focused on multiple genes or causative variants with moderate and additive effects on phenotype and rare allele frequency in the general population (160).



6.1 - ES hypoplasia is absent in our cohort of patients without MD

Our approach to find the genetic basis of ES hypoplasia will be based on the search for rare variants using the control population as a reference. This approach assumes that ES hypoplasia does not exist in the control population.

ES hypoplasia was identified in about 1 in 4 MD patients in the investigations performed by Eckhard *et al.*, and Bächinger *et al.*, (32,155). Given that there are 1-2 cases of MD in every 2000 people in the European population, the inferred prevalence of ES hypoplasia in the general population would be 1-2 per 10.000, or practically nonexistent. Nevertheless, less than 100 controls were contrasted in these trials, a few observations that cannot guarantee the non-existence of this finding in the general population. Therefore, the Chapter 1 of this thesis aims to confirm the absence of ES hypoplasia in the general population. For this purpose, we conducted a retrospective cross-sectional study to explore the prevalence of ES hypoplasia in the general adult population.

One problem with the study design was the requirement of CT scan with enough resolution in the ear region to show the bony boundaries of the vestibule, SSc, and AV. These specific CT are from patients coming from the ENT department, and therefore, the specialists who ordered these tests already suspected some type of audio-vestibular pathology. Thus, our cohort of patients cannot be referred to as a "control" population, because it is biased by the type of patients who attend the otolaryngology clinic. In consequence, the CT recruitment process was focused on avoiding the inclusion of patients who might have undiagnosed MD or who might develop it in the future. In this way, exclusion criteria included i) definitive diagnosis of MD, and ii) patients who had experienced episodes, overlapping or not, of at least two main symptoms of the disease (vertigo, SNHL or tinnitus) with less than 40 years old, since the onset of this pathology is usually late. Finally, we refer to this cohort as the "non-MD cohort".

After patients and CT recruitment, some patients in the non-MD cohort had clinical symptoms overlapping with MD, with 5 (3.2%) having vertigo, 3 (1.9%) having tinnitus, and 10% (6.4%) having SNHL. These patients were further examined and in no case they had experienced any other overlapping symptoms of MD.

In our cohort of non-MD patients, we did not find cases of ES hypoplasia in the 332 ears analyzed. This would indicate that ES hypoplasia is absent in patients without MD,



and if it exists, its prevalence is below 0.57% if we refer to the number of patients or below 0.3% if we think of the number of ears. The mean ATVA value for these patients was $95.6 \pm 9.8^\circ$, with a maximum of 126.63° and minimum of 65.95° . In Eckhard *et al.*, histological sections from 20 TB of controls for EH and MD were studied, where no ES hypoplasia was found (32). Sixty-two controls, where histology sections were available for 46 individuals and both histology sections and CT were available for 16 individuals were analyzed in Bächinger *et al.* Again, no ES hypoplasia was described and mean of ATVA values was $102.3 \pm 9.8^\circ$ (155).

Of course, 332 ears is not enough to ensure that ES hypoplasia does not exist in the population, when the estimated prevalence has been 1-2 per 10,000. In our initial design, 500 patients were included, making a total of 1000 ears. This is a longitudinal study that is yet to be completed, which is expected to increase the number of ears studied, and thereby decrease the estimated prevalence in our current calculations. However, this study represents a first step to ensure the absence of this finding in the general population, beyond the 20 and 62 controls analyzed in previous studies (32,155).

An interesting study was carried out with the same methodology by Jung *et al.*, (198) Their cohort of 301 patients is similar to our non-MD cohort, since it included adult cases with various otological diseases, differentiating four patient groups: MD, superior canal dehiscence (SCD), superior canal dehiscence syndrome (SCDS), and grouping the rest as a "Control" group. These authors did not find significant differences in the ATVA according to the established groups. In the 572 ears analyzed, 14 ears (2.3%) in 13 patients showed ATVA in the range of ES hypoplasia (>140 degrees). Only one of these patients had a diagnosis of MD, but in the ear contralateral to the ES hypoplasia. The rest showed SCDS, thin bone over the superior semicircular canal, intracochlear schwannoma, otosclerosis, or asymptomatic/presbycusis without MD. Consistent with our non-MD cohort, the mean ATVAs per group were between $105-108^\circ$. This study estimates a frequency of ES hypoplasia of 2.4% (if we refer to the number of ears), or 4.3% (if we focus on the number of individuals) in patients without MD. Thus, this study establishes a much higher prevalence than our research.

In our experience, the AVTA measurement is subject to some variability introduced by the user. In fact, some of these variations were even 15-20 degrees between observers. But, taking into account all measurements, only 4.5% (15 of 332 ears) showed poor interobserver agreement according to the Bland-Altman plot, and ATVA linear regression showed a positive correlation coefficient of 0.71. Since a difference of 15-20



degrees can perfectly mean the difference between the classification of an individual as "control" or "case" for ES hypoplasia, these cases could be studied later more deeply by both observers. A similar coefficient of 0.78 was also obtained by Bächinger *et al.*, although it was only tested in a randomly selected 14% of cases) (156). So, we conclude that in general, ATVA measures were robust and reproducible. However, Jung *et al.* are more critical of the method, indicating that it could be standardized with added restrictions to improve the reproducibility of the detected measures (198).

We have also studied the relationship of ATVA with age, sex and pathology to confirm that ATVA is independent of these variables. Since the size and shape of women skull is smaller than men's, we hypothesized that the TB could also be smaller in women (199). Age could also have affected, for example due to tissue degeneration over time, producing some variation that would affect VA. However, our results show no association of ATVA with the individual's age, sex, or pathology, being specific to the ES finding. Only a significant difference was found between tinnitus and mixed hearing loss. Nevertheless, some of these pathology groups are overrepresented, such as chronic otitis media with more than 100 individuals, meanwhile others have less than 10 individuals, such as vertigo, tinnitus, serous otitis media or mixed hearing loss. This is due to the fact that CT is usually performed in ENT for monitoring and diagnosis of chronic otitis media, cholesteatomas, otosclerosis, conductive-type hearing loss and to discard suspicions of secondary pathologies such as bone lesions or neoplasms, and for this reason these will be more represented.

6.2 - The characteristics of our MD and ES hypoplasia cohort are consistent with other patients with the same MD endotype

The classification of MD endophenotypes into hypoplastic and degenerative was postulated in 2019, so there are few studies that have used this methodology to study their cohorts of patients with MD. Thus, we can talk about the following cohorts of MD and ES hypoplasia: i) cohort of TB described by Eckhard *et al.*, 2019, with 9 individuals (32); ii) the Bächinger *et al.*, 2019 cohort, with 17 individuals (156); iii) the cohort of Jung *et al.*, 2023 with 11 individuals (198), and iv) our cohort with 42 individuals. The last three cohorts have been obtained using the same methodology: the ATVA analysis on CT images, and for this reason they will also be more easily comparable.

There is a high concordance between some clinical variables studied from ours and the Bächinger cohort, referring to sex, age, onset of first MD symptoms, presence of family history, and relation between the laterality of MD and ES hypoplasia. Both had a preponderance of men (81% vs 94%) and a similar proportion of cases with MD family history (14% vs 12%), in ours and Bächinger cohort, respectively. Patients developed first symptoms earlier in our cohort than Bächinger, with a difference of 6 years in the age mean (37 ± 11 vs 43 ± 9 years old) (156).

Considering the laterality of the MD, our cohort displays practically half each, with 57.1% of unilaterals and 42.9% bilaterals, being rather 70/30 in the Bächinger cohort, with 29.4% unilateral and 70.6% bilateral. Taking into account the laterality of ES hypoplasia referring to MD laterality, the number and proportion of individuals who showed i) bilateral MD and bilateral ES hypoplasia, ii) unilateral MD and ES hypoplasia, and iii) unilateral MD and ES hypoplasia bilateral were 18 (42.9%) and 5 (29.4%), 14 patients (33.3%) and 9 patients (52.9%), and 10 (23.8%) and 3 (17.6%), being the first data given corresponding to our cohort (n=42) and the second data from the Bächinger cohort (n=17). In both sets, bilateral ES hypoplasia always corresponds with bilateral MD, and unilateral ES hypoplasia was always found in the ipsilateral ear of MD symptoms (156). The exact numbers of patients with MD and ES hypoplasia concerning laterality are not specified in the study of TB (32). No hypoplastic ATVA ear was described by Jung *et al.*, in their MD group, but this may be due to such a limited sample of 11 MD individuals (198).

Focusing on unilateral MD patients, the authors hypothesized that patients with unilateral MD and unilateral ES hypoplasia have low risk of developing MD in the



contralateral ear, the same probability as any healthy ear (156). In fact, none of these contralateral ears showed other pathological symptoms such as the presence of EH. These individuals represent 33.3% (14 cases) in our cohort, and 52.9% (9 cases) in the Bächinger cohort. Conversely, it is expected that in patients with unilateral MD and bilateral ES hypoplasia the symptoms expand to finally become bilateral affection. Those cases consist of a total of 23.8% (10 cases) and 17.6% (3 cases) in our cohort and Bächinger one, respectively. In fact, Bächinger *et al.* verified posteriorly that around 69% of patients with bilateral ES hypoplasia and unilateral MD developed symptoms in the contralateral ear in an average of 12 years, meanwhile patients with unilateral ES hypoplasia and unilateral MD remained affected in initial ear (157). In our cohort, the years of evolution for this set of patients (10 individuals) is currently 10.3 ± 5.6 years. It would have been expected that in three patients with 16, 17 and 21 years of evolution, this progression or worsening would have already been observed.

6.3 - The abnormal development of the temporal bone, the ES, the ED and the VA are widely related to the appearance of MD

The definition of ES hypoplasia is relatively recent, but other abnormalities of the TB, the VA, the ED and the ES had been described since MD began to be studied. Stahle and Wildbrand described a lack of pneumatization, a shortened VA, and a narrowed VA exit to the PCF in 63 TB of MD patients (113). The findings of poor pneumatization were replicated by Sando and Ikeda, but also noticed hypoplasia of VA, in another cohort with 27 bones from patients with MD and EH versus 79 individuals with EH but without apparent otological disease (114). A decreased width of the ED isthmus and a collapsed ES lumen were also described in 25 EH and MD TB versus 25 controls (119). In Hebbar's research, loss of tubular complexity in the *pars canalicularis* of ES was observed, in addition to reduced ED and VA diameters in the region proximal to vestibule (200). The volume occupied by the ES has been compared between MD patients and healthy individuals from reconstructions and 3D modeling of TB. Thus, Bloch and Friss and Monsanto have reported that this space was significantly smaller in TB of patients with MD than in healthy individuals or cases with EH only (201,202). Finally, a displaced SS has also been observed in patients with MD (115). Regarding microstructural alterations, fibrosis processes in the ES epithelium and perisaccular tissue were found in MD specimens, including total absence of the epithelium, and collapse ES lumen (119,120). Similarly, Eckhard *et al.* reported the frequent finding of expelled epithelial cells, pyknotic nuclei, and fibrosis in the eES in histological sections of MD patients with ES degeneration and idiopathic EH (32).

Petrous part of the TB includes the otic capsule surrounding inner ear sensory organs. Most parts of the otic capsule reach adult-like proportions at mid-term during development. However, the distal region of the VA and the extraosseous ES undergoes changes in the postnatal stage and during several years, extending over the posterior surface of the TB lying in the dura mater still in growing. These changes include the opening of the AV to the PCF, generating an opening (operculum), which would rest on a spur of the TB. The shape, size, and extent of the operculum, the spur, the distal VA and the extraosseous ES vary broadly among adult skulls (203). Thus, environmental factors (such as middle ear infections) could affect the formation of the eES in individuals with risk genetic variants.

The features related to the hypoplastic ES endotype: a male predominance, bilateral affection, a tendency to early onset, presence of canal dehiscence in the SSC and PSC,



and findings of familial history of MD, SNHL or vertigo, suggest the hypothesis of a developmental or genetic cause. In this way, the alterations that could occur at the time of distal VA and eES formation would result in the observed histological abnormalities and clinical features. The temporal differences in the development of both areas of the otic capsule would explain why Bächinger *et al.* found that the entrance of the VA into the TB from the vestibule in adults is defined by a standard angle with very few variations, while the exit from the AV to the PCF in the operculum is much more variable (155). In fact, ATVA marker in TB of 14 patients with MD and ES hypoplasia and 42 fetuses was similar, meanwhile it differed significantly from 62 control adult bones. Thus, VA and ES development could have been arrested in an earlier stage in patients with MD and ES hypoplasia (155).

6.4 - Genetic analysis of ES hypoplasia in Meniere Disease

The results obtained from the GBA, the SV analysis and the functional analysis have pointed to candidate genes in several biological pathways, associated with some phenotypes or diseases, and supported by the IHC and WB expression assays. Some of these potential pathways could be altered as a result of burden of variants, which could ultimately produce the phenotype observed in our MD and ES hypoplastic patients.

With this in mind, the subsequent discussion is organized in three main sections, differentiating various groups of candidate genes and pathways that might be affected. They include: 6.4.1) genes and pathways involved in the development of audio-vestibular organs; 6.4.2) genes associated with bone remodeling, with a focus on the otic capsule and temporal bone; and 6.4.3) genes and pathways related with transmission of information by SGN from auditory or vestibular circuits to higher brain centers. In these pathways, at least one of our main candidate genes *ADAMTS18* or *SDK1* is represented, apart from other less significantly enriched genes involved in the same biological process, whose alteration could be having an additive effect to the phenotype.

6.4.1 - Candidate genes in the MD and ES hypoplastic cohort associated with audio-vestibular related function

6.4.1.1 - Candidate gene *ADAMTS18*

ADAMTS18 is a member of the ADAMTS family proteins (a domain similar to disintegrin and metalloproteinase with thrombospondin type 1 motifs). This family includes 19 different ADAMTS proteins whose main functions have been described in the formation and degradation of the extracellular matrix (ECM) in processes of tissue morphogenesis, repair and remodeling (204). The gene coding for this protein, *ADAMTS18*, was prioritized as one of the top candidate genes with enrichment for rare variants in our MD and ES hypoplasia cohort. A total of 7 variants in 15 patients was found, meaning they were present in 35.7% of our cases. The variants were widely shared among individuals, with 2 of them being found in 6 and 4 individuals, respectively.

Expression of *Adamts18* in mice has been located mostly in developing tissues, with its highest expression in embryonic development or early postnatal stages, such in the eye (E10.5 - E11.5), lung (E11.5 - E15.5), kidney (E10.5-P0), salivary glands (E13.5 - E14.5), lacrimal glands (E14.5 - E15.5), vascular systems (E10 - E16.5), small intestine,

adipose tissue (2 weeks postnatal), central nervous system (E18.5 - 2 weeks postnatal), and male and female reproductive tracts (1 - 6 weeks postnatal). In fact, several human GWAS association studies and animal models investigations have reported important roles of ADAMTS18 in the organogenesis of these tissues, including: lens, epithelial branching of the lung, kidney, salivary glands and lacrimal glands, formation of the aortic arch and common carotid artery and angiogenesis of the caudal venous plexus, organization of the fenestrated endothelium in the villi of the small intestine, development of visceral white adipose tissue, morphogenesis of cerebellum and hippocampus dentate gyrus cells, and formation of preputial gland and vagina in reproductive tracts (204). However, there are no studies that associate *ADAMTS18* with the development or normal physiology of the ear or inner ear, neither in the sensory nor in the structural part.

The inner ear sensory epithelia are composed of sensory HC and structural SC. Both organize and communicate through the intercellular junctions and the surrounding ECM (10). This matrix is mainly formed by collagen, tenascin, chondroitin sulfate proteoglycans and integrins (205). The importance of maintaining this matrix has also been highlighted, and the deregulation of its components has been associated with different abnormalities (206). So, deletion of the collagen receptor DDR1, involved in adhesion and migration functions, produces altered morphology of basal cells in the *stria vascularis*, HC and several types of SC, leading to deafness in mice (207). Alteration of matrix metalloproteases (MMP) have been related to development of SNHL (208–211). Induced elevated levels of MMP2, MMP9 and MMP14 lead to imbalance in ECM turnover and oxidative stress in the cochlea, producing disconnected tectorial membrane from HC, thinner *stria vascularis* and enlargement of spiral ligament fibroblasts (208). Exacerbated capillarization of cochlear ECM has been observed in mice models for Alport syndrome when inhibitors for MMP2, MMP9, MMP12 and MMP14 were administered, suggesting that these proteins are involved in basement membrane metabolism (210). Treatment of organ of Corti explant cultures with gentamicin induced MMP2 and MMP9 overexpression, meanwhile adding MMP inhibitors resulted in hair cell death, suggesting they maintain a basal expression with protective function (211). Moreover, other metallopeptidases of ADAMTS18 family have been revealed to have an inner ear purpose. Hu *et al.* found *Adamts1*, *Adamts2*, *Adamts5* and *Adamts8* expression by RNA-seq and RT-PCR in the sensory epithelium of the adult rat cochlea, where *Adamts1* showed the highest levels by far. Interestingly, after exposure to noise, an overexpression of *Adamts1* and *Adamts8* levels was observed (206). Moreover, Yamamoto *et al.*, identified that *Adamts1* acts as a marker in the differentiation pattern of the sensory and structural region of vestibule and

semicircular canals by RNA-seq in E13.5 mice during inner ear development, validating the expression by IHC (212).

In our IHC assay, the expression of Adamts18 is revealed in the sensory epithelia of P3 mice sections including the organ of Corti in the cochlea (in the inner and outer HC, SC, and *stria vascularis*), the macula of the utricle, and the *crista vascularis* of the SSC (Figure 5.16 and 5.17). In addition, western blot analysis confirms the expression in the sensory epithelia in the cochlea and vestibular organs (Figure 5.20). Besides, ADAMTS18 could be carrying out functions similar to those revealed by the studies of other metalloproteinases of the ADAMTS and MMP family mentioned above. These include i) the correct anchoring of HC and SC to basement membranes, but also HC attachment to the TM, otolithic membranes and cupula; ii) the maintaining of *stria vascularis* and spiral ligament integrity; and iii) a protective function against both chemical (cytotoxic molecules) and mechanical (acoustic trauma) damages. The *stria vascularis*, moreover, is a highly vascularized tissue, and ECM components play a decisive role in the formation of new vessels and capillaries. ADAMTS18 have been related to the angiogenesis of big vessels such as the aortic arch, the common carotid artery and the caudal venous plexus (dang 2018, ye 2021, lu 2020), but also endothelial sprouting (213), and several MMP proteins have been associated with vascularization of cochlear ECM (210). So ADAMTS18 could be involved in the regulation of the ECM in the *stria vascularis*, where it could be orchestrating blood vessels development.

In addition, our Adamts18 labeling is also observed in the boundaries of the membranous and osseous labyrinth both in the cochlear duct and vestibular organs (Figure 5.16 and 5.17). In this situation, Adamts18 would be remodeling the ECM that maintains the edges between these two diverse tissues, constituted of different cell types, and with functions as diverse as the correct reception of auditory-balance stimuli and the protective task of the otic capsule. In the western blot assays, the Adamts18 signal is observed with high intensity in the sensory epithelium of the cochlea ("Co" line), but also in the surrounding otic capsule ("O.C." line), although with less signal (Figure 5.20). However, we cannot know where this boundary zone between the two labyrinths has been dissected.

6.4.1.2 - Other candidate genes in the ES hypoplastic cohort related with MD audiovestibular phenotype

Other genes found in our analysis were related to inner ear disorders, though they appeared less significant than our candidate genes. Among them are Myosin VIIa (*MYO7A*), α -tectorin (*TECTA*) and whirlin (*WHRL*) (Figure 5.8 and Supplementary Table 2). Myosin VIIa and whirlin intervene in the interaction of actin cytoskeleton to the proteins forming the ankle-links and tip-links in the HC stereocilia (8). Specially, in the tip-links, they anchor the transmembrane region of protocadherin-15 and cadherin-23 to the actin fibers in the anterior and posterior stereocilia, respectively. Tip-link undergoes the tensile forces during the opening of MET channels in the mechanotransduction of both auditory and vestibular stimuli (7,8). On the other hand, *TECTA* is an essential component of the tectorial membrane, which interconnects the collagen fibers and anchors the TM to the surface of the stereocilia (151).

These genes were enriched in the terms "hearing impairment" and "non syndromic hearing loss" in the co-annotation produced between the DisGeNET and OMIM databases. *MYO7A* is associated with the genetic cause of some pathologies including Usher syndrome type IB (214), DFNA11 (215) and DFNB2 (216,217); *WHRN* with DFNB31 (218) and Usher syndrome type IID (219); and *TECTA* with DFNB21 (220). Usher syndrome is characterized by the association of hearing loss and retinitis pigmentosa (Ebermann 2007) and "DFNX" make reference to different types of non-syndromic SNHL autosomal dominant (DFNA) or recessive (DFNB). In addition, enrichment of rare variants in *MYO7A* and *TECTA* have been related with the pathophysiology of MD (103,144). The presence of variants in these genes could have an additive effect to the phenotype produced by our main candidates, contributing in this case to an erroneous perception or transmission of sound and balance stimuli that trigger the symptoms associated with MD.

6.4.2 - Candidate genes in the MD and ES hypoplastic cohort associated with bone remodeling

Normal bone morphogenesis during development and adult life resides in the process of bone turnover or remodeling, a highly coordinated process between bone resorption by osteoclasts and synthesis of new bone matrix by osteoblasts. Thus, old bone is replaced with new one, meanwhile osseous integrity, shape and size is maintained, except volume increases referring to growth (221). The turnover ratio differs between the

different osseous structures in the organism. The lower ratio is observed in the otic capsule, which explains why it is the hardest, and subsequently why its fractures are the most difficult to heal (222,223). In the dog, this rate has been estimated at 2.1% per year, compared with 7.4% in the humerus, or 13.9% for other cranial bones, and similar ratios have been replicated in other species. In addition, within the otic capsule itself, bone turnover is lower the closer the soft tissues are, where the remodeling ratio is estimated to be 0.13% or practically inhibited. These findings have led to the suspicion that membranous labyrinth itself controls this remodeling (222).

In the otic capsule, bone remodeling from cartilage to mature bone occurs by endochondral ossification. During this process, several zones can be morphologically differentiated (Figure 5.19, I): i) germinal stage or resting zone, with bone stem cells and nutrients; ii) proliferative zone, where chondrocytes proliferate, rapidly increasing in number, organizing themselves as a columnar mosaic; iii) hypertrophic zone, where the chondrocytes increase in size due to the entry of water, and synthesize and secrete high quantity of proteins that will form the bone ECM; and iii) ossification zone, where hypertrophic chondrocytes ossify to form mature bone (197). The edge with the ossified chondrocytes is called ossification front.

This process is orchestrated by numerous systemic and local factors, extra and intracellular receptors, osseous ECM components and transcription factors. Between them, it has been highlighted the role of: i) systemic factor such as growth hormone; ii) locally secreted soluble extracellular factors like insulin growth factor, Indian Hedgehog, parathyroid hormone-related peptide, bone morphogenetic (BMP) and transforming growth factor β (TGF- β) proteins, Wnt secreted family proteins and fibroblast growth factors; iii) components of the cartilage extracellular matrix; and iv) transcription factors such as Runx2, Sox9 and MEF2C (224). However, we will only delve into this discussion in those that have been found to be enriched in rare SNV/InDels or structural variants in our patients with MD and ES hypoplasia.

6.4.2.1 - Metalloproteinases of bone extracellular matrix

Among the components of the extracellular matrix, proteolytic enzymes have been widely studied trying to elucidate which ones are responsible for the degradation of the cartilage matrix components and therefore advancement of the ossification front. Metalloproteinases (MMP) and ADAMTS proteins are expected constituents, whose substrates include type II collagen and aggrecan, main components of bone ECM (224).

Our candidate protein Adamts18 is expressed in the osseous matrix in mice IHC sections. First, mild signal is observed in the boundaries of the membranous and osseous labyrinth in the cochlear and vestibular ducts, but does not invade chondrocytes (Figure 5.16 and 5.17). Supporting this, Adamts18 is only slightly observed in the otic capsule surrounding cochlear sensory epithelia in the “O.C.” line in the western blot analysis. At this stage, these chondrocytes surrounding the membranous labyrinth are in a hypertrophic state, with enlarged cytoplasm full of newly synthesized proteins that are to be secreted into the ECM. Second and more prominent Adamts18 labeling is observed in marginal areas of the otic capsule (Figure 5.19). The expression is revealed in the ECM, in an intermediate state between chondrocyte hypertrophy and ossification. In this stage, the chondrocytes die, tabication between cells is lost, and cytoplasm content is released together with ECM components, where Adamts18 could then be involved in its degradation. In this environment, the matrix is invaded by blood vessels, osteoclasts, and osteoblasts. Osteoclasts degrade cartilage debris and osteoblasts mineralize the matrix by deposition of hydroxyapatite (224). New IHC and western blot assays are necessary in these marginal areas of the temporal bone, where chondrocyte ossification begins, to analyze the possible role of Adamts18 in this stage.

The alteration of the Adamts18 protein function due to the genetic variants found in our cohort of patients with MD and ES hypoplasia could retain the ossification process, retaining chondrocytes in a late state of ossification. The most shared variant g.77434661G>C,P12R located in the signal peptide could affect the secretion of the protein from chondrocytes to the ECM, sequestering it intracellularly. A validation study in chondrocyte cell culture or in vivo model is needed to confirm these changes.

Some cellular and animal models have already been developed trying to elucidate the role of some metalloproteinases in the osseous matrix, with no clear results. *MMP13* or *MMP9* null mice and chondrocytes showed a decrement in the cell tabulation loss in late hypertrophic chondrocytes, and subsequent delay in the ossification front (225,226). On the other hand, mice with impaired Adamts-1, Adamts-4 and Adamts-5 grew normally, with no alteration in cartilage and osseous development. In those cases, authors assumed that other proteinases from these families could be supplying the function when any of them is impaired (224,227,228).

Also, in relation to bone metabolism, *ADAMTS18* has been associated with mineral density quantitative trait locus (QTL) in GWAS studies. Low bone mineral density in the femoral neck was related with various SNVs in *ADAMTS18* (rs16945612, rs11859065,

rs11864477, rs11860781) and *TGFBR3* (rs17131547) in a Caucasian cohort of 1000 individuals and replicated in others 4 cohorts. In fact, TGF β secreted polypeptides family have been related with local bone remodeling, and will be discussed in section 6.4.2.3. In addition, in one of these cohorts with 2995 Chinese individuals, *ADAMTS18* SNVs was also related to hip fracture QTL (229). Also, Koller *et al.*, described the association of the SNV rs1826601 in *ADAMTS18* with low mineral density of the femoral neck and lumbar spine in 1524 premenopausal European-American women, and the results were replicated in another cohort of 762 African-American women (230).

6.4.2.2 - Other candidate genes in the MD and ES hypoplastic cohort associated with extracellular matrix

Results from functional analysis reveal an enrichment of entities in some pathways including “collagen-containing extracellular matrix”, “extracellular matrix” and “extracellular matrix organization” according to GO - Cellular Compartments and Reactome. The encoded proteins from these pathways included some constituents of ECM such as collagens (*COL6A6* and *COL20A1*) (231), matrilin-4 (*MTN4*) (232) as mayor protein of cartilage matrix, and alpha-tectorin (*TECTA*) as the main non-collagenous components of the TM in the organ of Corti (151). WGS and GWAS analysis related *COL6A6* with osteoarthritis and ossification of thoracic spine (233,234), and matrilin-4 expression with dental pulps in wound-healing processes (235). Also, interactors between cells and ECM components are included, such as Nidogen 1 (*NID1*) and Integrin Subunit Alpha 1 (*ITGA1*). Nidogen 1 mediate in cell interaction with basement membranes and components of ECM, especially laminin, collagen iv and perlecan (236). Interestingly, Nidogen-1 enriched vesicles have been used to improve angiogenesis and bone regeneration targeting focal adhesion (237). In addition, WES analysis has pointed out *NID1* as candidate gene for autosomal dominant Dandy-Walker malformation and occipital cephaloceles, characterized by cerebellar hypoplasia, meningeal anomalies and skull defects (238). On the other hand, *ITGA1* form a cell-surface receptor for collagen and laminin (239). Several integrins including *ITGA1* have been shown to be expressed by osteoblast and osteoblast in the bone cartilage ECM, having a role in the control of cartilage differentiation during ossification process (240,241). Enzymatic activities were also represented with our candidate *ADAMTS18* and the Proteoglycan Like Sulfated Glycoprotein or papilin (*PAPLN*). Papilin is another *ADAMTS*-like proteins involved in procollagen maturation, extracellular matrix proteolysis in morphogenesis and angiogenesis (242). On the other hand, Inter-Alpha-Trypsin Inhibitor Heavy Chain 4 (*ITH4*)

act as inhibitor of serine-type endopeptidase enzymes in the ECM (243). Finally, LTBP2 and LTBP3 regulate TGF- β activation in the extracellular space, and require binding to ECM components such as fibronectin or fibrillin for activation (244). Its implication will be discussed in the next section.

Although the enrichment in variants in these genes is not as significant and highly shared between individuals as our main candidate protein ADAMTS18, they do have a common biological function. If some of these proteins also have a role in the ECM of otic capsule or inner ear, the alterations produced by the enrichment in variants in these genes would have an additive effect to the phenotype produced by ADAMTS18, contributing to malformations such as the abrupt termination of ES observed in our ES hypoplastic patients.

6.4.2.3 - Other candidate genes in the ES hypoplastic cohort related with bone development and remodeling

Among the genes with SVs shared in the higher number of our MD and ES hypoplasia patients, the Protein Activator Of Interferon Induced Protein Kinase (*PRKRA*) and Transforming Growth Factor Beta 2 (*TGFB2*) genes have been associated with phenotypes that included ear or craniofacial developmental abnormalities.

The first of them, *PRKRA*, showed a deletion of around 3000bp in 3 different individuals, classified as “pathogenic”. This gene codes for a kinase that is activated by dsRNA, related to the regulation of gene silencing and apoptosis. In the mice blastocyst, *Prkra* is expressed in the developing ear at E12, and in the anterior skull base and mandible at E16. Various studies disrupting *Prkra* in mice, resulting in absent protein levels, showed defects in ear, craniofacial development and growth (245–247). Those alterations included wide cranial sutures, hypoplastic interparietal bone, prominent bossing of the forehead, shortened nose, hypoplastic nasal turbinates, hypoplastic mandibular condyle and microtia. The ears had hypoplastic pinnae and external auditory canals, malformed middle ear ossicles and reduced middle ear space and tympanic membrane, resulting in hearing impairment (247). However, alterations of the temporal bone or the otic capsule is not specifically described, and the malformation of the external and middle ear could indicate that the hearing loss found in the mutant mouse has a conductive basis. For this reason, this phenotype differs somewhat from that observed in our patients with MD and ES hypoplasia.

On the other hand, *TGFB2* is a transcription factor known to regulate multiple developmental processes from blastocyst to adulthood, playing an essential role in tissue development in heart, eyes, ear, organs of urogenital tract, skeleton, and craniofacial tissues (248). It encodes for TGF β 2, one of the three members of Transforming growth factor (TGF β) secreted polypeptides family, comprising TGF β 1, TGF β 2 and TGF β 3. TGF β proteins are involved in local regulation of bone development and turnover, synthesized by osteoblast and osteoclast, and secreted to the mineralized bone matrix. Several *in vivo* and *in vitro* studies have proven the great effects of TGF β protein in the stimulation of osteoblastic activity, induction of ECM components secretion, modulation of osteoprogenitor cell proliferation, differentiation of osteoclast and bone formation (221).

Several investigations have assessed the effects of *TGFB2* in the inner ear and craniofacial bones. On the one hand, the *Tgfb2*-null mice developed by Sandford *et al.*, showed defective epithelial-mesenchymal maturation in the spiral limbus, incomplete canalization of *scala vestibuli*, and spatial separation of sensory epithelia and basilar membrane. Its craniofacial abnormalities consisted of smaller bone sizes and subsequent wider fontanels because of reduced ossification (248). On the other hand, the selective overexpression of *Tgfb2* in bone in transgenic mice produces a phenotype similar to human osteoporosis, with low bone mineralization leading to bone loss. The highest immunoreactivity was observed in osteoblast (221). Altered audition have been also described by Chang *et al.*, where deregulated transcription factors *Tgfb2* and *Runx2* gave rise to excessively hardened otic capsule bone triggering hearing loss, although display normal cochlear sensory epithelia (249).

The CNV in *TGFB2* in our MD and ES hypoplastic cohort consists of an increase in the number of copies in 4 patients. This could result in a rise in product levels similar to the mutant described by Erlenbacher and Derynck, where they described a low bone mineralization and gradual bone loss in the clavicle, along with an increase in osteoblastic matrix deposition and osteoclastic matrix resorption (221).

Interestingly, two of the genes enriched in rare variants resulting from GBA, *LTBP2* and *LTBP3*, regulate the activity of TGF β members. These two molecules are part of the LTBP, or latent transforming growth factor (TGF)- β binding protein family, located in the ECM. Their non-covalent binding to some members of the TGF β family creates a complex that maintains TGF β proteins in an inactive latency state in the extracellular matrix. (244,250). In animal models and humans, similar phenotypes have been observed with bone abnormalities in the spine, teeth, maxillofacial bones, and skull. Craniofacial

malformations generate a shortening in the length of the face, which subsequently produces a bulging of the cranial vault. This is produced by premature ossification because of the decrease in TGFB (251–253). In our MD and ES hypoplastic cohort, *LTBP2* displayed 5 variants in 5 individuals and *LTBP3* 4 variants in 7 individuals.

The variants in *TGFB2* and *LTBP* genes could also alter bone maturation in the whole otic capsule or bony canal conforming VA, having an additive effect to *ADAMTS18*. TGFβ2 is synthesized by osteoblasts and osteoclasts and secreted into ECM, and these two cell types invade the remodeling bone at the same chondrocyte stage in which *ADAMTS18* has been observed in our IHC, presumably degrading the matrix. In fact, two of the four patients with the CNV in TGFβ2 also have the more shared candidate variant g.7743466G>C in *ADAMTS18*, corresponding to patients B and F in Table 5.3 and Figure 5.9, and patient F also display one of the *LTBP3* variants.

6.4.3 - Candidate genes in the MD and ES hypoplastic cohort associated with neurogenesis and neuronal circuits

6.4.3.1 - Candidate gene *SDK1*

Sdks family are single-pass transmembrane proteins that participate in the formation and maintenance of trans-synaptic interactions in different neuronal circuits. In vertebrates, the two types of Sdks, Sdk1 and Sdk2, have been widely described in the retina (254). There, several layers can be distinguished, where the retinal ganglion cells that transmit visual stimuli synapse with interneurons that carry the information to higher centers. The connections of the same layer transmit information of the same type of stimulus, differentiating for example movement of a specific orientation, edges or color contrasts (255). In mouse, Sdk1 and Sdk2 are expressed in different neuronal subsets in different synaptic layers of the retina, and rarely together in the same cell (256). So, it has been hypothesized that Sdk1 and Sdk2 would be involved in the transmission of different visual characteristics (254).

In our cohort of patients with MD and ES hypoplasia, we have found an enrichment of 12 rare SNPs in 14 individuals in *SDK1* gene (Figure 5.21). Six of these variants, which include those variants shared among more individuals, are found in Ig-like domains. Crystallographic and structured-guided mutagenesis analysis performed by Goodman et al., verified that specifically the Ig1-4 domains, adopting a horseshoe conformation, mediate the binding of different Sdk proteins together to form homophilic dimers, but also

interact with neighboring cells to mediate in cell-cell adhesion (257). Sdk dimers tend to be homophilic (ie, SDK1 with SDK1, or SDK2 with SDK2), although heterophilic join SDK1-SDK2 can occur with weak strength. However, in a situation of high competition the homophilic union will always occur preferentially (257). Our most represented variant g.3951870C>T,P367L is present in 4 individuals and located in Ig-like 3 and produces a change of proline to lysine. Proline is a voluminous hydrophobic amino acid usually located in the protein to create turns in the polypeptide conformation. Its modification to a polar charged lysine could disturb the three-dimensional tertiary structure. A not very destabilizing alteration is expected in the other two variants found in Ig-like 3 domain, g.3951025C>T,A317V and g.3951861C>T,A364V modifying alanine to valine change, both residues with similar characteristics. Other variants in Ig1-4 domains include g.3619104C>T,T108M in Ig-like 1 and g.3962743G>A,G441R in Ig-like 4, each only in one individual. Lastly, variant g.3974407C>T,S619L in two patients, found in the Ig-like 6 domain could also modify tertiary conformation introducing a positive residue.

The remaining six variants are found in the FNIII domains, but they are present in singletons. The function of the FNIII domains is less understood, but it has been suggested they fortify the adhesion by interacting with the neighboring cell membrane (254). Of note g.4220247A>G,N1893S in the FNIII 3 remove an asparagine that is glycosylated post-traductionally, which could further alter the cell fate of the protein.

None of the variants was found in the short intracellular region, comprising the Postsynaptic density/Disc large/ZO-1 (PDZ) binding domain. The last 6 C-terminal amino acids of this PDZ motif are highly conserved across species. In vertebrates, Sdk1 and Sdk2 differentiate by this sequence, being -TGFSSFV in Sdk1 and -AGFSSFV in Sdk2. The differences in this hexapeptide define the intracellular interactors and the synaptic localization of Sdks proteins (254). Sdk1 PDZ domain is associated with scaffolding molecules of the Membrane-Associated Guanylate kinase with Inverted orientation (MAGI) and Polychaetoid protein (the *Drosophila* homologue of Zonula Occludens-1, ZO-1), both belonging to the MAGUK family (PDZ/membrane-associated guanylate kinase molecules) (254,258,259). MAGI directly interacts with other transmembrane proteins important in cell-cell adhesion, such as neuroligins and cadherins at the synapse (258). On the other hand, Polychaetoid was discovered in *Drosophila* sdk mutant showing eye abnormalities, where it worked as Sdk adapter to cytoskeleton, maintaining cell-cell tension during remodeling epithelia (254,259). Interestingly, one of these scaffolding proteins MAGI takes part of the tip-links in the membrane of the HC stereocilia (260). It interacts with the intracellular PDZ C-terminal domain of cadherin-23 through its PDZ4

domain in the posterior stereocilia, anchoring it to the actin backbone along with Harmonin-b. MAGI-1 labeling is detected from the developing to adult stereocilia, colocalizing with cadherin-23 (260). Although SDK1 has not been described as forming part of stereocilia, it acts in a similar way to cadherin-23 in tip-links, a transmembrane protein that bind to scaffolding proteins of the MAGUK family through PDZ domain, such as MAGI-1. Therefore, it is necessary to study the expression patterns of SDK1 in the sensory organs of the inner ear to confirm if it could develop a physiological role.

Sdks have been related to some neurodevelopmental and neurological disorders in mice, including addiction or depression (254). Thus, increased expression of Sdk1 has been observed in some brain areas including the nucleus accumbens after cocaine use (261). On the other hand, its expression is differential in the brain between control mice and those with chronic social fatigue, and its overexpression in the hippocampus increases susceptibilities to stress (262,263).

In humans, GWAS analyses have linked the *SDK1* gene to autism spectrum disorders (264–268) and attention deficit-hyperactivity (269,270). An interesting study carried out by Hromatka *et al.* associated polymorphism in various genes, including SDK1, with motion sickness (271). Its main symptoms include dizziness, nausea, vomiting, headache and sweating, and may also be accompanied by migraines, vertigo or morning sickness. Although the exact cause of this condition is still unknown, some theories suggest that it appear when the brain receives conflicting information from eye (static signals from surrounding objects) and ear (noticed acceleration in the vestibular system) during movement, especially during transportation (271). The genetic association included genes related to the development of the eye and inner ear, balance, cranial development, nervous system, glucose homeostasis, or hypoxia. Those related to the ear consist of *TSHZ1*, associated with ear deformities in mice in the external auditory canal and the skull (272); or *MUTED*, whose alteration produces hypopigmentation that induce postural defect and balance abnormalities in mice due to otolith deficiency in the vestibular system (273). Lastly, nine genes were associated with synapse formation and neurological pathways, including *SDK1*. The relationship of SDK1 with this condition is interesting because it shows symptomatological similarities with MD, including altered transference of vestibular information. According to that, Astigarraga *et al.* evidenced that *Drosophila* Sdk protein accumulate specifically in synaptic layers responsible for motion detection, and *Sdk* mutant exhibit optomotor defects as a consequence of disorganization of connections between photoreceptors and lamina neurons(274).



One of the few studies that directly relates *SDK1* to hearing function was carried out by Pretipré *et al.* (275) They performed single-cell RNA-seq in mouse inner ear neurons at different stages of development. They describe distinct transcriptional patterns that define the course of SGN diversification, discovering that the establishment of final SGN subpopulations occurs during HC innervation in cochlear sensory epithelia. *Sdk1* was expressed in SGN during the process, in higher levels in non-specialized SGN in early stages. Other cell-cell adhesion molecules were also found to be involved in the maturation and differentiation of SGN (275).

As in the retina, afferents that innervate other sensory epithelia synapse with interneurons from different neuronal divisions. In the ear, afferents that interact with HC synaptic boutons in the cochlea and vestibular organs synapse with the SGN and VGN in superior ganglion, respectively (22). Although there is no well-supported evidence, and only the study carried out by Petitpré *et al.* demonstrates the expression of *Sdk1* in the SGN in the mouse cochlea during development and differentiation, the *Sdk* family proteins could carry out a similar function in the ear (275). In this way, they would facilitate the interaction and adhesion between the cell membranes of the SGN and VGN in the synapse with interneurons from the vestibular and cochlear divisions of cranial nerve VIII. The correct transmission of this information is necessary for a correct perception of the audio-vestibular stimuli, altered in our patients with MD and ES hypoplasia.

6.5 - ES hypoplasia MD endophenotype is produced by alterations in the development of audio-vestibular organs, otic capsule and neural circuits inside inner ear

The study of MD is intricate due to several factors. There is a wide range of symptom presentations, varying in severity and often not showing a complete set of clinical signs. The age at which symptoms begin can be unpredictable and usually occurs later in life. Additionally, other conditions with similar symptoms can overlap with MD, further complicating the diagnosis (82,85). Regarding the etiology, different factors are taken into account, including an immune component, a genetic origin, and endolymphatic flow disorders, including EH (26,95,103). In fact, EHs have been the most consistent findings in the sensory organs of MD patients, especially in the cochlea and saccule (26). EH were attributed as the origin of the symptoms, since the accumulation of endolymph would increase the pressure within the membranous labyrinth, causing altered excitation of the sensory epithelia (26,117). However, it was later hypothesized that EH could be rather the consequence of an inadequate endolymph drainage (117). This new consideration took into account other abnormalities found in the non-sensory organs of the inner ear, the ED and the ES, such as narrowing in their diameter and generalized fibrosis of their epithelia, collapsed ES lumen and loss of tubules in the *pars canalicularis* (32,119,120,200–202). Especially, this segment contains MRC responsible for maintaining the endolymph ionic composition, and RRC in charge of protein synthesis and secretion that regulate osmotic pressure (35,39–41). The eES also rests on the SS, acting as a vascular regulator of both ear and intracranial pressure (115). Supporting this function, molecules of the vasopressin and aldosterone pathways, as well as other natriuretic peptides have been found expressed by the ES epithelium (32,42,45,47,50). In addition to soft tissues, other defects have been found in TB of MD patients, like shortened or thinner VA, or narrowed VA exit to the PCF (113,114,200). In summary, the accumulation of endolymph creating EH would be rather the consequence of an altered flow of endolymph from the cochlea and the vestibule towards the ES and SS, produced by the anomalies observed in ED, ES and VA.

In line with the above, Andreas Eckhard and David Bächinger defined two endotypes within MD disease based on histopathological malformation of ES (32,156). Specifically, in the ES hypoplastic endotype, the ES abruptly disappears at the level of the operculum, with a total absence of the extraosseous region (32,155). These ES hypoplastic patients have a family history of SNHL, vertigo or MD and a tendency to



present early onset, male predominance, TB abnormalities and higher bilateral prevalence than general MD patients (156). In accordance with these facts, the authors suggest ES hypoplasia has a genetic basis that is generated during development. Thus, the aim of this work was to find the genetic basis of ES hypoplasia in MD patients. Given that MD is a complex disease that has a multifactorial genetic basis resulting from causal variants and environmental factors, our genetic approach was focused on finding an enrichment of variants in multiple causative genes with moderate and additive effects on phenotype. For this purpose, we followed a gene burden analysis (GBA) with rare SNV and InDels, structural variant discovery and candidate genes functional analysis on a cohort of 42 patients with MD and ES hypoplasia.

Given that Eckhard and Bächinger investigations estimate that 1 in 4 MD have ES hypoplasia, and in the European population MD is found in approximately 1 in 2000 individuals, the inferred prevalence of ES hypoplasia would be 1-2 in 10,000 individuals, or practically absent in the general population. In the process of variant filtering in our ES hypoplastic cohort, and since the allele frequency is obtained from databases of reference populations, we should also assume that ES hypoplasia in the normal population is non-existent. However, these authors consulted less than 100 CT controls, which is not enough to confirm its absence (155). For this reason, a complementary study was carried out as *Chapter 1* of this thesis. More than 300 ears of otologic patients without MD were contrasted and ES hypoplasia was not found, placing its prevalence below 0.57% in the general population.

The genetic analysis performed in our cohort of patients with MD and ES hypoplasia, considering the enrichment in rare SNPs and InDels and the presence of structural variants, together with the functional analysis, have pointed out certain candidate genes and different biological processes or diseases. Expression validation tests using IHC and WB have supported some of these possible pathways that could be altered as a consequence of the variants, explaining the associated phenotype in the patients. These include a possible alteration in the development and function of the cochlear and vestibular sensory epithelia, an impairment in the transmission of sensory information received from the sensory epithelia to higher central nervous system centers, and abnormalities in the development and remodeling of the bone extracellular matrix, with the consequent malformations in the otic capsule.

First, certain candidate genes have been associated with the development of the sensory organs of the inner ear. This includes some genes previously known to take part

in HC stereocilia backbone or tip-links, such as *MYO7A* and *WHRL*, or in the tectorial membrane such as *TECTA* (7,8,151). Its involvement in phenotypes associated with audio-vestibular pathologies have been confirmed by many studies, and are related with different types of SNHL (215–218,220), Usher syndrome (214,219) or MD (103,144). On the other hand, we have probed that our new candidate *ADAMTS18*, is widely expressed in several P3 mouse sensory tissues, including organ of Corti in the cochlea, the macula of the utricle, and the *crista vascularis* of the semicircular canals. This metalloproteinase takes part of ECM in numerous tissues, where it participates in morphogenesis, repair and remodeling, especially during development (204). Abundant studies on animal models and cell cultures, in which the expression of ECM components have been altered, such as extracellular receptors and proteases, result in various abnormalities of the sensory epithelia in the inner ear (206–208,210,211). For this reason, we have hypothesized that *ADAMTS18* could be carrying out similar functions, remodeling the assembly between cells and extracellular membranes, maintaining the integrity between tissues, and allowing the formation of new structures, such as blood vessels. However, more functional studies will be necessary to discern its function in the physiopathology of the disease.

Second, the candidate gene *SDK1* is related to cell-cell adhesion at neuronal synapses (254). Although only one study has shown the expression of *Sdk1* in mice in SGN during development, a function similar to its role in the retina might be expected (275). So, this protein would be part of the connections between synapse of interneurons from the spiral and vestibular ganglion and afferents that innervate HC in the sensory epithelia (254,275). In summary, abnormalities due to the accumulation of variants in all these genes could modify both the perception and the transmission of audio-vestibular stimuli, generating the symptoms associated with MD.

Third, bone remodeling, specifically in the otic capsule, could be affected. *ADAMTS18* expression is observed at the border of the membranous and osseous labyrinths surrounding the vestibular organs and the cochlea, but also in marginal zones invading the bone ECM in a stage between late chondrocyte hypertrophy and ossification. GWAS studies have related the presence of polymorphisms in *ADAMTS18* with QTL as bone mineral density (229,230). Functional analysis revealed several variant enriched genes in “extracellular matrix” along with *ADAMTS18*, including the other metalloproteinase *PAPLN*, components such as collagens and *MTN4*, matrix cell interactors, and some transcription factors. Among the latter, we highlight the regulatory ligands of the TGF- β family (*LTBP*). Surprisingly, one CNV included an increase in *TGFB2* copies. Both *LTBP* ligand and *TGFB2* factors have been widely studied for modulating the



function of osteoblasts during bone formation, and their annulment in animal models produce bone loss and abnormalities in the otic capsule and sensory tissues (221,248,249). The impairment produced by this set of genes could be broadly associated with the abnormal development of the otic capsule, generating abnormalities in the temporal bones of MD, in the AV, and subsequently in the ED and ES, like the eES truncation observed in our ES hypoplastic patients.

The characterization of different endotypes within a complex and symptomatological very heterogeneous disease, such as MD, can help to stratify the different types of patients. Therefore, the identification of markers, whether histopathological or molecular, are promising to improve diagnosis and clinical decision-making, and predict the evolution and prognosis of the disease. Here, we have identified several genes and biological processes that might be altered by the accumulation of rare variants in our MD and ES hypoplasia endophenotype, that illustrate the possible pathophysiology of MD.



7. – Conclusions

Conclusiones



Conclusions

The development of this doctoral dissertation has allowed us to draw the following conclusions:

1. ES hypoplasia is a very rare finding, which has not been found in our cohort of patients without MD, estimating its prevalence below 0.57% in the general population, lower than sporadic MD prevalence.
2. ES hypoplasia is closely associated with the development of MD. The diagnosis of MD coincides in all cases with the ear affected by ES hypoplasia, whether they are bilateral or unilateral cases. Follow-up over time will be necessary to determine what percentage of patients with unilateral MD and bilateral ES hypoplasia end up developing disease in the contralateral ear.
3. The burden analysis of rare variants together with the discovery of structural variants is a competent approach to find candidate genes in complex endophenotypes, such as ES hypoplasia in MD. Among the pointed genes, better candidates with the highest number of rare variants and whose variants are shared in the greatest number of were *ADAMTS18* and *SDK1*.

Functional analysis of these genes has highlighted various biological processes that could be affected. These include: i) a possible alteration in the development and function of the sensory epithelia of the cochlea and vestibular system; ii) an impairment in the transmission of audio-vestibular information to higher information centers; and iii) abnormalities in the remodeling of the extracellular matrix bone, with consequent malformations in the otic capsule. Together, they could explain the features of the ES hypoplastic endophenotype in our MD patients.

Conclusiones

El desarrollo de esta disertación doctoral ha permitido esbozar las siguientes conclusiones:

1. La hipoplasia del SE es un hallazgo muy raro, el cual no ha sido encontrado en nuestra cohorte de pacientes sin EM, estimando su prevalencia por debajo del 0.57% en la población general, inferior a la de la enfermedad de Meniere esporádica.
2. La hipoplasia del SE está íntimamente asociada con el desarrollo de EM. El diagnóstico de EM coincide en todos los casos con el oído afectado por la SE hipoplasia, ya sean casos bilaterales o unilaterales. Un seguimiento en el tiempo será necesario para determinar qué porcentaje de pacientes con EM unilateral e hipoplasia SE bilateral terminan desarrollando afección en el oído contralateral.
3. El análisis agregado de variantes raras junto con el descubrimiento de variantes estructurales es una buena aproximación para encontrar genes candidatos en endofenotipos complejos, como lo es la hipoplasia del SE en la EM. Entre los genes destacados, los mejores candidatos con mayor número de variantes raras y cuyas variantes se comparten en la máxima cantidad de individuos fueron *ADAMTS18* y *SDK1*.
4. El análisis funcional de estos genes ha señalado diversos procesos biológicos que podrían verse afectados. Estos incluyen: i) una posible alteración en el desarrollo y la función de los epitelios sensoriales de la cochlea y el sistema vestibular; ii) un deterioro en la transmisión de la información audio-vestibular a los centros superiores de información; y iii) anomalías en la remodelación de la matriz extracelular ósea, con las consiguientes malformaciones en la cápsula ótica. Juntos, podrían explicar los rasgos del endofenotipo hipoplásico del SE en la EM.



8. – Limitations and future directions



Our cohort of sporadic patients with MD and ES hypoplasia has only 42 patients. Our candidate genes are selected based on the variant burden, taking those with greater accumulation in affected individuals than in controls. However, the large difference in individuals between our cohort and reference databases may overrepresent the effect of rare variants through the calculation of parameters such as Odd ratios. Recruitment of patients with this endophenotype should continue, and new genetic analysis should be performed.

In this same direction, the consistency of the genotype-phenotype associations gain strength if they are replicated in other cohorts. To our knowledge, this is the first genetic study of MD and ES hypoplasia patients, but new studies will be carried out. It will be interesting to see different cohorts confirming the implications of these genes.

Our study is based on exome analysis. Thus, we may be missing important information in non-coding regions of the genome that may also contribute to the phenotype. A future analysis should include genome sequencing of these patients, to analyse all types of variants that may be altering regulatory functions.

The methodology for the analysis of SV is not as developed as for SNV and short InDels. Thus, a very low level of replication has been found between the LSV obtained between the two contrasted tools, and other tools should have been used for CNV calling. In addition, we missed a good database of SV allele frequencies during the process. We should also have validated the candidate SVs using wet lab techniques, in addition to their visualization in IGV. Nevertheless, the study of structural variants would be better approached by whole genome sequencing, since the calling of longer variants would be limited by the capture regions of the exome.

The recruitment of samples and clinical information in relatives and controls of our familial patients has not been sufficient to carry out segregation analysis with the ES hypoplasia. Further recruitment and better characterization of these families should be performed.

Our expression validations, both IHC and WB, are carried out on wild type mice, where we have been able to demonstrate the expression pattern in the inner ear and otic capsule under normal conditions. As a more valid approach, it should have been used: i) mice altered for the expression of these candidate genes or, ii) mice developed with the same variants as those found in this thesis. Of course, the work with orthologs in other



animal models, and in human temporal bone, both in controls and in patients with MD would be very helpful.

Finally, since our work is based on the hypothesis of a genetic origin of ES hypoplasia during development, these new experiments should be tested at various stages of development. In this study, unfortunately, only mice on postnatal day 3 have been used.



9. – References

1. Purves D, Augustine G, Fitzpatrick D, Hall W, LaMantia AS, McNamara J, et al. The Auditory System. In: Neuroscience. 3rd ed. Sunderland, Mass: Sinauer Associates, Publishers; 2004. p. 283–314.
2. Northcutt RG. The evolutionary biology of hearing. Springer; 1992. 21–48 p.
3. Rask-Andersen H, Bredberg G, Lyttkens L, Löf G. THE FUNCTION OF THE ENDOLYMPHATIC DUCT? AN EXPERIMENTAL STUDY USING IONIC LANTHANUM AS A TRACER: A PRELIMINARY REPORT. *Ann N Y Acad Sci.* 1981 Nov;374(1 Vestibular an):11–9.
4. Kämpfe Nordström C. The Human Vestibular Aqueduct, Endolymphatic Duct and Sac: A Morphological Study Using Micro-ct, Super Resolution Immunohistochemistry and Synchrotron Phase Contrast Imaging. [Uppsala, Sweden]: Uppsala University; 2020.
5. Driver EC, Kelley MW. Development of the cochlea. *Development.* 2020 Jun 15;147(12):dev162263.
6. Rask-Andersen H, Liu W, Erixon E, Kinnefors A, Pfaller K, Schrott-Fischer A, et al. Human Cochlea: Anatomical Characteristics and their Relevance for Cochlear Implantation. *Anat Rec Adv Integr Anat Evol Biol.* 2012 Nov;295(11):1791–811.
7. Zheng W, Holt JR. The Mechanosensory Transduction Machinery in Inner Ear Hair Cells. *Annu Rev Biophys.* 2021 May 6;50(1):31–51.
8. McGrath J, Roy P, Perrin BJ. Stereocilia morphogenesis and maintenance through regulation of actin stability. *Semin Cell Dev Biol.* 2017 May;65:88–95.
9. Stelma F, Bhutta MF. Non-syndromic hereditary sensorineural hearing loss: review of the genes involved. *J Laryngol Otol.* 2014 Jan;128(1):13–21.
10. Wan G, Corfas G, Stone JS. Inner ear supporting cells: Rethinking the silent majority. *Semin Cell Dev Biol.* 2013 May;24(5):448–59.
11. Waissbluth S, Maass JC, Sanchez HA, Martínez AD. Supporting Cells and Their Potential Roles in Cisplatin-Induced Ototoxicity. *Front Neurosci.* 2022 Apr 27;16:867034.
12. Goodyear RJ, Richardson GP. Structure, Function, and Development of the Tectorial Membrane: An Extracellular Matrix Essential for Hearing. In: Current Topics in Developmental Biology [Internet]. Elsevier; 2018 [cited 2023 Jul 15]. p. 217–44. Available from: <https://linkinghub.elsevier.com/retrieve/pii/S0070215318300383>
13. Andrade LR, Salles FT, Grati M, Manor U, Kachar B. Tectorins crosslink type II collagen fibrils and connect the tectorial membrane to the spiral limbus. *J Struct Biol.* 2016 May;194(2):139–46.
14. Avan P, Le Gal S, Michel V, Dupont T, Hardelin JP, Petit C, et al. Otogelin, otogelin-like, and stereocilin form links connecting outer hair cell stereocilia to each other and the tectorial membrane. *Proc Natl Acad Sci.* 2019 Dec 17;116(51):25948–57.
15. Ghaffari R, Aranyosi AJ, Freeman DM. Longitudinally propagating traveling waves of the mammalian tectorial membrane. *Proc Natl Acad Sci.* 2007 Oct 16;104(42):16510–5.
16. Gavara N, Chadwick RS. Collagen-Based Mechanical Anisotropy of the Tectorial Membrane: Implications for Inter-Row Coupling of Outer Hair Cell Bundles. Gribble PL, editor. *PLoS ONE.* 2009 Mar 18;4(3):e4877.
17. Strimbu CE, Prasad S, Hakizimana P, Fridberger A. Control of hearing sensitivity by tectorial membrane calcium. *Proc Natl Acad Sci.* 2019 Mar 19;116(12):5756–64.
18. Jeng J, Harasztosi C, Carlton AJ, Corns LF, Marchetta P, Johnson SL, et al. MET currents and otoacoustic emissions from mice with a detached tectorial membrane indicate the extracellular matrix regulates Ca²⁺ near stereocilia. *J Physiol.* 2021 Apr;599(7):2015–36.
19. Zdebik AA, Wangemann P, Jentsch TJ. Potassium Ion Movement in the Inner Ear: Insights from Genetic Disease and Mouse Models. *Physiology.* 2009 Oct;24(5):307–16.
20. Thulasiram MR, Ogier JM, Dabdoub A. Hearing Function, Degeneration, and Disease: Spotlight on the Stria Vascularis. *Front Cell Dev Biol.* 2022 Mar 4;10:841708.
21. Hibino H, Kurachi Y. Molecular and Physiological Bases of the K⁺ Circulation in the Mammalian Inner Ear. *Physiology.* 2006 Oct;21(5):336–45.
22. Lysakowski A. Anatomy of the Vestibular System. In: Cummings Otolaryngology - Head and Neck Surgery [Internet]. Elsevier; 2010

- [cited 2023 Jul 1]. p. 1850–65. Available from: <https://www.elsevier.com/books-and-journals/deleted-doi>
23. Purves D, Augustine G, Fitzpatrick D, Hall W, LaMantia AS, McNamara J, et al. The Vestibular System. In: Neuroscience. 3rd ed. Sunderland, Mass: Sinauer Associates, Publishers; 2004. p. 315–35.
 24. Sterkers O, Ferrary E, Amiel C. Production of inner ear fluids. *Physiol Rev.* 1988 Oct;68(4):1083–128.
 25. Kim SH, Kim BG, Kim JY, Roh KJ, Suh MJ, Jung J, et al. Electrogenic transport and K⁺ ion channel expression by the human endolymphatic sac epithelium. *Sci Rep.* 2015 Dec 14;5(1):18110.
 26. Paparella MM, Djalilian HR. Etiology, pathophysiology of symptoms, and pathogenesis of Meniere's disease. *Otolaryngol Clin North Am.* 2002 Jun;35(3):529–45.
 27. Guild SR. The circulation of the endolymph. *Am J Anat.* 1927 Mar;39(1):57–81.
 28. Ogura Y, Clemis JD. A Study of the Gross Anatomy of the Human Vestibular Aqueduct. *Ann Otol Rhinol Laryngol.* 1971 Dec;80(6):813–25.
 29. Lundquist PG, Kimura R, Wersäll J. Ultrastructural Organization of the Epithelial Lining in the Endolymphatic Duct and Sac in the Guinea Pig. *Acta Otolaryngol (Stockh).* 1964 Jan;57(1–2):65–80.
 30. Friberg U, Jansson B, Rask-Andersen H, Bagger-Sjoberg D. Variations in Surgical Anatomy of the Endolymphatic Sac. *Arch Otolaryngol - Head Neck Surg.* 1988 Apr 1;114(4):389–94.
 31. Oehler MC, Chakeres DW, Schmalbrock P. Reformatted planar 'Christmas tree' MR appearance of the endolymphatic sac. *AJNR Am J Neuroradiol.* 1995 Aug;16(7):1525–8.
 32. Eckhard AH, Zhu M, O'Malley JT, Williams GH, Loffing J, Rauch SD, et al. Inner ear pathologies impair sodium-regulated ion transport in Meniere's disease. *Acta Neuropathol (Berl).* 2019 Feb;137(2):343–57.
 33. Furuta H, Mori N, Fujita M, Sakai S. Ultrastructure of the Endolymphatic Sac in the Mouse. *Cells Tissues Organs.* 1991;141(3):193–8.
 34. Dahlmann A, Von Düring M. The endolymphatic duct and sac of the rat: a histological, ultrastructural, and immunocytochemical investigation. *Cell Tissue Res.* 1995 Nov;282(2):277–89.
 35. Klaus Qvortrup, Jørgen Rostgaard, N. The Endolymphatic Sac, a Potential Endocrine Gland? *Acta Otolaryngol (Stockh).* 1999 Jan;119(2):194–9.
 36. Zechner G, Altmann F. Histological Studies on the Human Endolymphatic Duct and Sac. *ORL.* 1969;31(2):65–83.
 37. Friberg U, Rask-Andersen H, Bagger-Sjoberg D. Human Endolymphatic Duct: An Ultrastructural Study. *Arch Otolaryngol - Head Neck Surg.* 1984 Jul 1;110(7):421–8.
 38. Danckwardt-Lillieström N, Friberg U, Kinnefors A, Rask-Andersen H. Ultrastructural analysis of 20 intraosseous endolymphatic sacs from patients with cerebello-pontine angle tumours. *Auris Nasus Larynx.* 2000 Oct;27(4):311–21.
 39. Mori N, Miyashita T, Inamoto R, Matsubara A, Mori T, Akiyama K, et al. Ion transport its regulation in the endolymphatic sac: suggestions for clinical aspects of Meniere's disease. *Eur Arch Otorhinolaryngol.* 2017 Apr;274(4):1813–20.
 40. Kim SH, Nam GS, Choi JY. Pathophysiologic Findings in the Human Endolymphatic Sac in Endolymphatic Hydrops: Functional and Molecular Evidence. *Ann Otol Rhinol Laryngol.* 2019 Jun;128(6_suppl):76S-83S.
 41. Honda K, Kim SH, Kelly MC, Burns JC, Constance L, Li X, et al. Molecular architecture underlying fluid absorption by the developing inner ear. *eLife.* 2017 Oct 10;6:e26851.
 42. Møller MN, Kirkeby S, Vikeså J, Nielsen FC, Cayé-Thomasen P. The human endolymphatic sac expresses natriuretic peptides: Human ES Expresses Natriuretic Peptides. *The Laryngoscope.* 2017 Jun;127(6):E201–8.
 43. Beitz E, Kumagami H, Krippeit-Drews P, Ruppertsberg JP, Schultz JE. Expression pattern of aquaporin water channels in the inner ear of the rat. *Hear Res.* 1999 Jun;132(1–2):76–84.
 44. Couloigner V, Berrebi D, Teixeira M, Paris R, Florentin A, Grayeli AB, et al. Aquaporin-2 in the human endolymphatic sac. *Acta Otolaryngol (Stockh).* 2004 May 1;124(4):449–53.

45. Taguchi D, Takeda T, Kakigi A, Takumida M, Nishioka R, Kitano H. Expressions of Aquaporin-2, Vasopressin Type 2 Receptor, Transient Receptor Potential Channel Vanilloid (TRPV)1, and TRPV4 in the Human Endolymphatic Sac. *The Laryngoscope*. 2007 Apr;117(4):695–8.
46. Nishimura M, Kakigi A, Takeda T, Takeda S, Doi K. Expression of aquaporins, vasopressin type 2 receptor, and Na⁺-K⁺-Cl⁻ cotransporters in the rat endolymphatic sac. *Acta Otolaryngol (Stockh)*. 2009 Jan;129(8):812–8.
47. Maekawa C, Kitahara T, Kizawa K, Okazaki S, Kamakura T, Horii A, et al. Expression and Translocation of Aquaporin-2 in the Endolymphatic Sac in Patients with Meniere's Disease: AQP2 in Meniere's disease. *J Neuroendocrinol*. 2010 Nov;22(11):1157–64.
48. Takumida M, Kakigi A, Egami N, Nishioka R, Anniko M. Localization of aquaporins 1, 2, and 3 and vasopressin type 2 receptor in the mouse inner ear. *Acta Otolaryngol (Stockh)*. 2012 Jul 6;1–7.
49. Takeda T, Takeda S, Kitano H, Okada T, Kakigi A. Endolymphatic hydrops induced by chronic administration of vasopressin. *Hear Res*. 2000 Feb;140(1–2):1–6.
50. Marshall AF, Jewells VL, Kranz P, Lee YZ, Lin W, Zdanski CJ. Magnetic resonance imaging of guinea pig cochlea after vasopressin-induced or surgically induced endolymphatic hydrops. *Otolaryngol Neck Surg*. 2010 Feb;142(2):260–5.
51. Mori N, Wu D. Low-amiloride-affinity Na⁺ channel in the epithelial cells isolated from the endolymphatic sac of guinea-pigs. *Pflügers Arch Eur J Physiol*. 1996 Nov 18;433(1–2):58–64.
52. Kim SH, Park HY, Choi HS, Chung HP, Choi JY. Functional and Molecular Expression of Epithelial Sodium Channels in Cultured Human Endolymphatic Sac Epithelial Cells. *Otol Neurotol*. 2009 Jun;30(4):529–34.
53. Matsubara A, Miyashita T, Inamoto R, Hoshikawa H, Mori N. Cystic fibrosis transmembrane conductance regulator in the endolymphatic sac of the rat. *Auris Nasus Larynx*. 2014 Oct;41(5):409–12.
54. Wu D, Mori N. Outward K⁺ current in epithelial cells isolated from intermediate portion of endolymphatic sac of guinea pigs. *Am J Physiol-Cell Physiol*. 1996 Nov 1;271(5):C1765–73.
55. Wu D, Mori N. Extracellular ATP-induced inward current in isolated epithelial cells of the endolymphatic sac. *Biochim Biophys Acta BBA - Biomembr*. 1999 Jun;1419(1):33–42.
56. Miyashita T, Tatsumi H, Furuta H, Mori N, Sokabe M. Calcium-Sensitive Nonselective Cation Channel Identified in the Epithelial Cells Isolated from the Endolymphatic Sac of Guinea Pigs. *J Membr Biol*. 2001 Jul 15;182(2):113–22.
57. Ishibashi T, Takumida M, Akagi N, Hirakawa K, Anniko M. Expression of transient receptor potential vanilloid (TRPV) 1, 2, 3, and 4 in mouse inner ear. *Acta Otolaryngol (Stockh)*. 2008 Jan;128(12):1286–93.
58. Kumagami H, Terakado M, Sainoo Y, Baba A, Fujiyama D, Fukuda T, et al. Expression of the Osmotically Responsive Cationic Channel TRPV4 in the Endolymphatic Sac. *Audiol Neurotol*. 2009;14(3):190–7.
59. Mizukoshi F, Bagger-Sjöbäck D, Rask-Andersen H, Wersäll J. Cytochemical Localization of Na-K ATPase in the Guinea Pig Endolymphatic Sac. *Acta Otolaryngol (Stockh)*. 1988 Jan;105(3–4):202–8.
60. Peters TA, Kuijpers W, Curfs JHAJ. Occurrence of NaK-ATPase isoforms during rat inner ear development and functional implications. *Eur Arch Otorhinolaryngol*. 2001 Feb 28;258(2):67–73.
61. Stanković KM, Brown D, Alper SL, Adams JC. Localization of pH regulating proteins H⁺ATPase and exchanger in the guinea pig inner ear. *Hear Res*. 1997 Dec;114(1–2):21–34.
62. Dou H. Co-expression of Pendrin, Vacuolar H⁺-ATPase 4-Subunit and Carbonic Anhydrase II in Epithelial Cells of the Murine Endolymphatic Sac. *J Histochem Cytochem*. 2004 Oct 1;52(10):1377–84.
63. Lim DJ, Karabinas C, Trune DR. Histochemical localization of carbonic anhydrase in the inner ear. *Am J Otolaryngol*. 1983 Jan;4(1):33–42.
64. Takumida M, Bagger-Sjöbäck D, Rask-Andersen H. Ultrastructural Localization of Carbonic Anhydrase and Its Possible Role in the Endolymphatic Sac. *ORL*. 1988;50(3):170–5.
65. Furuta H, Mori N, Sakai S ichi. Immunohistochemical Localization of Carbonic Anhydrase in the Endolymphatic Sac of the Mouse and Guinea Pig. *ORL*. 1993;55(1):13–7.

66. Wu D, Mori N. Evidence for the presence of a Na⁺-H⁺ exchanger in the endolymphatic sac epithelium of guinea-pigs. *Pflügers Arch Eur J Physiol.* 1998 May 25;436(2):182–8.
67. Son EJ, Moon IS, Kim SH, Kim SJ, Choi JY. Interferon- γ suppresses Na⁺-H⁺ exchanger in cultured human endolymphatic sac epithelial cells. *J Cell Biochem.* 2009 Aug 1;107(5):965–72.
68. Royaux IE, Belyantseva IA, Wu T, Kachar B, Everett LA, Marcus DC, et al. Localization and Functional Studies of Pendrin in the Mouse Inner Ear Provide Insight About the Etiology of Deafness in Pendred Syndrome. *JARO - J Assoc Res Otolaryngol.* 2003 Sep 1;4(3):394–404.
69. Lee HJ, Yang WS, Park HW, Choi HS, Kim SH, Kim JY, et al. Expression of Anion Exchangers in Cultured Human Endolymphatic Sac Epithelia: *Otol Neurotol.* 2012 Dec;33(9):1664–71.
70. Møller MN, Kirkeby S, Vikeså J, Nielsen FC, Cayé-Thomasen P. Gene Expression in the Human Endolymphatic Sac: The Solute Carrier Molecules in Endolymphatic Fluid Homeostasis. *Otol Neurotol.* 2015 Jun;36(5):915–22.
71. Akiyama K, Miyashita T, Mori T, Mori N. Expression of the Na⁺-K⁺-2Cl⁻ cotransporter in the rat endolymphatic sac. *Biochem Biophys Res Commun.* 2007 Dec;364(4):913–7.
72. Kakigi A, Nishimura M, Takeda T, Taguchi D, Nishioka R. Expression of aquaporin1, 3, and 4, NKCC1, and NKCC2 in the human endolymphatic sac. *Auris Nasus Larynx.* 2009 Apr;36(2):135–9.
73. Akiyama K, Miyashita T, Mori T, Inamoto R, Mori N. Expression of thiazide-sensitive Na⁺-Cl⁻ cotransporter in the rat endolymphatic sac. *Biochem Biophys Res Commun.* 2008 Jul;371(4):649–53.
74. Kämpfe Nordström C, Danckwardt-Lillieström N, Laurell G, Liu W, Rask-Andersen H. The Human Endolymphatic Sac and Inner Ear Immunity: Macrophage Interaction and Molecular Expression. *Front Immunol.* 2019 Feb 1;9:3181.
75. Rask-Andersen H, Stahle J. Immunodefence of the Inner Ear?: Lymphocyte-Macrophage Interaction in the Endolymphatic Sac. *Acta Otolaryngol (Stockh).* 1980 Jan;89(3–6):283–94.
76. Ikeda M, Morgenstern C. Immune Response of the Endolymphatic Sac to Horseradish Peroxidase: Immunologic Route from the Middle Ear to the Inner Ear. *Ann Otol Rhinol Laryngol.* 1989 Dec;98(12):975–9.
77. Møller MN, Kirkeby S, Vikeså J, Nielsen FC, Cayé-Thomasen P. Gene expression demonstrates an immunological capacity of the human endolymphatic sac: Immunological Capacity of Human Endolymphatic Sac. *The Laryngoscope.* 2015 Aug;125(8):E269–75.
78. Zhang W, Dai M, Fridberger A, Hassan A, DeGagne J, Neng L, et al. Perivascular-resident macrophage-like melanocytes in the inner ear are essential for the integrity of the intrastrial fluid–blood barrier. *Proc Natl Acad Sci.* 2012 Jun 26;109(26):10388–93.
79. O'Malley JT, Nadol JB, McKenna MJ. Anti CD163+, Iba1+, and CD68+ Cells in the Adult Human Inner Ear: Normal Distribution of an Unappreciated Class of Macrophages/Microglia and Implications for Inflammatory Otopathology in Humans. *Otol Neurotol.* 2016 Jan;37(1):99–108.
80. Liu H, Chen L, Giffen KP, Stringham ST, Li Y, Judge PD, et al. Cell-Specific Transcriptome Analysis Shows That Adult Pillar and Deiters' Cells Express Genes Encoding Machinery for Specializations of Cochlear Hair Cells. *Front Mol Neurosci.* 2018 Oct 1;11:356.
81. Bruss DM, Shohet JA. *Neuroanatomy, Ear.* In: StatPearls [Internet]. Treasure Island (FL): StatPearls Publishing; 2023 [cited 2023 Jul 23]. Available from: <http://www.ncbi.nlm.nih.gov/books/NBK551658/>
82. Perez-Carpena P, Lopez-Escamez JA. Current Understanding and Clinical Management of Meniere's Disease: A Systematic Review. *Semin Neurol.* 2020 Feb;40(01):138–50.
83. Nakashima T, Pyykkö I, Arroll MA, Casselbrant ML, Foster CA, Manzoor NF, et al. Meniere's disease. *Nat Rev Dis Primer.* 2016 May 12;2(1):16028.
84. Gibson WPR. Hypothetical Mechanism for Vertigo in Meniere's Disease. *Otolaryngol Clin North Am.* 2010 Oct;43(5):1019–27.
85. Espinosa-Sanchez JM, Lopez-Escamez JA. Menière's disease. In: *Handbook of Clinical Neurology* [Internet]. Elsevier; 2016 [cited 2023 Jul 2]. p. 257–77. Available from: <https://linkinghub.elsevier.com/retrieve/pii/B9780444634375000194>

86. Frejo L, Soto-Varela A, Santos-Perez S, Aran I, Batuecas-Caletrio A, Perez-Guillen V, et al. Clinical Subgroups in Bilateral Meniere Disease. *Front Neurol* [Internet]. 2016 Oct 24 [cited 2022 Mar 6];7. Available from: <http://journal.frontiersin.org/article/10.3389/fneur.2016.00182/full>
87. Belinchon A, Perez-Garrigues H, Tenias JM, Lopez A. Hearing assessment in Meniere's disease: Hearing in Meniere's Disease. *The Laryngoscope*. 2011 Mar;121(3):622–6.
88. Romero Sánchez I, Pérez Garrigues H, Rodríguez Rivera V. Clinical characteristics of tinnitus in Ménière's disease. *Acta Otorrinolaringol Engl Ed*. 2010 Jan;61(5):327–31.
89. Perez-Carpena P, Martinez-Martinez M, Martínez Carranza RA, Batuecas-Caletrio A, Lopez-Escamez JA. A tinnitus symphony in 100 patients with Meniere's disease. *Clin Otolaryngol*. 2019 Nov;44(6):1176–80.
90. Lempert T, Olesen J, Furman J, Waterston J, Seemungal B, Carey J, et al. Migraña vestibular: criterios diagnósticos. Documento de consenso de la Bárány Society y la International Headache Society. *Acta Otorrinolaringol Esp*. 2013 Nov;64(6):428–33.
91. Lopez-Escamez JA, Dlugaiczyk J, Jacobs J, Lempert T, Teggi R, Von Brevern M, et al. Accompanying Symptoms Overlap during Attacks in Ménière's Disease and Vestibular Migraine. *Front Neurol* [Internet]. 2014 Dec 15 [cited 2023 Jul 2];5. Available from: <http://journal.frontiersin.org/article/10.3389/fneur.2014.00265/abstract>
92. Flook M, Frejo L, Gallego-Martinez A, Martin-Sanz E, Rossi-Izquierdo M, Amor-Dorado JC, et al. Differential Proinflammatory Signature in Vestibular Migraine and Meniere Disease. *Front Immunol*. 2019 Jun 4;10:1229.
93. Radtke A, Lempert T, Gresty MA, Brookes GB, Bronstein AM, Neuhauser H. Migraine and Meniere's disease: Is there a link? *Neurology*. 2002 Dec 10;59(11):1700–4.
94. Tyrrell JS, Whinney DJD, Ukoumunne OC, Fleming LE, Osborne NJ. Prevalence, Associated Factors, and Comorbid Conditions for Ménière's Disease. *Ear Hear*. 2014 Jul;35(4):e162–9.
95. Flook M, Lopez Escamez JA. Meniere's Disease: Genetics and the Immune System. *Curr Otorhinolaryngol Rep*. 2018 Mar;6(1):24–31.
96. Gazquez I, Soto-Varela A, Aran I, Santos S, Batuecas A, Trinidad G, et al. High Prevalence of Systemic Autoimmune Diseases in Patients with Ménière's Disease. Means RE, editor. *PLoS ONE*. 2011 Oct 28;6(10):e26759.
97. Kim SY, Lee CH, Yoo DM, Min C, Choi HG. Association Between Asthma and Meniere's Disease: A Nested Case–Control Study. *The Laryngoscope*. 2022 Apr;132(4):864–72.
98. Derebery MJ. Allergic and Immunologic Features of Ménière's Disease. *Otolaryngol Clin North Am*. 2011 Jun;44(3):655–66.
99. Frejo L, Gallego-Martinez A, Requena T, Martin-Sanz E, Amor-Dorado JC, Soto-Varela A, et al. Proinflammatory cytokines and response to molds in mononuclear cells of patients with Meniere disease. *Sci Rep*. 2018 Apr 13;8(1):5974.
100. Ciorba A, Corazzi V, Bianchini C, Aimoni C, Pelucchi S, Skarzyński PH, et al. Autoimmune inner ear disease (AIED): A diagnostic challenge. *Int J Immunopathol Pharmacol*. 2018 Jan;32:205873841880868.
101. Frejo L, Martin-Sanz E, Teggi R, Trinidad G, Soto-Varela A, Santos-Perez S, et al. Extended phenotype and clinical subgroups in unilateral Meniere disease: A cross-sectional study with cluster analysis. *Clin Otolaryngol*. 2017 Dec;42(6):1172–80.
102. Morrison AW, Bailey MES, Morrison GAJ. Familial Ménière's disease: clinical and genetic aspects. *J Laryngol Otol*. 2009 Jan;123(1):29–37.
103. Parra-Perez AM, Lopez-Escamez JA. Types of Inheritance and Genes Associated with Familial Meniere Disease. *J Assoc Res Otolaryngol* [Internet]. 2023 Apr 6 [cited 2023 Jul 2]; Available from: <https://link.springer.com/10.1007/s10162-023-00896-0>
104. Requena T, Espinosa-Sanchez JM, Cabrera S, Trinidad G, Soto-Varela A, Santos-Perez S, et al. Familial clustering and genetic heterogeneity in Meniere's disease. *Clin Genet*. 2014 Mar;85(3):245–52.
105. Martín-Sierra C, Gallego-Martinez A, Requena T, Frejo L, Batuecas-Caletrio A, Lopez-Escamez JA. Variable expressivity and genetic heterogeneity involving DPT and SEMA3D genes in autosomal dominant familial Meniere's disease. *Eur J Hum Genet*. 2017 Feb;25(2):200–7.

106. Pyykkö I, Nakashima T, Yoshida T, Zou J, Naganawa S. Ménière's disease: a reappraisal supported by a variable latency of symptoms and the MRI visualisation of endolymphatic hydrops. *BMJ Open*. 2013;3(2):e001555.
107. House JW, Doherty JK, Fisher LM, Derebery MJ, Berliner KI. Meniere's Disease: Prevalence of Contralateral Ear Involvement: *Otol Neurotol*. 2006 Apr;27(3):355–61.
108. Lopez-Escamez JA, Carey J, Chung WH, Goebel JA, Magnusson M, Mandalà M, et al. Diagnostic criteria for Ménière's disease. *J Vestib Res*. 2015 Mar 1;25(1):1–7.
109. Schuknecht HF, Northrop C, Igarashi M. Cochlear Pathology After Destruction Of The Endolymphatic Sac In The Cat. *Acta Otolaryngol (Stockh)*. 1968 Jan;65(1–6):479–87.
110. Koskas HJ, Linthicum FH, House WF. Membranous ruptures in Meniere's disease: Existence, location, and incidence. *Otolaryngol Neck Surg*. 1983 Feb;91(1):61–7.
111. Rauch SD, Merchant SN, Thedinger BA. Meniere's Syndrome and Endolymphatic Hydrops: Double-Blind Temporal Bone Study. *Ann Otol Rhinol Laryngol*. 1989 Nov;98(11):873–83.
112. Merchant SN, Adams JC, Nadol JB. Pathophysiology of Ménière's Syndrome: Are Symptoms Caused by Endolymphatic Hydrops?: *Otol Neurotol*. 2005 Jan;26(1):74–81.
113. Stahle J, Wilbrand HF. The Temporal Bone in Patients with Meniere's Disease. *Acta Otolaryngol (Stockh)*. 1983 Jan;95(1–4):81–94.
114. Sando I, Ikeda M. Pneumatization and Thickness of the Petrous Bone in Patients with Meniere's Disease: A Histopathological Study. *Ann Otol Rhinol Laryngol*. 1985 Jul;94(4_suppl):2–5.
115. Paparella MMS H. The significance of the lateral sinus in Meniere's disease. 1989 p. 139–46.
116. Nadol JB, Thornton AR. Ultrastructural Findings in a Case of Meniere's Disease. *Ann Otol Rhinol Laryngol*. 1987 Jul;96(4):449–54.
117. Baloh RW. Harold Schuknecht and Pathology of the Ear: *Otol Neurotol*. 2001 Jan;22(1):113–22.
118. Momin SR, Melki SJ, Alagramam KN, Megerian CA. Spiral ganglion loss outpaces inner hair cell loss in endolymphatic hydrops. *The Laryngoscope*. 2009;NA-NA.
119. Ikeda M, Sando I. Endolymphatic Duct and Sac in Patients with Meniere's Disease: A Temporal Bone Histopathological Study. *Ann Otol Rhinol Laryngol*. 1984 Nov;93(6):540–6.
120. Arenberg IK, Lemke C, Shambaugh GE. Viral Theory for Ménière's Disease and Endolymphatic Hydrops: Overview and New Therapeutic Options for Viral Labyrinthitis. *Ann N Y Acad Sci*. 1997 Dec;830(1):306–13.
121. Kimura RS, Schuknecht HF. Membranous Hydrops in the Inner Ear of the Guinea Pig after Obliteration of the Endolymphatic Sac. *ORL*. 1965;27(6):343–54.
122. Hahn HJ, Kwak SG, Kim DK, Kim JY. A Nationwide, Population-based Cohort Study on Potential Autoimmune Association of Ménière Disease to Atopy and Vitiligo. *Sci Rep*. 2019 Mar 13;9(1):4406.
123. Hwang G, Saadi R, Patel VA, Liaw J, Isildak H. Thyroid Dysfunction in Ménière's Disease: A Comprehensive Review. *ORL*. 2021;83(4):219–26.
124. Lopez-Escamez JA, Saenz-Lopez P, Gazquez I, Moreno A, Gonzalez-Oller C, Soto-Varela A, et al. Polymorphisms of CD16A and CD32 Fcγ receptors and circulating immune complexes in Ménière's disease: a case-control study. *BMC Med Genet*. 2011 Dec;12(1):2.
125. Kim SH, Kim JY, Lee HJ, Gi M, Kim BG, Choi JY. Autoimmunity as a Candidate for the Etiopathogenesis of Meniere's Disease: Detection of Autoimmune Reactions and Diagnostic Biomarker Candidate. Sokolowski B, editor. *PLoS ONE*. 2014 Oct 17;9(10):e111039.
126. Pathak S, Goldofsky E, Vivas EX, Bonagura VR, Vambutas A. IL-1β Is Overexpressed and Aberrantly Regulated in Corticosteroid Nonresponders with Autoimmune Inner Ear Disease. *J Immunol*. 2011 Feb 1;186(3):1870–9.
127. Vambutas A, Lesser M, Mulooley V, Pathak S, Zahtz G, Rosen L, et al. Early efficacy trial of anakinra in corticosteroid-resistant autoimmune inner ear disease. *J Clin Invest*. 2014 Sep 2;124(9):4115–22.
128. Gallego-Martinez A, Lopez-Escamez JA. Genetic architecture of Meniere's disease. *Hear Res*. 2020 Nov;397:107872.

129. Frejo L, Requena T, Okawa S, Gallego-Martinez A, Martinez-Bueno M, Aran I, et al. Regulation of Fn14 Receptor and NF- κ B Underlies Inflammation in Meniere's Disease. *Front Immunol*. 2017 Dec 13;8:1739.
130. Moleon MDC, Martinez-Gomez E, Flook M, Peralta-Leal A, Gallego JA, Sanchez-Gomez H, et al. Clinical and Cytokine Profile in Patients with Early and Late Onset Meniere Disease. *J Clin Med*. 2021 Sep 7;10(18):4052.
131. Huang C, Wang Q, Pan X, Li W, Liu W, Jiang W, et al. Up-Regulated Expression of Interferon-Gamma, Interleukin-6 and Tumor Necrosis Factor-Alpha in the Endolymphatic Sac of Meniere's Disease Suggesting the Local Inflammatory Response Underlies the Mechanism of This Disease. *Front Neurol*. 2022 Feb 23;13:781031.
132. Nakanishi H, Kawashima Y, Kurima K, Chae JJ, Ross AM, Pinto-Patarroyo G, et al. *NLRP3* mutation and cochlear autoinflammation cause syndromic and nonsyndromic hearing loss DFNA34 responsive to anakinra therapy. *Proc Natl Acad Sci [Internet]*. 2017 Sep 12 [cited 2023 Jul 23];114(37). Available from: <https://pnas.org/doi/full/10.1073/pnas.1702946114>
133. Duke WW. MÉNIÈRE'S SYNDROME CAUSED BY ALLERGY. *JAMA J Am Med Assoc*. 1923 Dec 29;81(26):2179.
134. Derebery MJ. Allergic management of Meniere's disease: An outcome study. *Otolaryngol Neck Surg*. 2000 Feb;122(2):174–82.
135. Keles E, Gödekmerdan A, Kalidag T, Kaygusuz I, Yalçın S, Cengiz Alpay H, et al. Ménière's disease and allergy: allergens and cytokines. *J Laryngol Otol [Internet]*. 2004 Sep [cited 2023 Jul 23];118(09). Available from: http://www.journals.cambridge.org/abstract_S0022215104001859
136. Ma Y, Sun Q, Zhang K, Bai L, Du L. High level of IgE in acute low-tone sensorineural hearing loss: A predictor for recurrence and Meniere Disease transformation. *Am J Otolaryngol*. 2021 Mar;42(2):102856.
137. Roomiani M, Dehghani Firouzabadi F, Delbandi AA, Ghalehbaghi B, Daneshi A, Yazdani N, et al. Evaluation of Serum Immunoreactivity to Common Indigenous Iranian Inhalation and Food Allergens in Patients with Meniere's Disease. *Immunol Invest*. 2022 Apr 3;51(3):705–14.
138. Zhang N, Lyu Y, Guo J, Liu J, Song Y, Fan Z, et al. Bidirectional Transport of IgE by CD23 in the Inner Ear of Patients with Meniere's Disease. *J Immunol*. 2022 Feb 15;208(4):827–38.
139. Dagli M, Goksu N, Eryilmaz A, Mocan Kuzey G, Bayazit Y, Gun BD, et al. Expression of histamine receptors (H1, H2, and H3) in the rabbit endolymphatic sac: an immunohistochemical study. *Am J Otolaryngol*. 2008 Jan;29(1):20–3.
140. Egami N, Kakigi A, Takeda T, Takeda S, Nishioka R, Hyodo M, et al. Type 1 Allergy-Induced Endolymphatic Hydrops and the Suppressive Effect of H1-Receptor Antagonist (Olopatadine Hydrochloride). *Otol Neurotol*. 2014 Mar;35(3):e104–9.
141. Møller MN, Kirkeby S, Vikeså J, Nielsen FC, Caye-Thomasen P. Expression of histamine receptors in the human endolymphatic sac: the molecular rationale for betahistine use in Menieres disease. *Eur Arch Otorhinolaryngol*. 2016 Jul;273(7):1705–10.
142. Takumida M, Takumida H, Anniko M. Localization of histamine (H₁, H₂, H₃ and H₄) receptors in mouse inner ear. *Acta Otolaryngol (Stockh)*. 2016 Jun 2;136(6):537–44.
143. Escalera-Balsera A, Roman-Naranjo P, Lopez-Escamez JA. Systematic Review of Sequencing Studies and Gene Expression Profiling in Familial Meniere Disease. *Genes*. 2020 Nov 27;11(12):1414.
144. Roman-Naranjo P, Parra-Perez AM, Escalera-Balsera A, Soto-Varela A, Gallego-Martinez A, Aran I, et al. Defective α -tectorin may involve tectorial membrane in familial Meniere disease. *Clin Transl Med [Internet]*. 2022 Jun [cited 2023 Jul 23];12(6). Available from: <https://onlinelibrary.wiley.com/doi/10.1002/ctm2.829>
145. Frykholm C, Klar J, Tomanovic T, Ameer A, Dahl N. Stereocilin gene variants associated with episodic vertigo: expansion of the DFNB16 phenotype. *Eur J Hum Genet*. 2018 Dec;26(12):1871–4.
146. Skarp S, Kanervo L, Kotimäki J, Sorri M, Männikkö M, Hietikko E. Whole-exome sequencing suggests multiallelic inheritance for childhood-onset Ménière's disease. *Ann Hum Genet*. 2019 Nov;83(6):389–96.
147. Mehrjoo Z, Kahrizi K, Mohseni M, Akbari M, Arzhanghi S, Jalalvand K, et al. Limbic System Associated Membrane Protein Mutation in an

- Iranian Family Diagnosed with Ménière's Disease. *Arch Iran Med.* 2020 May 1;23(5):319–25.
148. Roman-Naranjo P, Gallego-Martinez A, Soto-Varela A, Aran I, Moleon M del C, Espinosa-Sanchez JM, et al. Burden of Rare Variants in the OTOG Gene in Familial Meniere's Disease. *Ear Hear.* 2020 Nov;41(6):1598–605.
149. Roman-Naranjo P, Moleon MDC, Aran I, Escalera-Balsera A, Soto-Varela A, Bächinger D, et al. Rare coding variants involving MYO7A and other genes encoding stereocilia link proteins in familial meniere disease. *Hear Res.* 2021 Sep;409:108329.
150. Simmler MC, Cohen-Salmon M, El-Amraoui A, Guillaud L, Benichou JC, Petit C, et al. Targeted disruption of Otog results in deafness and severe imbalance. *Nat Genet.* 2000 Feb;24(2):139–43.
151. Kim DK, Kim JA, Park J, Niazi A, Almishaal A, Park S. The release of surface-anchored α -tectorin, an apical extracellular matrix protein, mediates tectorial membrane organization. *Sci Adv.* 2019 Nov;5(11):eaay6300.
152. Michalski N, Michel V, Bahloul A, Lefevre G, Barral J, Yagi H, et al. Molecular Characterization of the Ankle-Link Complex in Cochlear Hair Cells and Its Role in the Hair Bundle Functioning. *J Neurosci.* 2007 Jun 13;27(24):6478–88.
153. Gallego-Martinez A, Requena T, Roman-Naranjo P, Lopez-Escamez JA. Excess of Rare Missense Variants in Hearing Loss Genes in Sporadic Meniere Disease. *Front Genet.* 2019 Feb 15;10:76.
154. Gallego-Martinez A, Requena T, Roman-Naranjo P, May P, Lopez-Escamez JA. Enrichment of damaging missense variants in genes related with axonal guidance signalling in sporadic Meniere's disease. *J Med Genet.* 2020 Feb;57(2):82–8.
155. Bächinger D, Luu NN, Kempfle JS, Barber S, Zürrer D, Lee DJ, et al. Vestibular Aqueduct Morphology Correlates With Endolymphatic Sac Pathologies in Meniere's Disease—A Correlative Histology and Computed Tomography Study. *Otol Neurotol.* 2019 Jun;40(5):e548–55.
156. Bächinger D, Brühlmann C, Honegger T, Michalopoulou E, Monge Naldi A, Wettstein VG, et al. Endotype-Phenotype Patterns in Meniere's Disease Based on Gadolinium-Enhanced MRI of the Vestibular Aqueduct. *Front Neurol.* 2019 Apr 5;10:303.
157. Bächinger D, Schuknecht B, Długaiczek J, Eckhard AH. Radiological Configuration of the Vestibular Aqueduct Predicts Bilateral Progression in Meniere's Disease. *Front Neurol.* 2021 Jun 8;12:674170.
158. Rabbani B, Tekin M, Mahdieh N. The promise of whole-exome sequencing in medical genetics. *J Hum Genet.* 2014 Jan;59(1):5–15.
159. Fernandez-Marmiesse A, Gouveia S, Couce ML. NGS Technologies as a Turning Point in Rare Disease Research , Diagnosis and Treatment. *Curr Med Chem.* 2018 Jan 30;25(3):404–32.
160. Manolio TA, Collins FS, Cox NJ, Goldstein DB, Hindorff LA, Hunter DJ, et al. Finding the missing heritability of complex diseases. *Nature.* 2009 Oct;461(7265):747–53.
161. Escaramís G, Docampo E, Rabionet R. A decade of structural variants: description, history and methods to detect structural variation. *Brief Funct Genomics.* 2015 Sep;14(5):305–14.
162. Manolio TA. Genomewide Association Studies and Assessment of the Risk of Disease. Feero WG, Guttmacher AE, editors. *N Engl J Med.* 2010 Jul 8;363(2):166–76.
163. Gibson G. Rare and common variants: twenty arguments. *Nat Rev Genet.* 2012 Feb;13(2):135–45.
164. Garcia M, Juhos S, Larsson M, Olason PI, Martin M, Eisfeldt J, et al. Sarek: A portable workflow for whole-genome sequencing analysis of germline and somatic variants. *F1000Research.* 2020 Sep 4;9:63.
165. Van Der Auwera GA, Carneiro MO, Hartl C, Poplin R, Del Angel G, Levy-Moonshine A, et al. From FastQ Data to High-Confidence Variant Calls: The Genome Analysis Toolkit Best Practices Pipeline. *Curr Protoc Bioinforma [Internet].* 2013 Oct [cited 2023 Aug 16];43(1). Available from: <https://onlinelibrary.wiley.com/doi/10.1002/0471250953.bi11110s43>
166. DePristo MA, Banks E, Poplin R, Garimella KV, Maguire JR, Hartl C, et al. A framework for variation discovery and genotyping using next-generation DNA sequencing data. *Nat Genet.* 2011 May;43(5):491–8.
167. Danecek P, Bonfield JK, Liddle J, Marshall J, Ohan V, Pollard MO, et al. Twelve years of SAMtools and BCFtools. *GigaScience.* 2021 Jan 29;10(2):giab008.

168. Auwera G van der, O'Connor BD. Genomics in the cloud: using Docker, GATK, and WDL in Terra. First edition. Sebastopol, CA: O'Reilly Media; 2020. 467 p. massive parallel sequencing data. F1000Research. 2017 Jun 30;6:664.
169. McLaren W, Gil L, Hunt SE, Riat HS, Ritchie GRS, Thormann A, et al. The Ensembl Variant Effect Predictor. *Genome Biol.* 2016 Dec;17(1):122.
170. Chen S, Francioli LC, Goodrich JK, Collins RL, Kanai M, Wang Q, et al. A genome-wide mutational constraint map quantified from variation in 76,156 human genomes [Internet]. *Genetics*; 2022 Mar [cited 2023 Aug 16]. Available from: <http://biorxiv.org/lookup/doi/10.1101/2022.03.20.485034>
171. Kircher M, Witten DM, Jain P, O'Roak BJ, Cooper GM, Shendure J. A general framework for estimating the relative pathogenicity of human genetic variants. *Nat Genet.* 2014 Mar;46(3):310–5.
172. Richards S, Aziz N, Bale S, Bick D, Das S, Gastier-Foster J, et al. Standards and Guidelines for the Interpretation of Sequence Variants: A Joint Consensus Recommendation of the American College of Medical Genetics and Genomics and the Association for Molecular Pathology. *Genet Med Off J Am Coll Med Genet.* 2015 May;17(5):405–24.
173. Exome Aggregation Consortium, Lek M, Karczewski KJ, Minikel EV, Samocha KE, Banks E, et al. Analysis of protein-coding genetic variation in 60,706 humans [Internet]. *Genomics*; 2015 Oct [cited 2023 Jul 11]. Available from: <http://biorxiv.org/lookup/doi/10.1101/030338>
174. Shyr C, Tarailo-Graovac M, Gottlieb M, Lee JJ, Van Karnebeek C, Wasserman WW. FLAGS, frequently mutated genes in public exomes. *BMC Med Genomics.* 2014 Dec;7(1):64.
175. Van Camp G, Smith RJH. Hereditary Hearing Loss Homepage. <https://hereditaryhearingloss.org>.
176. Chen X, Schulz-Trieglaff O, Shaw R, Barnes B, Schlesinger F, Källberg M, et al. Manta: rapid detection of structural variants and indels for germline and cancer sequencing applications. *Bioinformatics.* 2016 Apr 15;32(8):1220–2.
177. Eisfeldt J, Vezzi F, Olason P, Nilsson D, Lindstrand A. TIDDIT, an efficient and comprehensive structural variant caller for massive parallel sequencing data. F1000Research. 2017 Jun 30;6:664.
178. Talevich E, Shain AH, Botton T, Bastian BC. CNVkit: Genome-Wide Copy Number Detection and Visualization from Targeted DNA Sequencing. *PLOS Comput Biol.* 2016 Apr 21;12(4):e1004873.
179. Geoffroy V, Guignard T, Kress A, Gaillard JB, Solli-Nowlan T, Schalk A, et al. AnnotSV and knotAnnotSV: a web server for human structural variations annotations, ranking and analysis. *Nucleic Acids Res.* 2021 Jul 2;49(W1):W21–8.
180. Lek M, Karczewski KJ, Minikel EV, Samocha KE, Banks E, Fennell T, et al. Analysis of protein-coding genetic variation in 60,706 humans. *Nat Publ Group.* 2016 Aug;536(7616):285–91.
181. Karczewski KJ, Francioli LC, Tiao G, Cummings BB, Alföldi J, Wang Q, et al. The mutational constraint spectrum quantified from variation in 141,456 humans. *Nature.* 2020 May 28;581(7809):434–43.
182. Kim DE, Chivian D, Baker D. Protein structure prediction and analysis using the Robetta server. *Nucleic Acids Res.* 2004 Jul 1;32(Web Server):W526–31.
183. Mortuza SM, Zheng W, Zhang C, Li Y, Pearce R, Zhang Y. Improving fragment-based ab initio protein structure assembly using low-accuracy contact-map predictions. *Nat Commun.* 2021 Dec;12(1):5011.
184. Zheng W, Zhang C, Li Y, Pearce R, Bell EW, Zhang Y. Folding non-homologous proteins by coupling deep-learning contact maps with I-TASSER assembly simulations. *Cell Rep Methods.* 2021 Jul;1(3):100014.
185. Jumper J, Evans R, Pritzel A, Green T, Figurnov M, Ronneberger O, et al. Highly accurate protein structure prediction with AlphaFold. *Nature.* 2021 Aug 26;596(7873):583–9.
186. Fiser A, Šali A. Modeller: Generation and Refinement of Homology-Based Protein Structure Models. In: *Methods in Enzymology* [Internet]. Elsevier; 2003 [cited 2023 Aug 21]. p. 461–91. Available from: <https://linkinghub.elsevier.com/retrieve/pii/S0076687903740208>
187. Pucci F, Kwasigroch JM, Rooman M. SCooP: an accurate and fast predictor of protein stability curves as a function of temperature. Valencia A, editor. *Bioinformatics.* 2017 Nov 1;33(21):3415–22.

188. Robinson JT, Thorvaldsdóttir H, Wenger AM, Zehir A, Mesirov JP. Variant Review with the Integrative Genomics Viewer. *Cancer Res.* 2017 Nov 1;77(21):e31–4.
189. Köressaar T, Lepamets M, Kaplinski L, Raime K, Andreson R, Remm M. Primer3_masker: integrating masking of template sequence with primer design software. Hancock J, editor. *Bioinformatics.* 2018 Jun 1;34(11):1937–8.
190. Ye J, Coulouris G, Zaretskaya I, Cutcutache I, Rozen S, Madden TL. Primer-BLAST: A tool to design target-specific primers for polymerase chain reaction. *BMC Bioinformatics.* 2012 Dec;13(1):134.
191. Garcia-Moreno A, López-Domínguez R, Villatoro-García JA, Ramirez-Mena A, Aparicio-Puerta E, Hackenberg M, et al. Functional Enrichment Analysis of Regulatory Elements. *Biomedicines.* 2022 Mar 3;10(3):590.
192. Scheffer DI, Shen J, Corey DP, Chen ZY. Gene Expression by Mouse Inner Ear Hair Cells during Development. *J Neurosci.* 2015 Apr 22;35(16):6366–80.
193. Ushakov K, Koffler-Brill T, Rom A, Perl K, Ulitsky I, Avraham KB. Genome-wide identification and expression profiling of long non-coding RNAs in auditory and vestibular systems. *Sci Rep.* 2017 Aug 17;7(1):8637.
194. Elkon R, Milon B, Morrison L, Shah M, Vijayakumar S, Racherla M, et al. RFX transcription factors are essential for hearing in mice. *Nat Commun.* 2015 Oct 15;6(1):8549.
195. Cai T, Jen HI, Kang H, Klisch TJ, Zoghbi HY, Groves AK. Characterization of the Transcriptome of Nascent Hair Cells and Identification of Direct Targets of the Atoh1 Transcription Factor. *J Neurosci.* 2015 Apr 8;35(14):5870–83.
196. Pesenti ME, Raisch T, Conti D, Walstein K, Hoffmann I, Vogt D, et al. Structure of the human inner kinetochore CCAN complex and its significance for human centromere organization. *Mol Cell.* 2022 Jun;82(11):2113–2131.e8.
197. Fuente R, García-Bengoia M, Fernández-Iglesias Á, Gil-Peña H, Santos F, López JM. Cellular and Molecular Alterations Underlying Abnormal Bone Growth in X-Linked Hypophosphatemia. *Int J Mol Sci.* 2022 Jan 15;23(2):934.
198. Jung D, Nagururu N, Hui F, Pearl MS, Carey JP, Ward BK. 2D Measurements of the Angle of the Vestibular Aqueduct Using CT Imaging. *Brain Sci.* 2022 Dec 26;13(1):47.
199. Toneva DH, Nikolova SY, Tasheva-Terzieva ED, Zlatareva DK, Lazarov NE. Sexual dimorphism in shape and size of the neurocranium. *Int J Legal Med.* 2022 Nov;136(6):1851–63.
200. Hebbbar GK, Rask-Andersen H, Linthicum FH. Three-Dimensional Analysis of 61 Human Endolymphatic Ducts and Sacs in Ears with and without Meniere's Disease. *Ann Otol Rhinol Laryngol.* 1991 Mar;100(3):219–25.
201. Bloch SL, Friis M. Objective Measurement of the Human Endolymphatic Sac Dimensions in Ménière's Disease. *Otol Neurotol.* 2011 Oct;32(8):1364–9.
202. Monsanto RDC, Pauna HF, Kwon G, Schachern PA, Tsuprun V, Paparella MM, et al. A three-dimensional analysis of the endolymph drainage system in Ménière disease. *The Laryngoscope* [Internet]. 2017 May [cited 2023 Aug 14];127(5). Available from: <https://onlinelibrary.wiley.com/doi/10.1002/lary.26155>
203. Watzke D, Bast TH. The development and structure of the otic (endolymphatic) sac. *Anat Rec.* 1950 Mar;106(3):361–79.
204. Nie J, Zhang W. Secreted protease ADAMTS18 in development and disease. *Gene.* 2023 Mar;858:147169.
205. Tsuprun V, Santi P. Ultrastructure and immunohistochemical identification of the extracellular matrix of the chinchilla cochlea. *Hear Res.* 1999 Mar;129(1–2):35–49.
206. Hu BH, Cai Q, Hu Z, Patel M, Bard J, Jamison J, et al. Metalloproteinases and Their Associated Genes Contribute to the Functional Integrity and Noise-Induced Damage in the Cochlear Sensory Epithelium. *J Neurosci.* 2012 Oct 24;32(43):14927–41.
207. Meyer Zum Gottesberge AM, Gross O, Becker-Lendzian U, Massing T, Vogel WF. Inner ear defects and hearing loss in mice lacking the collagen receptor DDR1. *Lab Invest.* 2008 Jan;88(1):27–37.
208. Kundu S, Tyagi N, Sen U, Tyagi SC. Matrix imbalance by inducing expression of metalloproteinase and oxidative stress in cochlea of hyperhomocysteinemic mice. *Mol Cell Biochem.* 2009 Dec;332(1–2):215–24.
209. Nam SI, Yu GI, Kim HJ, Park KO, Chung JH, Ha E, et al. A polymorphism at -1607 2G in

- the matrix metalloproteinase-1 (MMP-1) increased risk of sudden deafness in Korean population but not at -519A/G in MMP-1: MMP-1 Polymorphism and Risk of Sudden Deafness. *The Laryngoscope*. 2011 Jan;121(1):171–5.
210. Gratton MA, Rao VH, Meehan DT, Askew C, Cosgrove D. Matrix Metalloproteinase Dysregulation in the Stria Vascularis of Mice with Alport Syndrome. *Am J Pathol*. 2005 May;166(5):1465–74.
211. Setz C, Brand Y, Radojevic V, Hanusek C, Mullen PJ, Levano S, et al. Matrix metalloproteinases 2 and 9 in the cochlea: expression and activity after aminoglycoside exposition. *Neuroscience*. 2011 May;181:28–39.
212. Yamamoto R, Ohnishi H, Omori K, Yamamoto N. In silico analysis of inner ear development using public whole embryonic body single-cell RNA-sequencing data. *Dev Biol*. 2021 Jan;469:160–71.
213. Mushimiyimana I, Niskanen H, Beter M, Laakkonen JP, Kaikkonen MU, Ylä-Herttuala S, et al. Characterization of a functional endothelial super-enhancer that regulates ADAMTS18 and angiogenesis. *Nucleic Acids Res*. 2021 Aug 20;49(14):8078–96.
214. Well D, Blanchard S, Kaplan J, Guilford P, Gibson F, Walsh J, et al. Defective myosin VIIA gene responsible for Usher syndrome type 1B. *Nature*. 1995 Mar;374(6517):60–1.
215. Liu XZ, Walsh J, Tamagawa Y, Kitamura K, Nishizawa M, Steel KP, et al. Autosomal dominant non-syndromic deafness caused by a mutation in the myosin VIIA gene. *Nat Genet*. 1997 Nov;17(3):268–9.
216. Liu XZ, Walsh J, Mburu P, Kendrick-Jones J, Cope MJTV, Steel KP, et al. Mutations in the myosin VIIA gene cause non-syndromic recessive deafness. *Nat Genet*. 1997 Jun;16(2):188–90.
217. Weil D, Küssel P, Blanchard S, Lévy G, Levi-Acobas F, Drira M, et al. The autosomal recessive isolated deafness, DFNB2, and the Usher 1B syndrome are allelic defects of the myosin-VIIA gene. *Nat Genet*. 1997 Jun;16(2):191–3.
218. Mburu P, Mustapha M, Varela A, Weil D, El-Amraoui A, Holme RH, et al. Defects in whirlin, a PDZ domain molecule involved in stereocilia elongation, cause deafness in the whirler mouse and families with DFNB31. *Nat Genet*. 2003 Aug;34(4):421–8.
219. Ebermann I, Scholl HPN, Charbel Issa P, Becirovic E, Lamprecht J, Jurklics B, et al. A novel gene for Usher syndrome type 2: mutations in the long isoform of whirlin are associated with retinitis pigmentosa and sensorineural hearing loss. *Hum Genet*. 2007 Mar 12;121(2):203–11.
220. Mustapha M. An alpha-tectorin gene defect causes a newly identified autosomal recessive form of sensorineural pre-lingual non-syndromic deafness, DFNB21. *Hum Mol Genet*. 1999 Mar 1;8(3):409–12.
221. Erlebacher A, Derynck R. Increased expression of TGF-beta 2 in osteoblasts results in an osteoporosis-like phenotype. *J Cell Biol*. 1996 Jan 1;132(1):195–210.
222. Frisch T, Overgaard S, Sørensen MS, Bretlau P. Estimation of Volume Referent Bone Turnover in the Otic Capsule after Sequential Point Labeling. *Ann Otol Rhinol Laryngol*. 2000 Jan;109(1):33–9.
223. Zehnder AF, Kristiansen AG, Adams JC, Merchant SN, McKenna MJ. Osteoprotegerin in the Inner Ear May Inhibit Bone Remodeling in the Otic Capsule. *The Laryngoscope*. 2005 Jan;115(1):172–7.
224. Mackie EJ, Ahmed YA, Tatarczuch L, Chen KS, Mirams M. Endochondral ossification: How cartilage is converted into bone in the developing skeleton. *Int J Biochem Cell Biol*. 2008;40(1):46–62.
225. Stickens D, Behonick DJ, Ortega N, Heyer B, Hartenstein B, Yu Y, et al. Altered endochondral bone development in matrix metalloproteinase 13-deficient mice. *Development*. 2004 Dec 1;131(23):5883–95.
226. Vu TH, Shipley JM, Bergers G, Berger JE, Helms JA, Hanahan D, et al. MMP-9/Gelatinase B Is a Key Regulator of Growth Plate Angiogenesis and Apoptosis of Hypertrophic Chondrocytes. *Cell*. 1998 May;93(3):411–22.
227. Little CB, Mittaz L, Belluoccio D, Rogerson FM, Campbell IK, Meeker CT, et al. ADAMTS-1-Knockout mice do not exhibit abnormalities in aggrecan turnover in vitro or in vivo. *Arthritis Rheum*. 2005 May;52(5):1461–72.
228. Stanton H, Rogerson FM, East CJ, Golub SB, Lawlor KE, Meeker CT, et al. ADAMTS5 is the major aggrecanase in mouse cartilage in vivo and in vitro. *Nature*. 2005 Mar;434(7033):648–52.
229. Xiong DH, Liu XG, Guo YF, Tan LJ, Wang L, Sha BY, et al. Genome-wide Association and

- Follow-Up Replication Studies Identified ADAMTS18 and TGFBR3 as Bone Mass Candidate Genes in Different Ethnic Groups. *Am J Hum Genet.* 2009 Mar;84(3):388–98.
230. Koller DL, Ichikawa S, Lai D, Padgett LR, Doheny KF, Pugh E, et al. Genome-Wide Association Study of Bone Mineral Density in Premenopausal European-American Women and Replication in African-American Women. *J Clin Endocrinol Metab.* 2010 Apr 1;95(4):1802–9.
231. Fitzgerald J, Holden P, Hansen U. The expanded collagen VI family: new chains and new questions. *Connect Tissue Res.* 2013 Nov;54(6):345–50.
232. Klatt AR, Nitsche DP, Kobbe B, Macht M, Paulsson M, Wagener R. Molecular Structure, Processing, and Tissue Distribution of Matrilin-4. *J Biol Chem.* 2001 May;276(20):17267–75.
233. Gari MA, AlKaff M, Alsehli HS, Dallol A, Gari A, Abu-Elmagd M, et al. Identification of novel genetic variations affecting osteoarthritis patients. *BMC Med Genet.* 2016 Oct;17(S1):68.
234. Liang C, Wang P, Liu X, Yang C, Ma Y, Yong L, et al. Whole-genome sequencing reveals novel genes in ossification of the posterior longitudinal ligament of the thoracic spine in the Chinese population. *J Orthop Surg.* 2018 Dec;13(1):324.
235. Chen C, Wei X, Ling J, Xie N. Expression of Matrilin-2 and -4 in Human Dental Pulp during Dentin-Pulp Complex Wound Healing. *J Endod.* 2011 May;37(5):642–9.
236. Ho MSP, Böse K, Mokkapatil S, Nischt R, Smyth N. Nidogens—Extracellular matrix linker molecules. *Microsc Res Tech.* 2008 May;71(5):387–95.
237. Cheng P, Cao T, Zhao X, Lu W, Miao S, Ning F, et al. Nidogen1-enriched extracellular vesicles accelerate angiogenesis and bone regeneration by targeting Myosin-10 to regulate endothelial cell adhesion. *Bioact Mater.* 2022 Jun;12:185–97.
238. Darbro BW, Mahajan VB, Gakhar L, Skeie JM, Campbell E, Wu S, et al. Mutations in Extracellular Matrix Genes *NID1* and *LAMC1* Cause Autosomal Dominant Dandy-Walker Malformation and Occipital Cephaloceles. *Hum Mutat.* 2013 Aug;34(8):1075–9.
239. Calderwood DA, Tuckwell DS, Eble J, Kühn K, Humphries MJ. The Integrin $\alpha 1$ A-domain Is a Ligand Binding Site for Collagens and Laminin. *J Biol Chem.* 1997 May;272(19):12311–7.
240. Clover J, Dodds RA, Gowen M. Integrin subunit expression by human osteoblasts and osteoclasts *in situ* and in culture. *J Cell Sci.* 1992 Sep 1;103(1):267–71.
241. Salter DM, Godolphin JL, Gourlay MS. Chondrocyte heterogeneity: immunohistologically defined variation of integrin expression at different sites in human fetal knees. *J Histochem Cytochem.* 1995 Apr;43(4):447–57.
242. Apte SS. A Disintegrin-like and Metalloprotease (Reprolysin-type) with Thrombospondin Type 1 Motif (ADAMTS) Superfamily: Functions and Mechanisms. *J Biol Chem.* 2009 Nov;284(46):31493–7.
243. Pihl R, Jensen RK, Poulsen EC, Jensen L, Hansen AG, Thøgersen IB, et al. ITIH4 acts as a protease inhibitor by a novel inhibitory mechanism. *Sci Adv.* 2021 Jan 6;7(2):eaba7381.
244. Rifkin D, Sachan N, Singh K, Sauber E, Tellides G, Ramirez F. The role of LTBP5 in TGF beta signaling. *Dev Dyn.* 2022 Jan;251(1):75–84.
245. Dickerman BK, White CL, Chevalier C, Nalesso V, Charles C, Fouchécourt S, et al. Missense Mutation in the Second RNA Binding Domain Reveals a Role for Prkra (PACT/RAX) during Skull Development. Mossman KL, editor. *PLoS ONE.* 2011 Dec 14;6(12):e28537.
246. Rowe TM, Rizzi M, Hirose K, Peters GA, Sen GC. A role of the double-stranded RNA-binding protein PACT in mouse ear development and hearing. *Proc Natl Acad Sci.* 2006 Apr 11;103(15):5823–8.
247. Forman TE, Dennison BJC, Fantauzzo KA. The Role of RNA-Binding Proteins in Vertebrate Neural Crest and Craniofacial Development. *J Dev Biol.* 2021 Aug 27;9(3):34.
248. Sanford LP, Ormsby I, Groot ACG de, Sariola H, Friedman R, Boivin GP, et al. TGF β 2 knockout mice have multiple developmental defects that are non-overlapping with other TGF β knockout phenotypes. *Development.* 1997 Jul 1;124(13):2659–70.
249. Chang JL, Brauer DS, Johnson J, Chen CG, Akil O, Balooch G, et al. Tissue-specific calibration of extracellular matrix material properties by transforming growth factor- β

- and Runx2 in bone is required for hearing. *EMBO Rep.* 2010 Oct;11(10):765–71.
250. Rifkin DB, Rifkin WJ, Zilberberg L. LTBP in biology and medicine: LTBP diseases. *Matrix Biol.* 2018 Oct;71–72:90–9.
251. Morkmued S, Hemmerle J, Mathieu E, Laugel-Haushalter V, Dabovic B, Rifkin DB, et al. Enamel and dental anomalies in latent-transforming growth factor beta-binding protein 3 mutant mice. *Eur J Oral Sci.* 2017 Feb;125(1):8–17.
252. Dabovic B, Chen Y, Colarossi C, Zambuto L, Obata H, Rifkin D. Bone defects in latent TGF-beta binding protein (Ltbp)-3 null mice; a role for Ltbp in TGF-beta presentation. *J Endocrinol.* 2002 Oct 1;175(1):129–41.
253. Dabovic B, Levasseur R, Zambuto L, Chen Y, Karsenty G, Rifkin DB. Osteopetrosis-like phenotype in latent TGF- β binding protein 3 deficient mice. *Bone.* 2005 Jul;37(1):25–31.
254. Yamagata M. Structure and Functions of Sidekicks. *Front Mol Neurosci.* 2020 Aug 25;13:139.
255. Yamagata M, Sanes JR. Dscam and Sidekick proteins direct lamina-specific synaptic connections in vertebrate retina. *Nature.* 2008 Jan;451(7177):465–9.
256. Yamagata M, Sanes JR. Expression and Roles of the Immunoglobulin Superfamily Recognition Molecule Sidekick1 in Mouse Retina. *Front Mol Neurosci.* 2019 Jan 9;11:485.
257. Goodman KM, Yamagata M, Jin X, Mannepalli S, Katsamba PS, Ahlsén G, et al. Molecular basis of sidekick-mediated cell-cell adhesion and specificity. *eLife.* 2016 Sep 19;5:e19058.
258. Yamagata M, Sanes JR. Synaptic Localization and Function of Sidekick Recognition Molecules Require MAGI Scaffolding Proteins. *J Neurosci.* 2010 Mar 10;30(10):3579–88.
259. Letizia A, He D, Astigarraga S, Colombelli J, Hatini V, Llimargas M, et al. Sidekick Is a Key Component of Tricellular Adherens Junctions that Acts to Resolve Cell Rearrangements. *Dev Cell.* 2019 Aug;50(3):313–326.e5.
260. Xu Z, Peng AW, Oshima K, Heller S. MAGI-1, A Candidate Stereociliary Scaffolding Protein, Associates with the Tip-Link Component Cadherin 23. *J Neurosci.* 2008 Oct 29;28(44):11269–76.
261. Scobie KN, Damez-Werno D, Sun H, Shao N, Gancarz A, Panganiban CH, et al. Essential role of poly(ADP-ribosyl)ation in cocaine action. *Proc Natl Acad Sci.* 2014 Feb 4;111(5):2005–10.
262. Bagot RC, Cates HM, Purushothaman I, Lorsch ZS, Walker DM, Wang J, et al. Circuit-wide Transcriptional Profiling Reveals Brain Region-Specific Gene Networks Regulating Depression Susceptibility. *Neuron.* 2016 Jun;90(5):969–83.
263. Hultman R, Ulrich K, Sachs BD, Blount C, Carlson DE, Ndubuizu N, et al. Brain-wide Electrical Spatiotemporal Dynamics Encode Depression Vulnerability. *Cell.* 2018 Mar;173(1):166–180.e14.
264. Gai X, Xie HM, Perin JC, Takahashi N, Murphy K, Wenocur AS, et al. Rare structural variation of synapse and neurotransmission genes in autism. *Mol Psychiatry.* 2012 Apr;17(4):402–11.
265. Connolly JJ, Glessner JT, Hakonarson H. A Genome-Wide Association Study of Autism Incorporating Autism Diagnostic Interview-Revised, Autism Diagnostic Observation Schedule, and Social Responsiveness Scale: **Genome-Wide Association of ADI-R, ADOS, and SRS Items.** *Child Dev.* 2013 Jan;84(1):17–33.
266. Tsang KM, Croen LA, Torres AR, Kharrazi M, Delorenze GN, Windham GC, et al. A Genome-Wide Survey of Transgenerational Genetic Effects in Autism. *Zwick ME, editor. PLoS ONE.* 2013 Oct 24;8(10):e76978.
267. Butler M, Rafi S, Manzardo A. High-Resolution Chromosome Ideogram Representation of Currently Recognized Genes for Autism Spectrum Disorders. *Int J Mol Sci.* 2015 Mar 20;16(12):6464–95.
268. Narita A, Nagai M, Mizuno S, Ogishima S, Tamiya G, Ueki M, et al. Clustering by phenotype and genome-wide association study in autism. *Transl Psychiatry.* 2020 Aug 17;10(1):290.
269. De Araújo Lima L, Feio-dos-Santos AC, Belangero SI, Gadelha A, Bressan RA, Salum GA, et al. An integrative approach to investigate the respective roles of single-nucleotide variants and copy-number variants in Attention-Deficit/Hyperactivity Disorder. *Sci Rep.* 2016 Mar 7;6(1):22851.
270. Elia J, Gai X, Xie HM, Perin JC, Geiger E, Glessner JT, et al. Rare structural variants found in attention-deficit hyperactivity disorder are preferentially associated with



- neurodevelopmental genes. *Mol Psychiatry*. 2010 Jun;15(6):637–46.
271. Hromatka BS, Tung JY, Kiefer AK, Do CB, Hinds DA, Eriksson N. Genetic variants associated with motion sickness point to roles for inner ear development, neurological processes and glucose homeostasis. *Hum Mol Genet*. 2015 May 1;24(9):2700–8.
272. Coré N, Caubit X, Metchat A, Boned A, Djabali M, Fasano L. *Tshz1* is required for axial skeleton, soft palate and middle ear development in mice. *Dev Biol*. 2007 Aug;308(2):407–20.
273. Lyon MF, Meredith R. *Muted*, a new mutant affecting coat colour and otoliths of the mouse, and its position in linkage group XIV. *Genet Res*. 1969 Oct;14(2):163–6.
274. Astigarraga S, Douthit J, Tarnogorska D, Creamer MS, Mano O, Clark DA, et al. *Drosophila* Sidekick is required in developing photoreceptors to enable visual motion detection. *Development*. 2018 Jan 1;dev.158246.
275. Petitpré C, Faure L, Uhl P, Fontanet P, Filova I, Pavlinkova G, et al. Single-cell RNA-sequencing analysis of the developing mouse inner ear identifies molecular logic of auditory neuron diversification. *Nat Commun*. 2022 Jul 5;13(1):3878.
276. Yang J, Zhang Y. I-TASSER server: new development for protein structure and function predictions. *Nucleic Acids Res*. 2015 Jul 1;43(W1):W174–81.

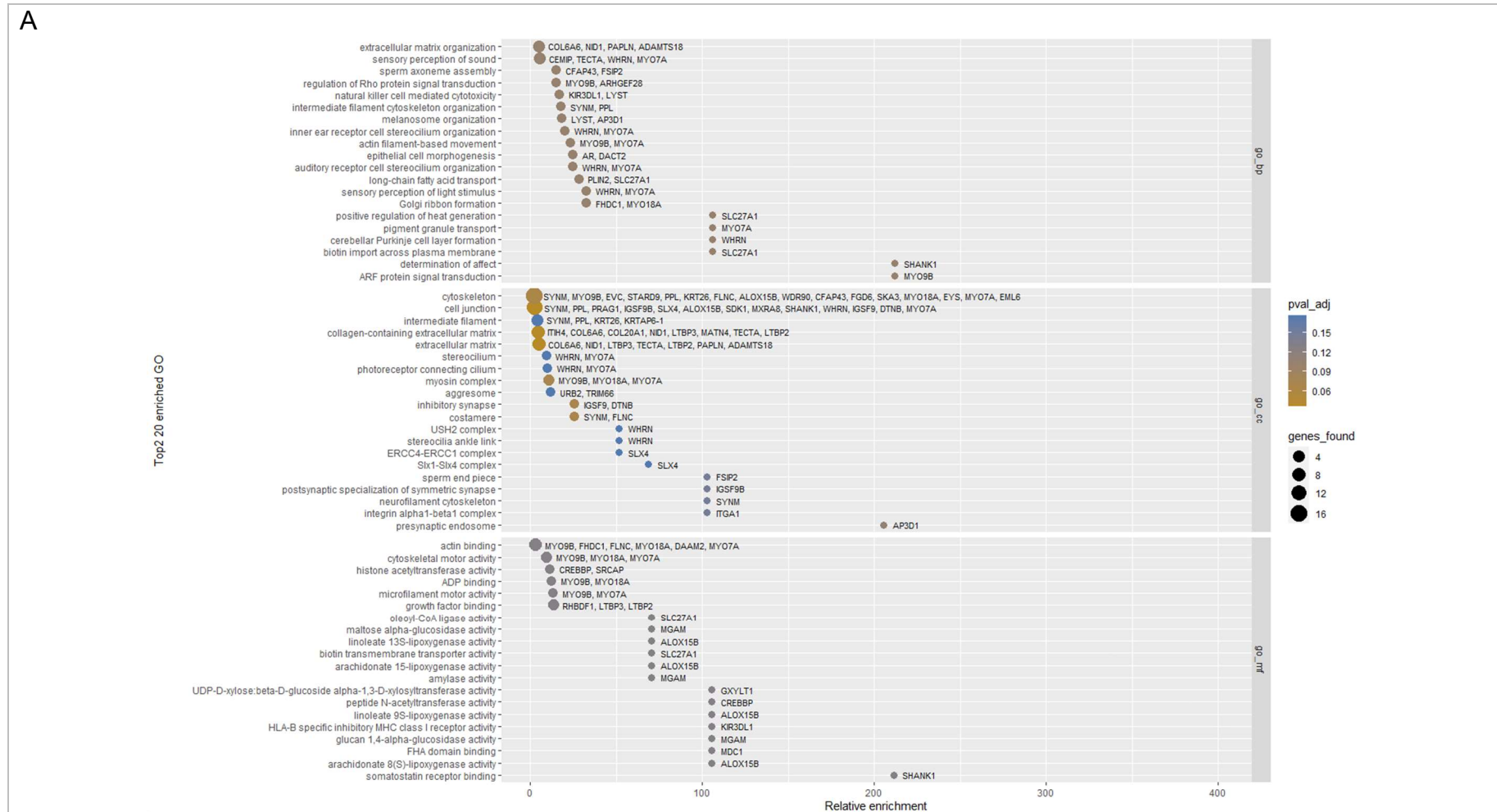


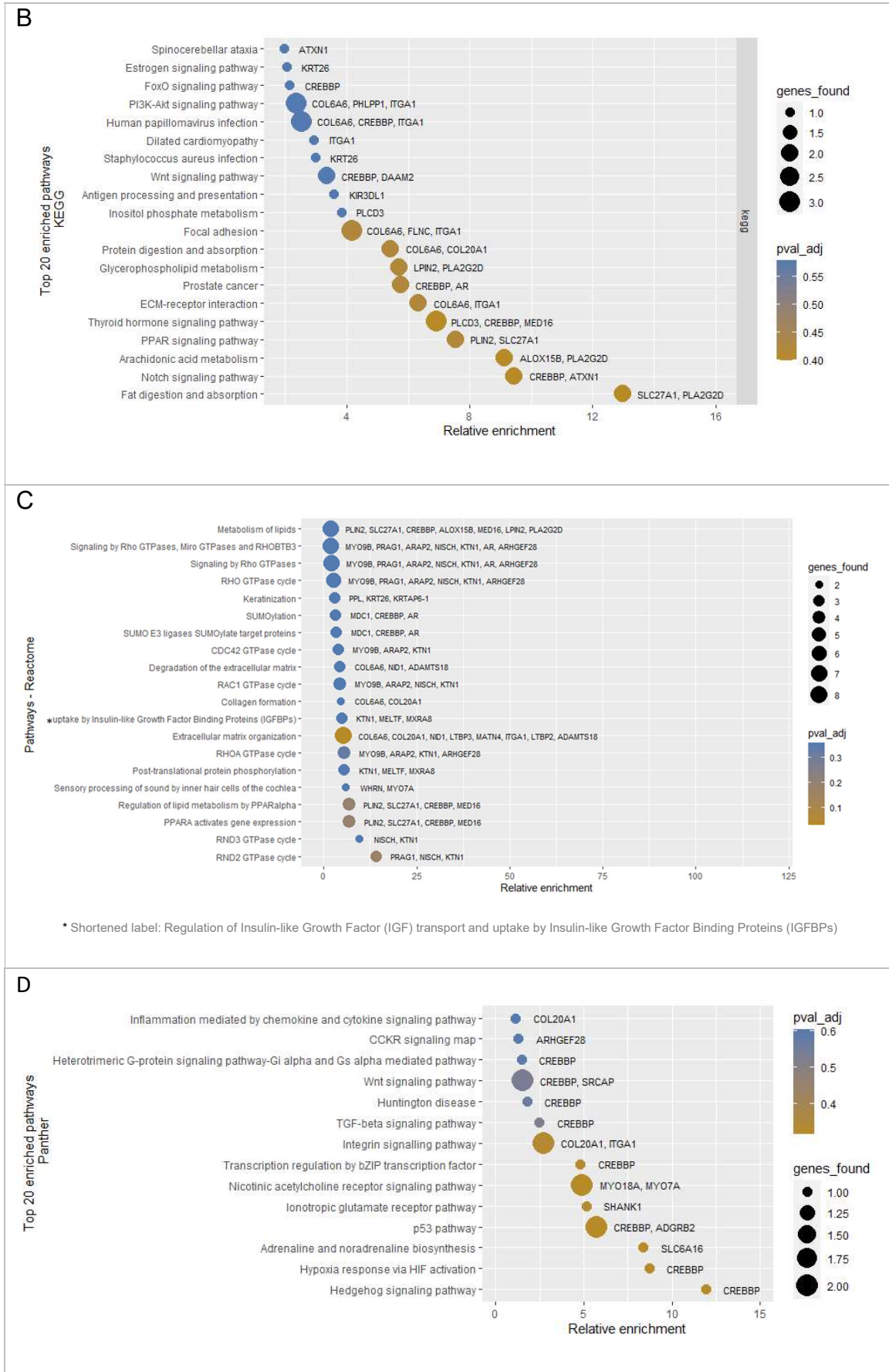
10. – Supplementary material

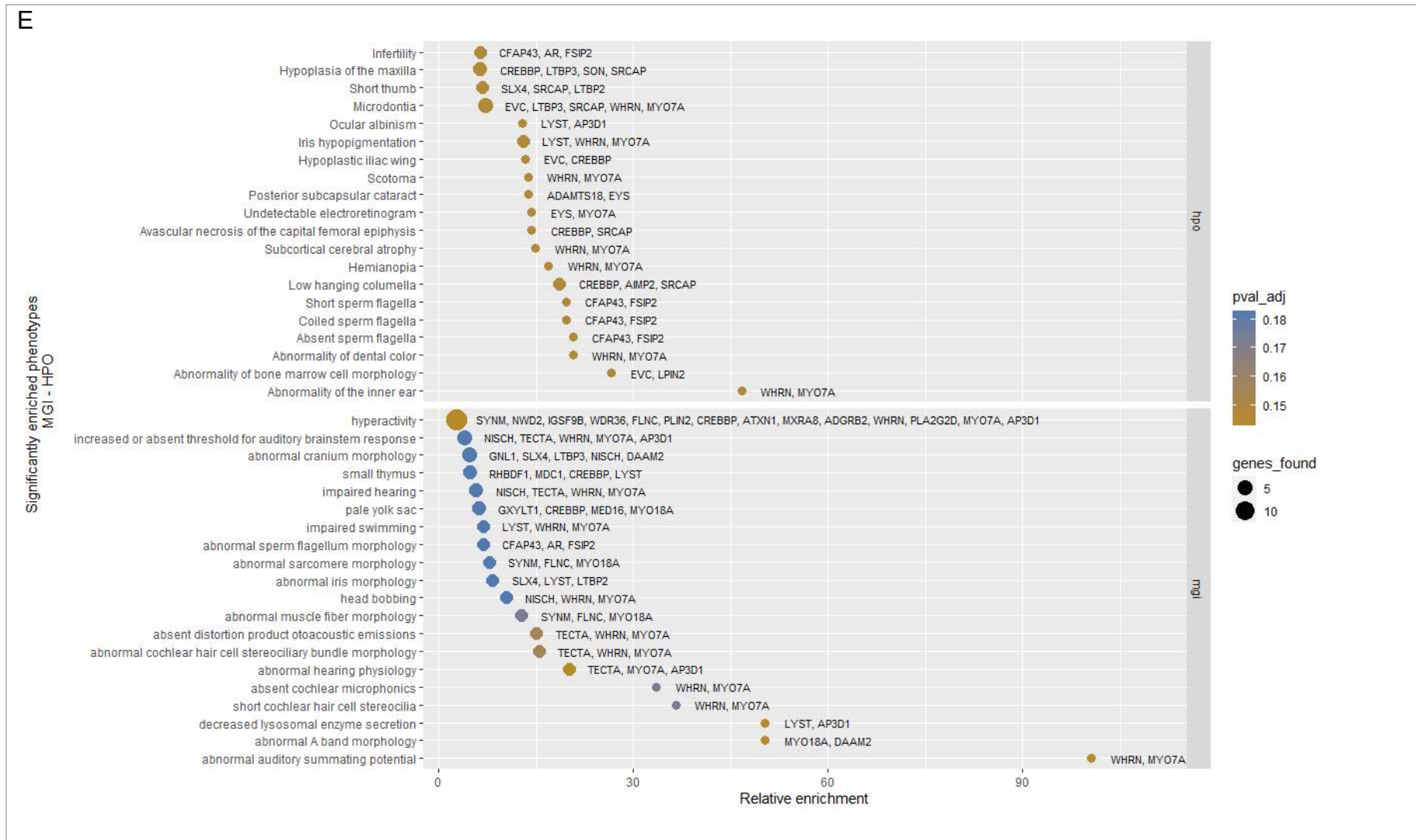


10.1 - Supplementary figures

Supplementary Figure 1 – Top 20 of the most enriched routes and pathways (although not significantly enriched) in the rest of databases contrasted in the functional analysis. A) GO including go_bp: biological processes; go_cc: cellular compartment; and go_mf: molecular function; B) KEGG; C) Reactome; D) Panther; E) Phenotype databases including MGI and HPO.









10.2 - Supplementary tables

Supplementary Table 1 – List of primers used to validate candidate variants in *ADAMTS18*, *SDK1* and *CENPP* genes.

Variant validation	Amplicon size	Primer sequence
ADAMTS18, 16-77367582G>A	269bp	FW: 3'- TGACACCCAACAGCACTCA - 5' RV: 3'- GGTCACCATCCTCAGTACT - 5'
ADAMTS18, 16-77434661G>C	193bp	FW: 5'- AGAGAAAAGGTGACATCGCG - 3' RV: 5'- ACCTGACCATGGAGTGCG - 3'
SDK1, 7-3951861C>T SDK1, 7-3951870C>T	257bp	FW: 5'- TGCCTGAGATGATGACCGTT-3' RV: 5'- ATGAAAAGAAAGCCGTCGC-3'
SDK1, 7-3951025C>T	236bp	FW: 5'- GGGTGCTCCTGTACTTAGAGT -3' RV: 5'- ATCCTTCTATCGTCGGCTCG -3'
CENPP, 9-92613131T>A	597bp	FW: 5'- AGTTTCTTACCCGGTTTAATGTTTT -3' RV: 5'- CATAGGCATCCGTCTCCAGAG -3'

Supplementary Table 2 – Complete list of the 94 genes enriched in rare variants as a result of GBA analysis.

Gene	N var	N ind	N het	N hom	% ind	gnomAD nfe					gnomAD global				
						OR	SE	lowCI	highCI	FDR pValue	OR	SE	lowCI	highCI	FDR pValue
<i>MYO9B</i>	13	18	18	0	42.86	2.62	0.21	1.73	3.96	4.7E-02	3.50	0.21	2.31	5.29	2.9E-05
<i>ADAMTS18</i>	7	15	15	0	35.71	4.28	0.25	2.60	7.05	9.7E-05	4.03	0.25	2.45	6.62	3.8E-04
<i>MDC1</i>	17	15	15	0	35.71	3.78	0.14	2.87	4.98	0.0E+00	2.33	0.14	1.77	3.06	1.6E-05
<i>SDK1</i>	12	14	14	0	33.33	3.69	0.23	2.34	5.81	1.8E-04	3.89	0.23	2.47	6.12	4.5E-05
<i>PAPLN</i>	11	13	13	0	30.95	3.71	0.26	2.22	6.19	4.7E-03	3.64	0.26	2.19	6.07	6.6E-03
<i>MELTF</i>	13	13	13	0	30.95	3.62	0.24	2.27	5.77	6.3E-04	4.04	0.24	2.54	6.45	4.1E-05
<i>COL6A6</i>	9	13	13	0	30.95	3.38	0.26	2.02	5.64	3.0E-02	4.90	0.26	2.93	8.17	1.1E-05
<i>AGBL1</i>	7	13	14	0	30.95	3.27	0.24	2.04	5.23	7.3E-03	3.83	0.24	2.39	6.12	2.0E-04
<i>KRTAP6-1</i>	1	12	12	0	28.57	4.15	0.29	2.33	7.38	1.2E-02	5.78	0.29	3.25	10.28	2.2E-05
<i>SKA3</i>	7	12	12	0	28.57	3.85	0.25	2.37	6.24	4.3E-04	5.43	0.25	3.35	8.81	6.4E-08
<i>ARHGEF28</i>	12	12	12	0	28.57	2.60	0.20	1.77	3.81	9.5E-03	2.63	0.20	1.79	3.85	7.0E-03
<i>STARD9</i>	14	11	11	0	26.19	8.72	0.24	5.46	13.92	1.1E-15	2.99	0.24	1.88	4.77	3.8E-02
<i>PRAG1</i>	6	11	11	0	26.19	4.50	0.31	2.47	8.20	8.0E-03	6.32	0.31	3.47	11.49	1.5E-05
<i>SYNM</i>	9	11	11	0	26.19	3.59	0.28	2.07	6.22	4.7E-02	5.32	0.28	3.07	9.22	2.3E-05
<i>FSIP2</i>	17	11	11	0	26.19	3.36	0.24	2.08	5.42	6.8E-03	4.25	0.24	2.63	6.86	3.0E-05
<i>GXYLT1</i>	1	10	10	0	23.81	30.13	0.34	15.35	59.15	0.0E+00	25.64	0.34	13.17	49.94	0.0E+00
<i>FER1L6</i>	7	10	10	0	23.81	5.18	0.32	2.76	9.69	2.6E-03	5.64	0.32	3.02	10.56	5.8E-04
<i>ARAP2</i>	9	10	10	0	23.81	4.05	0.29	2.29	7.18	1.5E-02	5.52	0.29	3.12	9.77	4.4E-05
<i>DAAM2</i>	7	9	9	0	21.43	10.97	0.34	5.66	21.30	1.3E-08	14.72	0.34	7.60	28.51	1.5E-11
<i>EYS</i>	8	9	9	0	21.43	4.88	0.34	2.52	9.43	2.3E-02	7.29	0.34	3.77	14.08	3.3E-05
<i>IGSF10</i>	7	9	9	0	21.43	4.60	0.31	2.53	8.37	5.3E-03	6.77	0.31	3.72	12.30	3.4E-06
<i>LPIN2</i>	4	8	8	0	19.05	8.03	0.36	3.97	16.26	6.4E-05	9.99	0.36	4.94	20.19	1.4E-06
<i>FGD6</i>	4	8	8	0	19.05	8.00	0.36	3.95	16.18	6.9E-05	11.28	0.36	5.58	22.80	1.4E-07
<i>WDR90</i>	8	8	8	0	19.05	7.63	0.34	3.94	14.78	1.6E-05	9.64	0.34	4.98	18.65	1.6E-07
<i>EVC</i>	7	8	8	0	19.05	7.28	0.34	3.75	14.10	3.8E-05	8.51	0.34	4.40	16.47	1.9E-06
<i>ADGRB2</i>	4	8	8	0	19.05	6.43	0.36	3.18	13.00	2.1E-03	8.78	0.36	4.35	17.74	1.3E-05
<i>COL20A1</i>	7	8	8	0	19.05	5.26	0.34	2.72	10.18	7.8E-03	7.18	0.34	3.71	13.89	4.5E-05
<i>IQCN</i>	10	8	8	0	19.05	3.68	0.25	2.24	6.04	2.4E-03	3.69	0.25	2.25	6.05	2.3E-03
<i>ZNF98</i>	1	7	7	0	16.67	86.63	0.41	38.44	195.22	0.0E+00	29.58	0.40	13.55	64.59	1.8E-13
<i>FLNC</i>	7	7	7	0	16.67	32.06	0.39	14.99	68.55	3.5E-15	26.51	0.38	12.51	56.17	1.1E-13
<i>DACT2</i>	6	7	7	0	16.67	23.96	0.39	11.24	51.09	1.8E-12	9.96	0.38	4.71	21.04	1.6E-05
<i>LYST</i>	7	7	7	0	16.67	16.06	0.38	7.56	34.09	4.5E-09	26.25	0.38	12.39	55.61	1.4E-13
<i>MAP3K9</i>	2	7	7	0	16.67	14.07	0.23	8.97	22.08	0.0E+00	18.80	0.23	11.99	29.46	0.0E+00
<i>RAB44</i>	7	7	7	0	16.67	12.93	0.38	6.10	27.40	2.3E-07	18.32	0.38	8.66	38.74	2.6E-10
<i>LTBP3</i>	4	7	7	0	16.67	9.32	0.38	4.39	19.80	5.7E-05	6.74	0.38	3.18	14.26	5.9E-03
<i>SLC6A16</i>	5	7	7	0	16.67	7.95	0.36	3.94	16.06	6.9E-05	7.54	0.36	3.74	15.20	1.6E-04



Gene	N var	N ind	N het	N hom	% ind	gnomAD nfe					gnomAD global				
						OR	SE	lowCI	highCI	FDR pValue	OR	SE	lowCI	highCI	FDR pValue
<i>MED16</i>	8	7	7	0	16.67	7.55	0.36	3.75	15.21	1.4E-04	11.54	0.36	5.73	23.23	6.8E-08
<i>LCMT2</i>	5	7	7	0	16.67	6.48	0.38	3.06	13.73	9.6E-03	9.35	0.38	4.42	19.79	4.7E-05
<i>NID1</i>	10	7	7	0	16.67	5.51	0.30	3.03	10.01	2.0E-04	5.76	0.30	3.18	10.46	7.9E-05
<i>FHDC1</i>	5	7	7	0	16.67	5.14	0.36	2.55	10.38	4.4E-02	7.81	0.36	3.87	15.74	8.8E-05
<i>PROB1</i>	6	6	6	0	14.29	65.47	0.43	28.35	151.23	0.0E+00	129.36	0.43	56.20	297.75	0.0E+00
<i>EML6</i>	7	6	6	0	14.29	16.02	0.38	7.54	34.00	4.7E-09	22.99	0.38	10.86	48.68	2.4E-12
<i>GCN1</i>	5	6	6	0	14.29	13.92	0.41	6.18	31.39	2.0E-06	20.97	0.41	9.32	47.18	1.8E-09
<i>PHLPP1</i>	4	6	6	0	14.29	12.58	0.42	5.57	28.38	9.9E-06	17.48	0.41	7.77	39.36	4.6E-08
<i>ATXN1</i>	6	6	6	0	14.29	10.42	0.41	4.63	23.43	1.3E-04	15.91	0.41	7.09	35.71	1.9E-07
<i>IGSF9</i>	6	6	6	0	14.29	10.34	0.41	4.60	23.24	1.5E-04	16.34	0.41	7.28	36.68	1.2E-07
<i>TMEM250</i>	4	6	6	0	14.29	9.84	0.41	4.37	22.18	3.2E-04	16.44	0.41	7.30	37.00	1.3E-07
<i>MYO7A</i>	7	6	6	0	14.29	8.77	0.38	4.15	18.56	1.2E-04	12.05	0.38	5.71	25.46	6.5E-07
<i>URB2</i>	5	6	6	0	14.29	8.74	0.41	3.88	19.65	1.5E-03	12.07	0.41	5.37	27.09	1.5E-05
<i>MGAM</i>	8	6	6	0	14.29	8.43	0.36	4.18	16.99	2.3E-05	6.95	0.36	3.46	13.98	5.0E-04
<i>KIAA1217</i>	6	6	6	0	14.29	8.34	0.38	3.94	17.66	2.7E-04	12.93	0.38	6.12	27.35	2.0E-07
<i>RHBDF1</i>	6	6	6	0	14.29	8.04	0.38	3.80	17.02	4.7E-04	13.47	0.38	6.37	28.49	9.5E-08
<i>ZBTB37</i>	2	6	6	0	14.29	8.00	0.42	3.53	18.15	6.0E-03	12.07	0.42	5.33	27.34	2.3E-05
<i>TMEM184A</i>	5	6	6	0	14.29	7.96	0.38	3.76	16.87	5.6E-04	10.34	0.38	4.89	21.87	9.5E-06
<i>KRT26</i>	4	6	6	0	14.29	7.57	0.41	3.36	17.04	9.3E-03	8.45	0.41	3.76	18.98	2.2E-03
<i>CFAP43</i>	6	6	6	0	14.29	7.43	0.41	3.31	16.67	1.1E-02	10.98	0.41	4.90	24.63	5.7E-05
<i>TECTA</i>	6	6	6	0	14.29	7.27	0.41	3.24	16.32	1.4E-02	10.52	0.41	4.69	23.58	1.1E-04
<i>LRRC8E</i>	5	6	6	0	14.29	7.17	0.41	3.19	16.12	1.7E-02	10.53	0.41	4.69	23.64	1.1E-04
<i>ITGA1</i>	4	6	6	0	14.29	7.16	0.41	3.18	16.11	1.8E-02	11.20	0.41	4.98	25.18	4.8E-05
<i>SLC27A1</i>	2	6	6	0	14.29	6.91	0.42	3.05	15.67	3.4E-02	10.20	0.42	4.50	23.09	2.4E-04
<i>WDR36</i>	4	6	6	0	14.29	6.72	0.38	3.17	14.26	6.3E-03	9.50	0.38	4.49	20.14	3.9E-05
<i>ZC3H13</i>	4	6	6	0	14.29	5.71	0.36	2.83	11.55	1.1E-02	8.64	0.36	4.28	17.45	1.8E-05
<i>KIR3DL1</i>	3	6	6	0	14.29	5.60	0.11	4.48	7.01	0.0E+00	6.51	0.11	5.21	8.14	0.0E+00
<i>ANKRD30B</i>	5	5	5	0	11.90	249.03	0.51	90.80	683.00	0.0E+00	294.70	0.49	113.77	763.36	0.0E+00
<i>NWD2</i>	5	5	5	0	11.90	83.02	0.47	32.88	209.62	1.0E-16	82.63	0.46	33.53	203.66	0.0E+00
<i>WHRN</i>	6	5	5	0	11.90	45.54	0.42	19.91	104.17	1.4E-15	71.22	0.42	31.34	161.87	0.0E+00
<i>AIMP2</i>	5	5	5	0	11.90	35.90	0.46	14.58	88.42	6.4E-11	50.53	0.46	20.66	123.58	7.8E-14
<i>CEMIP</i>	4	5	5	0	11.90	34.16	0.46	13.86	84.16	1.5E-10	9.30	0.45	3.84	22.55	7.6E-03
<i>LTBP2</i>	5	5	5	0	11.90	31.13	0.46	12.67	76.47	6.0E-10	34.54	0.45	14.18	84.15	6.0E-11
<i>ALOX15B</i>	3	5	5	0	11.90	22.42	0.46	9.14	55.02	1.0E-07	31.70	0.46	12.98	77.45	3.2E-10
<i>PLIN2</i>	2	5	5	0	11.90	16.75	0.46	6.82	41.16	7.4E-06	17.99	0.46	7.35	44.00	2.3E-06
<i>PLCD3</i>	5	5	5	0	11.90	15.69	0.42	6.95	35.41	3.1E-07	26.23	0.41	11.65	59.08	3.0E-11
<i>PPL</i>	5	5	5	0	11.90	11.34	0.45	4.67	27.57	7.7E-04	14.93	0.45	6.16	36.20	2.1E-05
<i>MXRA8</i>	3	5	5	0	11.90	11.02	0.45	4.52	26.87	1.2E-03	12.61	0.45	5.19	30.67	2.1E-04

Gene	N var	N ind	N het	N hom	% ind	gnomAD nfe					gnomAD global				
						OR	SE	lowCI	highCI	FDR pValue	OR	SE	lowCI	highCI	FDR pValue
GTF3C3	4	5	5	0	11.90	10.94	0.45	4.49	26.61	1.2E-03	16.87	0.45	6.95	40.98	4.1E-06
SLX4	7	5	5	0	11.90	10.91	0.38	5.15	23.10	4.0E-06	18.12	0.38	8.56	38.32	3.3E-10
ITIH4	3	5	5	0	11.90	10.70	0.45	4.39	26.08	1.7E-03	15.23	0.45	6.26	37.05	1.9E-05
KTN1	3	5	5	0	11.90	10.55	0.45	4.33	25.73	2.0E-03	15.04	0.45	6.18	36.60	2.2E-05
MATN4	3	5	5	0	11.90	10.50	0.45	4.31	25.60	2.2E-03	12.96	0.45	5.33	31.52	1.5E-04
GNL1	4	5	5	0	11.90	9.39	0.38	4.42	19.95	5.1E-05	12.27	0.38	5.79	26.02	5.8E-07
TRIM66	5	5	5	0	11.90	8.78	0.45	3.62	21.31	1.4E-02	9.14	0.45	3.77	22.13	8.9E-03
SHANK1	6	5	5	0	11.90	7.37	0.41	3.28	16.55	1.2E-02	8.45	0.41	3.77	18.94	2.1E-03
C1orf127	5	4	4	0	9.52	306.59	0.53	108.80	863.96	0.0E+00	49.12	0.46	20.09	120.09	1.3E-13
CREBBP	4	4	4	0	9.52	20.47	0.46	8.37	50.07	3.4E-07	33.17	0.45	13.60	80.89	1.3E-10
AP3D1	4	4	3	1	9.52	19.89	0.46	8.13	48.69	5.4E-07	31.87	0.46	13.06	77.76	2.7E-10
IGSF9B	4	4	4	0	9.52	18.84	0.46	7.71	46.05	1.1E-06	21.74	0.45	8.94	52.86	1.1E-07
DTNB	5	4	4	0	9.52	18.70	0.46	7.66	45.63	1.1E-06	19.51	0.45	8.04	47.34	4.9E-07
SRCAP	3	4	4	0	9.52	11.32	0.45	4.64	27.62	8.8E-04	13.59	0.45	5.59	33.07	8.2E-05
NISCH	4	4	4	0	9.52	11.28	0.45	4.63	27.45	8.6E-04	16.03	0.45	6.60	38.93	8.4E-06
ZNF215	4	4	4	0	9.52	11.05	0.45	4.54	26.90	1.1E-03	18.65	0.45	7.67	45.31	1.0E-06
PLA2G2D	2	4	4	0	9.52	10.25	0.46	4.19	25.10	3.3E-03	15.75	0.46	6.44	38.51	1.4E-05
MYO18A	5	4	4	0	9.52	9.05	0.45	3.73	21.96	1.0E-02	11.37	0.45	4.69	27.54	6.8E-04
SON	4	4	4	0	9.52	8.02	0.27	4.76	13.49	4.2E-11	11.91	0.27	7.09	20.03	1.0E-16
AR	3	2	3	0	4.76	8.90	0.31	4.87	16.25	1.1E-08	10.93	0.31	6.00	19.94	5.6E-11

Gene: variant enriched gene; N var: number of variants in the gene; N het and N hom indicate the number of individuals with variants in heterozygous and homozygous, respectively. % ind: percentage of individuals in the ES hypoplastic cohort with variants in this gene; OR: association score. OR significantly greater than 1 indicates that accumulation of rare variants in that gene increases the risk of developing the phenotype, being the magnitude of the association greater the further OR is from 1; SE, lowCI and highCI show the standard deviation, lower and upper confidence intervals of OR, respectively; p-value indicates the statistical significance of the association ($p < 0.05$), corrected by FDR multiple-testing. Association and statistical assessment were evaluated vs gnomAD nfe (soft grey header) and gnomAD global (dark grey header).

Supplementary Table 3 – Complete list of LSV

Tool	Gene/s	Chr	Start	End	Length	Type	AF cohort	N ind (hom/het)	GnomAD pLI	ExAC pLI	ACMG
Tiddit	<i>GRIK3</i>	1	36957455	36960066	2147	DUP	0.024	1 (1/0)	1	1	US
		1	36958632	36960275	1505	DEL	0.024	1 (1/0)	1	1	B
	<i>EXOC6B</i>	2	72213038	72214236	1198	INV	0.012	1 (0/1)	0.12	0.67	ND
	<i>CTD-3080P12.3</i>	5	1178178	1180671	2438	DEL	0.024	1 (1/0)	ND	ND	B
	<i>CNT -P2</i>	7	148375718	148379233	3457	DEL	0.024	1 (1/0)	0	0	B
	<i>MRGPRG; MRGPRG-AS1</i>	11	3217418	3222898	5346	DUP	0.024	1 (1/0)	ND	ND	US
	<i>RIMBP2</i>	12	130647393	130649324	1929	DEL	0.024	1 (1/0)	0.68	0.29	B
	<i>UNKL</i>	16	1372908	1374264	1153	DEL	0.024	1 (1/0)	0.82	0.1	US
	<i>WWP2</i>	16	69820783	69825180	4398	TDUP	0.012	1 (0/1)	0.16	0.98	US
	<i>LINC00917</i>	16	86345402	86352129	6596	INV	0.060	4 (1/3)	ND	ND	ND
	<i>SPIRE2</i>	16	89829650	89832014	2333	DEL	0.024	1 (1/0)	0	0	US
	<i>TCF25</i>	16	89907625	89908762	1138	TDUP	0.024	1 (1/0)	0.42	0.05	US
	<i>MSI2</i>	17	57610451	57612555	2103	DUP	0.024	1 (1/0)	0.99	0.96	US
	<i>TBC1D16</i>	17	80021923	80025068	3146	TDUP	0.071	3 (3/0)	0	0.01	US
	<i>HCN2</i>	19	605249	608624	3114	DUP	0.024	1 (1/0)	0.49	0.83	US
	<i>GPI</i>	19	34391361	34392770	1410	TDUP	0.024	1 (1/0)	0	0	US
	<i>ZNF888</i>	19	52918924	52921075	1994	DEL	0.024	1 (1/0)	ND	ND	US
	<i>ZNF665</i>	19	53185862	53188716	2765	DEL	0.024	1 (1/0)	0.01	0	B
	<i>LILRA1; LILRA2</i>	19	54576610	54597463	20854	TDUP	0.024	1 (1/0)	0	0	US
	<i>GUSBP11</i>	22	23683331	23685361	1920	DEL	0.024	1 (1/0)	ND	ND	US
<i>PARVB</i>	22	44112668	44114285	1527	DEL	0.012	1 (0/1)	0	0	B	



Manta	<i>CASP8</i>	2	201281925	201284727	-2792	DEL	0.119	6 (4/2)	0	0	US
	<i>CHROMR; PRKRA</i>	2	178436319	178441609	-5290	DEL	0.012	1 (0/1)	0.42	0.15	B
		2	178444501	178447508	-3007	DEL	0.036	3 (0/3)	0.42	0.15	LP
	<i>LOC285638</i>	5	109259373	109265435	-6047	DEL	0.012	1 (0/1)	ND	ND	US
	<i>EXOC2</i>	6	666376	667821	-1445	DEL	0.012	1 (0/1)	0	0	B
	<i>HLA-DRB1; HLA-DRB5; HLA-DRB6</i>	6	32519560	32581791	-62135	DEL	0.012	1 (0/1)	0	0	B
		13	21155811	21157923	-2110	DEL	0.012	1 (0/1)	0	0	B
	<i>SKA3</i>	13	21158122	21159902	-1776	DEL	0.060	5 (0/5)	0	0	B
		13	21158126	21161789	-3663	DEL	0.012	1 (0/1)	0	0	B
		13	21159987	21161790	-1802	DEL	0.060	5 (0/5)	0	0	B
	<i>MOSMO</i>	13	21161875	21167989	-6112	DEL	0.060	5 (0/5)	0	0	B
		16	22075699	22080695	-4996	DEL	0.012	1 (0/1)	ND	ND	B
	<i>WWP2</i>	16	69820782	69825118	4336	DUP	0.012	1 (0/1)	0.16	0.98	US

Gene/s: LSV mapped gene or genes; Chr: chromosome; Start and End: SV starting and ending position in GRCh38/Hg38; Length: size of SV in base pairs; Type of SV including DEL (deletion), DUP (duplication); INV (inversion); N ind (hom/het): number of individuals with the SV, specifying in brackets how many present SV in homozygosity and heterocigosity; pLI: probability of being Loss of Function variant intolerant gene in GnomAD and Exac databases. pLi >= 0.9 regions are considered as high-constrained. ACMG: American College of Medical Genetics guideline classification. LB: likely-benign; US: uncertain significance; LP: likely-pathogenic. ND: non-described.

Supplementary Table 4 – Complete list of CNV

Gene/s	Chr	Start	End	Length	Type	AF cohort	N ind (hom/het)	GnomAD pLi	ExAC pLi	ACMG	CN
<i>FBLIM1; FLJ37453; SPEN; UQCRHL</i>	1	15785058	15873799	-88741	DEL	0.024	1 (1/0)	1.00	1.00	LP	-2
<i>MIR548F3; TGFB2</i>	1	218346476	218441728	95252	DUP	0.048	4 (0/4)	1.00	0.99	P	+176, +256, +189, +57
<i>MYT1L</i>	2	1789112	1887121	-98009	DEL	0.071	3 (3/0)	1.00	1.00	LP	-2
<i>CFAP65; IHH; MIR3131; NHEJ1</i>	2	219033691	219076192	-42501	DEL	0.024	1 (1/0)	0.31	0.35	LP	-2
<i>ACVR2B; EXOG; SCN5A</i>	3	38483663	38549941	-66278	DEL	0.024	1 (1/0)	0.91	1.00	P	-2
<i>KIT</i>	4	54657917	54738936	81019	DUP	0.012	1 (0/1)	0.98	1.00	P	+15
<i>TSC1</i>	9	132895943	132928955	33012	DUP	0.024	2 (0/2)	1.00	1.00	P	+9, +10
<i>CPSF7; CYB561A3; TKFC; TMEM138; TMEM216</i>	11	61346832	61404704	-57872	DEL	0.048	2 (2/0)	1.00	0.99	P	-2
<i>CPSF7; CYB561A3; TMEM138; TMEM216</i>	11	61357732	61404704	-46972	DEL	0.024	1 (1/0)	1.00	0.99	P	-2
<i>CD276; NPTN</i>	15	73599488	73685083	-85595	DEL	0.024	1 (1/0)	0.99	0.99	P	-2
<i>FAHD1; LINC00254; MEIOB</i>	16	1828068	1884294	-56226	DEL	0.024	1 (1/0)	0.00	0.00	P	-2
<i>MIR3180-5; MIR4516; PKD1; RAB26</i>	16	2113160	2148324	-35164	DEL	0.024	1 (1/0)	1.00	1.00	P	-2
<i>GFOD2; RANBP10</i>	16	67677765	67726021	-48256	DEL	0.095	4 (4/0)	0.97	0.95	P	-2
<i>ANKRD11; ZNF778</i>	16	89228836	89268146	-39310	DEL	0.048	2 (2/0)	1.00	1.00	P	-2
<i>CHRN1; FGF11; SPEM3; TMEM102; ZBTB4</i>	17	7428856	7461760	-32904	DEL	0.012	1 (0/1)	1.00	1.00	P	-1
<i>CHD3; CYB5D1; NAA38</i>	17	7859908	7887081	-27173	DEL	0.071	3 (3/0)	1.00	1.00	LP	-2
<i>HSF5; RNF43</i>	17	58402639	58421864	-19225	DEL	0.071	3 (3/0)	0.98	0.74	LP	-2
<i>HSF5; RNF43; MTMR4;</i>	17	58402639	58491583	-88944	DEL	0.048	2 (2/0)	1.00	1.00	LP	-2



Gene/s	Chr	Start	End	Length	Type	AF cohort	N ind (hom/het)	GnomAD pLi	ExAC pLi	ACMG	CN
<i>METTL2A; TLK2</i>	17	62449643	62508553	-58910	DEL	0.071	3 (3/0)	1.00	1.00	P	-2
<i>CERS1; GDF1; UPF1</i>	19	18866520	18878756	-12236	DEL	0.071	3 (3/0)	1.00	1.00	P	-2
<i>LINC02575; LRRC3; LRRC3-DT; TRPM2; TSPEAR</i>	21	44441969	44499425	-57456	DEL	0.024	1 (1/0)	0.00	0.01	P	-2
<i>IQSEC2</i>	X	53233386	53321350	87964	DUP	0.012	1 (0/1)	1.00	0.98	P	+6
<i>ATP2B3; CCNQ; DUSP9; LOC105373383</i>	X	153580784	153647425	-66641	DEL	0.024	1 (1/0)	1.00	1.00	P	-2

Chr: chromosome; Start and End: SV starting and ending position in GRCh38/Hg38; Length: size of SV in base pairs; Type of SV including DEL (decreases in the number of copies) or DUP (increases in the number of copies); n ind: number of individuals with SV in homozygosity (n hom) and heterozygosity (n het); pLi: probability of being Loss of Function variant intolerant gene in GnomAD and Exac databases. pLi >= 0.9 regions are considered as high-constrained. ACMG: American College of Medical Genetics guideline classification. LP: likely-pathogenic; P: pathogenic. ND: non-described; CN: number of copies in the CNV. In duplications, increased number of copies are specified per individual. In deletions are indicated as -2 (homozygous deletion) or -1 (heterozygous deletion)

Supplementary Table 5 – Predicted structural models evaluation of CENPP

Protein (length)	Modelling method	Evaluation				
		Molprobit y Score	Verify3D	ERRAT	ProSA- Web	QMEANDisCo
CENPP 288aa	I-TASSER (184)	2.84	10.76	90.0000	-2.65	0.33 ± 0.05
	CI-TASSER (276)	3.98	67.36	80.0000	-5.67	0.37 ± 0.05
	C-QUARK (183)	3.00	52.43	85.1986	-5.59	0.36 ± 0.05
	Robetta-AB* (182)	0.81	74.65	85.6115	-7.18	0.41 ± 0.05
	AlphaFold2 (185)	1.26	62.06	91.2351	-5.31	0.46 ± 0.05

The CENPP structural model predicted by Alphafold2 is located at <https://alphafold.ebi.ac.uk/entry/Q6IPU0>. Molprobability Score, Verify3D, ERRAT, ProSA-web and QMEANDisCo metrics were used in the evaluation. Molprobability Score is a weighted logarithmic combination of different geometric scores such as clashscore, percentage of unfavored Ramachandran and percentage of bad sidechain rotamers, giving a number that reflects the crystallographic resolution at which those values would be expected. Lower values are better. Verify3D determines the compatibility of an atomic model (3D) with its own amino acid sequence (1D) by assigning a structural type based on its location and environment. A higher score indicated high-quality of the structure. The overall quality factor, ERRAT, analyzes the statistics of interactions between the different types of atoms and plots the value of the error function calculated by a comparison with highly refined structure statistics. As the generally accepted range for a high-quality model is >50, this analysis revealed that the backbone conformation and nonbonded interactions of all models were within the scope of a high-quality model. In the ProSA-web tool, the score is z-score defined as the energy separation between the native fold and the average of an ensemble of the misfolds in standard deviation units of the database. A z-score outside a range characteristic for native proteins of similar sizes indicated an erroneous structure. In this case, the z-score range of the overall quality of all models is in the range of the experimentally obtained structures. Finally, QMEANDisCo evaluates the agreement of pairwise distances between residues with sets of distance constraints extracted from structures homologous to the evaluated model, so the higher the score the better the model.

*Model used for the evaluation of the impact of the deletion found.



Original Research Articles

Original articles published during the performing of this doctoral thesis:

- Simoes JP, Schoisswohl S, Schlee W, Basso L, Bernal-Robledano A, Boecking B, Cima R, Denys S, Engelke M, Escalera-Balsera A, Gallego-Martinez A, Gallus S, Kikidis D, López-Escámez JA, Marcrum SC, Markatos N, Martin-Lagos J, Martinez-Martinez M, Mazurek B, Vassou E, Jarach CM, Mueller-Locatelli N, Neff P, Niemann U, Omar HK, Puga C, Schleicher M, Unnikrishnan V, Perez-Carpena P, Pryss R, Robles-Bolivar P, Rose M, Schecklmann M, Schiele T, Schobel J, Spiliopoulou M, Stark S, Vogel C, Wunder N, Zachou Z, Langguth B. The statistical analysis plan for the unification of treatments and interventions for tinnitus patients randomized clinical trial (UNITI-RCT). *Trials*. 2023 Jul 24;24(1):472. doi: 10.1186/s13063-023-07303-2. PMID: 37488627; PMCID: PMC10367236.
- Gallego-Martinez A, Escalera-Balsera A, Trpchevska N, Robles-Bolivar P, Roman-Naranjo P, Frejo L, Perez-Carpena P, Bulla J, Gallus S, Canlon B, Cederroth CR, Lopez-Escamez JA. Using coding and non-coding rare variants to target candidate genes in patients with severe tinnitus. *NPJ Genom Med*. 2022 Nov 30;7(1):70. doi: 10.1038/s41525-022-00341-w. PMID: 36450758; PMCID: PMC9712652.
- Robles-Bolivar P, Bächinger D, Parra-Perez AM, Román-Naranjo P, Escalera-Balsera A, Gallego-Martinez A, Eckhard AH, Lopez-Escamez JA. A novel nonsense variant in the CENPP gene segregates in a Swiss family with autosomal dominant low-frequency sensorineural hearing loss. *Eur J Hum Genet*. 2022 Nov;30(11):1301-1305.. doi: 10.1038/s41431-022-01184-w. Epub ahead of print. PMID: 36071244 <https://pubmed.ncbi.nlm.nih.gov/36071244/>

-----**This article supports this doctoral thesis**-----

- Stefan Schoisswohl, Berthold Langguth, Martin Schecklmann, Alberto Bernal-Robledano, Benjamin Boecking, Christopher R. Cederroth, Dimitra Chalanouli, Rilana Cima, Sam Denys, Juliane Dettling-Papargyris, Alba Escalera-Balsera, Juan Manuel Espinosa-Sanchez, Alvaro Gallego-Martinez, Efi Giannopoulou, Leyre Hidalgo-Lopez, Michael Hummel, Dimitris Kikidis, Michael Koller, Jose A. Lopez-Escamez, Steven C. Marcrum, Nikolaos Markatos, Juan Martin-Lagos, Maria Martinez-Martinez, Marta Martinez-Martinez, Maria Mata Ferron, Birgit Mazurek, Nicolas Mueller-Locatelli, Patrick Neff, Kevin Oppel, Patricia Perez-Carpena, Paula Robles-Bolivar, Matthias Rose, Tabea Schiele, Axel Schiller, Jorge Simoes, Sabine Stark, Susanne Staudinger, Alexandra Stege, Nicolas Verhaert & Winfried Schlee. Unification of Treatments and Interventions for Tinnitus Patients (UNITI): a study protocol for a multi-center randomized clinical trial. *Trials* 22, 875 (2021). <https://doi.org/10.1186/s13063-021-05835-z>